(12) INTERNATIONAL APPLICATION PUBLISHED UNDER THE PATENT COOPERATION TREATY (PCT)

(19) World Intellectual Property Organization
International Bureau

(43) International Publication Date
09 January 2025 (09.01.2025)

WIPO | PCT

(10) International Publication Number
WO 2025/010407 A2

(51) International Patent Classification:
C07F 15/00 (2006.01) *A61K 47/34* (2017.01)

(21) International Application Number:
PCT/US2024/036893

(22) International Filing Date:
05 July 2024 (05.07.2024)

(25) Filing Language: English

(26) Publication Language: English

(30) Priority Data:
63/525,052 05 July 2023 (05.07.2023) US

(71) Applicant: **THE UNIVERSITY OF CHICAGO** [US/US]; 5801 S. Ellis Avenue, Chicago, IL 60637 (US).

(72) Inventors: **LIN, Wenbin**; 1201 E. 56th Street, Chicago, IL 60637 (US). **XU, Ziwan**; 1127 E. 61st Street, Apt. 3, Chicago, IL 60637 (US). **ZHEN, Wenyao**; 1400 East 55th Place, Apt. 909S, Chicago, IL 60637 (US). **JIANG, Xiaomin**; 6128 Ellis Ave GL, Chicago, IL 60637 (US).

(74) Agent: **TAYLOR JR., Arles, A.**; Jenkins, Taylor, & Hunt, P.A., P.O. Box 710, Morrisville, NC 27560 (US).

(81) Designated States *(unless otherwise indicated, for every kind of national protection available)*: AE, AG, AL, AM, AO, AT, AU, AZ, BA, BB, BG, BH, BN, BR, BW, BY, BZ, CA, CH, CL, CN, CO, CR, CU, CV, CZ, DE, DJ, DK, DM, DO, DZ, EC, EE, EG, ES, FI, GB, GD, GE, GH, GM, GT, HN, HR, HU, ID, IL, IN, IQ, IR, IS, IT, JM, JO, JP, KE, KG, KH, KN, KP, KR, KW, KZ, LA, LC, LK, LR, LS, LU, LY, MA, MD, MG, MK, MN, MU, MW, MX, MY, MZ, NA, NG, NI, NO, NZ, OM, PA, PE, PG, PH, PL, PT, QA, RO, RS, RU, RW, SA, SC, SD, SE, SG, SK, SL, ST, SV, SY, TH, TJ, TM, TN, TR, TT, TZ, UA, UG, US, UZ, VC, VN, WS, ZA, ZM, ZW.

WO 2025/010407 A2

(54) Title: NANOSCALE METAL-ORGANIC FRAMEWORKS WITH X-RAY TRIGGERABLE PRODRUGS FOR COMBINATION RADIOTHERAPY, CHEMOTHERAPY, AND IMMUNOTHERAPY

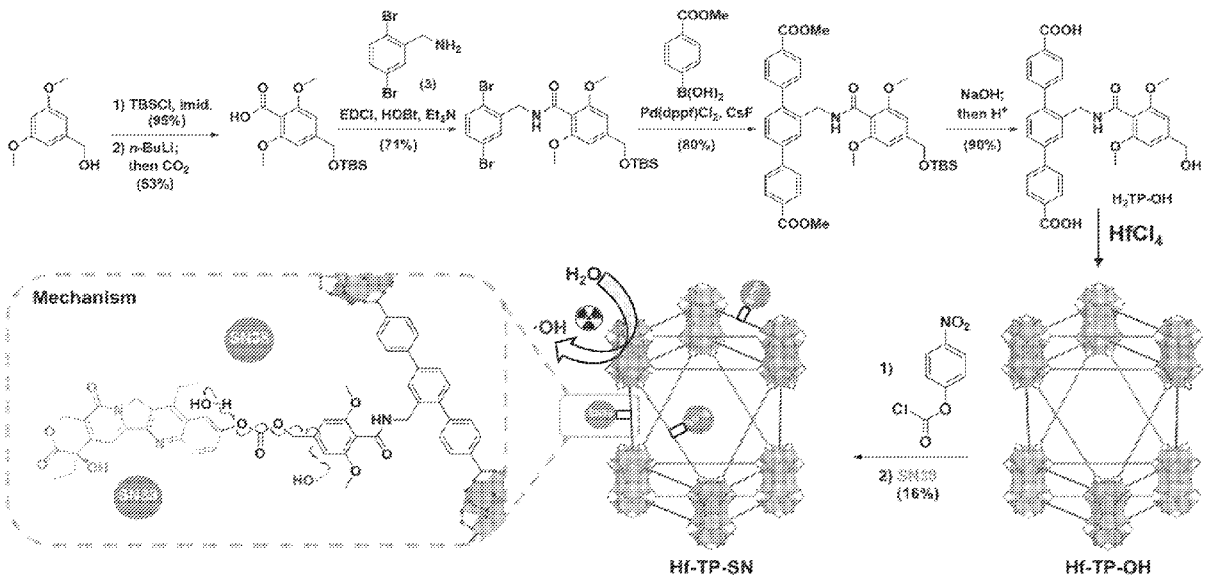

FIG. 1

(57) Abstract: A metal-organic framework (nMOF) including an X-ray sensitive prodrug is described. For instance, the MOF can include metal-containing secondary building units (SBU) that are linked together via organic bridging ligands where the SBU includes a metal cation that can absorb X-rays and where at least one organic bridging ligand is substituted by a monovalent moiety derived from a therapeutic agent, such as a chemotherapy and/or immunotherapy agent, via a group that includes a bond capable of radical-promoted bond cleavage. Methods of using the MOF to treat diseases, such as cancer, are also described. The methods can include the combination of radiotherapy or radiotherapy-radiodynamic therapy with chemotherapy or immunotherapy.

[Continued on next page]

(84) Designated States *(unless otherwise indicated, for every kind of regional protection available)*: ARIPO (BW, CV, GH, GM, KE, LR, LS, MW, MZ, NA, RW, SC, SD, SL, ST, SZ, TZ, UG, ZM, ZW), Eurasian (AM, AZ, BY, KG, KZ, RU, TJ, TM), European (AL, AT, BE, BG, CH, CY, CZ, DE, DK, EE, ES, FI, FR, GB, GR, HR, HU, IE, IS, IT, LT, LU, LV, MC, ME, MK, MT, NL, NO, PL, PT, RO, RS, SE, SI, SK, SM, TR), OAPI (BF, BJ, CF, CG, CI, CM, GA, GN, GQ, GW, KM, ML, MR, NE, SN, TD, TG).

Published:

— *without international search report and to be republished upon receipt of that report (Rule 48.2(g))*

DESCRIPTION

NANOSCALE METAL-ORGANIC FRAMEWORKS WITH X-RAY TRIGGERABLE PRODRUGS FOR COMBINATION RADIOTHERAPY, CHEMOTHERAPY, AND IMMUNOTHERAPY

CROSS REFERENCE TO RELATED APPLICATIONS

This application claims priority to and the benefit of U.S. Provisional Patent Application Serial No. 63/525,052, filed July 5, 2023, the disclosure of which is incorporated herein by reference in its entirety.

GOVERNMENT INTEREST

This invention was made with government support under Grant No. CA253655 awarded by the National Institutes of Health. The government has certain rights in the invention.

TECHNICAL FIELD

The presently disclosed subject matter relates to metal-organic frameworks (MOFs), e.g., nanoscale MOFs (nMOFs) comprising metal cations that absorb X-rays and organic bridging ligands that comprise X-ray sensitive prodrugs. The presently disclosed subject matter further relates to the use of the MOFs in treating diseases, such as cancer, e.g., via combinations of radiotherapy or immunotherapy with radiotherapy or radiotherapy-radiodynamic therapy.

ABBREVIATIONS

°C	=	degrees Celsius
%	=	percentage
ζ	=	zeta
μg	=	microgram
μl or μL	=	microliter
μM	=	micromolar
ACN	=	acetonitrile
APF	=	aminophenyl fluorescein
BMDC	=	bone marrow-derived dendritic cells
CLSM	=	confocal laser scanning microscopy
cm	=	centimeter

	DBP	=	bis(p-benzoato)porphyrin
	DCFH	=	2',7'-dichlorodihydrofluorescein
	$DMR_{10\%}$	=	dose modifying ratio at 10% survival fraction
	DMSO	=	dimethyl sulfoxide
	EA	=	ethyl acetate
	EC_{50}	=	half maximal effective concentration
	EtOH	=	ethanol
	g	=	gram
	Gy	=	gray
	h	=	hour
	Hf	=	hafnium
	IC_{50}	=	fifty percent inhibitory concentration
	IL	=	interleukin
	kg	=	kilogram
	M	=	molar
	mg	=	milligram
	min	=	minute
	mL	=	milliliter
	mm	=	millimeter
	mM	=	millimolar
	mmol	=	millimole
	MOF	=	metal-organic framework
	nm	=	nanometer
	nMOF	=	nanoscale metal-organic framework
	NMR	=	nuclear magnetic resonance
	PBS	=	phosphate buffered saline
	PXRD	=	powder X-ray diffraction
	QP	=	quaterphenyl
	R848	=	resiquimod
	ROS	=	reactive oxygen species
	RT	=	radiotherapy
	RT-RDT	=	radiotherapy-radiodynamic therapy
	SBU	=	secondary building unit
	SN38	=	7-ethyl-10-hydroxycamptothecin
	STING	=	stimulator of interferon genes

TEM	=	transmission electron microscopy
THF	=	tetrahydrofuran
TLR	=	Toll-like receptor
TP	=	terphenyl

BACKGROUND

Metal-organic frameworks (MOFs) are of increasing interest for biomedical applications due to their tunable compositions, large porosity, ease of surface functionalization, and biodegradability.[1-4] In particular, MOFs have found use as drug carriers.[5-10] Generally, three approaches have been used to load drugs into MOFs: direct encapsulation of drugs in the pores,[11-12] coordination of drugs to metal-cluster secondary building units (SBUs),[13] and covalent conjugation of drugs to the organic bridging ligands.[14] The first two approaches can result in premature drug release due to weak interactions between MOFs and drug molecules.[15] The third method can involve the use of an actionable trigger to release active drug from the prodrug-containing MOF.[16-17]

Accordingly, there is an ongoing need for additional MOF-based prodrug compositions comprising actionable triggers that can release drugs efficiently and on-demand, e.g., at a particular site in the body and/or at a particular time. There is also an ongoing need for additional methods of using MOF-based compositions to treat diseases, such as cancer, with improved activity and/or at lower doses and/or with reduced levels of side effects.

SUMMARY

This summary lists several embodiments of the presently disclosed subject matter, and in many cases lists variations and permutations of these embodiments. This summary is merely exemplary of the numerous and varied embodiments. Mention of one or more representative features of a given embodiment is likewise exemplary. Such an embodiment can typically exist with or without the feature(s) mentioned; likewise, those features can be applied to other embodiments of the presently disclosed subject matter, whether listed in this summary or not. To avoid excessive repetition, this summary does not list or suggest all possible combinations of such features.

In some embodiments, the presently disclosed subject matter provides a metal organic framework (MOF) comprising an X-ray sensitive prodrug, wherein the MOF comprises metal-containing secondary building units (SBUs) linked together via organic bridging

ligands, wherein at least one of the SBUs comprises a metal cation capable of absorbing X-rays, and wherein at least one of the organic bridging ligands is substituted by a group having the formula: -L-D, wherein L is a bivalent linker group comprising one or more bonds capable of radical-promoted bond cleavage and wherein D is a monovalent moiety of a therapeutic agent.

In some embodiments, the metal cation capable of absorbing X-rays is selected from the group comprising Hf, a lanthanide metal, Ta, W, Re, Os, Ir, Pt, Au, and Bi. In some embodiments, the metal cation capable of absorbing X-rays is an Hf cation, optionally wherein one or more of the SBUs comprise a Hf oxo cluster, optionally a Hf_6 oxo cluster or a Hf_{12} oxo cluster.

In some embodiments, L has the structure:

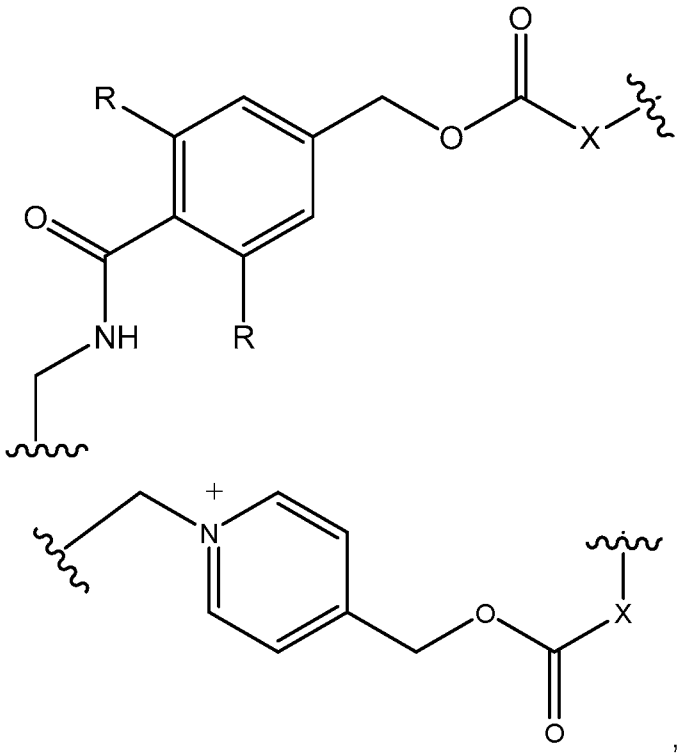

or

,

wherein: X is -O-, -NR'-, -O-X_1-O-, or NH-X_1-NH-, wherein R' is selected from H and alkyl, and X_1 is alkylene, optionally wherein R' is H or methyl and/or X_1 is propylene or ethylene; and each R is hydroxyl, oxyalkyl, optionally methoxy, or dialkylamino, optionally dimethylamino.

In some embodiments, the therapeutic agent is a therapeutic agent that comprises at least one functional group selected from a primary amino group, a secondary amino group, -C(=O)-NH_2, -C(=O)OH, a hydroxyl group, and a phenol. In some embodiments, the therapeutic agent is a chemotherapeutic agent or an immune modulator, optionally a TLR

agonist or a STING agonist. In some embodiments, the therapeutic agent is selected from the group comprising SN38, R848, imiquimod, VTX-378, DSR-6434, ioxoribine, TLR7/8 agonist 1, Cu-712-9, neoseptin-3, and diABZI.

In some embodiments, the at least one organic bridging ligand substituted by a group having the formula -L-D is an organic bridging ligand comprising a terphenyl (TP) moiety or a quaterphenyl (QP) moiety and at least two groups, which can be the same or different, selected from the group comprising a carboxylate group, an aromatic or non-aromatic nitrogen-containing group, a phenol, an acetylacetonate, a phosphonate, and a phosphate; optionally wherein the at least one organic bridging ligand has a structure selected from:

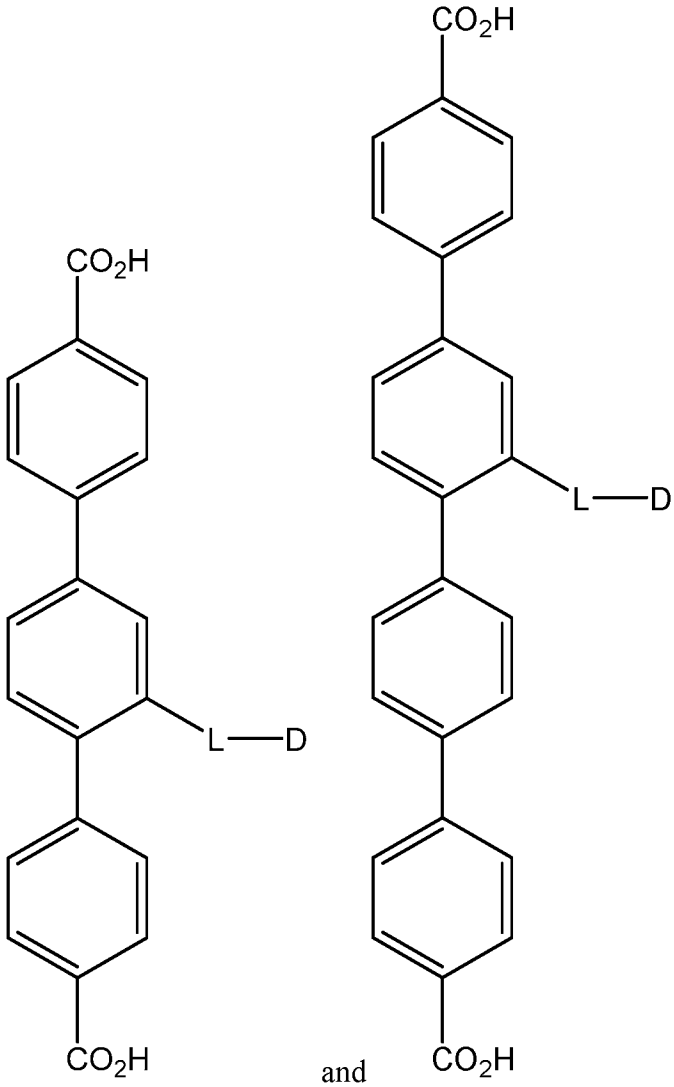

and .

In some embodiments, the MOF further comprises at least one photosensitizer, optionally wherein the MOF comprises at least one organic bridging ligand selected from the group consisting of a porphyrin, a chlorin, a chlorophyll, a phthalocyanine, a ruthenium-bipyridine complex, an iridium-phenylpyridine complex, or an iridium-bipyridine complex.

In some embodiments, the MOF comprises at least one organic bridging ligand comprising a porphyrin, optionally bis(p-benzoato)porphyrin (DBP).

In some embodiments, the presently disclosed subject matter provides a pharmaceutical composition comprising an MOF comprising an X-ray sensitive prodrug, wherein the MOF comprises metal-containing SBUs linked together via organic bridging ligands, wherein at least one of the SBUs comprises a metal cation capable of absorbing X-rays, and wherein at least one of the organic bridging ligands is substituted by a group having the formula: -L-D, wherein L is a bivalent linker group comprising one or more bonds capable of radical-promoted bond cleavage and wherein D is a monovalent moiety of a therapeutic agent.

In some embodiments, the presently disclosed subject matter provides a method of treating a disease in a subject in need thereof, the method comprising: (a) administering to the subject a MOF comprising an X-ray sensitive prodrug, wherein the MOF comprises metal-containing SBUs linked together via organic bridging ligands, wherein at least one of the SBUs comprises a metal cation capable of absorbing X-rays, and wherein at least one of the organic bridging ligands is substituted by a group having the formula: -L-D, wherein L is a bivalent linker group comprising one or more bonds capable of radical-promoted bond cleavage and wherein D is a monovalent moiety of a therapeutic agent, or a pharmaceutical composition of said MOF; and (b) irradiating at least a portion of the subject with X-rays. In some embodiments, the disease is cancer, optionally selected from the group comprising a head tumor, a neck tumor, a head and neck tumor, a breast tumor, a gynecological tumor, a brain tumor, a colorectal cancer, a lung cancer, mesothelioma, a soft tissue sarcoma, and a pancreatic cancer.

In some embodiments, D is a monovalent moiety of a chemotherapeutic agent, thereby providing to the subject, upon performing (b), a combination of (i) chemotherapy and (ii) radiotherapy (RT) or radiotherapy-radiodynamic therapy (RT-RDT). In some embodiments, the MOF comprises a photosensitizer, optionally DBP, thereby providing to the subject, upon performing (b), a combination of (i) chemotherapy and (ii) RT-RDT.

In some embodiments, D is monovalent moiety of SN38 and a higher percentage of SN38 is released from the MOF upon performing (b) compared to release from a comparable amount of a homogenous SN38 prodrug, optionally wherein the homogenous SN38 prodrug is MeO-SN.

In some embodiments, D is a monovalent moiety of an immune modulator, thereby providing to the subject, upon performing (b), a combination of (i) immunotherapy and (ii)

RT or RT-RDT. In some embodiments, the MOF comprises a photosensitizer, optionally DBP, thereby providing to the subject, upon performing (b) a combination of immunotherapy and RT-RDT.

In some embodiments, the method provides selective cytotoxicity and/or immune activation in a tumor.

In some embodiments, the presently disclosed subject matter provides a use of an MOF comprising an X-ray sensitive prodrug, wherein the MOF comprises metal-containing SBUs linked together via organic bridging ligands, wherein at least one of the SBUs comprises a metal cation capable of absorbing X-rays, and wherein at least one of the organic bridging ligands is substituted by a group having the formula: -L-D, wherein L is a bivalent linker group comprising one or more bonds capable of radical-promoted bond cleavage and wherein D is a monovalent moiety of a therapeutic agent; or a pharmaceutical composition comprising said MOF, in treating a disease, optionally cancer, in a subject in need thereof. In some embodiments, the use provides selective cytotoxicity and/or immune activation in a tumor.

Accordingly, it is an object of the presently disclosed subject matter to provide nanoscale metal-organic frameworks comprising X-ray sensitive prodrugs, as well as related pharmaceutical formulations, uses, and methods of treating disease.

An object of the presently disclosed subject matter having been stated hereinabove, and which is achieved in whole or in part by the presently disclosed subject matter, other objects will become evident as the description proceeds hereinbelow.

BRIEF DESCRIPTION OF THE DRAWINGS

Figure 1: A schematic drawing showing the synthesis of a nanoscale metal-organic framework (nMOF) comprising hafnium (Hf)-containing secondary building units (SBUs) and 2'-((4-(hydroxymethyl)-2,6-dimethoxybenzamido)methyl)-[1,1':4',1''-terphenyl]-4,4''-dicar-boxylic acid (H_2TP-OH) organic bridging ligands. This nMOF, i.e., Hf-TP-OH, is post-synthetically modified with a group comprising a monovalent moiety of 7-ethyl-10-hydroxycamptothecin (SN38) to afford Hf-TP-SN nMOF, an X-ray sensitive nMOF-based prodrug of SN38. The proposed mechanism for X-ray triggered release of SN38 from Hf-TP-SN is shown on the bottom left.

Figures 2A-2C: A series of micrograph images including (Figure 2A) the transmission electron microscopy (TEM) micrograph image and (Figure 2B) the high-resolution TEM (HRTEM) image and fast Fourier transform (FFT) pattern (inset) of a nanoscale metal-

organic framework (nMOF) comprising hafnium-containing secondary building units (SBUs) and 2'-((4-(Hydroxymethyl)-2,6-dimethoxybenzamido)methyl)-[1,1':4',1''-terphenyl]-4,4''-dicarboxylic acid (H_2TP-OH) organic bridging ligands, i.e., Hf-TP-OH. Figure 2C is the TEM image of the 7-ethyl-10-hydroxycamptothecin (SN38) post-synthetically modified nMOF, i.e., Hf-TP-SN. The scale bar in the lower left corner of each image represents 50 nanometers (nm).

Figures 3A-3D: A series of graphs showing (Figure 3A), the number averaged sizes (number expressed as a percentage (%) of the total population versus size in nanometers (nm)) of the nanoscale metal-organic frameworks (nMOFs) described for Figures 2A-2C, i.e., Hf-TP-OH and Hf-TP-SN, in ethanol; (Figure 3B) the zeta (ζ) -potentials of Hf-TP-OH and Hf-TP-SN in water (H_2O); (Figure 3C) the powder X-ray diffraction (PXRD) patterns (intensity versus 2 theta (2θ) of Hf-TP-OH, Hf-TP-SN, and the simulated pattern for Hf_{12}-TP MOF; and (Figure 3D) the PXRD patterns of freshly prepared Hf-TP-SN or Hf-TP-SN dispersed in phosphate buffered saline (PBS) for 1, 2, 4, 8 and 24 hours.

Figures 4A-4E: A series of graphs including (Figures 4A, 4B, and 4D) graphs showing the ultraviolet-visible (UV-Vis) absorption spectra (absorbance versus wavelength (in nanometers (nm))) of (Figure 4A) 7-ethyl-10-hydroxycamptothecin (SN38), a nanoscale metal-organic framework (nMOF) comprising hafnium-containing secondary building units (SBUs) and 2'-((4-(Hydroxymethyl)-2,6-dimethoxybenzamido)methyl)-[1,1':4',1''-terphenyl]-4,4''-dicarboxylic acid (H_2TP-OH) organic bridging ligands, i.e., Hf-TP-OH, and a digested SN-38-modified nMOF, i.e., Hf-TP-SN; (Figure 4B) H_2TP-OH at different concentrations from 2.17 milligrams per liter (mg/L) to 18.2 mg/L; and (Figure 4D) SN38 at different concentrations from 4 micromolar (μM) to 40 μM. Figures 4C and 4E are graphs showing the fitted standard curves (absorbance versus concentration) of H_2TP-OH (in mg/L) and SN38 (in μM), respectively, in dimethyl sulfoxide (DMSO).

Figures 5A-5D: A series of graphs including graphs showing (Figure 5A) total reactive oxygen species (ROS) signals and (Figure 5B) hydroxyl radical ($\cdot$OH) signal for samples comprising the nanoscale metal-organic frameworks (nMOFs) described for Figure 1, i.e., Hf-TP-OH and Hf-TP-SN measured by 2',7'-dichlorodihydrofluorescein (DCFH) assay and aminophenyl fluorescein (APF) assay, respectively, after different X-ray doses (1 to 10 Gray (Gy)). n = 6. For Figures 5A and 5B, hafnium (Hf) concentration was 40 micromolar (μM). Figures 5C and 5D are graphs showing the concentration (μM) of 7-ethyl-10-hydroxycamptothecin (SN38) released from the homogenous prodrug of SN38 (MeO-SN)

or the nMOF prodrug, i.e., Hf-TP-SN, after 10 Gy X-ray irradiation (Figure 5C) or after reaction with ·OH generated by the Fenton reaction (Figure 5D). Initial MeO-SN or Hf-TP-SN concentration was 100 μM.

Figures 6A-6D**:** Figures 6A and 6B are graphs showing the toxicity of the 2'-((4-(Hydroxymethyl)-2,6-dimethoxybenzamido)methyl)-[1,1':4',1''-terphenyl]-4,4''-dicarboxylic acid (i.e., H_2TP-OH) ligand (Figure 6A) and of the hafnium-containing nanoscale metal-organic framework (nMOF) prepared from the H_2TP-OH ligand (i,e Hf-TP-OH, Figure 6B). Toxicity is assessed as cell viability of mouse colon carcinoma (CT26) cells treated by (Figure 6A) H_2TP-OH without X-ray radiation (H_2TP-OH(-)) or (Figure 6B) Hf-TP-OH without X-ray radiation (Hf-TP-OH(-)) at the following concentrations: 0 micromolar (μM), 1.56 μM, 6.25 μM, 25 μM, or 100 μM. Figure 6C is a graph showing the survival fractions of CT26 cells after incubation with phosphate buffered saline (PBS), Hf-TP-OH, or Hf-TP-SN under different doses of X-ray irradiation (0 Gray (Gy), 2 Gy, 4 Gy, or 6 Gy). Figure 6D is a series of confocal laser scanning microscopy (CLSM) images of CT26 cells stained by hydroxyphenyl fluorescein (HPF, green) and Hoechst 33342 (blue, cell nucleus) for detecting the generation of ·OH. Images are shown for cells treated with PBS and no X-ray radiation (PBS(-)), PBS with X-ray radiation (PBS(+)), and Hf-TP-OH with X-ray radiation (Hf-TP-OH(+)). The scale bar in the lower right corner of the lower right image represents 25 micrometers (μm).

Figures 7A-7C: Figures 7A and 7B are graphs showing the cell viability curves of mouse colon carcinoma (CT26) cells treated by (Figure 7A) 7-ethyl-10-hydroxycamptothecin (SN38) without X-ray radiation (SN38(-)) or (Figure 7B) the dimethyl ester of a SN38-modified terphenyl bridging ligand without X-ray radiation (Me_2TP-SN38(-)). Graphs show cell viability (expressed as a percentage (%)) versus SN38 or Me_2TP-SN concentration (micromolar (μM)). Figure 7C is a graph showing the time-dependent cellular uptake of a hafnium-containing nanoscale metal-organic framework (nMOF) comprising an X-ray sensitive SN38 prodrug (Hf-TP-SN) quantified by inductively coupled plasma mass spectroscopy (ICP-MS). Hafnium (Hf) uptake (measured in nanomoles per 10^6 cells (nmol/10^6 cells)) is measured at 0, 1, 2, and 6 hours (h). n = 3.

Figures 8A-8D: ROS generation *in vitro*. Figure 8A is a series of confocal laser scanning microscopy (CLSM) images of mouse colon carcinoma (CT26) cells stained by 2',7'-dichlorofluorescein diacetate (DCFH-DA, top and bottom rows) and/or Hoechst (middle and bottom row) for detecting the generation of reactive oxygen species (ROS). Cells

were treated with (from left to right columns): phosphate buffered saline (PBS) without X-ray irradiation (PBS(-)); a hafnium (Hf) and terphenyl (TP) ligand-containing nanoscale metal-organic framework (nMOF) without a prodrug (Hf-TP-OH) and without irradiation (Hf-TP-OH(-)); a HF and TP-ligand containing nMOF comprising an X-ray sensitive 7-ethyl-10-hydroxycamptothecin prodrug (Hf-TP-SN) and without irradiation (Hf-TP-SN(-)); PBS with irradiation (PBS(+)); Hf-TP-OH with irradiation (Hf-TP-OH(+)); or Hf-TP-SN with irradiation (Hf-TP-SN(+)). Figure 8B is a graph showing the relative fluorescence intensity (ROS signal) from the CLSM images of Figure 8A as analyzed by Image J. Figure 8C is a graph showing the quantification of histograms of intracellular ROS signals of cells treated as described in Figure 8A by flow cytometry. Figure 8D is a graph showing the percentage of dichlorofluorescein-positive (DCF^+) CT26 cells after Hf-TP-OH(+) or Hf-TP-SN(+) treatment. X-ray dose was 3 Gray (Gy).

Figure 9: Confocal laser scanning microscopy (CLSM) images of mouse colon carcinoma (CT26) cells showing results of the phosphorylation of histone variant H2AX (γ-H2AX) assay and treated with phosphate buffered saline (PBS) with (+) or without (-) X-ray radiation; a hafnium (Hf) and terphenyl (TP)-ligand containing nanoscale metal organic framework nMOF without a prodrug (Hf-TP-OH) with (+) or without (-) X-ray radiation, or a HF and TP-containing nMOF comprising an X-ray sensitive 7-ethyl-10-hydroxycamptothecin prodrug (Hf-TP-SN) with (+) or without (-) X-ray radiation. The scale bar in the lower right corner of the image on the bottom right represents 10 micrometers (μm). X-ray dose was 3 Gray (Gy).

Figure 10: Immunogenic cell death. Representative flow cytometry dot plots showing cell apoptosis/death stained by fluorescein isothiocyanate (FITC)-annexin-V and propidium iodide (PI) in different treatment groups: phosphate buffered saline (PBS) with (+) or without (-) X-ray radiation; hafnium (Hf) and terphenyl (TP)-ligand containing nanoscale metal organic framework (nMOF) without a prodrug (Hf-TP-OH) with (+) or without (-) X-ray radiation; and Hf and TP-containing nMOF with an X-ray sensitive prodrug (Hf-TP-SN) with (+) and without (-) X-ray radiation.

Figures 11A-11D: *In vivo* anticancer efficacy. Figure 11A is a graph showing growth curves of subcutaneous mouse colon carcinoma (CT26) tumors implanted in BALB/c mice and after treatment with phosphate buffered saline (PBS), irinotecan, a hafnium (Hf) and terphenyl (TP)-ligand containing nanoscale metal organic framework (nMOF) without a prodrug (Hf-TP-OH), or a Hf and TP-containing nMOF with an X-ray sensitive 7-ethyl-10-hydroxycamptothecin prodrug (Hf-TP-SN) followed by X-ray irradiation (+). Data for PBS

and Hf-TP-SN treated mice not exposed to X-ray irradiation (-) is also shown. n = 5 per treatment group. Tumor growth is measured as tumor volume in cubic centimeters (cm^3) starting at day 6 after tumor implant. The arrow at 7 days indicates nMOF injection, whereas the other arrows indicate irradiation. Figure 11B is a graph showing the weights (in grams (g)) of the excised tumors at the endpoint (day 19) of mice treated as described for Figure 11A, while Figure 11C is a photographic image showing the excised tumors. Figure 11D is a graph showing relative body weights (expressed as a percentage) of CT26 bearing BALB/c mice after different treatments as a function of time (days) during the treatment regimen described for Figure 11A.

Figures 12: Microscopy images showing pathological changes of tumors from the treatments described for Figures 11A-11D. Top row shows detection of phosphorylation of histone variant H2AX (γ-H2AX); row second from top shows detection for antigen Kiel 67 (Ki67), a marker of proliferation; row second from the bottom shows detection for terminal deoxynucleotidyl transferase dUTP nick end labeling (TUNEL); and the bottom row shows hematoxylin and eosin (H&E) staining of excised mouse colon carcinoma (CT26) tumors after the treatments described for Figures 11A-11D. The scale bar in the bottom right corner of the image on the bottom right represents 50 micrometers (μm).

Figure 13: A series of images of hematoxylin and eosin (H&E) staining of hearts, livers, spleens, lungs, and kidneys of mouse colon carcinoma (CT26) tumor-bearing BALB/c mice in different treatment groups as described for Figures 11A-11D. The scale bar in the lower right corner of the image on the bottom right represents 200 micrometers (μm).

Figures 14A-14B: Synthesis of a Hf-DBP-QP-SN nanoscale metal-organic framework (nMOF) and proposed mechanism of action. Figure 14A is a schematic diagram showing the synthesis of a dicarboxylic acid quaterphenyl (H_2QP) bridging ligand containing a dimethoxy benzyl alcohol derivative. Figure 14B is a schematic diagram showing the synthesis of a hafnium (Hf)-bis-(p-benzoato)porphyrin (DBP)-quaterphenyl (QP) nMOF (i.e., Hf-DBP-QP) and its post-synthetic modification with 7-ethyl-10-hydroxycamptothecin (SN38) to afford a prodrug nMOF, i.e., Hf-DBP-QP-SN along with the proposed mechanism for X-ray triggered release of SN38 from Hf-DBP-QP-SN for synergistic radiotherapy-radiodynamic therapy (RT-RDT) and chemotherapy.

Figures 15A-15D: Transmission electron microscopy (TEM) and dynamic light scattering (DLS) characterization. Figures 15A and 15B show TEM images of (Figure 15A) nanoscale metal organic frameworks (nMOFs) containing hafnium (Hf) secondary building units and both bis(p-benzoato)porphyrin (DBP) and quaterphenyl (QP) bridging ligands (i.e.,

Hf-DBP-QP) and (Figure 15B) a Hf-DBP-QP nMOF post-synthetically modified as a prodrug of 7-ethyl-10-hydroxycamptothecin (Hf-DBP-QP-SN). The scale bars in the lower left of each image represent 100 nanometers (nm). Figure 15C is a graph showing the number-averaged sizes (percentage (%) versus size in nm) of the Hf-DBP-QP and HF-DBP-SN nMOFs. Figure 15D is a graph showing the zeta (ζ)-potentials of the Hf-DBP-QP and Hf-DBP-QP-SN nMOFs.

Figures 16A-16B: Crystallinity and stability of Hf-DBP-QP-SN. Figure 16A shows the powder x-ray diffraction (PXRD) patterns (intensity versus 2 theta (2θ)) of (bottom) a hafnium-bis(p-benzoato)porphyrin (Hf-DBP) nanoscale metal-organic framework (nMOF), (middle) a hafnium-bis(p-benzoato)porphyrin-quaterphenyl (Hf-DBP-QP) nMOF, and (top) a 7-ethyl-10-hydroxycamptothecin prodrug modified Hf-DBP-QP nMOF, i.e., Hf-DBP-QP-SN nMOF. Figure 16B is a graph showing the PXRD patterns (intensity versus 2θ) of (from top to bottom) Hf-DBP-QP-SN nMOF freshly prepared or after dispersion in phosphate buffered saline (PBS) for 1, 2, 4, 8, or 24 hours.

Figure 17: Ultraviolet-visible (UV-Vis) spectra (absorbance versus wavelength in nanometers (nm)) of 7-ethyl-10-hydroxycamptothecin (SN38), dicarboxyl-quaterphenyl (H_2QP) bridging ligand, bis(p-benzoato)porphyrin (H_2DBP) bridging ligand, and digested hafnium (Hf)-containing nanoscale metal-organic frameworks (nMOFs), including a nMOF containing both bis(p-benzoato)porphyrin and quaterphenyl bridging ligands (i.e., Hf-DBP-QP) and the same nMOF post-synthetically modified with SN38 (i.e., Hf-DBP-QP-SN) in dimethyl sulfoxide (DMSO).

Figures 18A-18D: Ultraviolet-visible (UV-Vis) standard curves for quantification. Figures 18A and 18C are the UV-Vis absorption spectra (absorbance versus wavelength in nanometers (nm)) of (Figure 18A) a dicarboxyl-quaterphenyl (H_2QP) bridging ligand and (Figure 18C) a bis(p-benzoato)porphyrin (H_2DBP) bridging ligand. Figures 18B and 18D are the fitted standard curves (absorbance versus concentration (in milligrams per liter (mg/L))) of (Figure 18B) H_2QP and (Figure 18D) H_2DBP.

Figures 19A-19C: Release mechanism and reactive oxygen species (ROS) generation in test tubes. Figure 19A is a schematic diagram showing a mechanism for X-ray triggered release of 7-ethyl-10-hydroxycamptothecin (SN38) from a hafnium (Hf)-containing nanoscale metal-organic framework (nMOF) comprising bis(p-benzoato)porphyrin and SN38-prodrug-contianing quarterphenyl bridging ligands, (Hf-DBP-QP-SN) via radiotherapy-radiodynamic therapy (RT-RDT). Figures 19B and 19C are graphs showing the

hydroxyl radical (·OH) signals (Figure 19B) and total ROS signals (Figure 19C) of phosphate buffered saline (PBS), hafnium-bis(p-benzoato)porphyrin (Hf-DBP) nMOF, hafnium-bis(p-benzoato)porphyrin-quarterphenyl (Hf-DBP-QP) nMOF, and SN-38 prodrug Hf-DBP-QP-SN nMOF by aminophenyl fluorescein (APF) assay and 2',7'-dichlorodihydrofluorescien (DCFH) assay, respectively, after different doses (0 to 10 Gray (Gy)) of X-ray radiation. n = 6. Hf concentration was 40 micromolar (μM).

Figures 20A-20B: Figures 20A and 20B are graphs showing the concentration of 7-ethyl-10-hydroxycamptothecin (SN38, micromolar (μM)) released from a homogenous methoxy-prodrug of SN38 (MeO-SN) or a hafnium (Hf)-containing metal organic framework (nMOF) prodrug comprising bis(p-benzoato)porphyrin and SN38-modifed quaterphenyl bridging ligands (i.e., Hf-DBP-QP-SN) (Figure 20A) after 10 Gray (Gy) X-ray irradiation or (Figure 20B) after reaction with hydroxy radical (·OH) generated by the Fenton reaction. Initial MeO-SN or Hf-DBP-QP-SN concentration was 100 μM.

Figure 21: A graph showing cell viability of mouse colon carcinoma (CT26) cells after incubation with a hafnium-containing metal organic framework (nMOF) comprising bis(p-benzoato)porphyrin and quaterphenyl bridging ligands (Hf-DBP-QP). The graph shows cell viability (as a percentage (%)) versus hafnium (Hf) concentration (micromolar (μM)).

Figures 22A-22C: Cytotoxicity of 7-ethyl-10-hydroxycamptothecin (SN38) and prodrugs. Figures 22A-22C are graphs showing the cell viability of mouse colon carcinoma (CT26) cells after incubation with different concentrations (micromolar (μm) of (Figure 22A) SN38 (Figure 22B) a SN38 modified quaterphenyl homogenous compound (Me_2QP-SN), and (Figure 22C) a SN38-prodrug nanoscale metal-organic framework (nMOG) comprising hafnium (Hf)-containing secondary building units and both bis(p-benzoato)porphyrin (DBP) and SN-38-modified quaterphenyl organic bridging ligands (Hf-DBP-QP-SN).

Figure 23: A graph showing the time-dependent cellular uptake of 7-ethyl-10-hydroxycamptothecin (SN38)-prodrug nanoscale metal-organic frameworks (nMOFs) comprising hafnium (Hf)-containing secondary building units and both bis(p-benzoato)porphyrin (DBP) and SN-38-modified quaterphenyl organic bridging ligands (Hf-DBP-QP-SN) as quantified by flow cytometry. Cell uptake is expressed as a percentage (%) and time is expressed in hours (h).

Figure 24: A graph showing the total reactive oxygen species (ROS) generation in mouse colon carcinoma (CT26) cancer cells after different treatments (phosphate buffered saline (PBS), a hafnium (Hf)-containing nanoscale metal-organic framework (nMOF) with

both bis(p-benzoato)porphyrin (DBP) and quaterphenyl organic bridging ligands (Hf-DBP-QP), or the Hf-DBP-QP nMOF modified as a prodrug of 7-ethyl-10-hydroxycamptothecin (SN38), i.e., Hf-DBP-QP-SN, all with (+) or without (-) X-ray irradiation), as probed by dichlorofluorescein-diacetate (DCFH-DA) and quantified by flow cytometry. The X-ray dose, is used, was 3 Gray (Gy).

Figure 25: A series of confocal light scanning microscopy (CLSM) images showing mouse colon carcinoma (CT26) cells after different treatments (phosphate buffered saline (PBS), a hafnium (Hf)-containing nanoscale metal-organic framework (nMOF) with both bis(p-benzoato)porphyrin (DBP) and quaterphenyl organic bridging ligands (Hf-DBP-QP), or the Hf-DBP-QP nMOF modified as a prodrug of 7-ethyl-10-hydroxycamptothecin (SN38), i.e., Hf-DBP-QP-SN, all with (+) or without (-) X-ray irradiation) stained by dichloroflurescein-diacetate (DCFH-DA, top and bottom rows) and Hoechst (middle and bottom rows) for reactive oxygen species (ROS) detection.

Figure 26: A series of confocal light scanning microscopy (CLSM) images showing mouse colon carcinoma (CT26) cells after different treatments (phosphate buffered saline (PBS), a hafnium (Hf)-containing nanoscale metal-organic framework (nMOF) with both bis(p-benzoato)porphyrin (DBP) and quaterphenyl organic bridging ligands (Hf-DBP-QP), or the Hf-DBP-QP nMOF modified as a prodrug of 7-ethyl-10-hydroxycamptothecin (SN38), i.e., Hf-DBP-QP-SN, all with (+) or without (-) X-ray irradiation) stained by hydroxyphenyl fluorescein (HPF, top and bottom rows) and Hoechst (middle and bottom rows) for hydroxy radical (·OH) detection.

Figures 27A-27D: Figure 27A is a pair of flow cytometric analysis of mouse colon carcinoma (CT26) cells treated with (right) or without (left) 7-ethyl-10-hydroxycamptothecin (SN38). Figure 27B is a series of confocal laser scanning microscopy (CLSM) images showing reactive oxygen species (ROS) generation (probed by dichlorofluorescein-diacetate (DCFH-DA)) in CT26 cells after incubation with SN38. The scale bar in the lower right of the image on the lower right represents 50 micrometers (μm). Figure 27C is a series of CLSM images showing hydroxy radical (·OH) generation (probed by hydroxyphenyl fluorescein (HPF)) in CT26 cells after incubation with SN38. The scale bar in the lower right of the image on the lower right represents 50 μm. Figure 27D is a series of CLSM images showing mitochondria membrane potentials (probed by 5,5,6,6'-tetrachloro-1,1',3,3'-tetraethylbenzimidazolyl carbocyanine iodide dye (JC-1)). The scale bar in the lower right of the image on the lower right represents 10 μm.

Figures 28A-28C. Clonogenic assay and immunogenetic cell death. Figure 28A is a graph showing the results of clonogenic assays showing radioenhancement of a hafnium (Hf)-containing nanoscale metal-organic framework (nMOF) containing bis(p-benzoato)porphyrin (DBP) and quaterphenyl (QP) organic bridging ligands (Hf-DBP-QP) and of the same nMOF modified as a prodrug of 7-ethyl-10-hydroxycamptothecin (Hf-DBP-QP-SN) on mouse colon carcinoma (CT26) cells upon radiation with different doses of X-rays (0 to 8 Gray (Gy). n=3. Figure 28B is a series of respective images of colony formation of CT26 cells after treatment with Hf-DBP-QP or Hf-DBP-QP-SN followed by 250 peak kilovoltage (kVp) X-ray irradiation. Figure 28C is a graph showing the quantification (as a percentage) of early apoptotic (top portion of each bar), late apoptotic (middle portion of bars with three sections or bottom portion of bars with two sections), and necrotic (bottom portion of bars with three portions) CT26 cells after incubation with Hf-DBP-QP or Hf-DBP-QP-SN with (+) or without (-) X-ray radiation (X-ray dose: 3 Gy).

Figure 29: A series of confocal light scanning microscopy (CLSM) images of mouse colon carcinoma (CT26) cells using the phosphorylation of histone variant H2AX (γ-H2AX) assay after different treatments (phosphate buffered saline (PBS), a hafnium (Hf)-containing nanoscale metal-organic framework (nMOF) with both bis(p-benzoato)porphyrin (DBP) and quaterphenyl organic bridging ligands (Hf-DBP-QP), or the Hf-DBP-QP nMOF modified as a prodrug of 7-ethyl-10-hydroxycamptothecin (SN38), i.e., Hf-DBP-QP-SN, all with (+) or without (-) X-ray irradiation). The scale bar in the lower left corner of the image on the lower right represents 10 micrometers (μm).

Figure 30A-30B: Figure 30A is a graph showing the growth curves of mouse colon carcinoma (CT26) tumors in BALB/c mice starting 6 days after inoculation with CT26 cells and using different treatments (phosphate buffered saline (PBS), a hafnium (Hf)-containing nanoscale metal-organic framework (nMOF) with both bis(p-benzoato)porphyrin (DBP) and quaterphenyl organic bridging ligands (Hf-DBP-QP), irinotecan, or the Hf-DBP-QP nMOF modified as a prodrug of 7-ethyl-10-hydroxycamptothecin (SN38), i.e., Hf-DBP-QP-SN, with (+) or without (-) X-ray irradiation (n = 5)). The arrow at day 7 indicates intrathecal (i.t.) injection of nMOF or other treatment and the other arrows indicate X-ray radiation. Figure 30B is a graph showing the relative body weights of CT26 tumor-bearing BALB/c mice being treated with the different treatments as a function of time (day) after tumor.

Figures 31: Microscopy images showing pathological changes of excised mouse colon carcinoma (CT26) tumors from the study described for Figures 30A and 30B at day 1 after the last X-ray radiation dose. The top row shows hematoxylin and eosin (H&E) staining

of excised tumors; the row second from the top shows detection for terminal deoxynucleotidyl transferase dUTP nick end labeling (TUNEL) in the excised tumors; the row second from the bottom shows detection of phosphorylation of histone variant H2AX (γ-H2AX) in the excised tumors; the bottom row shows detection for antigen Kiel 67 (Ki67), a marker of proliferation, in the excised tumors. The scale bar in the bottom right corner of the image on the bottom right represents 50 micrometers (μm).

Figure 32: A series of images of hematoxylin and eosin (H&E) staining of hearts, livers, spleens, lungs, and kidneys of mouse colon carcinoma (CT26) tumor-bearing BALB/c mice in different treatment groups as described for Figures 30A and 30B. The scale bar in the lower right corner of the image on the bottom right represents 200 micrometers (μm).

Figure 33: A graph showing the survival curves of mouse colon carcinoma (CT26) tumor-bearing BALB/c mice after different treatments as described for Figures 30A and 30B.

Figure 34 is a graph showing the interleukin-6 (IL-6) secretion (in picograms per milliliter (pg/mL)) of bone marrow-derived dendritic cells (BMDCs) after treatment with various concentrations (125 nanomolar (nM), 250 nM, 500 nM, or 1000 nM) of a nanoscale metal-organic framework (nMOF) comprising hafnium (Hf) secondary building units (SBUs), bis(p-benzoato)porphyrin (DBP) bridging ligands and quarterphenyl (QP) bridging ligands modified with an X-ray sensitive prodrug of resiquimod (R848) under various doses of X-ray irradiation (0 Gray (Gy), 1 Gy, 5 Gy, 10 Gy, or 50 Gy, bars from left to right for each concentration). The concentration refers to the conjugated R848.

Figures 35A-35C are a series of schematic drawings showing the chemical structures of metal-organic frameworks (MOFs) comprising exemplary prodrugs of immune modulators, including (Figure 35A) Toll-like receptor (TLR) 7/8 agonists; (Figure 35B) other TLR agonists; and (Figure 35C) stimulator of interferon genes (STING) agonists.

DETAILED DESCRIPTION

Heavy metal-based metal-organic frameworks (MOFs), e.g., nanoscale heavy metal-based metal-organic frameworks (nMOFs), can act as radiosensitizers for radiotherapy via enhanced energy deposition and reactive oxygen species (ROS) generation. According to aspects of the presently disclosed subject matter, MOFs (e.g., nMOFs) are provided comprising covalently conjugated, X-ray triggerable prodrugs that can harness the ROS for on-demand release of a therapeutic agent, thereby resulting in effective combination therapies.

According to some aspects of the presently disclosed subject matter, the presently disclosed MOFs provide X-ray triggered release of chemotherapy and/or immunotherapy agents, providing for selective cytotoxic or immune activation in tumors. This can greatly reduce the general toxicity associated with chemotherapy and/or immunotherapy agents when provided in more conventional form, improving their therapeutic indices.

Exemplary MOFs disclosed herein include nMOFs comprising an X-ray triggerable 7-ethyl-10-hydroxycamptothecin (SN38) prodrug and nMOFs with X-ray triggerable innate immune modulator prodrugs (e.g., resiquimod (R848) prodrugs) for synergistic radiotherapy (RT) and chemotherapy or immunotherapy. For example, upon X-ray irradiation, electron-dense Hf_{12} oxo cluster or other X-ray absorbing, metal-containing secondary building units (SBUs) can serve as radiosensitizers to enhance hydroxyl radical generation for the triggered release of the therapeutic agent (e.g., the SN38 or innate immune modulator) of the covalently attached prodrug via hydroxylation of a 3,5-dimethoxylbenzyl carbonate followed by 1,4-elimination. See Figure 1. An exemplary nMOF comprising a SN38 prodrug attached to a terphenyl-based bridging ligand, referred to herein as Hf-TP-SN, provided 5-fold higher release of SN38 from Hf-TP-SN than a comparable amount of a homogeneous counterpart, i.e., MeO-SN. As a result, and as described hereinbelow, Hf-TP-SN plus X-ray irradiation can induce significant cytotoxicity to cancer cells *in vitro* and efficiently inhibits tumor growth *in vivo* with a high tumor growth inhibition index of 0.965 in a murine colon carcinoma model.

The presently disclosed subject matter will now be described more fully hereinafter with reference to the accompanying Examples, in which representative embodiments are shown. The presently disclosed subject matter can, however, be embodied in different forms and should not be construed as limited to the embodiments set forth herein. Rather, these embodiments are provided so that this disclosure will be thorough and complete, and will fully convey the scope of the embodiments to those skilled in the art.

Unless otherwise defined, all technical and scientific terms used herein have the same meaning as commonly understood by one of ordinary skill in the art to which this presently described subject matter belongs. Although any methods, devices, and materials similar or equivalent to those described herein can be used in the practice or testing of the presently disclosed subject matter, representative methods, devices, and materials are now described. All publications, patent applications, patents, and other references mentioned herein are incorporated by reference in their entirety.

Throughout the specification and claims, a given chemical formula or name shall encompass all optical and stereoisomers, as well as racemic mixtures where such isomers and mixtures exist.

I. DEFINITIONS

While the following terms are believed to be well understood by one of ordinary skill in the art, the following definitions are set forth to facilitate explanation of the presently disclosed subject matter.

Following long-standing patent law convention, the terms “a”, “an”, and “the” refer to “one or more” when used in this application, including the claims. Thus, for example, reference to "a metal ion" includes a plurality of such metal ions, and so forth.

Unless otherwise indicated, all numbers expressing quantities of size, reaction conditions, and so forth used in the specification and claims are to be understood as being modified in all instances by the term “about”. Accordingly, unless indicated to the contrary, the numerical parameters set forth in this specification and attached claims are approximations that can vary depending upon the desired properties sought to be obtained by the presently disclosed subject matter.

As used herein, the term “about”, when referring to a value or to an amount of size (i.e., diameter), weight, concentration or percentage is meant to encompass variations of in one example ±20% or ±10%, in another example ±5%, in another example ±1%, and in still another example ±0.1% from the specified amount, as such variations are appropriate to perform the disclosed methods.

As used herein, the term “and/or” when used in the context of a listing of entities, refers to the entities being present singly or in combination. Thus, for example, the phrase “A, B, C, and/or D” includes A, B, C, and D individually, but also includes any and all combinations and subcombinations of A, B, C, and D.

The term “comprising”, which is synonymous with “including,” “containing,” or “characterized by” is inclusive or open-ended and does not exclude additional, unrecited elements or method steps. “Comprising” is a term of art used in claim language which means that the named elements are present, but other elements can be added and still form a construct or method within the scope of the claim.

As used herein, the phrase “consisting of” excludes any element, step, or ingredient not specified in the claim. When the phrase “consists of” appears in a clause of the body of a

claim, rather than immediately following the preamble, it limits only the element set forth in that clause; other elements are not excluded from the claim as a whole.

As used herein, the phrase "consisting essentially of" limits the scope of a claim to the specified materials or steps, plus those that do not materially affect the basic and novel characteristic(s) of the claimed subject matter.

With respect to the terms "comprising", "consisting of", and "consisting essentially of", where one of these three terms is used herein, the presently disclosed and claimed subject matter can include the use of either of the other two terms.

As used herein the term "alkyl" can refer to C_{1-20} inclusive, linear (*i.e.*, "straight-chain"), branched, or cyclic, saturated or at least partially and in some cases fully unsaturated (*i.e.*, alkenyl and alkynyl) hydrocarbon chains, including for example, methyl, ethyl, propyl, isopropyl, butyl, isobutyl, *tert*-butyl, pentyl, hexyl, octyl, ethenyl, propenyl, butenyl, pentenyl, hexenyl, octenyl, butadienyl, propynyl, butynyl, pentynyl, hexynyl, heptynyl, and allenyl groups. "Branched" refers to an alkyl group in which a lower alkyl group, such as methyl, ethyl or propyl, is attached to a linear alkyl chain. "Lower alkyl" refers to an alkyl group having 1 to about 8 carbon atoms (*i.e.*, a C_{1-8} alkyl), e.g., 1, 2, 3, 4, 5, 6, 7, or 8 carbon atoms. "Higher alkyl" refers to an alkyl group having about 10 to about 20 carbon atoms, e.g., 10, 11, 12, 13, 14, 15, 16, 17, 18, 19, or 20 carbon atoms. In certain embodiments, "alkyl" refers, in particular, to C_{1-8} straight-chain alkyls. In other embodiments, "alkyl" refers, in particular, to C_{1-8} branched-chain alkyls.

Alkyl groups can optionally be substituted (a "substituted alkyl") with one or more alkyl group substituents, which can be the same or different. The term "alkyl group substituent" includes but is not limited to alkyl, substituted alkyl, halo, arylamino, acyl, hydroxyl, aryloxyl, alkoxyl, alkylthio, arylthio, aralkyloxyl, aralkylthio, carboxyl, alkoxycarbonyl, oxo, and cycloalkyl. In some embodiments, there can be optionally inserted along the alkyl chain one or more oxygen, sulfur or substituted or unsubstituted nitrogen atoms, wherein the nitrogen substituent is hydrogen, lower alkyl (also referred to herein as "alkylaminoalkyl"), or aryl.

Thus, as used herein, the term "substituted alkyl" includes alkyl groups, as defined herein, in which one or more atoms or functional groups of the alkyl group are replaced with another atom or functional group, including for example, alkyl, substituted alkyl, halogen, aryl, substituted aryl, alkoxyl, hydroxyl, nitro, amino, alkylamino, dialkylamino, sulfate, and mercapto.

The term "aryl" is used herein to refer to an aromatic substituent that can be a single aromatic ring, or multiple aromatic rings that are fused together, linked covalently, or linked to a common group, such as, but not limited to, a methylene or ethylene moiety. The common linking group also can be a carbonyl, as in benzophenone, or oxygen, as in diphenylether, or nitrogen, as in diphenylamine. The term "aryl" specifically encompasses heterocyclic aromatic compounds. The aromatic ring(s) can comprise phenyl, naphthyl, biphenyl, diphenylether, diphenylamine and benzophenone, among others. In particular embodiments, the term "aryl" means a cyclic aromatic comprising about 5 to about 10 carbon atoms, e.g., 5, 6, 7, 8, 9, or 10 carbon atoms, and including 5- and 6-membered hydrocarbon and heterocyclic aromatic rings.

The aryl group can be optionally substituted (a "substituted aryl") with one or more aryl group substituents, which can be the same or different, wherein "aryl group substituent" includes alkyl, substituted alkyl, aryl, substituted aryl, aralkyl, hydroxyl, alkoxyl, aryloxyl, aralkyloxyl, carboxyl, acyl, halo, nitro, alkoxycarbonyl, aryloxycarbonyl, aralkoxycarbonyl, acyloxyl, acylamino, aroylamino, carbamoyl, alkylcarbamoyl, dialkylcarbamoyl, arylthio, alkylthio, alkylene, and –NR'R", wherein R' and R" can each be independently hydrogen, alkyl, substituted alkyl, aryl, substituted aryl, and aralkyl.

Thus, as used herein, the term "substituted aryl" includes aryl groups, as defined herein, in which one or more atoms or functional groups of the aryl group are replaced with another atom or functional group, including for example, alkyl, substituted alkyl, halogen, aryl, substituted aryl, alkoxyl, hydroxyl, nitro, amino, alkylamino, dialkylamino, sulfate, and mercapto.

Specific examples of aryl groups include, but are not limited to, cyclopentadienyl, phenyl, furan, thiophene, pyrrole, pyran, pyridine, imidazole, benzimidazole, isothiazole, isoxazole, pyrazole, pyrazine, triazine, pyrimidine, quinoline, isoquinoline, indole, carbazole, and the like.

"Heteroaryl" as used herein refers to an aryl group that contains one or more non-carbon atoms (e.g., O, N, S, Se, etc) in the backbone of a ring structure. Nitrogen-containing heteroaryl moieties include, but are not limited to, pyridine, imidazole, benzimidazole, pyrazole, pyrazine, triazine, pyrimidine, and the like.

"Aralkyl" refers to an –alkyl-aryl group, optionally wherein the alkyl and/or aryl moiety is substituted.

"Alkoxyl" or "oxyalkyl" refer to an alkyl–O– group wherein alkyl is as previously described. The term "alkoxyl" as used herein can refer to $C_{1\text{-}20}$ inclusive, linear, branched, or

cyclic, saturated or unsaturated oxo-hydrocarbon chains, including, for example, methoxyl, ethoxyl, propoxyl, isopropoxyl, butoxyl, *t*-butoxyl, and pentoxyl.

"Alkylene" refers to a straight or branched bivalent aliphatic hydrocarbon group having from 1 to about 20 carbon atoms, e.g., 1, 2, 3, 4, 5, 6, 7, 8, 9, 10, 11, 12, 13, 14, 15, 16, 17, 18, 19, or 20 carbon atoms. The alkylene group can be straight, branched or cyclic. The alkylene group also can be optionally unsaturated and/or substituted with one or more "alkyl group substituents." There can be optionally inserted along the alkylene group one or more oxygen, sulfur or substituted or unsubstituted nitrogen atoms (also referred to herein as "alkylaminoalkyl"), wherein the nitrogen substituent is alkyl as previously described. Exemplary alkylene groups include methylene (–CH_2–); ethylene (–CH_2-CH_2–); propylene (–$(CH_2)_3$–); cyclohexylene (–C_6H_{10}–); –CH=CH—CH=CH–; –CH=CH–CH_2–; –$(CH_2)_q$–N(R)–$(CH_2)_r$–, wherein each of q and r is independently an integer from 0 to about 20, e.g., 0, 1, 2, 3, 4, 5, 6, 7, 8, 9, 10, 11, 12, 13, 14, 15, 16, 17, 18, 19, or 20, and R is hydrogen or lower alkyl; methylenedioxyl (–O–CH_2–O–); and ethylenedioxyl (–O–$(CH_2)_2$–O–). An alkylene group can have about 2 to about 3 carbon atoms and can further have 6-20 carbons.

The term "arylene" refers to a bivalent aromatic group, e.g., a bivalent phenyl or napthyl group. The arylene group can optionally be substituted with one or more aryl group substituents and/or include one or more heteroatoms.

The term "amino" refers to the group –$N(R)_2$ wherein each R is independently H, alkyl, substituted alkyl, aryl, substituted aryl, aralkyl, or substituted aralkyl. The terms "aminoalkyl" and "alkylamino" can refer to the group –$N(R)_2$ wherein each R is H, alkyl or substituted alkyl, and wherein at least one R is alkyl or substituted alkyl. "Arylamine" and "aminoaryl" refer to the group –$N(R)_2$ wherein each R is H, aryl, or substituted aryl, and wherein at least one R is aryl or substituted aryl, e.g., aniline (i.e., -NHC_6H_5).

"Dialkylamino" refers to an –NRR' group wherein each of R and R' is independently an alkyl group and/or a substituted alkyl group as previously described. Exemplary alkylamino groups include ethylmethylamino, dimethylamino, and diethylamino.

The terms "halo", "halide", or "halogen" as used herein refer to fluoro, chloro, bromo, and iodo groups.

The terms "hydroxyl" and "hydroxy" refer to the –OH group.

The terms "mercapto" or "thiol" refer to the –SH group.

The terms "carboxylate" and "carboxylic acid" can refer to the groups –$C(=O)O^-$ and –C(=O)OH, respectively. The term "carboxyl" can also refer to the –C(=O)OH group. In some embodiments, "carboxylate" or "carboxyl" can refer to either the –$C(=O)O^-$ or –

C(=O)OH group. In some embodiments, when the term "carboxylate" is used in reference to an anion of a SBU, the term "carboxylate" can be used to refer to the anion HCO_2^- and, thus, can be synonymous with the term "formate".

The term "carbonate" refers to a compound or group comprising a -O-C(=O)-O moiety.

The term "phosphonate" refers to the $-P(=O)(OR)_2$ group, wherein each R can be independently H, alkyl, aralkyl, aryl, or a negative charge (i.e., wherein effectively there is no R group present to bond to the oxygen atom, resulting in the presence of an unshared pair of electrons on the oxygen atom). Thus, stated another way, each R can be present or absent, and when present is selected from H, alkyl, aralkyl, or aryl.

The term "phosphate" refers to the $-OP(=O)(OR')_2$ group, where R' is H or a negative charge.

The terms "bonding" or "bonded" and variations thereof can refer to either covalent or non-covalent bonding. In some cases, the term "bonding" refers to bonding via a coordinate bond.

The term "conjugation" can refer to a bonding process, as well, such as the formation of a covalent linkage or a coordinate bond.

The term "prodrug" as used herein refers to a chemical entity that, upon administration to a recipient, is capable of providing (directly or indirectly) a pharmaceutically active compound (e.g. a known pharmaceutically active compound) or an active metabolite or residue thereof, either based on conditions already present in at least a portion of the recipient and/or based on conditions that can be introduced deliberately to at least a portion of the recipient. In some embodiments, the pharmaceutically active compound can be referred to as the "parent drug" or "parent compound" of the prodrug. A prodrug can be a derivative of a pharmaceutically active compound that comprises one or more groups or bonds that can be cleaved under particular conditions, such as at a certain pH, in the presence of a particular type of enzyme, or in the presence of one or more other chemical entities). Such groups or bonds can include, but are not limited to, an ester, carbamate, carbonate, phosphate ester, azo group or amide, depending upon the particular conditions that can cleave the groups or bonds. In some, but not all, embodiments, the prodrug has less pharmaceutical activity than the parent compound (i.e., the pharmaceutically active compound upon which the structure of the prodrug is based and to which the prodrug can be transformed *in vivo*). In some embodiments, the prodrug compound has no measurable inhibitory activity prior to transformation to the parent compound.

As used herein, the term "metal-organic framework" or "MOF" refers to a solid two- or three-dimensional network comprising both metal and organic components, wherein the organic components include at least one, and typically more than one carbon atom. In some embodiments, the material is crystalline. In some embodiments, the material is amorphous. In some embodiments, the material is porous. In some embodiments, the metal-organic matrix material is a coordination polymer, which comprises repeating units of coordination complexes comprising a metal-based secondary building unit (SBU), such as a metal ion or metal complex, and a bridging polydentate (e.g., bidentate or tridentate) organic ligand. In some embodiments, the material contains more than one type of SBU or metal ion. In some embodiments, the material can contain more than one type of organic bridging ligand.

The term "nanoscale metal-organic framework" can refer to a nanoscale particle comprising an MOF.

The terms "nanoscale particle," "nanomaterial," and "nanoparticle" refer to a structure having at least one region with a dimension (e.g., length, width, diameter, etc.) of less than about 1,000 nm. In some embodiments, the dimension is smaller (e.g., less than about 500 nm, less than about 250 nm, less than about 200 nm, less than about 150 nm, less than about 125 nm, less than about 100 nm, less than about 80 nm, less than about 70 nm, less than about 60 nm, less than about 50 nm, less than about 40 nm, or even less than about 30 nm). In some embodiments, the dimension is between about 30 nm and about 250 nm (e.g., about 30, 40, 50, 60, 70, 80, 90, 100, 110, 120, 130, 140, 150, 160, 170, 180, 190, 200, 210, 220, 230, 240, or 250 nm).

In some embodiments, the nanoparticle is approximately spherical. When the nanoparticle is approximately spherical, the characteristic dimension can correspond to the diameter of the sphere. In addition to spherical shapes, the nanomaterial can be disc-shaped, plate-shaped (e.g., hexagonally plate-like), oblong, polyhedral, rod-shaped, cubic, or irregularly-shaped.

A "coordination complex" is a compound in which there is a coordinate bond between a metal ion and an electron pair donor, ligand or chelating group. Thus, ligands or chelating groups are generally electron pair donors, molecules or molecular ions having unshared electron pairs available for donation to a metal ion.

The term "coordinate bond" refers to an interaction between an electron pair donor and a coordination site on a metal ion resulting in an attractive force between the electron pair donor and the metal ion. The use of this term is not intended to be limiting, in so much as certain coordinate bonds also can be classified as having more or less covalent character (if

not entirely covalent character) depending on the characteristics of the metal ion and the electron pair donor.

As used herein, the term "ligand" refers generally to a species, such as a molecule or ion, which interacts, *e.g.*, binds, in some way with another species. More particularly, as used herein, a "ligand" can refer to a molecule or ion that binds a metal ion in solution to form a "coordination complex." See Martell, A. E., and Hancock, R. D., *Metal Complexes in Aqueous Solutions*, Plenum: New York (1996), which is incorporated herein by reference in its entirety. The terms "ligand" and "chelating group" can be used interchangeably. The term "bridging ligand" can refer to a group that bonds to more than one metal ion or complex, thus providing a "bridge" between the metal ions or complexes. Organic bridging ligands can have two or more groups with unshared electron pairs separated by, for example, an alkylene or arylene group. Groups with unshared electron pairs, include, but are not limited to, $–CO_2H$, $-NO_2$, amino, hydroxyl, thio, thioalkyl, $-B(OH)_2$, $-SO_3H$, PO_3H, phosphonate, and heteroatoms (e.g., nitrogen, oxygen, or sulfur) in heterocycles.

The term "coordination site" when used herein with regard to a ligand, e.g., a bridging ligand, refers to a unshared electron pair, a negative charge, or atoms or functional groups cable of forming an unshared electron pair or negative charge (e.g., via deprotonation under at a particular pH).

The term "small molecule" as used herein refers to a non-polymeric compound typically having a molecular weight below about 1000 daltons (Da), below about 900 Da, or below about 800 Da.

The term "photosensitizer" (PS) refers to a chemical compound or moiety that can be excited by light of a particular wavelength, typically visible or near-infrared (NIR) light, and produce a reactive oxygen species (ROS). For example, in its excited state, the photosensitizer can undergo intersystem crossing and transfer energy to oxygen (O_2) (e.g., in tissues being treated by PDT) to produce ROSs, such as singlet oxygen ($^1O_2$). Any known type of a photosensitizer can be used in accordance with the presently disclosed subject matter. As described herein, in some embodiments, a PS can be excited (without exposure to light) via transfer of energy from a group that is capable of absorption of X-rays (e.g., an X-ray absorbing metal in a metal-containing SBU). Thus, in some embodiments, the PS can generate ROS, such as singlet oxygen, as part of a process referred to herein as "radiodynamic therapy" (RDT).

In some embodiments, the photosensitizer is a porphyrin, a chlorophyll, a dye, or a derivative or analog thereof, such as a porphyrin, chlorophyll or dye comprising one or more

additional aryl or alkyl group substituents, having one or more carbon-carbon double bonds replaced by a carbon-carbon single bond, and/or comprising a substituent (e.g., a substituted alkylene group) that can covalently substituted with a bond to an organic bridging ligand). In some embodiments, porphyrins, chlorins, bacteriochlorins, or porphycenes can be used. In some embodiments, the photosensitizer can have one or more functional groups, such as carboxylic acid, amine, or isothiocyanate, e.g., for using in attaching the photosensitizer to another molecule or moiety, such as an organic bridging ligand or a SBU, and/or for providing an additional site or sites to enhance coordination or to coordinate an additional metal or metals. In some embodiments, the photosensitizer is a porphyrin or a derivative or analog thereof. Exemplary porphyrins include, but are not limited to, hematoporphyrin, protoporphyrin and tetraphenylporphyrin (TPP). Exemplary porphyrin derivatives include, but are not limited to, pyropheophorbides, bacteriochlorophylls, chlorophyll a, benzoporphyrin derivatives, tetrahydroxyphenyl chlorins, purpurins, benzochlorins, naphthochlorins, verdins, rhodins, oxochlorins, azachlorins, bacteriochlorins, tolyporphyrins and benzobacteriochlorins. Porphyrin analogs include, but are not limited to, expanded porphyrin family members (such as texaphyrins, sapphyrins and hexaphyrins), porphyrin isomers (such as porphycenes, inverted porphyrins, phthalocyanines, and naphthalocyanines), and TPP substituted with one or more functional groups. In some embodiments, the porphyrin is bis(p-benzoato)porphyrin (DBP).

In some embodiments, the PS is a metal coordination complex comprising a metal (e.g., Ru or Ir) and one or more nitrogen donor ligands, e.g., one or more nitrogen-containing aromatic groups. In some embodiments, the one or more nitrogen donor ligands are selected from the group including, but not limited to, a bipyridine (bpy), a phenanthroline, a terpyridine, or a phenyl-pyridine (ppy), each of which can optionally be substituted with one or more aryl group substituents (e.g., on a carbon atom of the aromatic group).

The term “cancer” as used herein refers to diseases caused by uncontrolled cell division and/or the ability of cells to metastasize, or to establish new growth in additional sites. The terms “malignant”, “malignancy”, “neoplasm”, “tumor,” “cancer” and variations thereof refer to cancerous cells or groups of cancerous cells.

Particular types of cancer include, but are not limited to, skin cancers (e.g., melanoma), connective tissue cancers (e.g., sarcomas), adipose cancers, breast cancers, head and neck cancers, lung cancers (e.g., mesothelioma), stomach cancers, pancreatic cancers, ovarian cancers, cervical cancers, uterine cancers, anogenital cancers (e.g., testicular cancer), kidney cancers, bladder cancers, colorectal cancers (i.e., colon cancers or rectal cancers),

prostate cancers, central nervous system (CNS) cancers, retinal cancer, blood, neuroblastomas, multiple myeloma, and lymphoid cancers (e.g., Hodgkin's and non-Hodgkin's lymphomas).

The term "metastatic cancer" refers to cancer that has spread from its initial site (i.e., the primary site) in a patient's body.

The terms "anticancer drug", "chemotherapeutic", and "anticancer prodrug" refer to drugs (i.e., chemical compounds) or prodrugs known to, or suspected of being able to treat a cancer (i.e., to kill cancer cells, prohibit proliferation of cancer cells, or treat a symptom related to cancer). In some embodiments, the term "chemotherapeutic" as used herein refers to a non-PS molecule that is used to treat cancer and/or that has cytotoxic ability. Such more traditional or conventional chemotherapeutic agents can be described by mechanism of action or by chemical compound class, and can include, but are not limited to, alkylating agents (e.g., melphalan), anthracyclines (e.g., doxorubicin), cytoskeletal disruptors (e.g., paclitaxel), epothilones, histone deacetylase inhibitors (e.g., vorinostat), inhibitors of topoisomerase I or II (e.g., irinotecan or etoposide), kinase inhibitors (e.g., bortezomib), nucleotide analogs or precursors thereof (e.g., methotrexate), peptide antibiotics (e.g., bleomycin), platinum based agents (e.g., cisplatin or oxaliplatin), retinoids (e.g., tretinoin), and vinka alkaloids (e.g., vinblastine).

II. EXEMPLARY EMBODIMENTS OF THE PRESNETLY DISCLOSED SUBJECT MATTER

IIA. Nanoscale MOF with an X-ray Triggerable Prodrug for Synergistic Radiotherapy and Chemotherapy

Metal-organic frameworks (MOFs) are solid two- or three-dimensional networks comprising both metal and organic components. For example, MOFs can include repeating units of coordination complexes comprising a metal-based secondary building unit (SBU), such as a metal ion or metal complex, and a bridging polydentate (e.g., bidentate or tridentate) organic ligand. As described hereinabove, metal-organic frameworks (MOFs), particularly nanoscale MOFs (nMOFs), have recently gained interest as drug carriers.[5-10] While it is possible to associate drugs with MOFs in different ways, one approach involves covalently conjugating a therapeutic agent or agents of interest to an organic bridging ligand. The covalent linkage between the bridging ligand and the therapeutic agent can include a bond that is sensitive to (e.g., reactive or unstable to) particular conditions. This bond can be viewed as an actionable trigger that can be used to release the therapeutic agent at a time

and/or location of interest, e.g., after deliberately administering a treatment that can introduce the particular conditions to which the covalent linkage is sensitive. Among many possible triggers,[18-27] X-ray stands out as an external stimulus that could be useful as a trigger. X-rays are capable of deep tissue penetration,[28] image-guided precise dosing,[29-30] and radiotherapeutic effects through direct DNA damage and/or indirect cytotoxic effects (e.g., via generating reactive oxygen species (ROS)).[31-38]

Heavy metal-based nMOFs can act as radioenhancers by enhancing energy deposition and ROS generation.[39-41] According to one aspect of the presently disclosed subject matter provided herein are heavy metal-nMOFs with covalently conjugated drugs that can be efficiently triggered by X-rays to release the drugs via enhanced ROS generation and radiation-induced cleavage of the drug molecules for synergistic radiotherapy and chemotherapy while reducing the systemic exposure of chemotherapeutics. An example of such a nMOF disclosed herein is a Hf-TP-SN nMOF with an X-ray triggerable 7-ethyl-10-hydroxycamptothecin (SN38) prodrug for synergistic radiotherapy and chemotherapy. See Figure 1 and Examples 1 and 2, below. As a topoisomerase I inhibitor, SN38 is the active metabolite of irinotecan, a compound that has been used in the treatment of colorectal and pancreatic cancer.[42-43] As described hereinbelow, Hf-TP-SN was synthesized via a combination of pre-functionalization of terphenyl ligands with 3,5-dimethylbenzyl alcohol and post-synthetic modification with SN38 via a carbonate bond. Upon X-ray irradiation, electron-dense Hf_{12}-SBUs served as radiosensitizers to enhance ·OH generation, leading to 5-fold higher release of SN38 from Hf-TP-SN than a homogeneous counterpart. Hf-TP-SN not only enhanced the radiotherapeutic efficacy but also achieved chemotherapeutic effect through on-demand release of SN38. Such a chemoradiotherapy strategy can effectively reduce the radiation dose required for tumor regression and minimizes the side effects of chemotherapy via burst release of SN38 inside the cancer cells.

IIB. Mixed-Ligand Nanoscale MOFs for X-ray-Mediated Synergistic Radiotherapy-Radiodynamic Therapy and Chemotherapy

To improve the therapeutic effects and reduce the non-specific toxicity of traditional chemotherapeutics,[53,54] many nanotherapeutic systems have been designed to release active drugs using stimuli such as reactive oxygen species (ROS), enzymes, temperature, and light.[55,56] These stimuli-responsive nanotherapeutics undergo specific activation at the target site to release the pharmacologically active drugs.[57-59] In particular, ROS-responsive nanotherapeutics have emerged as a preferred antitumor strategy[60-62] as the ROS concentration in the tumor tissue can be higher than that in normal organs.[63] Various ROS-

responsive drug delivery systems with photodynamic effect or chemodynamic effect have been developed to enable ROS-triggered drug release.[64,65,37] However, the photodynamic effect relies on visible to near-infrared photons which cannot penetrate deeply into most tumor tissues whereas the chemodynamic effect relies on unusually high ROS concentrations in mouse tumors which could be absent in human tumors.[66-69] In addition, existing stimuli-responsive nanotherapeutics tend to have inefficient drug loading and premature release of active drugs. Thus, there is an ongoing need for biocompatible ROS-responsive nanotherapeutics which can be selectively triggered to increase intratumoral ROS level for localized and on-demand release of active drugs in tumors for enhanced antitumor efficacy.[70]

Radiotherapy (RT) has provided important curative and palliative treatments to more than half of all cancer patients with tissue-penetrating ionizing radiations to kill cancer cells by directly inducing DNA damage or indirectly generating ROS to decompose biomolecules and disrupt the redox balance.[71,41,72] Nanoscale metal–organic frameworks (nMOFs)[73,74,2] have shown exciting potential in RT and drug delivery because of their unique advantages, including highly porous structures, high surface areas, good biocompatibility, and molecular tunability.[75-77] For example, Hf-DBP (DBP = bis(p-benzoato)porphyrin) nMOF-mediated radiotherapy-radiodynamic therapy (RT-RDT) has been described.[78] Under X-ray irradiation, electron-dense Hf_{12} SBUs not only enhance hydroxyl radical (·OH) generation for RT, but also transfer energy to neighboring photosensitizing DBP ligands to generate $^1O_2$ for RDT. Thus, Hf-DBP can provide a nanoplatform for designing nanotherapeutics by incorporating a high loading of ROS-responsive prodrugs into the framework.

According to one aspect of the presently disclosed subject matter, herein is described a quaterphenyl dicarboxylate ligand (QP-SN) conjugated with 7-ethyl-10-hydroxycamptothecin (SN-38, an active metabolite of irinotecan)[79] via a ·OH responsive 3,5-dimethoxylbenzyl carbonate linkage. With a similar length as DBP ligand (19.3 vs 19.2 Å), QP-SN was introduced to Hf-DBP nMOF with photosensitizing DBP ligands to form a novel multi-functional mix-ligand Hf-DBP-QP-SN nMOF. In addition to Hf-DBP mediated RT-RDT process for enhanced radiation damage, Hf-DBP-QP-SN achieved tumor-selective chemotherapy via a cascade of ·OH generation from electron-dense Hf_{12} SBUs[80], hydroxylation of the 3,5-dimethoxylbenzyl carbonate at ortho positions, and subsequent 1,4-elimination to release SN38.[38] Under the irradiation of X-rays, Hf-DBP-QP-SN effectively suppressed tumor growth due to synergistic tumor-targeted RT-RDT and chemotherapy. See Figures 14A and 14B.

Also disclosed herein, according to an aspect of the presently disclosed subject matter, is a nMOF comprising a quaterphenyl dicarboxylate ligand conjugated to pomalidomide, a thalidomide analog antineoplastic agent, through a picolinium-containing X-ray sensitive linkage

IIC. MOFs with X-ray-triggerable Innate Immune Modulators for Synergistic Radiotherapy and Immunotherapy

According to one aspect of the presently disclosed subject matter, provided herein are MOFs comprising X-ray-triggerable innate immune modulator prodrugs, which can be used for combination radiotherapy and immunotherapy or combination radiotherapy-radiodynamic therapy and immunotherapy. As an example of a MOF comprising a X-ray-triggerable innate immune modulate prodrug, a MOF (i.e., HF-DBP-QP-R848) was prepared comprising a prodrug of R848, as described hereinbelow. See Scheme 7, below.

III. NMOFS WITH X-RAY TRIGGED PRODRUGS AND METHODS AND USES THEREOF

In some embodiments, the presently disclosed subject matter provides a MOF (e.g., a nMOF) comprising an irradiation-sensitive prodrug (e.g., a prodrug comprising a bond sensitive to X-rays or other ionizing radiation, or a bond sensitive to a product produced by absorption of X-rays or other ionizing radiation by another component of the MOF). For example, the prodrug can include a bond that is sensitive to radicals (e.g., hydroxyl radicals) produced by X-ray adsorption of a metal ion. In some embodiments, the presently disclosed subject matter provides a MOF (e.g., a porous nMOF) comprising an X-ray sensitive prodrug, wherein the MOF comprises metal-containing secondary building units (SBUs) linked together via organic bridging ligands, wherein at least one of the SBUs comprises a metal cation capable of absorbing X-rays, and wherein at least one of the organic bridging ligands is substituted by a group having the formula: -L-D, wherein L is a bivalent linker group comprising one or more bonds capable of radical-promoted bond cleavage and wherein D is a monovalent moiety of a therapeutic agent.

Thus, in some embodiments, the presently disclosed nMOF comprises periodic repeats of metal-based SBUs and organic bridging ligands, wherein each SBU is bonded to at least one other SBU via coordinative bonding to the same organic bridging ligand and wherein one or more of the SBUs contain cations of a high Z-metal that can absorb ionizing irradiation energy, such as X-ray, γ-ray, β-irradiation, or proton irradiation. In some

embodiments, one or more of the SBUs are metal-oxo clusters with a structure that strongly absorbs ionizing irradiation energy. In some embodiments, the metal cation capable of absorbing X-rays is a cation of an element selected from the group comprising Hf, the lanthanide metals (La, Ce, Pr, Nd, Pm, Sm, Eu, Gd, Tb, Dy, Ho, Er, Tm, Yb, and Lu), Ba, Ta, W, Re, Os, Ir, Pt, Au, Pb, and Bi. In some embodiments, the one or more SBUs comprise combinations of metals (either in the same SBU or in different SBUs). In some embodiments, the SBUs are metal oxo clusters comprising one or more of Hf, a lanthanide metal, Ba, Ta, W, Re, Os, Ir, Pt, Au, and Bi. In some embodiments, the oxo clusters comprise anions selected from oxide (O^{2-}), hydroxide (OH^-), S^{2-}, SH^-, and formate (HCO_2^-). In some embodiments, the oxo clusters are capped with anions derived from a strongly coordinating modulator, such as a monocarboxylic acid. Thus, in some embodiments, the oxo clusters are capped with an anion selected from the group including, but not limited to, acetate, formate, benzoate, and trifluoroacetate.

In some embodiments, the metal cation capable of absorbing X-rays is an Hf cation. In some embodiments, one or more of the SBUs comprise a Hf oxo cluster. For example, one or more of the SBUs can be selected from the group including, but not limited to an Hf_6 oxo cluster (e.g., $Hf_6O_4(OH)_4(HCO_2)_{12}$), a Hf_{12} oxo cluster (e.g., $Hf_{12}O_8(OH)_{14}(HCO_2)_{18}$), an Hf_{18} oxo cluster (e.g., $Hf_{18}O_{12}(OH)_{24}(HCO_2)_{24}$) and an Hf_{24} oxo cluster (e.g., $Hf_{24}O_{16}(OH)_{34}(HCO_2)_{30}$). In some embodiments, one or more of the SBUs comprise a Hf_6 oxo cluster (e.g., $[Hf_6O_4(OH)_4(HCO_2)_6]$) or an Hf_{12} oxo cluster. In some embodiments, one or more of the SBUs comprise a Hf_6 oxo cluster. In some embodiments, one or more of the SBUs comprise a Hf_{12} oxo cluster.

In some embodiments, L has the structure:

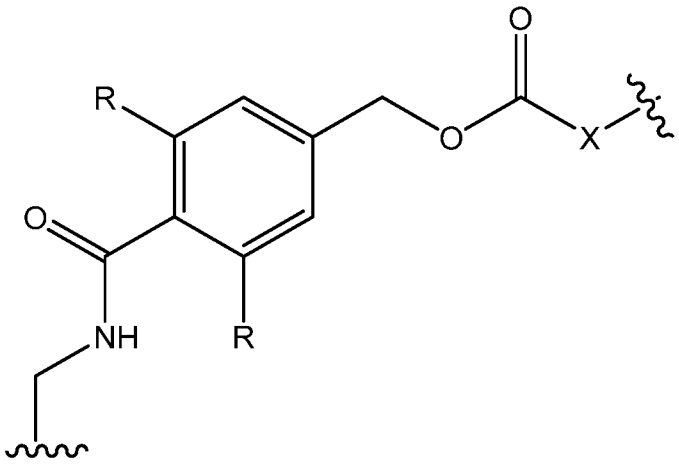

or

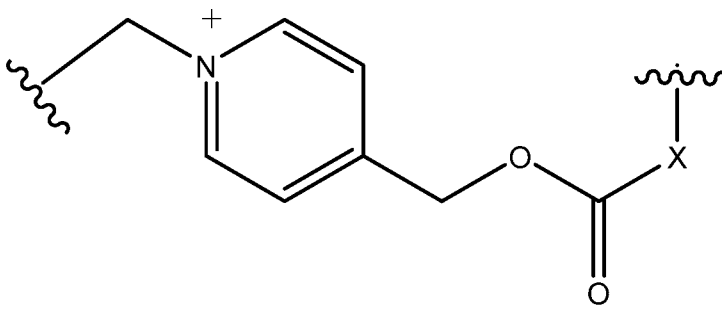

wherein: X is selected from the group comprising -O-, -NR'-, -O-X_1-O-, and -NH-X_1-NH-, wherein R' is selected from H and alkyl, and X_1 is alkylene; and each R is selected from the group comprising hydroxyl, oxyalkyl, and dialkylamino. In some embodiments, X is selected from -O- and -NR'- (e.g., -NH-).

In some embodiments, L has the structure:

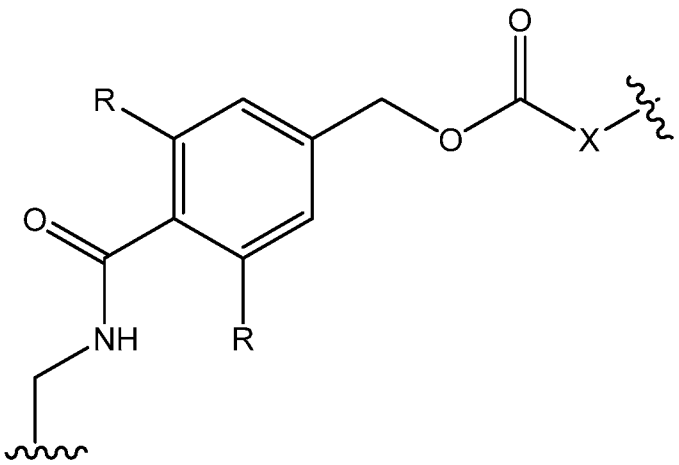

,

wherein: X is selected from the group comprising -O-, -NR'-, -O-X_1-O-, and -NH-X_1-NH-, wherein R' is selected from H and alkyl, and X_1 is alkylene; and each R is selected from the group comprising hydroxyl, oxyalkyl, and dialkylamino. In some embodiments, R' is H or C1-C6 alkyl. In some embodiments, R' is methyl. In some embodiments, each R is oxyalkyl (e.g., C1-C6 oxyalkyl). In some embodiments, each R is methoxy. In some embodiments, each R is dialkylamino. In some embodiments, the dialkylamino is dimethylamino. In some embodiments, X_1 is propylene or ethylene. In some embodiments, X is -O- or -NR'-. In some embodiments, X is -O- and L comprises a radical sensitive carbonate.

In some embodiments, L has the structure:

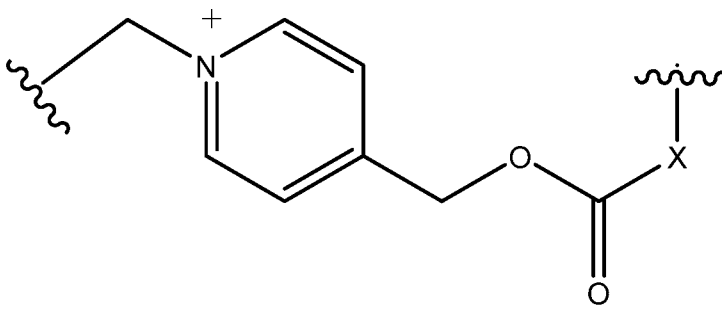

wherein: X is selected from the group comprising -O-, -NR'-, -O-X_1-O-, and -NH-X_1-NH-, wherein R' is selected from H and alkyl, and X_1 is alkylene. In some embodiments, X is selected from -O- and -NR'-. In some embodiments, X is -NH-.

Any suitable therapeutic agent can be used. In some embodiments, the parent therapeutic agent is a therapeutic agent that comprises at least one functional group for covalently bonding the therapeutic agent to L. In some embodiments, the at least one functional group is selected from the group comprising a primary amino group (i.e., -NH_2), a secondary amino group (e.g., -NH(alkyl)), amido (i.e., -C(=O)-NH_2), carboxylate (i.e., -C(=O)OH), a hydroxyl group, and a phenol. The functional group can be used to form a portion of the group L (i.e., to provide one or more atoms to the structure of L). Thus, in some embodiments, D is the monovalent moiety that would be provided if the bond attaching the functional group to the therapeutic agent were cleaved. For example, if the functional group is a carboxylate, D is the monovalent moiety that has the same structure as the parent therapeutic agent but with a free bonding site where the carboxylate group is in the parent therapeutic agent. If the functional group is a hydroxy or phenol group, D can have the same structure as the parent therapeutic agent but with a free bonding site where the hydroxy or phenol OH group is in the parent therapeutic agent.

In some embodiments, the therapeutic agent is a chemotherapeutic agent or an immune modulator (i.e., a small molecule chemotherapeutic agent or small molecule immune modulator). In some embodiments, the chemotherapeutic agent is a topoisomerase inhibitor. In some embodiments, the chemotherapeutic agent is camptothecin or an analog and/or metabolite thereof, such as SN38. In some embodiments, the chemotherapeutic agent is pomalidomide, lenalidomide, or another thalidomide analog chemotherapeutic agent (e.g., another amino-substituted thalidomide analog chemotherapeutic agent). In some embodiments, the immune modulator is a TLR agonist or a STING agonist. In some embodiments, the therapeutic agent is selected from SN38, R848 (resiquimod), imiquimod, VTX-378 (motolimod), DSR-6434, ioxoribine, TLR7/8 agonist 1, Cu-712-9, neoseptin-3, and

diABZI. See Figures 35A-35C, which shows MOF prodrugs of exemplary immune modulators. In some embodiments, the therapeutic agent is R848.

In some embodiments, the at least one organic bridging ligand substituted by a group having the formula -L-D is an organic bridging ligand comprising an arylene group (e.g., a terphenyl (TP) moiety or a quaterphenyl (QP) moiety) and at least two groups, which can be the same or different, capable of coordinating with an SBU. In some embodiments, the at least two groups capable of coordinating with an SBU are selected from the group including, but not limited to, a carboxylate group, an aromatic or non-aromatic nitrogen-containing group (e.g., pyridine), a phenol, an acetylacetonate, a phosphonate, and a phosphate. In some embodiments, the at least one organic bridging ligand has a structure selected from:

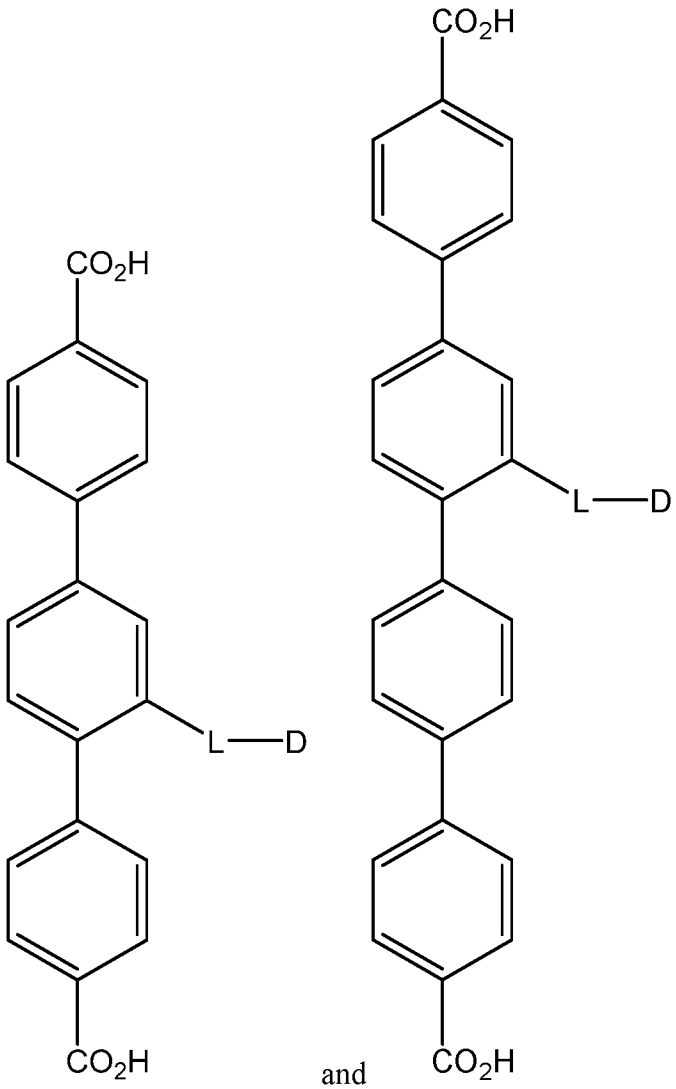

In some embodiments, the MOF further comprises at least one photosensitizer (PS). In some embodiments, the MOF comprises at least one organic bridging ligand that is

covalently attached to a PS or that is, itself, a PS. In some embodiments, the MOF comprises at least one organic bridging ligand comprising a porphyrin, a chlorin, a chlorophyll, a phthalocyanine, a ruthenium-bipyridine complex, iridium-phenylpyridine complex, or an iridium-bipyridine complex. In some embodiments, the PS or PS containing bridging ligands can generate reactive oxygen species (ROS) such as singlet oxygen ($^1O_2$), superoxide ($\cdot O_2^-$), hydrogen peroxide (H_2O_2), and hydroxyl radicals ($\cdot OH$), upon absorption of ionizing irradiation by the MOF (e.g., by the metal cation of a SBU). In some embodiments, the MOF comprises at least one organic bridging ligand comprising a porphyrin, optionally bis(p-benzoato)porphyrin (DBP). Thus, in some embodiments, the MOF is a mixed ligand MOF comprising at least two different organic bridging ligands, one that comprises a covalently attached radical sensitive prodrug and one that comprises a PS that can generate ROS when the MOF absorbs ionizing radiation.

In some embodiments, the presently disclosed subject matter provides a pharmaceutical composition comprising an MOF of the presently disclosed subject matter (e.g., a nMOF comprising a radical sensitive prodrug). The composition can comprise the MOF of the presently disclosed subject matter and a pharmaceutically acceptable carrier.

In some embodiments, the presently disclosed subject matter provides a method of treating a disease a disease in a subject in need thereof, the method comprising: (a) administering to the subject a MOF (e.g., a nMOF) of the presently disclosed subject matter, or a pharmaceutical composition thereof; and (b) irradiating at least a portion of the subject with X-rays. In some embodiments, the disease is cancer or another proliferative disease or pathogenic infection. In some embodiments, the disease is cancer. In some embodiments, the cancer is selected from the group including, but not limited to, a head tumor, a neck tumor, a head and neck tumor, a breast tumor, a gynecological tumor, a brain tumor, a colorectal cancer, a lung cancer, mesothelioma, a soft tissue sarcoma, and a pancreatic cancer.

The subject can be exposed to the ionizing irradiation energy in any suitable manner and/or using any suitable equipment, such as that currently being used for delivering X-rays in a medical or veterinary setting. In some embodiments, the X-ray source and/or output can be refined to enhance disease treatment. For instance, the X-rays can be generated using a peak voltage, current and/or, optionally, a filter chosen to minimize DNA damage in the patient due to X-ray irradiation and maximize X-ray absorption by the scintillator.

In some embodiments, the subjects are irradiated with a linear accelerator (LINAC), using conventional techniques, Intensity-Modulated Radiation Therapy (IMRT), Image

Guided Radiation Therapy (IGRT), or Stereotactic Body Radio Therapy (SBRT), a ^{60}Co radiation source, an implanted radioactive seed such as the ones used in brachytherapy, an orthovoltage or supervoltage X-ray irradiator, a high energy electron beam generated from LINAC, or a proton source. In some embodiments, the irradiating can comprise generating X-rays using a tungsten or another metal target, Cobalt-60 sources (cobalt unit), linear accelerators (linacs), Ir-192 sources, and Cesium-137 sources. In some embodiments, the irradiating comprises passing the X-rays (e.g., the X-rays generated using a tungsten target) or other ionizing radiation through a filter prior to irradiation the subject. In some embodiments, the filter can comprise an element with an atomic number of at least 20. In some embodiments, the filter comprises copper (Cu). In some embodiments, the filter can have a thickness that is less than about 5 millimeters (mm). In some embodiments, the filter can have a thickness of less than about 4 mm (e.g., less than about 3 mm, less than out 1 mm, less than about 0.5 mm, less than about 0.4 mm, less than about 0.3 mm, less than about 0.2 mm, or less than about 0.1 mm).

The X-rays can be generated using a peak voltage, current and/or, optionally, a filter chosen to minimize DNA damage in the patient due to X-ray irradiation and maximize X-ray absorption by the scintillator. In some embodiments, the X-rays are generated using a peak voltage that is less than about 230 kVp. In some embodiments, the peak voltage is less than about 225 kVp, less than about 200 kVp, less than about 180 kVp, less than about 160 kVp, less than about 140 kVp, less than about 120 kVp, less than about 100 kVp, or less than about 80 kVp. In some embodiments, the X-rays are generated using a peak voltage that is about 120 kVp.

The X-rays can be provided in a single dose or fractionated into several smaller doses. Thus, in some embodiments, step (b) comprises irradiating at least a portion of the subject with X-rays one or more times (e.g., 1, 2, 3, 4, 5, 6, 7, 8, 9, or 10 times).

In some embodiments, X-rays are generated by placing radioactive sources inside the subject on a temporary or permanent basis. In some embodiments, a MOF of the presently disclosed subject matter is injected along with the implantation of a radioactive source.

In some embodiments, the methods can further comprise administering to the subject an additional treatment (e.g., an additional cancer and/or immunotherapy treatment). The additional cancer treatment can be selected on the basis of the cancer being treated and/or on other factors, such as the patient's treatment history, overall health, etc., in accordance with the best judgement of the treating physician. The additional cancer treatment can be selected from the group including, but not limited to, surgery, radiotherapy, conventional

chemotherapy, toxin therapy, immunotherapy, cryotherapy and gene therapy. In some embodiments, the additional cancer treatment can comprise administering to the patient a conventional chemotherapeutic, such as, but not limited to, a platinum-containing agent (e.g., cisplatin or oxaliplatin or a prodrug thereof), doxorubicin, daunorubicin, docetaxel, mitoxanthrone, paclitaxel, digitoxin, digoxin, and septacidin or another conventional chemotherapeutic known in the art. The additional chemotherapeutic agent can be present in the MOF (e.g., encapsulated or coordinatively or covalently bonded to the MOF). Alternatively, the additional chemotherapeutic agent can be present in the same pharmaceutical composition or formulation as the MOF or in a separate pharmaceutical composition or formulation, administered prior to, simultaneously with, or after administration of the pharmaceutical composition or formulation comprising the MOF and/or the irradiation.

In some embodiments, the additional cancer treatment can involve administering to the patient a drug formulation selected from the group comprising a polymeric micelle formulation, a liposomal formulation, a dendrimer formulation, a polymer-based nanoparticle formulation, a silica-based nanoparticle formulation, a nanoscale coordination polymer formulation, a nanoscale metal-organic framework formulation, and an inorganic nanoparticle (gold, iron oxide nanoparticles, etc.) formulation. In some embodiments, the drug formulation can be a formulation including a conventional chemotherapeutic.

In some embodiments, D is a monovalent moiety of a chemotherapeutic agent, thereby providing to the subject, upon performing the irradiating of (b), a combination of chemotherapy and either radiotherapy (RT) or radiotherapy-radiodynamic therapy (RT-RDT). In some embodiments, the MOF comprises a PS (e.g., a DBP bridging ligand) and the method provides combination of chemotherapy and RT-RDT. In some embodiments, D is a monovalent moiety of SN38. In some embodiments, a higher percentage of the SN38 (or other chemotherapeutic agent) is released from the MOF upon performing the irradiating of (b) compared to the release of SN38 (or other chemotherapeutic agent) from a homogenous prodrug comprising the SN38 monovalent moiety (or other chemotherapeutic agent-derived monovalent moiety). The term “homogenous prodrug” as used herein refers to a prodrug that is free of coordination bonding and/or that is not a MOF. In some embodiments, the homogenous SN38 prodrug is MeO-SN.

In some embodiments, D is a monovalent moiety of an immune modulator, thereby providing to the subject, upon performing the irradiating of (b), a combination of immunotherapy and either RT or RT-RDT. In some embodiments, the MOF comprises a PS

(e.g., a DBP bridging ligand) and the method provides, upon performing the irradiating of (b), a combination of immunotherapy and RT-RDT.

The presently disclosed methods can provide more selective treatment than use of a non-MOF (e.g., homogenous) prodrug or free therapeutic agent. For example, as release of the therapeutic agent is triggered by radicals that are themselves generated upon absorption of ionizing radiation (e.g., X-rays) by the MOF, release of the therapeutic agent can be controlled by directing the X-ray radiation treatment to regions at or near a disease site (e.g., a tumor). Thus, in some embodiments, the method provides selective cytotoxicity and/or immune activation in a tumor (i.e., higher cytotoxicity and/or immune activation in a tumor than in surrounding non-diseased tissue). Thus, the presently disclosed methods can provide an improved therapeutic index for the therapeutic agent. In some embodiments, the presently disclosed method can provide effective results using a lower dose of X-ray radiation than conventional radiotherapy.

In some embodiments, the presently disclosed MOF or a pharmaceutical composition thereof can be used in treating a disease or in the manufacture of a composition for treating a disease in a subject in need thereof. In some embodiments, the disease is cancer or another proliferative disease or pathogenic infection. In some embodiments, the disease is cancer. In some embodiments, the cancer is selected from a head tumor, a neck tumor, a head and neck tumor, a breast tumor, a gynecological tumor, a brain tumor, a colorectal cancer, a lung cancer, mesothelioma, a soft tissue sarcoma, and a pancreatic cancer. In some embodiments, the use is a use performed in combination with exposing at least a portion of the subject to ionizing radiation (e.g., X-rays). In some embodiments, the use provides selective cytotoxicity and/or immune activation in a tumor (i.e., higher cytotoxicity and/or immune activation in a tumor than in surrounding non-diseased tissue). Thus, the presently disclosed uses can provide an improved therapeutic index for the therapeutic agent. The present method selectively releases chemotherapeutic agents and immune modulators in tumors during radiotherapy without causing significant systemic exposure of these agents, thereby reducing the toxicity from conventional systemic administration of chemotherapy and immunotherapy.

IV. PHARMACEUTICAL COMPOSITIONS/FORMULATIONS

In some embodiments, the presently disclosed subject matter provides a pharmaceutical composition or formulation comprising a MOF (e.g., a nMOF) as described herein and a pharmaceutically acceptable carrier, e.g., a pharmaceutically acceptable carrier

that is pharmaceutically acceptable in humans. In some embodiments, the composition can also include other components, such as, but not limited to anti-oxidants, buffers, bacteriostatics, bactericidal antibiotics, suspending agents, thickening agents, and solutes that render the composition isotonic with the bodily fluids of a subject to whom the composition is to be administered.

The compositions of the presently disclosed subject matter comprise, in some embodiments, a composition that includes a pharmaceutically acceptable carrier. Any suitable pharmaceutical formulation can be used to prepare the compositions for administration to a subject. In some embodiments, the composition and/or carriers can be pharmaceutically acceptable in humans.

For example, suitable formulations can include aqueous and non-aqueous sterile injection solutions that can contain anti-oxidants, buffers, bacteriostatics, bactericidal antibiotics, and solutes that render the formulation isotonic with the bodily fluids of the subject; and aqueous and non-aqueous sterile suspensions that can include suspending agents and thickening agents. The formulations can be presented in unit-dose or multi-dose containers, for example sealed ampoules and vials, and can be stored in a frozen or freeze-dried (lyophilized) condition requiring only the addition of sterile liquid carrier, for example water for injections, immediately prior to use. Some exemplary ingredients are sodium dodecyl sulfate (SDS), in one example in the range of 0.1 to 10 mg/ml, in another example about 2.0 mg/ml; and/or mannitol or another sugar, for example in the range of 10 to 100 mg/ml, in another example about 30 mg/ml; and/or phosphate-buffered saline (PBS).

It should be understood that in addition to the ingredients particularly mentioned above, the formulations of this presently disclosed subject matter can include other agents conventional in the art having regard to the type of formulation in question. For example, sterile pyrogen-free aqueous and non-aqueous solutions can be used.

V. SUBJECTS

The methods and compositions disclosed herein can be used on a sample either *in vitro* (for example, on isolated cells or tissues) or *in vivo* in a subject (i.e. living organism, such as a patient). In some embodiments, the subject or patient is a human subject, although it is to be understood that the principles of the presently disclosed subject matter indicate that the presently disclosed subject matter is effective with respect to all vertebrate species, including mammals, which are intended to be included in the terms “subject” and “patient”. Moreover, a mammal is understood to include any mammalian species for which employing

the compositions and methods disclosed herein is desirable, particularly agricultural and domestic mammalian species.

As such, the methods of the presently disclosed subject matter are particularly useful in warm-blooded vertebrates. Thus, the presently disclosed subject matter concerns mammals and birds. More particularly provided are methods and compositions for mammals such as humans, as well as those mammals of importance due to being endangered (such as Siberian tigers), of economic importance (animals raised on farms for consumption by humans), and/or of social importance (animals kept as pets or in zoos) to humans, for instance, carnivores other than humans (such as cats and dogs), swine (pigs, hogs, and wild boars), rodents (such as rats, mice, hamsters, guinea pigs, etc.), ruminants (such as cattle, oxen, sheep, giraffes, deer, goats, bison, and camels), and horses. Also provided is the treatment of birds, including the treatment of those kinds of birds that are endangered, kept in zoos or as pets (e.g., parrots), as well as fowl, and more particularly domesticated fowl, for example, poultry, such as turkeys, chickens, ducks, geese, guinea fowl, and the like, as they are also of economic importance to humans. Thus, also provided is the treatment of livestock including, but not limited to domesticated swine (pigs and hogs), ruminants, horses, poultry, and the like.

VI. ADMINISTRATION

Suitable methods for administration of a composition of the presently disclosed subject matter include, but are not limited to intravenous and intratumoral injection, oral administration, subcutaneous administration, intraperitoneal injection, intracranial injection, and rectal administration. Alternatively, a composition can be deposited at a site in need of treatment in any other manner, for example by spraying a composition within the pulmonary pathways. The particular mode of administering a composition of the presently disclosed subject matter depends on various factors, including the distribution and abundance of cells to be treated and mechanisms for metabolism or removal of the composition from its site of administration. For example, relatively superficial tumors can be injected intratumorally. By contrast, internal tumors can be treated following intravenous injection.

In some embodiments, the method of administration encompasses features for regionalized delivery or accumulation at the site to be treated. In some embodiments, a composition is delivered intratumorally. In some embodiments, selective delivery of a composition to a target is accomplished by intravenous injection of the composition followed by photodynamic treatment (light irradiation) of the target.

For delivery of compositions to pulmonary pathways, compositions of the presently disclosed subject matter can be formulated as an aerosol or coarse spray. Methods for preparation and administration of aerosol or spray formulations can be found, for example, in U.S. Patent Nos. 5,858,784; 6,013,638; 6,022,737; and 6,136,295.

VII. DOSES

An effective dose of a composition of the presently disclosed subject matter is administered to a subject. An "effective amount" is an amount of the composition sufficient to produce detectable treatment. Actual dosage levels of constituents of the compositions of the presently disclosed subject matter can be varied so as to administer an amount of the composition that is effective to achieve the desired effect for a particular subject and/or target. The selected dosage level can depend upon the activity of the composition and the route of administration.

After review of the disclosure herein of the presently disclosed subject matter, one of ordinary skill in the art can tailor the dosages to an individual subject, taking into account the particular formulation, method of administration to be used with the composition, and nature of the target to be treated. Such adjustments or variations, as well as evaluation of when and how to make such adjustments or variations, are well known to those of ordinary skill in the art.

EXAMPLES

The following Examples have been included to provide guidance to one of ordinary skill in the art for practicing representative embodiments of the presently disclosed subject matter. In light of the present disclosure and the general level of skill in the art, those of skill can appreciate that the following Examples are intended to be exemplary only and that numerous changes, modifications, and alterations can be employed without departing from the scope of the presently disclosed subject matter.

EXAMPLE 1

METHODS FOR PREPARATION AND STUDIES WITH Hf-TP-SN nMOF

Synthesis of Organic Ligands and Molecular Prodrugs:

4-(((*tert*-Butyldimethylsilyl)oxy)methyl)-2,6-dimethoxybenzoic acid (3). A solution of imidazole (6.08 g, 0.089 mol) and 3,5-dimethoxybenzyl alcohol (**1**, 5 g, 0.030 mol) in dry

dichloromethane (DCM, 60 mL) was combined with tert-butyldimethylsilyl chloride (TBSCl, 6.74 g, 0.045 mol) and stirred at room temperature (RT) for 2 hours. Excess TBSCl was quenched by 2 mL methanol (MeOH); the resulting solution was condensed via rotary evaporation and then purified by flash silica gel column chromatography to give *tert*-butyl((3,5-dimethoxybenzyl)oxy)dimethylsilane (**2**, 8 g, 0.028 mol, 95%). ^{1}H NMR (400 MHz, Chloroform-*d*) δ 6.52-6.47 (m, 2H), 6.34 (s, 1H), 4.69 (s, 2H), 3.79 (s, 6H), 0.95 (s, 9H), 0.10 (s, 6H); ^{13}C NMR (101 MHz, $CDCl_3$) δ 160.91, 144.23, 103.85, 99.05, 64.99, 55.42, 26.09, 18.57, -5.11. HR-MS (ESI, positive mode): *m/z* calc'd for $C_{15}H_{27}O_3Si$ $[M+H]^+$: 283.1729, found 283.1727.

Compound **2** (10 g, 0.035 mol) was dissolved in dry tetrahydrofuran (THF, 100 mL) and cooled to 0 °C under N_2, to which 1.6 M n-butyllithium in hexanes (22.2 mL, 0.035 mol) was added dropwise; the resulting mixture was then stirred at RT for 1 hour. Dry ice (10 g, 0.227 mol) was added afterwards, and the reaction mixture was allowed to stand at RT overnight. The resulting solution was condensed via rotary evaporation and water (50 mL) was added to the residue, which was extracted with ethyl acetate (EA, 20 mL) twice. The aqueous layer was carefully acidified with 1M hydrochloric acid (dropwise) until the pH reached about 3. The white precipitate was separated via filtration, washed with water, dried under vacuum, and purified by column chromatography to give **3** (6.1 g, 0.019 mol, 53%). ^{1}H NMR (400 MHz, Chloroform-*d*) δ 6.60 (s, 2H), 4.74 (s, 2H), 3.88 (s, 6H), 0.96 (s, 8H), 0.12 (s, 6H); ^{13}C NMR (101 MHz, $CDCl_3$) δ 168.75, 158.57, 146.94, 109.33, 101.59, 64.73, 56.35, 26.01, 18.51, -5.12. HR-MS (ESI, positive mode): *m/z* calc'd for $C_{16}H_{27}O_5Si$ $[M+H]^+$: 327.1628, found 327.1695.

2,5-Dibromobenzyl amine (6). 2,5-Dibromobenzyl amine (**6**) was prepared based on reported procedures with modification in the second step.[51] To a solution of 7M ammonia (NH_3) in MeOH (100 mL, 0.70 mol) was added methyl 2,5-dibromobenzoate (**4**, 10.0 g, 0.034 mol) at RT; the resulting dissolved solution was evenly separated into five 20-mL vials, sealed, and stirred for 3 days. The white precipitate formed was separated and collected via filtration, dispersed in hexanes (100 mL), recollected via filtration, and dried under vacuum to produce 2,5-dibromobenzamide (**5**, 8.58 g, 0.031 mol, 90%). ^{1}H NMR (400 MHz, Chloroform-*d*) δ 7.78 (d, J = 2.4 Hz, 1H), 7.48 (d, J = 8.5 Hz, 1H), 7.42 (dd, J = 8.5, 2.4 Hz, 1H), 6.02 (d, J = 63.0 Hz, 2H); ^{13}C NMR (101 MHz, $CDCl_3$) δ 167.63, 138.29, 135.14, 134.84, 133.00, 121.79, 117.98. HR-MS (ESI, positive mode): *m/z* calc'd for $C_7H_6Br_2NO$ $[M+H]^+$: 279.8796, found 279.8790.

1M borane-tetrahydrofuran complex (BH_3 in THF) was added in excess (35 mL, 0.035 mol) to **5** (4.11 g, 0.0144 mol); the resulting mixture was stirred at reflux for 24 hours and then quenched with concentrated HCl (3.5 mL). The solution was then refluxed for 2 more hours and cooled to RT. The suspension was filtered to obtain the white solid, which was then dissolved in water and basified to pH~10 by addition of sat. sodium carbonate (Na_2CO_3) while the solution was stirring. The reaction mixture was extracted with EA (30 mL) 3 times. The combined organic phase was dried over sodium sulfate (Na_2SO_4), filtered, and evaporated to give **6** (2.91 g, 0.011 mol, 74.6%). ^{1}H NMR (400 MHz, Chloroform-*d*) δ 7.55 (d, *J* = 2.6 Hz, 1H), 7.39 (d, *J* = 8.5 Hz, 1H), 7.24 (dd, *J* = 8.4, 2.4 Hz, 1H), 3.88 (s, 2H); ^{13}C NMR (101 MHz, $CDCl_3$) δ 144.34, 134.22, 131.99, 131.45, 122.07, 121.76, 46.65. HR-MS (ESI, positive mode): *m/z* calc'd for $C_7H_8Br_2N$ $[M+H]^+$: 265.9003, found 265.8999.

4-(((*tert*-Butyldimethylsilyl)oxy)methyl)-*N*-(2,5-dibromobenzyl)-2,6-dimethoxybenzamide (7). Compound **6** (1 g, 3.77 mmol), **3** (1.23 g, 3.77 mmol), EDCI (1.536 g, 8.0 mmol), HOBt (0.6486 g, 4.8 mmol), and triethylamine (TEA, 1.3675 mL) were combined in 75 mL dry DCM under Ar. The resulting mixture was stirred at RT for 12 hours before 10 mL H_2O was added and the mixture was extracted by DCM (3x20 mL); the combined organic phase was then dried over Na_2SO_4, filtered, evaporated, and separated via column chromatography to give **7** (1.534 g, 2.68 mmol, 71%). ^{1}H NMR (400 MHz, Chloroform-*d*) δ 7.83 (dd, *J* = 2.4, 0.9 Hz, 1H), 7.39 (dd, *J* = 8.4, 0.9 Hz, 1H), 7.24 (d, *J* = 2.4 Hz, 1H), 6.58 (d, *J* = 1.0 Hz, 2H), 6.17 (t, *J* = 6.5 Hz, 1H), 4.73 (d, *J* = 1.0 Hz, 2H), 4.68 (d, *J* = 6.4 Hz, 2H), 3.88 (d, *J* = 0.9 Hz, 6H), 0.96 (d, *J* = 0.9 Hz, 9H), 0.11 (d, *J* = 0.9 Hz, 6H); ^{13}C NMR (101 MHz, $CDCl_3$) δ 166.22, 157.58, 145.50, 139.87, 133.93, 131.86, 121.83, 121.53, 113.82, 101.42, 64.90, 56.04, 43.48, 26.03, 18.53, -5.09. HR-MS (ESI, positive mode): *m/z* calc'd for $C_{23}H_{32}Br_2NO_4Si$ $[M+H]^+$: 574.0447, found 574.0463.

Dimethyl 2'-((4-(((tert-butyldimethylsilyl)oxy)methyl)-2,6-dimethoxybenzamido)-methyl)-[1,1':4',1''-terphenyl]-4,4''-dicarboxylate (8). To **7** (1 g, 0.0017 mol) was added (4-(methoxycarbonyl)phenyl)boronic acid (0.942 g, 0.0052 mol), CsF (1.591 g, 0.0105 mol), and Pd(dppf)Cl_2 (0.128 g, 0.00017 mol); the solids were collected in a Schlenk flask and put under vacuum. Degassed dioxane (45 mL) was added to the flask; the resulting solution was stirred at 90 °C for 3 days, after which the solution was allowed to cool to RT, filtered through celite, rid of dioxane via rotary evaporation, dried under vacuum and purified via column chromatography to yield **8** (0.95 g, 1.4 mmol, 80%). ^{1}H NMR (400 MHz, Chloroform-*d*) δ 8.15 – 8.10 (m, 4H), 7.99 (d, *J* = 1.9 Hz, 1H), 7.78 – 7.72 (m, 2H), 7.60 (dd, *J* = 7.9, 1.9 Hz, 1H), 7.51 – 7.45 (m, 2H), 7.36 (d, *J* = 7.9 Hz, 1H), 6.53 (s, 2H), 5.98 (t, *J* =

6.0 Hz, 1H), 4.70 (s, 2H), 4.68 (d, *J* = 6.0 Hz, 2H), 3.96 (d, *J* = 2.8 Hz, 6H), 3.71 (s, 6H), 0.94 (s, 9H), 0.10 (s, 6H); ^{13}C NMR (101 MHz, $CDCl_3$) δ 167.11, 167.01, 166.13, 157.55, 145.34, 145.30, 145.02, 140.23, 140.05, 136.57, 130.49, 130.24, 129.85, 129.48, 129.39, 129.27, 127.30, 127.20, 126.09, 114.05, 101.43, 64.88, 56.00, 52.37, 52.33, 41.48, 26.02, 18.52, -5.10. HR-MS (ESI, positive mode): *m/z* calc'd for $C_{39}H_{46}NO_8Si$ $[M+H]^+$: 684.2993, found 684.3101.

2'-((4-(Hydroxymethyl)-2,6-dimethoxybenzamido)methyl)-[1,1':4',1''-terphenyl]-4,4''-dicarboxylic acid (H_2TP-OH). To **8** (0.6911 g, 1.01 mmol) was added NaOH (4.04 g, 101 mmol, 50 eq. per ester group) and MeOH and H_2O in a 1:1 ratio (20 mL: 20 mL). The resulting mixture was stirred at 40 °C for 1 day; it was then allowed to cool to RT before being acidified (while being stirred) to pH~1-2 by addition of concentrated HCl; the acidic solution was left to stir for 2 hours to ensure the completion of the acid-base reaction. The resulting solution was filtered, washed with H_2O and dried under vacuum to produce H_2TP-OH (**9**, 0.493 g, 0.91 mmol, 90%).^{1}H NMR (400 MHz, DMSO-d_6) δ 12.99 (s, 2H), 8.63 (t, *J* = 6.0 Hz, 1H), 8.11 – 8.03 (m, 4H), 7.97 (d, *J* = 2.0 Hz, 1H), 7.88 – 7.82 (m, 2H), 7.72 (dd, *J* = 8.0, 1.9 Hz, 1H), 7.63 – 7.56 (m, 2H), 7.40 (d, *J* = 8.0 Hz, 1H), 6.63 (s, 2H), 4.49 (s, 2H), 4.37 (d, *J* = 5.9 Hz, 2H), 3.63 (s, 6H). sSee Figure 15. ^{13}C NMR (101 MHz, DMSO-d_6) δ 167.14, 167.12, 164.90, 156.53, 145.24, 144.26, 144.16, 139.30, 138.55, 137.25, 130.10, 130.01, 129.80, 129.70, 129.42, 129.38, 126.77, 126.34, 125.29, 114.89, 101.87, 62.90, 55.55, 25.81. See Figure 16. HR-MS (ESI, positive mode): *m/z* calc'd for $C_{31}H_{28}NO_8$ $[M+H]^+$: 542.1815, found 542.1780.

Dimethyl 2'-((4-(hydroxymethyl)-2,6-dimethoxybenzamido)methyl)-[1,1':4',1''-terphenyl]-4,4''-dicarboxylate (9). Compound **8** (500 mg, 0.730 mmol) was added to tetrabutylammonium fluoride solution in THF (1M, 5 mL) and stirred at RT for 2 hours. 10 mL saturated NH_4Cl solution was added and THF was removed via rotary evaporation. White precipitate was filtered and washed with water to produce compound **9** (395 mg, 0.694 mmol, 95%). ^{1}H NMR (400 MHz, Chloroform-d) δ 8.16 – 8.11 (m, 4H), 7.97 (d, J = 12.9 Hz, 1H), 7.75 (dd, J = 8.5, 2.3 Hz, 2H), 7.64 – 7.59 (m, 1H), 7.53 – 7.45 (m, 2H), 7.37 (dd, J = 7.9, 3.3 Hz, 1H), 6.56 (s, 2H), 5.96 (t, J = 6.3 Hz, 1H), 4.81 – 4.64 (m, 4H), 3.96 (d, J = 3.1 Hz, 6H), 3.73 (s, 6H). ^{1}H NMR (400 MHz, DMSO-d_6) δ 8.63 (t, *J* = 5.9 Hz, 1H), 8.09 (dd, *J* = 12.7, 7.9 Hz, 4H), 7.98 (s, 1H), 7.88 (d, *J* = 8.0 Hz, 2H), 7.74 (d, *J* = 8.1 Hz, 1H), 7.63 (d, *J* = 7.9 Hz, 2H), 7.41 (d, *J* = 7.8 Hz, 1H), 6.63 (s, 2H), 5.27 (s, 1H), 4.49 (s, 2H), 4.37 (d, *J* = 5.8 Hz, 2H), 3.90 (d, *J* = 4.4 Hz, 6H), 3.62 (s, 6H). ^{13}C NMR (101 MHz, DMSO-d_6) δ 166.08, 166.04, 164.88, 156.51, 145.24, 144.64, 144.51, 139.23, 138.43, 137.28, 130.12, 129.87,

129.59, 129.23, 128.65, 128.56, 126.93, 126.37, 125.35, 114.87, 101.87, 62.89, 55.56, 52.24, 52.21, 40.15. HR-MS (ESI, positive mode): *m/z* calc'd for $C_{33}H_{32}NO_8$ $[M+H]^+$: 570.2128, found 570.2111.

Dimethyl (S)-2'-((4-(((((4,11-diethyl-4-hydroxy-3,14-dioxo-3,4,12,14-tetrahydro-1H-pyrano[3',4':6,7]indolizino[1,2-b]quinolin-9-yl)oxy)carbonyl)-oxy)methyl)-2,6-dimethoxy-benzamido)methyl)-[1,1':4',1''-terphenyl]-4,4''-dicarboxylate (Me_2TP-SN). Compound **10** (500 mg, 0.878 mmol), 4-nitrophenyl chloroformate (442 mg, 2.195 mmol), TEA (366 µL, 2.634 mmol) were combined in dry DCM (30 mL) under Ar and stirred for 1 day at RT. The resulting solution was quenched with 5 mL H_2O and extracted with DCM, dried over Na_2SO_4, filtered, concentrated by rotary evaporation, and then dried completely under vacuum to produce dimethyl 2'-((2,6-dimethoxy-4-((((4-nitrophenoxy)carbonyl)oxy)methyl)-benzamido)methyl)-[1,1':4',1''-terphenyl]-4,4''-dicarboxylate (**10**), which was used directly in the next step without purification.

To a solution of **10** (500 mg, 0.681 mmol) in DCM (20 mL) was added SN38 (668 mg, 1.702 mmol) and TEA (284 µL, 2.043 mmol); the resulting mixture was stirred at RT for 1 day before being washed with H_2O and extracted with DCM (3x20 mL). The organic phases were combined, dried over Na_2SO_4, filtered, concentrated by rotary evaporation, dissolved in minimal DCM, and purified via large TLC plate chromatography (5% MeOH in DCM) to give Me_2TP-SN (134 mg, 0.136 mmol, 20%). ^{1}H NMR (400 MHz, Chloroform-*d*) δ 8.24 (d, *J* = 9.2 Hz, 1H), 8.13 (ddd, *J* = 10.2, 6.1, 2.8 Hz, 4H), 7.99 (d, *J* = 1.9 Hz, 1H), 7.91 (d, *J* = 2.6 Hz, 1H), 7.78 – 7.74 (m, 2H), 7.74 – 7.69 (m, 4H), 7.64 (s, 1H), 7.64 – 7.60 (m, 2H), 7.50 (d, *J* = 8.3 Hz, 2H), 7.42 (d, *J* = 7.9 Hz, 1H), 6.65 (s, 2H), 6.07 (t, *J* = 6.0 Hz, 1H), 5.73 (d, *J* = 16.3 Hz, 1H), 5.26 (d, *J* = 11.3 Hz, 4H), 4.77 (d, *J* = 6.1 Hz, 2H), 3.95 (d, *J* = 2.4 Hz, 6H), 3.75 (s, 6H), 3.14 (q, *J* = 7.7 Hz, 2H), 1.89 (ddt, *J* = 16.9, 14.2, 7.1 Hz, 2H), 1.38 (t, *J* = 7.7 Hz, 3H), 1.03 (t, *J* = 7.3 Hz, 3H). See Figure 17. ^{13}C NMR (101 MHz, $CDCl_3$) δ 174.00, 167.09, 165.58, 157.77, 157.74, 153.40, 152.33, 150.31, 149.88, 147.65, 146.90, 145.54, 145.36, 145.10, 140.67, 140.05, 139.67, 139.30, 137.72, 136.46, 132.48, 131.75, 131.00, 130.72, 130.36, 130.24, 129.99, 129.25, 129.22, 127.56, 127.52, 127.44, 127.24, 127.13, 126.99, 126.12, 124.72, 118.84, 116.13, 114.26, 104.32, 98.24, 72.89, 70.61, 66.47, 56.25, 52.34, 52.32, 49.51, 41.60, 31.75, 23.32, 14.13, 7.96. See Figure 18. HR-MS (ESI, positive mode): *m/z* calc'd for $C_{56}H_{50}N_3O_{14}$ $[M+H]^+$: 988.3293, found 988.3273.

(S)-4,11-diethyl-4-hydroxy-3,14-dioxo-3,4,12,14-tetrahydro-1H-pyrano[3',4':6,7]-indolizino[1,2-b]quinolin-9-yl (3,5-dimethoxybenzyl) carbonate (MeO-SN). Compound **1** (500 mg, 2.972 mmol), 4-nitrophenyl chloroformate (1.497 g, 7.430 mmol), TEA (1.240 mL,

8.916 mmol) were combined in dry DCM (50 mL) under Ar and stirred for 1 day at RT. The resulting solution was quenched with 5 mL H_2O and extracted with DCM, dried over Na_2SO_4, filtered, concentrated by rotary evaporation, and then dried completely under vacuum to produce dimethyl 3,5-dimethoxybenzyl (4-nitrophenyl) carbonate (**11**), which was used directly in the next step without purification.

To a solution of **11** (500 mg, 1.500 mmol) in DCM (30 mL) was added SN38 (1471 mg, 3.750 mmol) and TEA (626 µL, 4.500 mmol); the resulting mixture was stirred at RT for 1 day before being washed with H_2O and extracted with DCM (3 x 20 mL). The organic phases were combined, dried over Na_2SO_4, filtered, concentrated by rotary evaporation, dissolved in minimal DCM, and purified via column chromatography to give MeO-SN (264 mg, 0.450 mmol, 30%).^{1}H NMR (400 MHz, $CDCl_3$) δ 8.25 (d, *J* = 9.2 Hz, 1H), 7.92 (d, *J* = 2.6 Hz, 1H), 7.68 (s, 1H), 7.65 (dd, *J* = 9.2, 2.6 Hz, 1H), 6.61 (d, *J* = 2.3 Hz, 2H), 6.47 (t, *J* = 2.3 Hz, 1H), 5.74 (d, *J* = 16.4 Hz, 1H), 5.30 (d, *J* = 16.5 Hz, 1H), 5.26 (d, *J* = 3.6 Hz, 4H), 3.82 (s, 6H), 3.15 (q, *J* = 7.7 Hz, 2H), 1.88 (dq, *J* = 17.0, 7.1 Hz, 2H), 1.39 (t, *J* = 7.7 Hz, 3H), 1.03 (t, *J* = 7.4 Hz, 3H). See Figure 19. ^{13}C NMR (101 MHz, $CDCl_3$) δ 173.93, 161.23, 157.72, 153.41, 151.89, 150.38, 150.10, 147.10, 146.56, 146.09, 136.73, 132.03, 127.60, 127.55, 125.08, 119.01, 114.27, 106.44, 100.87, 98.68, 72.90, 70.80, 66.43, 55.58, 49.57, 31.77, 23.40, 14.10, 7.96. Figure 20. HR-MS (ESI, positive mode): *m/z* calc'd for $C_{32}H_{31}N_2O_9$ $[M+H]^+$: 587.2030, found 587.2009.

MOF Synthesis and characterization:

Synthesis of Hf-TP-OH. $HfCl_4$ and H_2TP-OH were separately dissolved in dimethylformamide (DMF) at a concentration of 2 mg/mL. 500 µL $HfCl_4$ solution and 500 µL H_2TP-OH were then combined in a 1-dram vial with the addition of 1 µL trifluoracetic acid and 5 µL water as modulators. The mixture was heated in an oven at 80 °C for 1 day, after which the white precipitate was collected by centrifugation and sequentially washed with DMF, 1% triethylamine (TEA) in ethanol (EtOH) (v/v), and EtOH to afford Hf-TP-OH in 88% yield based on H_2TP-OH.

Synthesis of Hf-TP-SN via post-synthetic modification. 10 mL Hf-TP-OH was washed with dry acetonitrile (ACN) twice and dispersed in ACN with a ligand concentration of 3.0 mM. 4-nitrophenyl chloroformate (15.1 mg, 75 µmol), and TEA (12.5 µL, 90 µmol) were then added, and the solution was stirred for 2 days to afford Hf-TP-NO_2 nMOF. The mixture was then centrifuged, washed with ACN for 3 times and redispersed in ACN before the addition of SN38 (11.8 mg, 30 µmol) and TEA (6.3 µL, 45 µmol); the solution was then

stirred for 2 more days. The as-synthesized Hf-TP-SN was washed with 10% dimethyl sulfoxide (DMSO) in ACN 6 times and dispersed in EA for storage.

Digestion of Hf-MOFs for UV-Vis spectroscopic measurements. 50 μL Hf-TP-OH or Hf-TP-SN solution, 900 μL DMSO and 50 μL H_3PO_4 were mixed and sonicated for 1 hour and let stand overnight, after which the mixture was diluted to a proper concentration for UV-Vis measurement. The absorbance of H_2TP-OH at 304 nm was used to calculate the concentration of H_2TP-OH in Hf-TP-OH or Hf-TP-SN after comparison with the standard curve of H_2TP-OH in DMSO, while the absorbance of SN38 at 390 nm was used to calculate the concentration of SN38 in Hf-TP-SN after comparison with the standard curve of SN38 in DMSO.

Digestion of Hf-TP-SN for quantification of SN38 by LC-MS. 100 μL 1M $NaHCO_3$ solution was added to 100 μL Hf-TP-SN dispersion in water (total SN concentration: 100 μM). The mixture was sealed and sonicated for 20 minutes, after which 100 μL PBS (200 mM, pH 4.0) was added to adjust the pH to 7. 100 μL saturated NaCl solution and 150 μL ethyl acetate (EA) were then added before vortexing the mixture for 1 minute. The EA layer after centrifugation was analyzed with LC-MS. For HPLC, absorption of SN38 at 380 nm was used to calculate the concentration of free SN38 after comparison with the standard curve of SN38 in EA. For LC-MS, extracted ion chromatogram (EIC) at m/z value of 393.1450 was used to calculate the concentration of free SN38 after comparison with the standard curve of SN38 in EA.

Stability of Hf-TP-SN in PBS. Hf-TP-SN was dispersed in 1 mL PBS (1 mM) with a Hf concentration of 5.2 mM. 200 uL suspension was taken after incubation for 1, 2, 4, 8, and 24 hours and centrifuged for PXRD measurement.

Total ROS generation in test tubes. Total ROS generation under irradiation was detected by the 2',7'-dichlorodihydrofluorescein (DCFH) assay following reported procedures.[46] 1 mL DCFH-DA (1mM) in DMSO was hydrolyzed by 4 mL NaOH (0.01 M) solution in the dark for 30 minutes and stopped by adding 20 mL PBS (25 mM, pH 7.4). The freshly prepared DCFH was then added to the PBS suspension (pH 7, 10 mM) of Hf-TP-OH or Hf-TP-SN at the same Hf concentration. In the final mixture, the concentration of DCFH was 10 μM while the concentration of Hf was 40 μM. The PBS solution with the same DCFH concentration served as a blank control. 100 μL of each suspension was added to 96-well plates (n = 6) and then irradiated with X-ray at 0, 1, 2, 3, 5, or 10 Gy, respectively. The fluorescence signal (em. 520/20 nm) was collected with a Synergy HTX microplate reader (ex. 485/20 nm; Agilent Technologies, Santa Clara, California, United States of America).

Hydroxyl radical generation in test tubes. Hydroxyl radical (·OH) generation under irradiation was detected by the APF assay. APF assay was added to the PBS suspension of Hf-TP-OH or Hf-TP-SN at the same Hf concentration. In the final mixture, the concentration of APF was 5 μM while that of Hf was 40 μM. The PBS solution with the same APF concentration served as a blank control. 100 μL of each suspension was added to 96-well plates (n = 6) and then irradiated with X-ray at 0, 1, 2, 3, 5, or 10 Gy, respectively. The fluorescence signal (em. 520/20 nm) was collected with a Synergy HTX microplate reader (ex. 485/20 nm; Agilent Technologies, Santa Clara, California, United States of America).

Hydroxyl radical triggered SN38 release in test tubes. Hf-TP-SN or MeO-SN was dispersed in H_2O at the same concentration of total SN38 (100 μM). $FeCl_3$, (+)-Sodium L-ascorbate, $Na_2(EDTA)\cdot 2H_2O$ (ethylenediaminetetraacetic acid, disodium salt dihydrate) was firstly dissolved in water to reach a concentration of 10 mM separately (10.5 mM for $Na_2(EDTA)\cdot 2H_2O$). Then, 100 μL of each solution and 50 μL H_2O_2 (200 mM in H_2O) was added to Hf-TP-SN or MeO-SN solution to generate hydroxyl radical in situ and to trigger the release of SN38. For control group, only H_2O_2 was added. After 8h incubation at RT, additional 100 μL 1M $NaHCO_3$ was added to Hf-TP-SN to digest the nMOF, after which the mixture was sealed and sonicated for 20 minutes before the addition of 100 μL PBS (200 mM, pH 4) to adjust the pH to 7. 100 μL saturated NaCl solution and 150 μL ethyl acetate (EA) were added before vortexing the Hf-TP-SN or MeO-SN mixture for 1 minute. The EA layer after centrifugation was analyzed by LC-MS.

X-ray triggered release in test tubes. Hf-TP-SN or MeO-SN were dispersed in H_2O (10 mM, pH = 7.4) at the same concentration of total SN38 (100 μM). 100 μL Hf-TP-SN or MeO-SN suspension was irradiated with 10 Gy X-ray. 100 μL 1M $NaHCO_3$ was added to Hf-TP-SN to digest the nMOF, after which the mixture was sealed, sonicated for 20 minutes, and sat 15h before the addition of 100 μL PBS (200 mM, pH 4.0) to adjust the pH to 7. 100 μL saturated NaCl solution and 150 μL ethyl acetate (EA) were added before vortexing the Hf-TP-SN or MeO-SN mixture for 1 minute. The EA layer after centrifugation was analyzed by HPLC.

In vitro experiments:

Dark toxicity. CT26 cells were cultured in RPMI-1640 medium supplemented with 10% fetal bovine serum, 1% HyClone penicillin-streptomycin 100X solution, and cultured in a humidified atmosphere containing 5% CO_2 at 37°C. The cytotoxicity of H_2TP-OH, Hf-TP-OH, and Hf-TP-SN on CT26 cells was detected by MTS assay. CT26 cells were seeded in 96-well plates at a density of 2500 cells/well. Different concentrations of H_2TP-OH, Hf-TP-

OH and Hf-TP-SN were added and 24 hours later 10% (v/v) of MTS reagent was added to each well. 90 minutes later the absorbance of each well at 490 nm was read by a Synergy HTX plate reader (Agilent Technologies, Santa Clara, California, United States of America) to calculate cell viability.

Clonogenic assay. CT26 cells were seeded in 6-well plates at a density of 1.5×10^5 cells/well and cultured overnight. The cells were incubated with PBS, Hf-TP-OH, or Hf-TP-SN at an equivalent metal concentration of 50 μM for 4 hours, and then irradiated with 0, 2, 4, 6 and 8 Gy X-ray ($n = 3$). The cells were washed with PBS twice and then trypsinized to afford single cell suspensions. The cells were counted and diluted, then 200 cells were seeded in each well of 6-well plates and cultured in 2 mL medium for another 7 days. Then, the plates were rinsed once with PBS, fixed by 4% paraformaldehyde for 20 minutes, and washed with PBS twice at RT. After that, the 6-well plates were scanned with a cell analysis system sold under the tradename INCUCYTE® S3 (Sartorius Bioanalytical Instruments, Inc., Brooklyn Center, Minnesota, United States of America) in the whole well mode with a 4× objective. The colonies were identified with software available under the tradename INCUCYTE® 2021A (Sartorius Bioanalytical Instruments, Inc., Brooklyn Center, Minnesota, United States of America) in a cellular resolution and the confluence was used as a parameter to calculate the plating efficiency (PE) and surviving fraction (SF):

$$PE = \text{Confluence}\ (0\ Gy, PBS)/\text{Cell}\ \#\ (0\ Gy, PBS)$$

$$SF\ (D, MOF) = \text{Confluence}\ (D, MOF)/\text{Cell}\ \#\ (D, MOF) \times \text{PE}$$

Where D was the radiation dose and Cell # (*D, MOF*) was the number of cells seeded for a certain radiation dose D and a certain treatment group.

The dose modifying ratio at a 10% ($DMR_{10\%}$) was used as a parameter to assess radiosensitization effect and defined as the ratio of doses under reference conditions to produce a 10%[52]:

$$DMR_{10\%} = DMR_{10\%}\ (PBS) / DMR_{10\%}\ (MOF)$$

Hydroxyl radical generation. To demonstrate ·OH generation, CT26 cells were seeded in cell culture dishes at a density of 1.5×10^5 and cultured overnight. Hf-TP-OH was added at an equivalent Hf concentration of 50 μM and further incubated in a 37°C incubator for 4 hours. The cells were washed with PBS solution 3 times and 1 mL cell culture medium containing with 10 μM HPF was added and incubated at 37°C for another 30 minutes. Then the cells were irradiated with X-ray (3 Gy) and cultured in the cell incubator for another 24 h.

After that, the cells were washed with PBS for three times and further incubated with Hoechst 33342 (10 μg mL^{-1}) in PBS for 10 minutes in the cell incubator. Finally, the cells were washed with PBS 3 times and observed on a Leica Stellaris 8 confocal microscope (Leica Microsystems, Wetzlar, Germany).

Dark toxicity. The cytotoxicity of SN38 and Me_2TP-SN on CT26 cells were detected by MTS assay. CT26 cells were seeded in 96-well plates at a density of 2500 cells/well. Different concentrations of SN38 and Me_2TP-SN were added and 48 hours later, 10% (v/v) of MTS reagent was added to each well. 90 minutes later the absorbance of each well at 490 nm was read by a Synergy HTX plate reader (Agilent Technologies, Santa Clara, California, United States of America) to calculate cell viability.

Cellular uptake. The cellular uptake of Hf-TP-SN (Hf: 50 μM) was evaluated on CT26 cells. The cells were seeded in 6-well plates at a density of 2×10^5/well and cultured overnight. Hf-TP-SN was added at a Hf concentration of 50 μM into the medium ($n = 3$). The cells were incubated in a 37 °C incubator for 1, 2, and 6 hours. At each time point, the medium was aspirated, the cells were washed with PBS three times, collected by centrifugation, and counted with a hemocytometer. The cell pellets were digested with nitric acid for 24 h and the concentration of Hf was detected by ICP-MS.

ROS generation. To demonstrate the generation of ROS, CT26 cells were seeded in cell culture dishes at a density of 1.5×10^5 and cultured overnight. Hf-TP-SN or Hf-TP-OH was added at a Hf concentration of 50 μM and further incubated in a 37°C incubator for 4 hours. The cells were washed with PBS solution 3 times and 1 mL cell culture medium containing with 30 μM DCFH-DA was added and incubated at 37°C for another 30 minutes. Then the cells were irradiated with X-ray (3 Gy) and cultured in the cell incubator for another 24 h. After that, the cells were washed with PBS three times and further incubated with Hoechst 33342 (10 μg mL^{-1}) in PBS for 10 minutes. Finally, cells were washed with PBS 3 times and observed on a Leica Stellaris 8 confocal microscope (Leica Microsystems, Wetzlar, Germany).

DNA damage. For CLSM imaging, CT26 cells were seeded in cell culture dishes at a density of 1.5×10^5. The cells were treated in the same way as in the clonogenic assay. 24 hours after radiation, the cells were washed with PBS and fixed with 4% paraformaldehyde at RT for 20 minutes. The cells were again rinsed with PBS, blocked and permeabilized with 5% FBS + 0.3% Triton-X in PBS at RT for 1 hour. After blocking, cells were incubated with the γ-H2AX primary antibody (1:500) in 1% BSA + 0.3% Triton-X in PBS at RT for 1 hour.

The cells were then washed with PBS and incubated with the Alexa Fluor 488 conjugated secondary antibody (1:3000) in 1% BSA + 0.3% Triton-X in PBS at RT for 1 hour. Afterwards, the cells were washed with PBS and further incubated with Hoechst 33342 (10 μg mL^{-1}) in PBS for 10 minutes at 37 °C to visualize cell nuclei, respectively. Finally, cells were washed with PBS 3 times and observed on a Leica Stellaris 8 confocal microscope (Leica Microsystems, Wetzlar, Germany).

Apoptotic cell death. To quantify apoptosis, CT26 cells were seeded in 6-well plates at a density of 1.5 × 10^5/well and cultured overnight. Hf-TP-OH or Hf-TP-SN was added at an equivalent metal concentration of 50 μM for 4 hours and irradiated with X-ray (3 Gy). 24 hours later, the cells were washed with PBS, trypsinized to afford single cell suspensions, cells were stained with the dead cell apoptosis kit with annexin V Alexa Fluor 488 & PI following the manufacturer's protocol and resuspended in the binding buffer for flow cytometric analysis (Annexin-V in FITC channel, PI in PE-dazzle 594 channel).

In vivo experiments:

Anti-cancer efficacy. BALB/c mice (6-8 weeks) were obtained from Charles River Laboratories, Inc (Wilmington, Massachusetts, United States of America) and bred in house at the animal facility at the University of Chicago (Chicago, Illinois, United States of America). To evaluate the in vivo therapeutic efficacy, CT26 tumor models were established on BALB/c mice by inoculating 2 × 10^6 cells/mouse subcutaneously onto the right flanks at day 0, respectively. When CT26 tumors reached ~85 mm^3, the mice were randomized for treatments. PBS, irinotecan, Hf-TP, or Hf-TP-SN was intratumorally injected with an equivalent metal dose of 0.5 μmol in 20 μL PBS and SN38 dose of 0.047 μmol in 20 μL PBS. The dose of irinotecan was 0.047 μmol in 20 μL PBS. 6-8 hours later, the mice were anaesthetized with 2.5% (v/v) isoflurane/O_2 and mounted onto the X-Rad 225 irradiator. The CT26 tumors were irradiated with 2 Gy X-ray/fraction for 3 consecutive days. The length and width of tumor tissues were measured with an electronic caliper (tumor volume = length × $width^2/2$) and body weights were monitored with an electronic scale. At the endpoint of the experiments, the mice were euthanized, and the tumors and major organs were sectioned for hematoxylin-eosin (H&E) staining to evaluate general toxicity. The tumor growth inhibition index (TGI) was defined as the equation below:[13]

$$TGI = 1 - \frac{\frac{T_e}{T_s} \Big/ \frac{C_e}{C_s}}{1 - \frac{C_s}{C_e}}$$

where T_e, T_s, C_e, and C_s represent average tumor volumes of treated mice at endpoint, treated mice at starting-point, control mice at endpoint and control mice at starting-point, respectively.

Immunohistochemistry analysis. To evaluate DNA damage and tumor proliferation after different treatments, a group of CT26-bearing mice were established and treated in the same way as in antitumor efficacy experiments. The mice were euthanized one day after the last irradiation. The tumors were excised and fixed in 4% PFA for 48 h and 70% ethanol for 1 day. The tissues were embedded in paraffin, sectioned and stained for H&E, γ-H2AX, Ki67 and TUNEL by Human Tissue Resource Center at the University of Chicago. Briefly, the slides were deparaffinized and rehydrated using xylenes and serial dilutions of ethanol to distilled water. Then the slides were treated with antigen retrieval buffer (AR9640; Leica Biosystems, Wetzlar, Germany) and heated in a steamer at 97°C for 20 minutes. After washing with tris-buffered saline (TBS), the slides were incubated with primary γ-H2AX antibody (1:400) or primary Ki67 antibody (Thermo Fisher Scientific, Clone# SP6, 1:400; Thermo Fisher Scientific, Waltham, Massachusetts, United States of America) at RT for 1 hour in a wet chamber. The slides were washed with TBS, then γ-H2AX and Ki67 slides were incubated with anti-rabbit-polymer (Bond Polymer Refine Detection, Leica Biosystems, DS9800; Leica Biosystems, Wetzlar, Germany) for 30 minutes at RT. The antigen-antibody binding was detected with the 3,3′-Diaminobenzidine (DAB) (DAKO, K3468; Agilent Technologies, Santa Clara, California, United States of America) system. Tissue sections were then immersed in hematoxylin for counterstaining and covered with cover glasses. The slides were scanned on a CRi Pannoramic SCAN 40× whole slide scanner (3DHISTECH LTD, Budapest, Hungary). The images were analyzed with QuPath-0.2.3 software.

EXAMPLE 2

Hf-TP-SN nMOF

Synthesis and characterization of Hf-TP-SN:

SN38 was conjugated to Hf-TP-OH nMOF via the 3,5-dimethoxylbenzyl carbonate linkage, which can be cleaved by hydroxyl radical (·OH).[38] Hf-TP-SN was synthesized via a combination of pre-functionalization and post-synthetic modification. See Figure 1. The terphenyl dicarboxylate ligand was pre-functionalized with dimethoxybenzyl alcohol via an amide bond, incorporated into a Hf-nMOF, and then post-synthetically modified with SN38 via a carbonate bond.

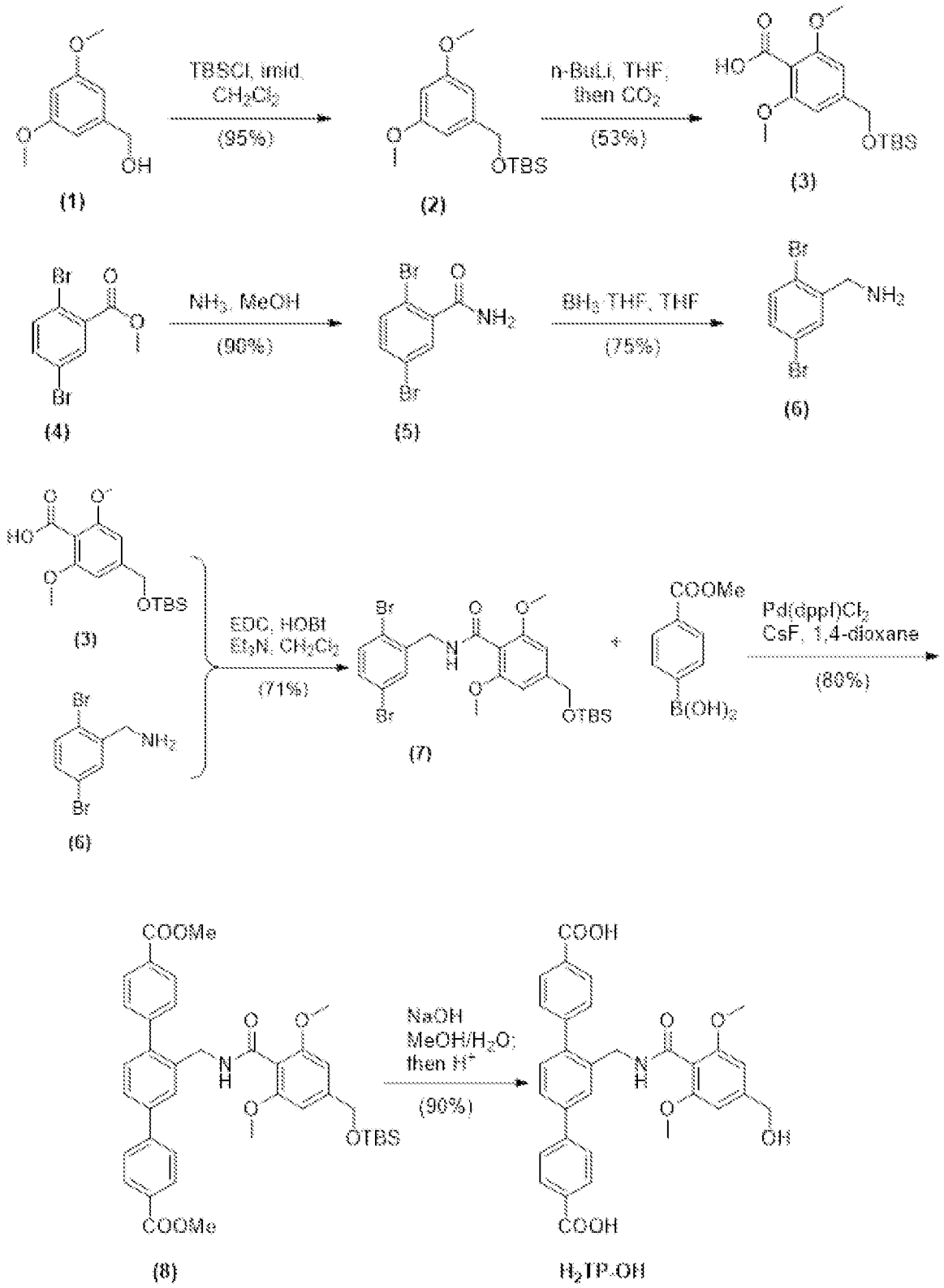

Scheme 1. Synthetic route for H_2TP-OH.

First, the dicarboxylic acid H_2TP-OH was synthesized in five steps starting from 3,5-dimethoxylbenzyl alcohol (**1**) via protection with *tert*-butyldimethylsilyl group, lithiation and

carboxyl group installation, coupling with 2,5-dibromobenzylamine via an amide bond, Suzuki coupling with (4-(methoxycarbonyl)phenyl)boronic acid, and base-catalyzed hydrolysis. See Scheme 1. Next, Hf-TP-OH nMOF with Hf_{12} SBUs was synthesized via a solvothermal reaction between $HfCl_4$, H_2TP-OH, trifluoracetic acid, and water in *N, N*-dimethylformamide at 80 °C for 1 day. Finally, Hf-TP-OH was treated with 4-nitrophenyl chloroformate followed by SN38 to afford Hf-TP-SN.

Hf-TP-OH and Hf-TP-SN both displayed a nanoplate morphology with a diameter of ~70 nm and a thickness of ~10 nm by transmission electron microscopy (TEM). See Figures 2A and 2C. The high-resolution TEM (HRTEM) image and its fast Fourier transform (FFT) pattern of Hf-TP-OH demonstrated the crystallinity and 6-fold symmetry, consistent with the projection of Hf_{12}-TP structure along the vertical direction. See Figure 2B.

The number-averaged sizes of Hf-TP-OH and Hf-TP-SN were 125 ± 4 and 124 ± 2 nm (see Figure 3A), respectively, while their ζ-potentials were -11.2 ± 1.2 and -10.3 ± 0.4 mV (see Figure 3B), respectively, suggesting that Hf-TP-OH maintained the nanoscale size and surface charge after post-synthetic modification. Powder X-ray diffraction (PXRD) studies confirmed that Hf-TP-SN and Hf-TP-OH adopted the same structure as Hf_{12}-TP MOF consisting of $Hf_{12}(\mu_3\text{-}O)_8(\mu_3\text{-}OH)_8(\mu_2\text{-}OH)_6$ SBUs and TP ligand in a *hcp* topology.[44] See Figure 3C. Moreover, Hf-TP-SN retained its crystallinity after incubation in PBS (1 mM, pH 7.4) for 24 hours (see Figure 3D), ensuring its stability for biological applications.

UV-Vis spectroscopic analysis of digested Hf-TP-SN indicated ~16% of TP-OH ligands were conjugated with SN38 (see Figures 4A-4E) after comparing the absorbance of TP-OH ligand and SN38 with their standard curves.

Liquid chromatography-mass spectrometry (LC-MS) analysis indicated the trapping of 2.6% free SN38 (relative to total SN38) in the pores after digesting Hf-TP-SN using $NaHCO_3$[45] and extraction with ethyl acetate. After determining the Hf content by inductively coupled plasma mass spectrometry (ICP-MS), the formula of Hf-TP-SN was determined as $Hf_{12}(\mu_3\text{-}O)_8(\mu_3\text{-}OH)_8(\mu_2\text{-}OH)_6(\text{TP-SN})_{1.08}(\text{TP-OH})_{5.66}(OH)_{4.52}(H_2O)_{4.52}(\text{SN38})_{0.03}$.

ROS generation and X-ray triggered release:

A molecular counterpart, Me_2TP-SN, was synthesized from Me_2TP-OTBS (**5**) to support the post-synthetic modification and to examine the cytotoxicity of the prodrug. See Scheme 2. Because of low aqueous solubility of Me_2TP-SN, MeO-SN was synthesized from **1** and used as a homogeneous control. See Scheme 3.

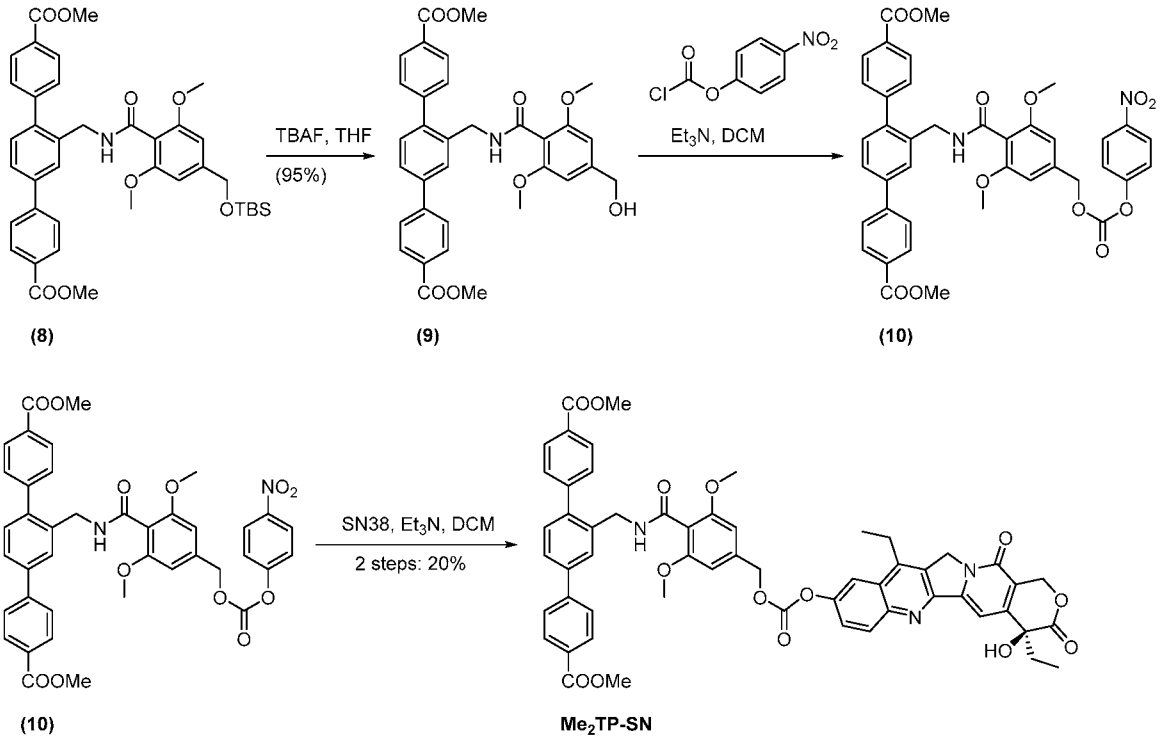

Scheme 2. Synthesis of Me_2TP-SN.

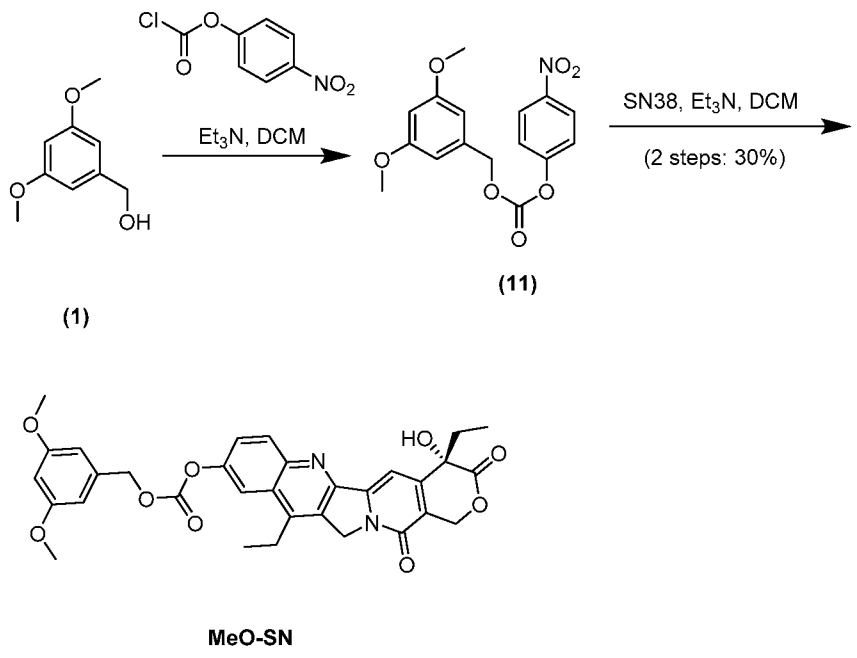

Scheme 3. Synthesis of MeO-SN.

ROS generation was evaluated by 2',7'-dichlorodihydrofluorescein (DCFH) assay.[46] The total ROS signals in PBS, Hf-TP-OH, and Hf-TP-SN groups all increased linearly with X-ray doses. The relative enhancements of Hf-TP-OH and Hf-TP-SN over PBS were 47% and 19%, respectively See Figure 5A. Aminophenyl fluorescein (APF) assay showed that Hf-

TP-OH and Hf-TP-SN enhanced ·OH generation by 96% and 59%, respectively, over PBS. See Figure 5B. The reduced ROS and hydroxyl radical signals from Hf-TP-SN are likely due to the consumption of ·OH by the 3,5-dimethoxylbenzyl carbonate linkage to release SN38.

High performance-liquid chromatography analyses showed that Hf-TP-SN released ~1.35% of total SN38 after 10 Gy X-ray irradiation, which was 5-fold higher than SN38 released from MeO-SN under identical conditions. See Figure 5C. The triggered release of SN38 was confirmed using OH generated by the Fenton reaction;[47] Hf-TP-SN showed 14.8-fold higher SN38 release than MeO-SN under this condition. See Figure 5D. These results showed that upon X-ray irradiation, electron-dense Hf_{12} SBUs serve as radiosensitizers to enhance ·OH generation for the triggered release of SN38 via hydroxylation of the 3,5-dimethoxylbenzyl carbonate followed by 1,4-elimination. See Figure 1.

In vitro experiments:

MTS assays revealed that H_2TP-OH ligand and Hf-TP-OH nMOF did not show obvious cytotoxicity to CT26 colon carcinoma cells at a TP concentration of 100 μM (see Figures 6A and 6B), indicating their non-toxic nature without X-ray irradiation. On the other hand, clonogenic assay showed that Hf-TP-OH possessed strong radiosensitizing property with a dose modifying ratio at 10% survival fraction ($DMR_{10\%}$) of 1.255 (see Figure 6C) due to enhanced ·OH generation via radiosensitization as probed by hydroxyphenyl fluorescein (HPF) assay. See Figure 6D.

The cytotoxicity of SN38 and Me_2TP-SN38 was also evaluated. While SN38 showed a half-maximal inhibitory concentration (IC_{50}) of 0.584 μM (see Figure 7A),[33] Me_2TP-SN38 had much lower cytotoxicity with an IC_{50} of 13.5 μM (see Figure 7B), suggesting the successful construction of SN38 prodrug via the dimethoxybenzyl carbonate masking group.

The cellular uptake of Hf-TP-SN was examined before investigation of its cytotoxicity. Hf-TP-SN showed efficient and time-dependent cellular uptake as quantified by ICP-MS. See Figure 7C. To confirm X-ray triggered release of SN38, we detected the cytotoxicity of Hf-TP-SN on CT26 cells with varying doses of X-ray by clonogenic assay [denoted Hf-TP-SN(+)]. Hf-TP-SN showed a significantly increased $DMR_{10\%}$ of 2.566 over Hf-TP-OH (1.255), likely due to the combined chemo-radiotherapeutic effects of the released SN38 and X-ray irradiation. See Figure 6C. Interestingly, confocal laser scanning microscopy (CLSM) and flow cytometry studies show that Hf-TP-OH(+) and Hf-TP-SN(+) exhibited 2.29- and 9.30-fold higher intracellular ROS signals than PBS(+), respectively, at an X-ray dose of 3 Gy. See Figures 8A-8D. The stronger ROS signal in Hf-TP-SN(+) group likely

resulted from the oxidative pressure of the released SN38 on the cells and the radiosensitizing effect of electron-dense Hf_{12} SBUs.[48]

DNA double strand breaks (DSBs) were investigated in CT26 cells via detecting the expression of γ-H2AX, a phosphorylated protein biomarker for DSBs.[49] PBS(+) induced a small amount of red γ-H2AX fluorescence due to X-ray's ability to cause DNA damage.[50] More pronounced DSBs were observed in Hf-TP-OH(+) and Hf-TP-SN(+) groups, while no fluorescence was observed in Hf-TP-OH(-) group (see Figure 9), which supports potent radiosensitization by Hf-nMOFs. Hf-TP-SN(-) also showed significantly enhanced γ-H2AX signal over PBS control, likely due to the entrapped SN38 in the pores of Hf-TP-SN. Free SN38 inhibits the nuclear enzyme topoisomerase I during DNA replication, leading to DSBs.[42-43]

Cell death pathways were evaluated with the annexin V Alexa fluor 488 and propidium iodide (PI) cell apoptosis kit. More than 85% cells remained healthy in Hf-TP-OH(-) group, confirming that Hf-TP-OH exhibited negligible cytotoxicity. While Hf-TP-OH(+) and Hf-TP-SN(-) groups showed 77.5% and 59.6% healthy cells, respectively, Hf-TP-SN(+) treatment significantly reduced the percentage of healthy cells to 46.3%. See Figure 10. This result suggests synergistic therapeutic effects of Hf-TP-SN(+) due to the radiosensitizing effect of the nMOF and potent chemotherapeutic effect of the released SN38.

In vivo experiments:

A subcutaneous CT26 tumor model was established to assess the *in vivo* anticancer efficacy of Hf-TP-SN(+). CT26 tumor-bearing mice were intratumorally injected with PBS, irinotecan (a prodrug of SN38, 0.046 μmol),[34] Hf-TP-OH (0.5 μmol Hf), or Hf-TP-SN (0.5 μmol Hf and 0.046 μmol SN38). Six to eight hours later, the tumors were exposed to X-ray at the dose of 2 Gy. X-ray irradiation was repeated on two consecutive days (for a total of 6 Gy). Tumor volumes and mouse body weights were monitored daily until the PBS(-) end point. See Figures 11A-11D. While PBS(+) moderately inhibited tumor growth with a tumor growth inhibition index (TGI) of 0.468, irinotecan(+) and Hf-TP-OH(+) enhanced tumor growth inhibition with TGIs of 0.695 and 0.869, respectively. Hf-TP-SN(+) potently regressed tumors with a TGI value of 0.965 and completed tumor eradication in 40% mice. In contrast, Hf-TP-SN(-) treatment modestly inhibited tumor growth with a TGI of 0.362. The impressive *in vivo* therapeutic effects of Hf-TP-SN(+) resulted from synergistic actions of nMOF-mediated radiosensitization and X-ray triggered release of SN38 from Hf-TP-SN. The mice in all treatment groups showed steady body weights (see Figure 11D), suggesting the lack of general toxicity.

One day after the last X-ray irradiation, tumor slices were processed to evaluate pathological changes via γ-H2AX, Ki67, terminal deoxynucleotidyl transferase mediated dUTP-biotin nick end labeling (TUNEL), and hematoxylin and eosin (H&E) staining. See Figure 12. Hf-TP-SN(+) treatment increased the expression of γ-H2AX (see Figure 12, top row) reduced cell proliferation with lower Ki67 signal (see Figure 12, row second from top), and increased cell apoptosis in TUNEL staining. See Figure 12, row second from bottom. H&E staining showed distinctive cellular damage in the tumors treated with Hf-TP-OH(+) and Hf-TP-SN(+); minimal cellular damage was observed in PBS(+) and irinotecan(+) groups. See Figure 12, bottom row.

Furthermore, histology of the hearts, livers, spleens, lungs, and kidneys of treated mice did not show any abnormality (see Figure 13), supporting the safety of Hf-TP-SN(+) treatment in mice.

Summary of Studies with Hf-TP-SN:

A nMOF, Hf-TP-SN nMOF, was prepared comprising an X-ray triggerable SN38 prodrug for synergistic radiotherapy and chemotherapy. More particularly, Hf-TP-SN was synthesized via a combination of pre-functionalization of terphenyl ligands with 3,5-dimethylbenzyl alcohol and post-synthetic modification with SN38 via a carbonate bond. Upon X-ray irradiation, electron-dense Hf_{12}-SBUs served as radiosensitizers to enhance OH generation, leading to 5-fold higher release of SN38 from Hf-TP-SN than a homogeneous counterpart. Hf-TP-SN not only enhanced the radiotherapeutic efficacy but also achieved chemotherapeutic effect through on-demand release of SN38. Such a chemoradiotherapy strategy effectively reduces the radiation dose required for tumor regression and minimizes the side effects of chemotherapy via burst release of SN38 inside cancer cells. As the post-synthetic modification step only requires a hydroxyl or amino group in a drug for nucleophilic substitution, a variety of therapeutic agents can be grafted onto the Hf-TP-OH to form novel Hf-TP-conjugated drugs for disease management. This highlights the use of nMOFs in multi-modality cancer treatment via on-demand, triggered release of therapeutic agents.

EXAMPLE 3

METHODS FOR PREPARATION AND STUDIES WITH Hf-DBP-QP-SN

Synthesis of H_2QP and Me_2QP-SN:

(4,4'-Dibromo-[1,1'-biphenyl]-2-yl)methanamine (15). 2,7-Dibromo-9*H*-fluoren-9-one (**12**, 6 g, 17.8 mmol) and KOH (15.6 g, 0.278 mol) were dissolved in diphenyl ether

(Ph_2O, 80 mL) and refluxed for 18 hrs. After the solution was cooled to room temperature, concentrated HCl (21.5 mL) was added dropwise to adjust the pH to 1-2. The precipitate was collected via filtration and washed with H_2O to remove excess KCl and then hexane to remove excess Ph_2O, and finally dried under vacuum to give 4,4'-dibromo-[1,1'-biphenyl]-2-carboxylic acid (**13**, 6.32 g, 17.8 mmol, 99%). ^{1}H NMR (400 MHz, $CDCl_3$): δ 8.10 (d, J = 2.2 Hz, 1H), 7.69 (dd, J = 8.2, 2.1 Hz, 1H), 7.55 – 7.50 (m, 2H), 7.23 – 7.15 (m, 3H);^{13}C NMR (101 MHz, $CDCl_3$) δ 168.92, 141.21, 139.09, 135.25, 133.76, 132.67, 131.49, 130.16, 129.87, 123.35, 122.23, 121.72, 119.03. HR-MS (ESI, positive mode): *m/z* calc'd for $C_{13}H_9Br_2O_2$ $[M-H]^-$: 354.8798, found 354.8835.

$SOCl_2$ (15 mL) was added to compound **13** (6.32 g, 17.8 mmol) and the mixture was refluxed at 80 °C for 6 h to produce 4,4'-dibromo-[1,1'-biphenyl]-2-carbonyl chloride. The unreacted $SOCl_2$ was removed by distilling under reduced pressure. 25-28% NH_3• H_2O (100 mL) was added slowly to 4,4'-dibromo-[1,1'-biphenyl]-2-carbonyl chloride with vigorous stirring overnight. The resulting solution was filtered with water (to remove any NH_4Cl salt) and hexane before being dried under vacuum to afford 4,4'-dibromo-[1,1'-biphenyl]-2-carboxamide (**14**, 5.67 g, 15.9 mmol, 90%). ^{1}H NMR (400 MHz, chloroform-d): δ 7.88 (d, J = 2.1 Hz, 1H), 7.63 (dd, J = 8.3, 2.1 Hz, 1H), 7.59 – 7.54 (m, 2H), 7.33 – 7.28 (m, 2H), 7.21 (d, J = 8.2 Hz, 1H), 5.49 (s, 1H), 5.27 (s, 1H); ^{13}C NMR (101 MHz, $CDCl_3$) δ 169.41, 138.03, 137.58, 136.21, 133.82, 132.16, 132.00, 130.36, 122.92, 122.28. HR-MS (ESI, positive mode): *m/z* calc'd for $C_{13}H_{10}Br_2NO$ $[M+H]^+$: 355.9109, found 355.9111.

Compound **14** (5.67 g, 15.9 mmol) was dissolved in 1M BH_3 in THF (56.0 mL, 56 mmol) and stirred at reflux for 24 h before being quenched with concentrated HCl (6 mL). The solution was refluxed for 2 more hours, cooled to room temperature, and basified by addition of saturated Na_2CO_3 to pH = ~10. The solution was then partitioned with water (15 mL) and AcOEt (30 mL) to separate the organic phase from the aqueous phase, extracted with CH_2Cl_2 (3 × 30 mL). The combined organic phase was dried with Na_2SO_4, filtered, condensed via rotary evaporation, and then purified by silica gel column chromatography to give (4,4'-dibromo-[1,1'-biphenyl]-2-yl)methanamine (**15**, 4.07 g, 11.9 mmol, 75%). ^{1}H NMR (400 MHz, chloroform-d): δ 7.68 (s, 1H), 7.59 – 7.53 (m, 2H), 7.47 – 7.41 (m, 1H), 7.23 – 7.16 (m, 2H), 7.07 (d, J = 8.2 Hz, 1H), 3.78 (s, 2H); ^{13}C NMR (101 MHz, $CDCl_3$) δ 139.05, 138.96, 131.71, 131.60, 131.19, 130.76, 130.02, 122.26, 121.87, 43.85. HR-MS (ESI, positive mode): *m/z* calc'd for $C_{13}H_{12}Br_2N$ $[M+H]^+$: 341.9316, found 341.9313.

4-(((*tert*-Butyldimethylsilyl)oxy)methyl)-N-((4,4'-dibromo-[1,1'-biphenyl]-2-yl)methyl)-2,6-dimethoxybenzamide (16). Compound **3** (1.20 g, 3.68 mmol), 1-(3-dimethylaminopropyl)-3-ethylcarbodiimide hydrochloride (EDCI, 0.846 g, 4.42 mmol), hydroxybenzotriazole (HOBt, 0.596 g, 4.42 mmol), TEA (615 uL, 4.42 mmol), and compound **15** (1.255 g, 3.68 mmol) were combined in CH_2Cl_2 (70 mL). The resulting mixture was degassed and then stirred at room temperature for 12 h. The reaction mixture was then partitioned between EA and water, and the aqueous layer was extracted with EA twice. The combined organic phase was then dried over Na_2SO_4, filtered, concentrated by rotary evaporation, and separated with column chromatography to give compound **16** (1.00 g, 1.54 mmol, 42%). ^{1}H NMR (400 MHz, chloroform-d): δ 7.89 (d, J = 2.0 Hz, 1H), 7.60 – 7.51 (m, 2H), 7.44 (dd, J = 8.1, 2.1 Hz, 1H), 7.23 – 7.15 (m, 2H), 7.08 (d, J = 8.1 Hz, 1H), 6.56 (t, J = 0.8 Hz, 2H), 5.94 (t, J = 6.1 Hz, 1H), 4.72 (t, J = 0.8 Hz, 2H), 4.56 (d, J = 6.2 Hz, 2H), 3.87 (d, J = 1.1 Hz, 6H), 0.95 (d, J = 1.1 Hz, 9H), 0.11 (d, J = 1.1 Hz, 6H); ^{13}C NMR (101 MHz, $CDCl_3$) δ 166.02, 157.39, 145.28, 138.76, 138.44, 138.07, 131.63, 131.21, 130.75, 130.63, 130.12, 122.27, 121.90, 113.79, 101.24, 64.78, 55.90, 40.90, 30.94, 25.89, 18.40, -5.23. HR-MS (ESI, positive mode): *m/z* calc'd for $C_{29}H_{36}Br_2NO_4Si$ $[M+H]^+$: 650.0760, found 650.0795.

Dimethyl 2''-((4-(((tert-butyldimethylsilyl)oxy)methyl)-2,6-dimethoxybenzamido)methyl)-[1,1':4',1'':4'',1'''-quaterphenyl]-4,4'''-dicarboxylate (17). To compound **16** (1.00 g, 1.54 mmol) was added (4-(methoxycarbonyl)phenyl)boronic acid (0.832 g, 4.62 mmol), CsF (0.702 g, 4.62 mmol), [1,1′-bis(diphenylphosphino)ferrocene]dichloropalladium(II) ($Pd(dppf)Cl_2$, 0.113 g, 0.154 mol), and the solid mixture was degassed followed by the addition of degassed dioxane (30 mL). The resulting solution was stirred at 90 °C under N_2 for 3 days. The mixture was filtered before the removal of dioxane under reduced pressure, extracted with EA, and purified by column chromatography to yield compound **17** (0.784 g, 1.03 mmol, 67%). ^{1}H NMR (400 MHz, chloroform-d): δ 8.13 (ddd, J = 8.2, 6.5, 1.6 Hz, 4H), 7.99 (s, 1H), 7.78 – 7.74 (m, 2H), 7.61 (dt, J = 7.9, 1.6 Hz, 1H), 7.54 – 7.45 (m, 2H), 7.41 (dd, J = 7.9, 1.4 Hz, 1H), 6.53 (s, 2H), 6.05 (t, J = 6.3 Hz, 1H), 4.76 (d, J = 5.9 Hz, 2H), 4.70 (s, 2H), 3.99 – 3.92 (m, 6H), 3.70 (d, J = 1.6 Hz, 6H), 0.98 – 0.88 (m, 9H), 0.15 – 4 (m, 6H); ^{13}C NMR (101 MHz, $CDCl_3$) δ 233.82, 232.85, 224.23, 212.11, 211.99, 211.87, 207.34, 206.84, 206.34, 205.93, 203.37, 197.33, 197.04, 196.92, 196.70, 195.90, 195.86, 194.11, 193.96, 193.84, 193.74, 192.73,

180.80, 168.13, 131.56, 122.68, 118.99, 108.25, 97.75, 92.70, 85.20, 61.57. HR-MS (ESI, positive mode): *m/z* calc'd for $C_{45}H_{50}NO_8Si$ $[M+H]^+$: 760.3306, found 760.3311.

2''-((4-(hydroxymethyl)-2,6-dimethoxybenzamido)methyl)-[1,1':4',1'':4'',1'''-quaterphenyl]-4,4'''-dicarboxylic acid (H_2QP). To compound **17** (1 g, 1.32 mmol) was added NaOH (5.28 g, 132 mmol) and MeOH and H_2O in a 1:1 ratio (20 mL: 20 mL). The resulting mixture was stirred at 40 °C for 1 day, acidified with 1M HCl to pH = 1-2, filtered, washed with water and methanol, and dried under vacuum to afford **H_2QP** (0.728 g, 1.18 mmol, 90%). ^{1}H NMR (400 MHz, DMSO-*d*$_6$) δ 13.00 (s, 2H), 8.65 (t, *J* = 6.0 Hz, 1H), 8.11 – 8.03 (m, 4H), 7.98 (d, *J* = 1.9 Hz, 1H), 7.93 – 7.81 (m, 6H), 7.73 (dd, *J* = 7.9, 2.0 Hz, 1H), 7.62 – 7.56 (m, 2H), 7.43 (d, *J* = 7.9 Hz, 1H), 6.64 (s, 2H), 5.29 (t, *J* = 5.8 Hz, 1H), 4.49 (d, *J* = 5.1 Hz, 2H), 4.44 (d, *J* = 5.9 Hz, 2H), 3.63 (s, 6H). See Figure 42. ^{13}C NMR (101 MHz, DMSO-*d*$_6$) δ 167.15, 166.07, 164.94, 156.58, 156.54, 145.23, 144.68, 144.24, 143.87, 139.85, 139.71, 139.61, 138.21, 138.04, 138.00, 137.81, 137.41, 137.37, 130.19, 130.02, 129.90, 129.88, 129.73, 128.57, 127.03, 127.00, 126.89, 126.84, 126.73, 126.15, 125.27, 114.94, 101.89, 62.91, 55.57, 55.54, 52.20. **See Figure 41.** HR-MS (ESI, positive mode): *m/z* calc'd for $C_{37}H_{32}NO_8$ $[M+H]^+$: 618.2128, found 618.2120.

Dimethyl (*S*)-2''-((4-(((((4,11-diethyl-4-hydroxy-3,14-dioxo-3,4,12,14-tetrahydro-1*H*-pyrano[3',4':6,7]indolizino[1,2-*b*]quinoline-9-yl)oxy)carbonyl)-oxy)methyl)-2,6-dimethoxy-benzamido)methyl)-[1,1':4',1'':4'',1'''-quaterphenyl]-4,4'''-dicarboxylate (Me_2QP-SN). Compound **9** (1.0 g, 1.32 mmol) was added tetrabutylammonium fluoride solution in THF (1M, 5 mL) and stirred at room temperature for 2 h. 10 mL saturated NH_4Cl solution was added and THF was removed via rotary evaporation. White precipitate was filtered and washed with water to produce dimethyl 2''-((4-(hydroxymethyl)-2,6-dimethoxybenzamido)methyl)-[1,1':4',1'':4'',1'''-quaterphenyl]-4,4'''-dicarboxylate (**18**, 0.809 g, 1.25 mmol, 95%). ^{1}H NMR (400 MHz, DMSO-*d*$_6$) δ 8.65 (t, *J* = 6.0 Hz, 1H), 8.09 (dd, *J* = 11.5, 8.2 Hz, 4H), 7.98 (d, *J* = 2.0 Hz, 1H), 7.93 (d, *J* = 8.2 Hz, 2H), 7.88 (d, *J* = 7.9 Hz, 4H), 7.77 – 7.69 (m, 1H), 7.60 (d, *J* = 8.0 Hz, 2H), 7.43 (d, *J* = 7.9 Hz, 1H), 6.63 (s, 2H), 5.29 (t, *J* = 5.7 Hz, 1H), 4.49 (d, *J* = 5.7 Hz, 2H), 4.43 (d, *J* = 6.0 Hz, 2H), 3.89 (s, 6H), 3.62 (s, 6H). ^{13}C NMR (101 MHz, DMSO-*d*$_6$) δ 166.14, 165.02, 156.58, 145.27, 144.72, 144.28, 139.88, 139.75, 138.09, 137.86, 137.43, 130.25, 129.93, 128.60, 127.08, 127.04, 126.94, 126.18, 125.33, 114.95, 101.93, 62.95, 55.62, 52.26. HR-MS (ESI, positive mode): *m/z* calc'd for $C_{39}H_{36}NO_8$ $[M+H]^+$: 646.2441, found 646.2440.

Compound 18 (500 mg, 0.774 mmol), 4-nitrophenyl chloroformate (390 mg, 1.94 mmol), TEA (322 μL, 2.322 mmol) were combined in dry DCM (30 mL) under Ar and

stirred for 1 day at RT. The resulting solution was quenched with 5 mL H_2O and extracted with DCM, dried over Na_2SO_4, filtered, concentrated by rotary evaporation, and then dried completely under vacuum to afford dimethyl 2''-((2,6-dimethoxy-4-((((4-nitrophenoxy)carbonyl)oxy)methyl)benzamido)-methyl)-[1,1':4',1'':4'',1'''-quaterphenyl]-4,4'''-dicarboxylate (**19**), which was used directly in the next step without purification. HR-MS (ESI, positive mode): *m/z* calc'd for $C_{46}H_{39}N_2O_{12}$ $[M+H]^+$: 811.2505, found 811.2542.

To a mixture of **19** in DCM (20 mL) was added SN38 (589 mg, 1.500 mmol) and TEA (250 µL, 1.80 mmol); the resulting mixture was stirred at room temperature for 1 day before being washed with H_2O and extracted with DCM (3 × 20 mL). The organic phases were combined, dried over Na_2SO_4, filtered, concentrated by rotary evaporation, dissolved in minimal DCM, and purified via thin layer chromatography (5% MeOH in DCM) to give **Me_2QP-SN** (0.165 g, 0.155 mmol, 20%). ^{1}H NMR (400 MHz, Chloroform-*d*) δ 8.27 (d, *J* = 9.2 Hz, 1H), 8.14 (ddd, *J* = 8.5, 6.4, 1.9 Hz, 5H), 7.99 (d, *J* = 1.9 Hz, 1H), 7.93 (d, *J* = 2.6 Hz, 1H), 7.79 – 7.75 (m, 2H), 7.72 (dt, *J* = 8.6, 1.9 Hz, 4H), 7.68 (s, 1H), 7.67 – 7.60 (m, 2H), 7.53 – 7.49 (m, 2H), 7.43 (d, *J* = 7.9 Hz, 1H), 6.65 (s, 2H), 6.02 (t, *J* = 6.0 Hz, 1H), 5.75 (d, *J* = 16.4 Hz, 1H), 5.31 (d, *J* = 16.3 Hz, 1H), 5.27 (d, *J* = 3.1 Hz, 4H), 4.77 (d, *J* = 6.0 Hz, 3H), 3.96 (d, *J* = 1.9 Hz, 7H), 3.76 (s, 7H), 3.64 (s, 2H), 3.16 (q, *J* = 7.7 Hz, 3H), 2.26 – 2.18 (m, 3H), 1.38 (d, *J* = 7.7 Hz, 2H), 1.04 (t, *J* = 7.4 Hz, 3H), 0.91 – 0.85 (m, 3H). See Figure 44. ^{13}C NMR (101 MHz, CDCl3) δ 174.00, 167.09, 165.58, 157.77, 157.74, 153.40, 152.33, 150.31, 149.88, 147.65, 146.90, 145.54, 145.36, 145.10, 140.67, 140.05, 139.67, 139.30, 137.72, 136.46, 132.48, 131.75, 131.00, 130.72, 130.36, 130.24, 129.99, 129.25, 129.22, 127.56, 127.52, 127.44, 127.24, 127.13, 126.99, 126.12, 124.72, 118.84, 116.13, 114.26, 104.32, 98.24, 72.89, 70.61, 66.47, 56.25, 52.34, 52.32, 49.51, 41.60, 31.75, 23.32, 14.13, 7.96. See Figure 43. HR-MS (ESI, positive mode): *m/z* calc'd for $C_{62}H_{54}N_3O_{14}$ $[M+H]^+$: 1064.3606, found 1064.3596.

Synthesis and characterization of Hf-DBP-QP-SN:

Synthesis of Hf-DBP-QP. $HfCl_4$, H_2DBP and H_2QP-OH were separately dissolved in DMF at a concentration of 2, 3.5 and 3.5 mg/mL, respectively. 500 µL $HfCl_4$ solution, 100 µL H_2DBP and 400 µL H_2QP-OH were then combined in a 1-dram vial with the addition of 55 µL acetic acid and 5 µL water as modulators. The mixture was heated in an oven at 80 °C for 2 days. The purple precipitate was collected by centrifugation and sequentially washed with DMF, 1% triethylamine (TEA) in ethanol (EtOH) (v/v), and EtOH, and then dispersed in EtOH for storage.

Synthesis of Hf-DBP-QP-SN. 10 mL Hf-DBP-QP was washed with dry acetonitrile (ACN) twice and dispersed in ACN with a QP concentration of 2.0 mM. 4-Nitrophenyl chloroformate (10.1 mg, 50 μmol), and TEA (8.3 μL, 60 μmol) were then added, and the solution was stirred for 2 days to afford Hf-DBP-QP-NO_2 nMOF. The mixture was then centrifuged, washed with ACN three times and redispersed in ACN before the addition of SN38 (7.9 mg, 20 μmol) and TEA (4.2 μL, 30 μmol); the solution was then stirred for 2 more days. The as-synthesized Hf-DBP-QP-SN was washed with 10% dimethyl sulfoxide (DMSO) in ACN 6 times and dispersed in EA for storage.

MOF Digestion for UV-Vis Spectroscopic Measurement. 50 μL Hf-DBP-QP or Hf-DBP-QP-SN solution, 900 μL DMSO, and 50 μL H_3PO_4 were mixed and sonicated for 1 h. The mixture was diluted to a proper concentration for UV-Vis measurement. The absorption of H_2QP at 304 nm was used to calculate the concentration of H_2QP-OH in Hf-DBP-QP after comparison with the standard curve of H_2QP-OH in DMSO while the absorption of H_2DBP at 408 nm was used to calculate the concentration of H_2DBP in Hf-DBP-QP or Hf-DBP-QP-SN after comparison with the standard curve of H_2DBP in DMSO.

Digestion of Hf-DBP-QP-SN for Quantification of SN38 by HPLC. 10 μL Hf-DBP-QP-SN dispersion in EA (Hf concentration of ~1.5 mM) and 100 μL TFA/EA mixture (v/v=1:9) was combined and sonicated for 15min. The supernatant was obtained by centrifugation and analyzed by HPLC. The absorption of SN38 at 380 nm was used to calculate the concentration of SN38 after comparison with the standard curve of SN38 in EA.

Digestion of Hf-DBP-QP-SN for Quantification of SN38 by LC-MS. 100 μL 1M $NaHCO_3$ solution was added to 100 μL Hf-DBP-QP-SN dispersion in PBS (SN concentration of approximately 100 μM). The mixture was sealed and sonicated for 20 min. 100 μL saturated NaCl solution and 150 μL ethyl acetate (EA) were added and the mixture was vortexed for 1 min. The EA layer after centrifugation was analyzed by LC-MS.

Stability Test of Hf-DBP-QP-SN in PBS. Hf-DBP-QP-SN was dispersed in 1 mL PBS (1 mM) with a Hf concentration of 5 mM. 200 uL suspension was taken after incubation for 1, 2, 4, 8, and 24 h and centrifuged for PXRD measurement.

Total ROS Generation in Test Tubes. Total ROS generation under irradiation was detected by the 2',7'-dichlorodihydrofluorescein (DCFH) assay. 1 mL DCFH-DA (1mM) in DMSO was hydrolyzed by 4 mL NaOH (0.01 M) solution in the dark for 30 minutes and stopped by adding 20 mL PBS (25 mM, pH 7.4). The freshly prepared DCFH was then added to the PBS suspension (pH 7, 10 mM) of Hf-DBP, Hf-DBP-QP or Hf-DBP-QP-SN at the same Hf concentration. In the final mixture, the concentration of DCFH was 5 μM while the

concentration of Hf was 40 μM. The PBS solution with the same DCFH concentration served as a blank control. 100 μL of each suspension was added to 96-well plates (n = 6) and then irradiated with X-ray at 0, 1, 2, 3, 5, or 10 Gy, respectively. The fluorescence signal (em. 520/20 nm) was collected with a Synergy HTX microplate reader (ex. 485/20 nm; Agilent Technologies, Santa Clara, California, United States of America).

Hydroxyl radical generation in Test Tubes. Hydroxyl radical (·OH) generation under irradiation was detected by the APF assay. APF assay was added to the PBS suspension of Hf-DBP, Hf-DBP-QP or Hf-DBP-QP-SN at the same Hf concentration. In the final mixture, the concentration of APF was 5 μM while that of Hf was 40 μM. The PBS solution with the same APF concentration served as a blank control. 100 μL of each suspension was added to 96-well plates (n = 6) and then irradiated with X-ray at 0, 1, 2, 3, 5, or 10 Gy, respectively. The fluorescence signal (em. 520/20 nm) was collected with a Synergy HTX microplate reader (ex. 485/20 nm; Agilent Technologies, Santa Clara, California, United States of America).

Hydroxyl Radical Triggered SN38 Release in Test Tubes. Hf-DBP-QP-SN or MeO-SN was dispersed in H_2O at the same concentration of total SN38 (100 μM). $FeCl_3$, (+)-Sodium L-ascorbate, $Na_2(EDTA)\cdot 2H_2O$ (ethylenediaminetetraacetic acid, disodium salt dihydrate) was firstly dissolved in water to reach a concentration of 10 mM separately (10.5 mM for $Na_2(EDTA)\cdot 2H_2O$). Then, 100 μL of each solution and 50 μL H_2O_2 (200 mM in H_2O) was added to Hf-DBP-QP-SN or MeO-SN solution to generate hydroxyl radical in situ and to trigger the release of SN38. For control group, only H_2O_2 was added. After 8h incubation at room temperature, additional 100 μL 1M $NaHCO_3$ was added to Hf-DBP-QP-SN to digest the nMOF, after which the mixture was sealed and sonicated for 20 minutes before the addition of 100 μL PBS (200 mM, pH 4) to adjust the pH to 7. 100 μL saturated NaCl solution and 150 μL ethyl acetate (EA) were added before vortexing the Hf-DBP-QP-SN or MeO-SN mixture for 1 minute. The EA layer after centrifugation was analyzed by LC-MS.

X-ray Triggered Release in Test Tube. Hf-DBP-QP-SN or MeO-SN were dispersed in H_2O (10 mM, pH = 7.4) at the same concentration of total SN38 (100 μM). 100 μL Hf-DBP-QP-SN or MeO-SN suspension was irradiated with 10 Gy X-ray. 100 μL 1M $NaHCO_3$ was added to Hf-DBP-QP-SN to digest the nMOF, after which the mixture was sealed, sonicated for 20 minutes, and sat 15h before the addition of 100 μL PBS (200 mM, pH 4.0) to adjust the pH to 7. 100 μL saturated NaCl solution and 150 μL ethyl acetate (EA) were added

before vortexing the Hf-DBP-QP-SN or MeO-SN mixture for 1 min. The EA layer after centrifugation was analyzed by LC-MS.

In vitro experiments:

Dark Toxicity. CT26 cells were cultured in RPMI-1640 medium supplemented with 10% fetal bovine serum (filtered, VWR International, Radnor, Pennsylvania, United States of America), 1% Penicillin-Streptomycin 100X solution sold under the tradename HYCLONE® HyClone Laboratories, Logan, Utah, United States of America), and cultured in a humidified atmosphere containing 5% CO_2 at 37°C. Mycoplasma was tested on a regular basis using a detection kit sold under the tradename MYCOALERT® (Lonza Walkersville, Inc., Walkersville, Maryland, United States of America)

The cytotoxicity of H_2QP ligand, Hf-DBP-QP and Hf-DBP-QP-SN on CT26 cells were detected by MTS assay. CT26 cells were seeded in 96-well plates at a density of 2500 cells/well. Different concentrations of Hf-DBP-QP-SN were added and 24 hours later 10% (v/v) of MTS reagent was added to each well. 90 minutes later the absorbance of each well at 490 nm was read by a Synergy HTX plate reader (Agilent Technologies, Santa Clara, California, United States of America) to calculate cell viability.

The cytotoxicity of SN38 and Me_2QP-SN on CT26 cells were detected by MTS assay. CT26 cells were seeded in 96-well plates at a density of 2500 cells/well. Different concentrations of SN38 or Me_2QP-SN were added and 48 hours later 10% (v/v) of MTS reagent was added to each well. 90 minutes later the absorbance of each well at 490 nm was read by a Synergy HTX plate reader (Agilent Technologies, Santa Clara, California, United States of America) to calculate cell viability.

Cellular Uptake. CT26 cells were seeded in 6-well plates at a density of 2×10^5/well and cultured overnight. Hf-DBP-QP (Hf: 50 μM) and Hf-DBP-QP-SN (Hf: 50 μM) was added at an equivalent metal concentration into medium (n = 3) and incubated for 1, 2, 3, 4 and 6 hours in a 37 °C incubator. At each time point, the medium was aspirated, the cells were washed with PBS for three times, collected by centrifugation, and counted with a hemocytometer. Then, the uptake of Hf-DBP-QP and Hf-DBP-QP-SN were detected on a flow cytometer (sold under the tradename LSRFORTESSA™ 4-15 HTS, BD Biosciences, Franklin Lakes, New Jersey, United States of America) and analyzed by FlowJo software (FlowJo LLC, Ashland, Oregon, United States of America).

Intracellular ROS Generation. To demonstrate the generation of total ROS, CT26 cells were seeded in the cell culture dishes at a density of 1.5×10^5 and cultured overnight. Hf-DBP-QP-SN or Hf-DBP-QP was added at an equivalent metal concentration of 50 μM and

further incubated in a 37 ℃ incubator for 4 hours. The cells were washed with PBS solution for 3 times and 1 mL cell culture medium containing with 20 μM DCFH-DA was added and incubated at 37 ℃ for another 30 min. Then, the cells were irradiated with X-ray (3 Gy) and continued to be cultured in the cell incubator for another 12 h. After that, cells were washed by PBS for three times and collected by centrifugation and counted with a hemocytometer. Then, the generation of total ROS was detected on a flow cytometer (sold under the tradename LSRFORTESSA™ 4-15 HTS, BD Biosciences, Franklin Lakes, New Jersey, United States of America) and analyzed by FlowJo software (FlowJo LLC, Ashland, Oregon, United States of America).

To demonstrate the generation of total ROS, CT26 cells were seeded in the cell culture dishes at a density of 1.5×10^5 and cultured overnight. Hf-DBP-QP-SN or Hf-DBP-QP was added at an equivalent metal concentration of 50 μM and further incubated in a 37 ℃ incubator for 4 hours. The cells were washed with PBS solution for 3 times and 1 mL cell culture medium containing with 30 μM DCFH-DA was added and incubated at 37 ℃ for another 30 min. Then the cells were irradiated with X-ray (3 Gy) and continued to be cultured in the cell incubator for another 24 h. After that, cells were washed by PBS for three times and further incubated with Hoechst 33342 (10 μg mL^{-1}) in PBS for 10 min in the cell incubator. Finally, cells were washed by PBS 3 times and observed on a Leica Stellaris 8 confocal microscope (Leica Microsystems, Wetzlar, Germany) and analysis was done with Image J software (National Institutes of Health (NIH), United States of America).

The generation of ·OH in cancer cells was also detected according to the similar method as above. Typically, CT26 cells were seeded in the cell culture dishes at a density of 1.5×10^5 and cultured overnight. Hf-DBP-QP-SN or Hf-DBP-QP was added at an equivalent metal concentration of 50 μM and further incubated in a 37 ℃ incubator for 4 hours. The cells were washed with PBS solution for 3 times and 1 mL cell culture medium containing with 10 μM HPF was added and incubated at 37℃ for another 30 min. Then the cells were irradiated with X-ray (3 Gy) and continued to be cultured in the cell incubator for another 24 h. After that, cells were washed by PBS for three times and further incubated with Hoechst 33342 (10 μg mL^{-1}) in PBS for 10 min in the cell incubator. Finally, cells were washed by PBS for 3 times and observed on a Leica Stellaris 8 confocal microscope (Leica Microsystems, Wetzlar, Germany) and analysis was done with Image J software (NIH, United States of America).

Apoptotic Cell Death. To quantify the apoptosis, CT26 cells were seeded in 6-well plates at a density of 2×10^5/well and cultured overnight. Hf-DBP-QP or Hf-DBP-QP-SN

was added at an equivalent metal concentration of 50 μM for 4 hours and irradiated with X-ray (3 Gy). 24 hours later, the cells were washed with PBS, trypsinized to afford single cell suspensions, The cells were stained with the dead cell apoptosis kit with annexin V Alexa Fluor 488 & PI and resuspended in the binding buffer for flow cytometric analysis (Annexin-V in FITC channel, PI in PE-dazzle 594 channel).

Clonogenic Assay. RT250 orthovoltage X-ray machine model (Philips, Andover, Massachusetts, United States of America) with fixed setting at 250 kVp, 15 mA and a built-in 1 mm Cu filter was used for X-ray irradiation in test tube and *in vitro* experiments. CT26 cells were seeded in 6-well plates at a density of 1.5×10^5 cells/well and cultured overnight. The cells were incubated with PBS, Hf-DBP-QP, or Hf-DBP-QP-SN at an equivalent metal concentration of 50 μM for 4 hours, and then irradiated with 0, 2, 4, 6 Gy X-ray ($n = 3$). The cells were washed with PBS twice and then trypsinized to afford single cell suspensions. The cells were counted and diluted, then 200 cells were seeded in each well of 6-well plates and cultured in 2 mL medium for another 7 days. When an appropriate colony size was observed, the plates were rinsed once with PBS, fixed by 4% paraformaldehyde for 20 minutes at room temperature, and washed with PBS once. The 6-well plates were then scanned and analyzed with a cell analysis system sold under the tradename INCUCYTE® S3 (Sartorius Bioanalytical Instruments, Inc., Brooklyn Center, Minnesota, United States of America) in the whole well mode with a 4× objective. The colonies were identified with software sold under the tradename INCUCYTE® 2021A (Sartorius Bioanalytical Instruments, Inc., Brooklyn Center, Minnesota, United States of America) in a cellular resolution and the confluence was used as a parameter to calculate the plating efficiency (PE)and surviving fraction (SF):

$$PE = \frac{Confluence\ (0\ Gy, PBS)}{Cell\#\ (0\ Gy, PBS)} \qquad SF(D, MOF) = \frac{Confluence\ (D, MOF)}{Cell\#\ (D, MOF) \times PE}$$

Where was the radiation dose and was the number of cells seeded for a certain radiation dose D and a certain treatment group.

The dose modifying ratio at a 10% ($DMR_{10\%}$) was used as a parameter to assess radiosensitization effect and defined as the ratio of doses under reference conditions to produce a 10% SF:

$$DMR_{10\%} = \frac{D_{PBS}}{D_{MOF}}$$

DNA Damage. For CLSM imaging, CT26 cells were seeded in cell culture dishes at a density of 1.5×10^5 . The cells were treated in the same way as in the clonogenic assay. 24 hours after radiation, the cells were washed with PBS and fixed with 4% paraformaldehyde at room temperature for 20 minutes. The cells were again rinsed with PBS, blocked and permeabilized with 5% FBS + 0.3% Triton-X in PBS at room temperature for 1 hour. After blocking, the cells were incubated with the γ-H2AX primary antibody (1:500) in 1% BSA + 0.3% Triton-X in PBS at 4 °C overnight. The cells were then washed with PBS and incubated with the Alexa Fluor 488 conjugated secondary antibody (1:3000) in 1% BSA + 0.3% Triton-X in PBS at room temperature for 1 hour. Afterwards, the cells were washed with PBS and further incubated with Hoechst 33342 (10 μg mL^{-1}) in PBS for 10 min at 37 °C to visualize cell nuclei, respectively. Finally, cells were washed by PBS for 3 times and observed on a Leica Stellaris 8 confocal microscope (Leica Microsystems, Wetzlar, Germany).

In vivo experiments:

Anti-cancer Efficacy. X-RAD 225 image-guided biological irradiator (Precision X-ray Inc., Madison, Connecticut, United States of America) was used with voltage at 225 kVp, current at 13 mA, a 0.3 mm Cu filter, and a 15 mm collimator for animal therapy. The X-ray dose rate of X-RAD 225 was 0.04167 Gy/second. BALB/c mice (6-8 weeks) were obtained from Charles River Laboratories, Inc (Wilmington, Massachusetts, United States of America) and bred in house. To evaluate the in vivo therapeutic efficacy of Hf-DBP-QP-SN, CT26 tumor model was established on BALB/c mice by inoculating 2×10^6 cells/mouse subcutaneously onto the right flanks at day 0, respectively. When CT26 tumors reached to ~105 mm^3, the mice were randomized for irradiation treatment. PBS, Hf-QP, or Hf-DBP-QP-SN was intratumorally injected with an equivalent metal dose of 0.5 μmol and SN38 dose of 0.0373 μmol in 20 μL PBS (n = 5). 6-8 hours later, the mice were anaesthetized with 2.5% (v/v) isoflurane/O_2 and mounted onto the X-Rad 225 irradiator. The CT26 tumors were irradiated with 2 Gy X-ray/fraction for 3 consecutive days. The length and width of tumor tissues were measured with an electronic caliper (tumor volume = length × $width^2/2$) and body weights were monitored with an electronic scale. At the endpoint of the experiments, the mice were euthanized, and the tumors and major organs were sectioned for hematoxylin-eosin (H&E) staining to evaluate general toxicity. The tumor growth inhibition index (TGI) was defined as the equation below:

$$TGI = (1 - \frac{\frac{T_e}{T_s} / \frac{C_e}{C_s}}{1 - \frac{C_s}{C_e}}) \times 100\%$$

where T_e, T_s, C_e, and represent average tumor volumes of treated mice at endpoint, treated mice at starting-point, control mice at endpoint and control mice at starting-point, respectively.

Immunohistochemistry Analysis. The histological slides were scanned on a CRi Pannoramic SCAN 40x whole slide scanner (3DHISTECH LTD, Budapest, Hungary). To evaluate DNA damage and tumor proliferation after different treatments, a group of CT26-bearing mice were established and treated in the same way as described above, but euthanized one day after the last irradiation. The tumors were excised and fixed in 4% PFA for 48 h and 70% ethanol for 1 day. The tissues were embedded in paraffin, sectioned and stained for H&E, γ-H2AX, Ki67 and TUNEL. Briefly, the slides were deparaffinized and rehydrated using xylenes and serial dilutions of ethanol to distilled water. Then the slides were treated with antigen retrieval buffer (AR9640; Leica Biosystems, Wetzlar, Germany) and heated in a steamer over 97°C for 20 minutes). After washing with tris-buffered saline (TBS), the slides were incubated with primary γ-H2AX antibody (1:400) or primary Ki67 antibody (Clone# SP6, 1:400; Thermo Fisher Scientific, Waltham, Massachusetts, United States of America) at room temperature for 1 hour in a wet chamber. The slides were washed with TBS, then γ-H2AX and Ki67 slides were incubated with anti-rabbit-polymer (Bond Polymer Refine Detection, DS9800; Leica Biosystems, Wetzlar, Germany) for 30 minutes at room temperature. The antigen-antibody binding was detected with the 3,3′-Diaminobenzidine (DAB) (DAKO, K3468; Agilent Technologies, Santa Clara, California, United States of America) system. Tissue sections were then immersed in hematoxylin for counterstaining and covered with cover glasses. The slides were scanned on a CRi Pannoramic SCAN 40× whole slide scanner (3DHISTECH LTD, Budapest, Hungary) and analyzed with the QuPath-0.2.3 software.

EXAMPLE 4

Hf-DBP-QP-SN

Synthesis and characterization of Hf-DBP-QP-SN:

The 5,15-di (p-benzoato)porphyrin ligand (H_2DBP) was synthesized following reported procedures.[81] The quaterphenyl dicarboxylic acid (H_2QP) with 3,5-dimethoxyl benzyl alcohol was synthesized from 2,7-dibromo-9*H*-fluoren-9-one (**12**) in 6 steps via intramolecular ring-opening, amide formation with ammonia, borane reduction, amide coupling with 4-(((tert-butyldimethylsilyl)oxy)methyl)-2,6-dimethoxybenzoic acid, Suzuki coupling with (4-(methoxycarbonyl)phenyl)boronic acid, and base-catalyzed hydrolysis. The

mix-ligand nMOF, Hf-DBP-QP, was synthesized solvothermally by heating a mixture of $HfCl_4$, H_2DBP, H_2QP, acetic acid, and water in *N, N*-dimethylformamide at 80 °C for 1 day. Finally, Hf-DBP-QP was postsynthetically modified by treatment with 4-nitrophenyl chloroformate followed by SN38 to afford Hf-DBP-QP-SN with SN38 conjugated to the QP ligand via a hydroxyl radical-responsive 3,5-dimethoxyl benzyl carbonate linkage.[38]

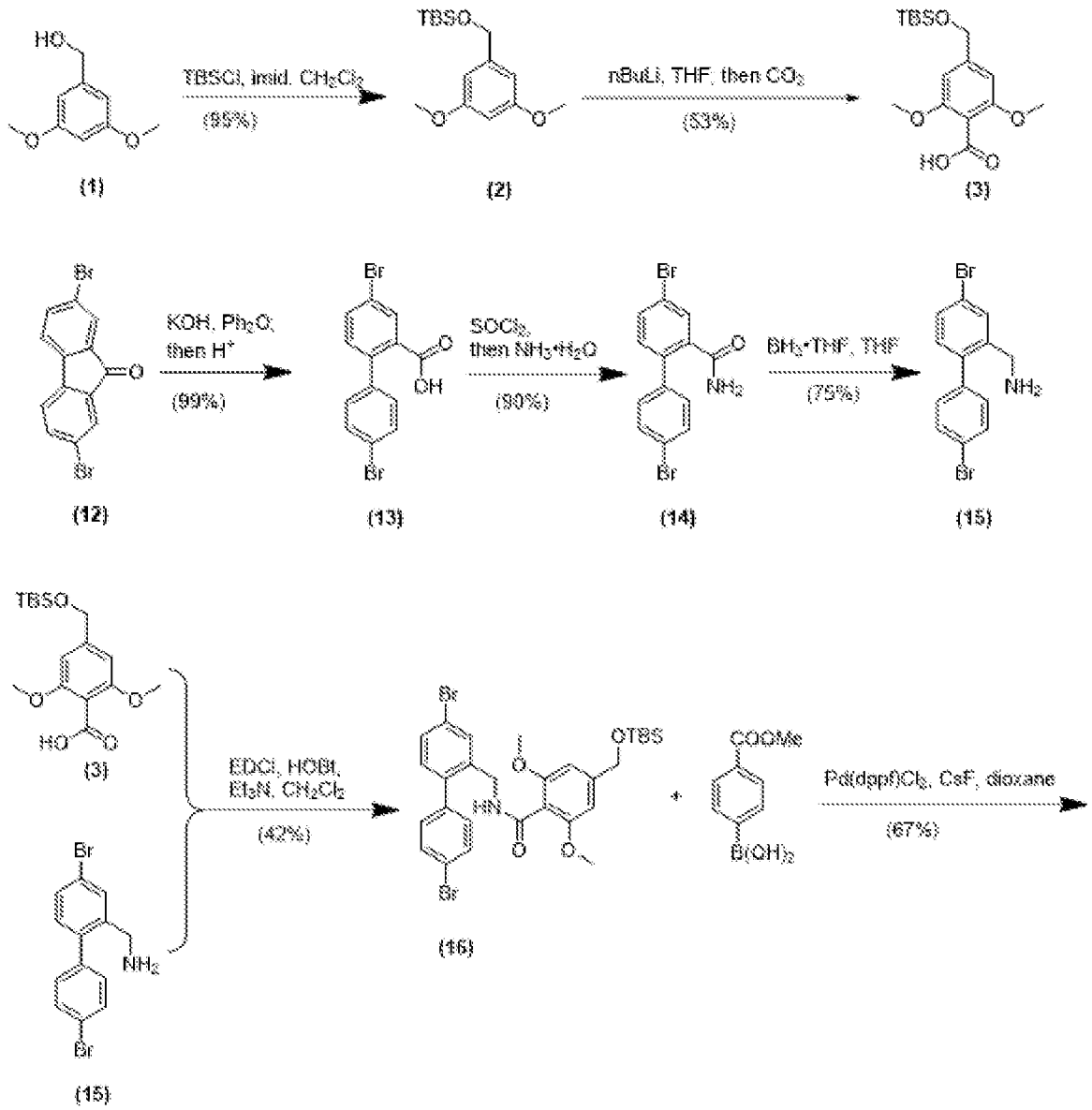

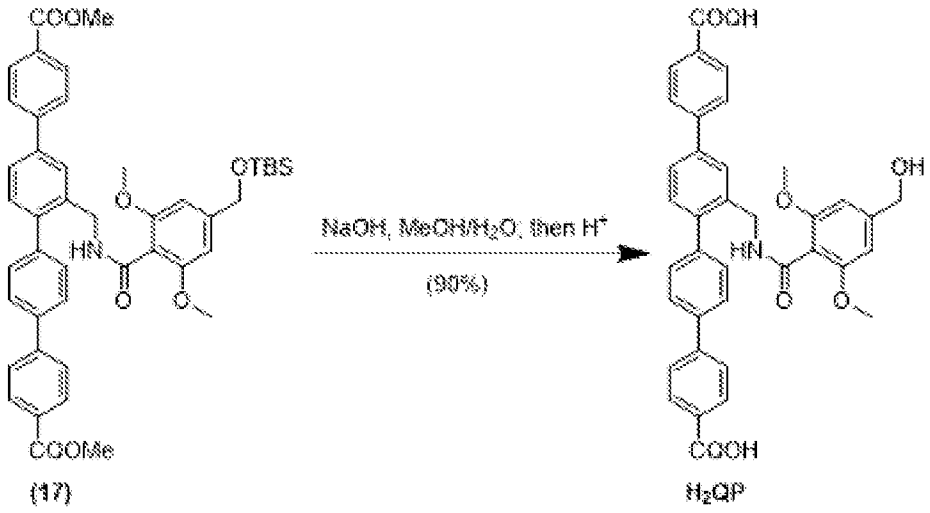

Scheme 4. Synthesis of H_2QP.

Hf-DBP-QP displayed a similar nanoplate morphology as previously reported Hf-DBP with a diameter of ~ 120 nm and a thickness of ~20 nm by transmission electron microscopy (TEM). See Figure 15A. After postsynthetic modification, Hf-DBP-QP-SN retained the nanoplate morphology without obvious variation of diameters. See Figure 15B. The number-averaged sizes of Hf-DBP-QP and Hf-DBP-QP-SN were measured to be 81 ± 3 nm and 96 ± 3 nm (see Figure 15C), respectively, while their ζ-potentials were -18.4 ± 0.8 mV and -21.7 ± 0.5 mV (see Figure 15D), respectively, by dynamic light scattering (DLS).

Powder X-ray diffraction (PXRD) studies showed both Hf-DBP-QP and Hf-DBP-QP-SN displayed similar patterns as Hf-DBP, corresponding to the Hf_{12}-nMOF structure with $Hf_{12}(\mu_3\text{-}O)_8(\mu_3\text{-}OH)_8(\mu_2\text{-}OH)_6$ SBUs and linear dicarboxylate ligands in a *hcp* topology.[39] See Figure 16A. Moreover, Hf-DBP-QP-SN retained its crystallinity after incubation in PBS (1mM, pH 7.4) for 24 hours (see Figure 16B), suggesting the good stability of Hf-DBP-QP-SN in physiologically relevant environments.

UV-Vis spectroscopic analysis of digested Hf-DBP-QP determined the QP/DBP ratio to be 3.29 (see Figure 17) by comparing the absorbance of QP and DBP ligands with their standard curves (see Figures 18A-18D), which was consistent with the QP/DBP ratio (3.55) used in the synthesis.

The total loading of SN38 was quantified by high performance liquid chromatography (HPLC) after digesting Hf-DBP-QP-SN in 10% trifluoracetic acid in EA, indicating ~25% of QP ligands were conjugated with SN38. Liquid chromatography-mass spectrometry (LC-MS) analysis indicated the trapping of 1.5% free SN38 (relative to total SN38) in the pores after

digesting Hf-DBP-QP-SN using $NaHCO_3$ and extraction with ethyl acetate. After determining the Hf content by inductively coupled plasma-mass spectrometry (ICP-MS), the formula of Hf-DBP-QP-SN was determined to be $Hf_{12}(\mu_3\text{-}O)_8(\mu_3\text{-}OH)_8(\mu_2\text{-}OH)_6(QP\text{-}SN)_{0.88}(QP)_{2.74}(DBP)_{1.36}(OH)_{8.04}(H_2O)_{8.04}(SN38)_{0.01}$.

A molecular counterpart, Me_2QP-SN, was synthesized from compound **17** using the same synthetic route to support the post-synthetic modification and to examine the toxicity of the prodrug. See Scheme 5. Because of low aqueous solubility of Me_2QP-SN, we synthesized MeO-SN from compound **1** and used it as a homogeneous control. See Scheme 3, above.

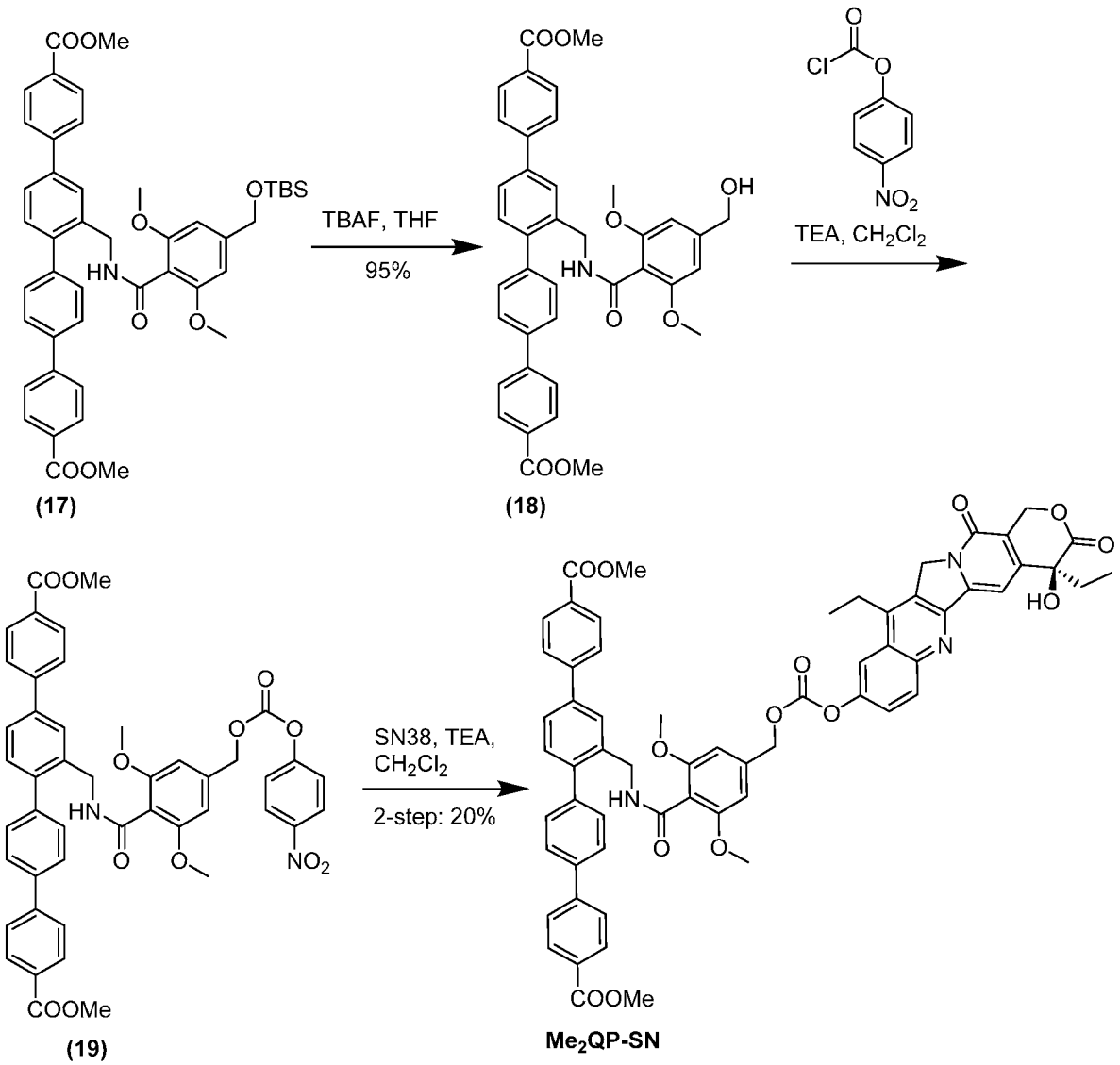

Scheme 5. Synthesis of Me_2QP-SN.

ROS generation and triggered release of SN38:

To confirm the proposed mechanism of chemotherapy via X-ray triggered release of SN38 via RT-RDT (see Figure 19A), ROS generation was evaluated by 2',7'-dichlorodihydrofluorescein (DCFH) assay[46] and ·OH generation by aminophenyl fluorescein (APF) assay. The ·OH signals in PBS, Hf-DBP, Hf-DBP-QP, and Hf-DBP-QP-SN groups all increased linearly with X-ray doses. Hf-DBP-QP and Hf-DBP enhanced ·OH generation by 20% and 21%, respectively, over PBS (see Figure 19B), while Hf-DBP-QP-SN consumed ·OH significantly to reduce ·OH generation by 13% from PBS group. In terms of total ROS, the relative enhancements of Hf-DBP and Hf-DBP-QP over PBS were 76% and 21%, respectively (see Figure 19C), while Hf-DBP-QP-SN was comparable with PBS. The reduced ROS and hydroxyl radical signals from Hf-DBP-QP-SN are likely due to the consumption of ·OH by the 3,5-dimethoxylbenzyl carbonate linkage to release SN38, while the incorporation of DBP ligand significantly improved total ROS signal by generating singlet oxygen through the RDT process.[82,83]

Next, LC-MS analyses were used to evaluate the release of SN38. Hf-DBP-QP-SN released ~3.3% of total SN38 after 10 Gy X-ray irradiation, which was 13-fold higher than SN38 released from MeO-SN under identical conditions (see Figure 20A), suggesting that electron-dense Hf_{12} SBUs could serve as radiosensitizers to enhance ·OH generation for the triggered release of SN38 via hydroxylation of the 3,5-dimethoxylbenzyl carbonate followed by 1,4-elimination. See Figure 20B. The successful release of SN38 was supported by using ·OH generated via the Fenton reaction;[47] Hf-DBP-QP-SN showed 14.8-fold higher SN38 release than MeO-SN under this condition (see Figure 20B) due to better dispersity of the SN38 prodrug in the nMOF.

In vitro experiments:

The cytotoxicity of H_2QP ligand and Hf-DBP-QP was assessed by 3-(4,5-dimethylthiazol-2-yl)-5-(3-carboxymethoxyphenyl)-2-(4-sulfo-phenyl)-2H-tetrazolium (MTS) assay on CT26 cells. No obvious toxicity was observed at a Hf concentration of up to 200 μM or at a H_2QP concentration of up to 60.33 μM. See Figure 21. This result suggests the biocompatibility of the mix-ligand Hf-DBP-QP nMOF.

Compared with the strong toxicity of SN38 with a low half maximal inhibitory concentration (IC_{50}) value of 0.672 μM[42] (see Figure 22A), Me_2QP-SN and Hf-DBP-QP-SN showed no obvious toxicity (see Figures 22B and 22C) at an equivalent SN38 concentration of up to 25 μM or a Hf concentration of up to 300 μM (corresponding to 22.3 μM SN38 in

Hf-DBP-QP-SN). This result shows that Me_2QP-SN and Hf-DBP-QP-SN serve as prodrugs with low intrinsic toxicity.

The uptake of the prepared nMOFs by cancer cells was determined. CT26 cells were incubated with Hf-DBP-QP-SN for 1, 2, 3, 4 and 6 h, and cellular content of DBP was detected by flow cytometry. See Figure 23. CT26 cells showed efficient uptake of Hf-DBP-QP-SN in a time-dependent manner.

DCFH-DA was then utilized to detect the generation of ROS in cancer cells. Flow cytometry analysis results showed that Hf-DBP-QP generated 1.80-fold higher ROS signals than PBS group under the radiation of 3 Gy X-ray. See Figure 24. Stronger ROS generation by Hf-DBP-QP was supported by confocal laser scanning macroscopy (CLSM) imaging. See Figure 25. This result suggests efficient ROS generation by Hf-DBP-QP via the RT-RDT process.

Hydroxyphenyl fluorescein (HPF), a specific probe of ·OH, was used to demonstrate the intracellular generation of ·OH. As shown in Figure 26, Hf-DBP-QP generated more ·OH than PBS under X-ray irradiation, which supported X-ray-triggered SN38 release from Hf-DBP-QP-SN.

Hf-DBP-QP-SN(+) generated 26.33% ROS^+ cells, which was significantly higher than Hf-DBP-QP(+) (4.82%). See Figures 27A-27D. This difference could be caused by the oxidative pressure by released SN38 molecules.[43]

Clonogenic assays were conducted to determine the radio-enhancement effects.[84] At the same Hf concentration of 50 μM μM, Hf-DBP-QP and Hf-DBP-QP-SN exhibited long-term anti-proliferative effect with a radiation enhancement factor (REF_{10}) of 1.147, and 2.52, respectively. See Figures 28A and 28B. The radioenhancement of Hf-DBP-QP likely resulted from RT-RDT process, while the higher radioenhancing effect of Hf-DBP-QP-SN was likely due to the synergistic effect between RT-RDT and chemotherapy resulted from the released SN38 triggered by ·OH.

Flow cytometry was used to assay the exposure of phosphatidylserine (PS) of CT26 cells by annexin V/propidium iodide (PI) apoptosis staining. See Figure 28C. Compared with PBS(-) and PBS(+) groups, Hf-DBP-QP(+) treatment gave an increased ratio of early and late apoptotic cells (29%), suggesting effective radioenhancement effect of Hf-DBP-QP. Hf-DBP-QP-SN(+) treatment showed an increase of necrosis, early and late apoptosis (44.81%), supporting the successful release of the SN38 to result in a higher proportion of apoptotic and necrotic cells than Hf-DBP-QP(+) treatment.

DNA damage was measured by γ-H2AX assay. See Figure 29. Hf-DBP-QP(+) treatment showed stronger red fluorescence than PBS(+) treated cells, suggesting the RT-RDT process could effectively lead to more DNA damage. Hf-DBP-QP-SN(+) treated cancer cells showed stronger DNA damage than Hf-DBP-QP(+) treated cells, likely due to DNA damage by released SN38. Taken together, Hf-DBP-QP-SN(+) treatment effectively generated ROS through the RT-RDT process and caused oxidative stress by the released SN38.

In vitro experiments:

The CT26 tumor model was established on BALB/c mice by inoculating 2×10^6 cells/mouse subcutaneously onto the right flanks. When the volume of CT26 tumors reached ~105 mm^3, the mice were randomized into six groups (n = 5) to receive PBS(-), Hf-DBP-QP-SN(-) (0.5 μmol Hf and 0.037 μmol SN38), PBS(+), irinotecan(+) (a prodrug of SN38: 0.037 μmol), Hf-DBP-QP(+), or Hf-DBP-QP-SN(+) treatment. Hf-DBP-QP-SN(-) exhibited no obvious tumor inhibition effect, supporting low toxicity of the nMOF nanotherapeutics. Irradiation of CT26 tumors with 2 Gy X-ray by 3 fractions moderately inhibited tumor growth with a tumor growth inhibition index (TGI) of 0.474, while Hf-DBP-QP(+) enhanced tumor growth inhibition with a TGI of 0.744. Irinotecan(+) exhibited a TGI of 0.641 due to the additive effect of radiotherapy and chemotherapy. Importantly, Hf-DBP-QP-SN(+) treatment gave an impressive TGI of 0.935 (see Figure 30A), demonstrating the synergistic effect between RT-RDT and chemotherapeutic effect of SN38 released from Hf-DBP-QP-SN in the tumors.

The therapeutic effects of Hf-DBP-QP-SN(+) and control groups were also evaluated by analyzing tumor slices by hematoxylin and eosin (H&E) and TdT-mediated dUTP nick end labeling (TUNEL) staining. See Figures 31. In the Hf-DBP-QP-SN(-) group, no damaged or apoptotic cancer cells were observed, suggesting insignificant premature release of SN38 in the absence of X-ray irradiation. In the PBS(+) group, only a small percentage of damaged cancer cells and TUNEL positive cells were observed, while Hf-DBP-QP(+) treatment reduced the number of viable cancer cells and increased TUNEL positive cells. Hf-DBP-QP-SN(+) treatment led to the most damaged and TUNEL positive cells, supporting the synergistic antitumor effects from RT-RDT and chemotherapy from released SN38. γ-H2AX and Ki67 staining further demonstrated that Hf-DBP-QP-SN(+) effectively induced the strongest DNA damage and inhibited tumor proliferation while greatly reducing systemic toxicity of traditional chemotherapeutic drugs. See Figure 31.

Importantly, the mice in all treatment groups showed similar and steady body weight growth patterns (see Figure 30B), suggesting the lack of toxicity from these treatments. The treatments did not cause any histological abnormality in major organs (see Figure 32), further supporting the safety of Hf-DBP-QP-SN(+) treatment. Finally, Hf-DBP-QP-SN(+) treatment significantly increased the median survival to 38 days from 29 days for Hf-DBP-QP(+) treatment. See Figure 33. For comparison, PBS(+) only modestly increased mouse median survival to 21 days from 18 days for PBS(-). These results showed that Hf-DBP-QP-SN served as an efficient radioenhancer and a novel nanotherapeutics for X-ray triggered release of SN38 for tumor-targeted and synergistic RT-RDT and chemotherapy without causing systemic toxicity.

Summary of Studies with Hf-DBP-QP-SN:

Accordingly, described herein is the successful design of a new functional ligand, QP-SN, with conjugated SN38 via a ·OH-cleavable linker. QP-SN and photosensitizing DBP ligands were used to prepare a novel mix-ligand nMOF, Hf-DBP-QP-SN, as a potent nMOF radiosensitizer and nanotherapeutic for RT-RDT and chemotherapy via X-ray triggered release of SN38 in tumors. Test tube, *in vitro*, and *in vivo* studies demonstrated that X-ray could precisely stimulate the release of SN38 from Hf-DBP-QP-SN in tumors through a cascade of ·OH generation under X-ray irradiation, hydroxylation of the 3,5-dimethoxylbenzyl carbonate at ortho positions, and subsequent 1,4-elimination to release SN38. Hf-DBP-QP-SN plus X-ray treatment significantly inhibit the tumor growth with a TGI of 0.935 via synergistic RT-RDT and X-ray induced chemotherapy. These findings suggest a new area of 'ionizing radiation'-mediated chemistry for on-demand prodrug activation. The local conversion of an inactive prodrug to an active drug via concurrent RT can potentially lead to much more tolerable treatment regimens without the debilitating adverse effects from concurrent radiotherapy and systemic chemotherapy.

EXAMPLE 5

Hf-DBP-QP-R848

As an example of a MOF comprising a X-ray-triggerable innate immune modulate prodrug, a MOF was prepared comprising a prodrug of R848, as described hereinbelow. See Scheme 7, below. For comparison, a homogenous R848 prodrug was also prepared. See Scheme 6, below. X-ray-triggerable prodrugs of other innate immune modulators (see Figures 35A-35C) can also be prepared.

Synthesis of MeO-R848:

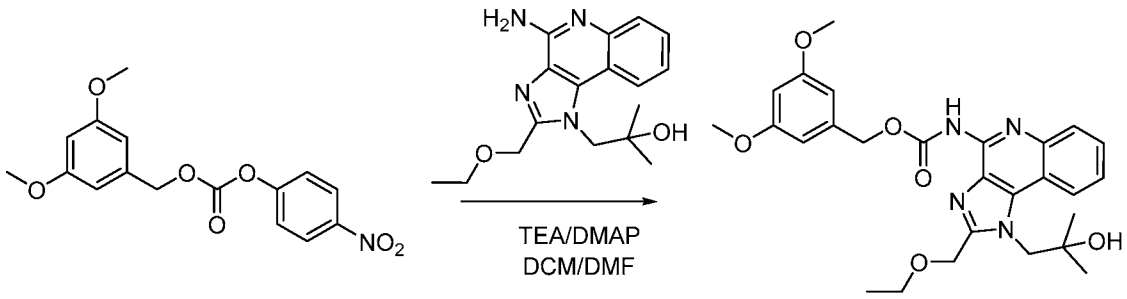

Scheme 6. Synthesis of Me-R848.

Dimethyl 3,5-dimethoxybenzyl (4-nitrophenyl) carbonate (50 mg, 0.15 mmol), R848 (47 mg, 0.15 mmol), TEA (45 mg, 0.45 mmol, 3 eq), DMAP (6 mg, 0.05, 0.33 eq) were combined in dry DMF (30 mL) and stirred for 1 day at RT. The resulting solution was concentrated by rotary evaporation, dried completely under vacuum and purified via column chromatography to produce 3,5-dimethoxybenzyl (2-(ethoxymethyl)-1-(2-hydroxy-2-methylpropyl)-1H-imidazo[4,5-c]quinolin-4-yl)carbamate (**MeO-R848,** 32 mg, Yield: 42 %). ^{1}H NMR (500 MHz, $CDCl_3$) δ 8.17 (t, *J* = 8.0 Hz, 2H), 8.02 (s, 2H), 7.62 (t, *J* = 7.7 Hz, 1H), 7.49 (t, *J* = 7.6 Hz, 1H), 6.64 (d, *J* = 2.4 Hz, 2H), 6.45 (t, *J* = 2.1 Hz, 1H), 5.28 (s, 2H), 4.92 (s, 2H), 4.80 (s, 2H), 3.83 (s, 6H), 3.67 (q, *J* = 6.9 Hz, 2H), 2.97 (s, 5H), 2.89 (s, 5H), 1.43 – 1.20 (m, 13H). HR-MS (ESI, positive mode): *m/z* calc'd for $C_{27}H_{32}N_4O_6$ $[M+H]^+$: 509.2322, found 509.2436.

Synthesis of Hf-DBP-QP-R848:

As shown in Scheme 7, below, Hf-DBP-QP-NO_2 nMOF (4.73 μmol based on QP) was redispersed in ACN before the addition of R848 (1.5 mg, 4.73 μmol) and TEA (1.2 μL, 10 μmol); the solution was then stirred for 3 days. The as-synthesized Hf-DBP-QP-R848 was washed with ACN 10 times to remove remaining R848 to less than 1% than conjugated R848. The measurement was quantified by LC-MS.

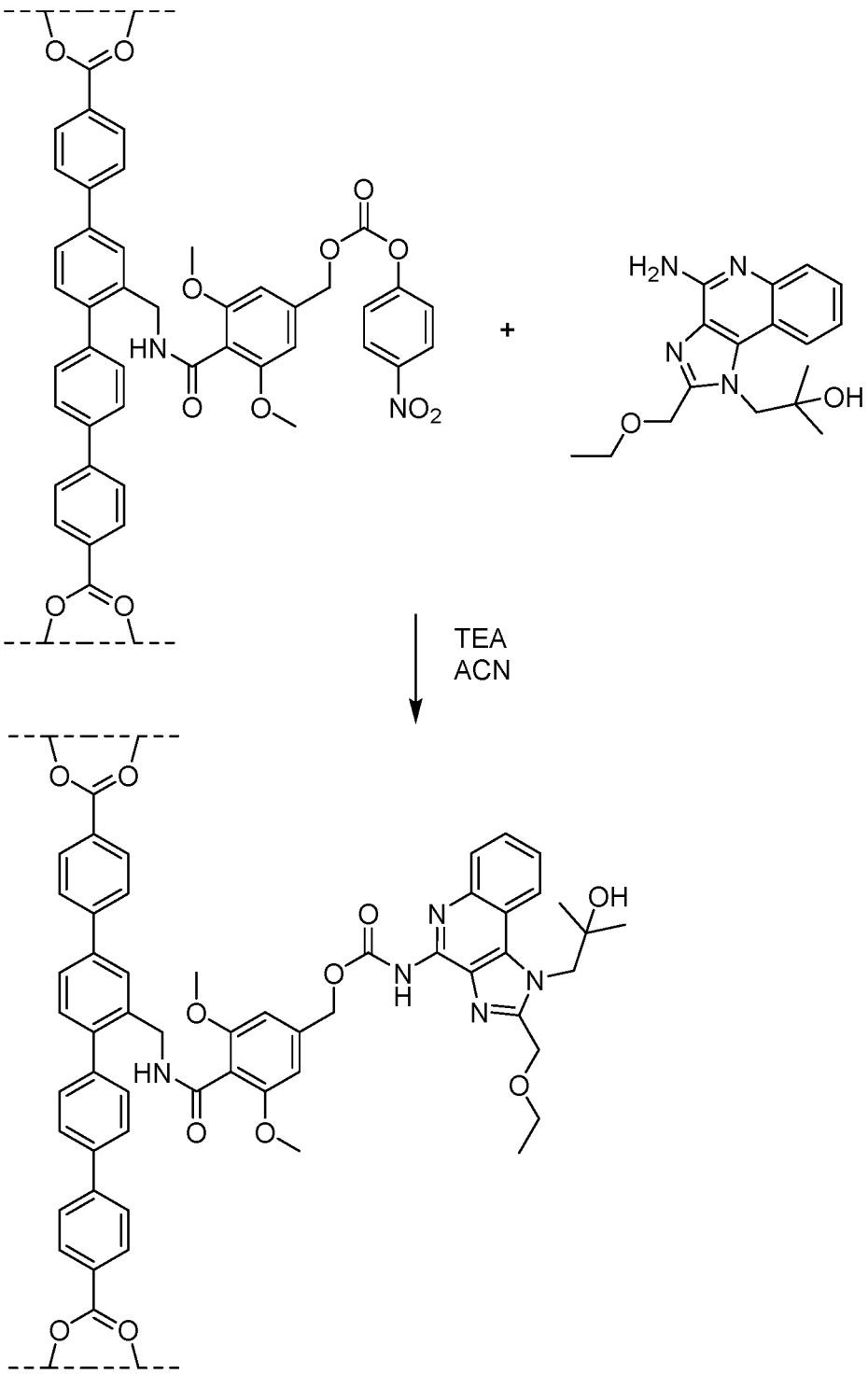

Scheme 7. Synthesis of Hf-DBP-QP-R848.

The free R848 measurement was conducted by disintegrating nMOF using a 1 M $NaHCO_3$ solution, diluting it with ACN, and then analyzing with LC-MS. For the measurement of conjugated R848, the carbamate was hydrolyzed using a 0.4 M NaOH

solution at 85 °C for 1 h. The resulting mixture was then diluted with ACN and analyzed using LC-MS.

Ex vivo TLR7/8 activation by Hf-DBP-QP-R848 with X-ray:

Bone marrow-derived dendritic cells (BMDCs) were obtained by the following procedure: Female C57BL/c mice aged 6 to 8 weeks were euthanized, and bone marrow cells were extracted from the femur and tibia using insulin syringes containing RPMI-1640. Sterile ACK buffer (Corning, Glendale, Arizona, United States of America) was used to lyse the red blood cells, and the remaining cells were cultured in RPMI-1640 complete medium supplemented with 20 ng/mL recombinant mouse granulocyte-macrophage colony-stimulating factor (GM-CSF, R&D Systems, Minneapolis, Minnesota, United States of America) and 10 ng/mL recombinant murine interleukin-4 (IL-4, PeproTech, Cranbury, New Jersey, United States of America). On day 4, the entire medium was discarded and replaced with a fresh, warm medium containing 20 ng/mL GM-CSF and 10 ng/mL IL-4. On day 6, the loosely attached cells in the semi-suspended state were collected by gentle pipetting, and the medium suspension containing these cells was designated as BMDCs. The purity of the cells was assessed using flow cytometry with CD11c-PE/Cy5.5 (N418) antibodies.

BMDCs were plated in 96-well plates at a density of 5×10^4 cells per well. Various concentrations of Hf-DBP-QP-R848 were irradiated with 0, 1, 5, 10, or 50 Gy and then added to the cells. The cells were incubated for 24 hours. The culture supernatants were collected and analyzed using enzyme-linked immunosorbent assay (ELISA) to measure IL-6 levels. See Figure 34. The EC_{50}s of Hf-DBP-QP-R848 under various doses of X-ray are described in Table 1, below.

Table 1. EC_{50} of Hf-DBP-QP-R848 to BMDCs under various doses of X-ray (nM based on conjugated R848)

0 Gy	1 Gy	5 Gy	10 Gy	50 Gy
456.8	319.2	316.9	334.7	284.3

EXAMPLE 6

Hf-DBP-QP-Pomalidomide

The radiation-sensitive release of N-alkyl-picolinium-based prodrugs has recently been reported.[85] As described in Schemes 8 and 9, below, a pomalidomide prodrug nMOF

was prepared containing a bridging ligand with a picolinium-based linkage that can be cleaved via a radiation-induced radical-promoted mechanism.

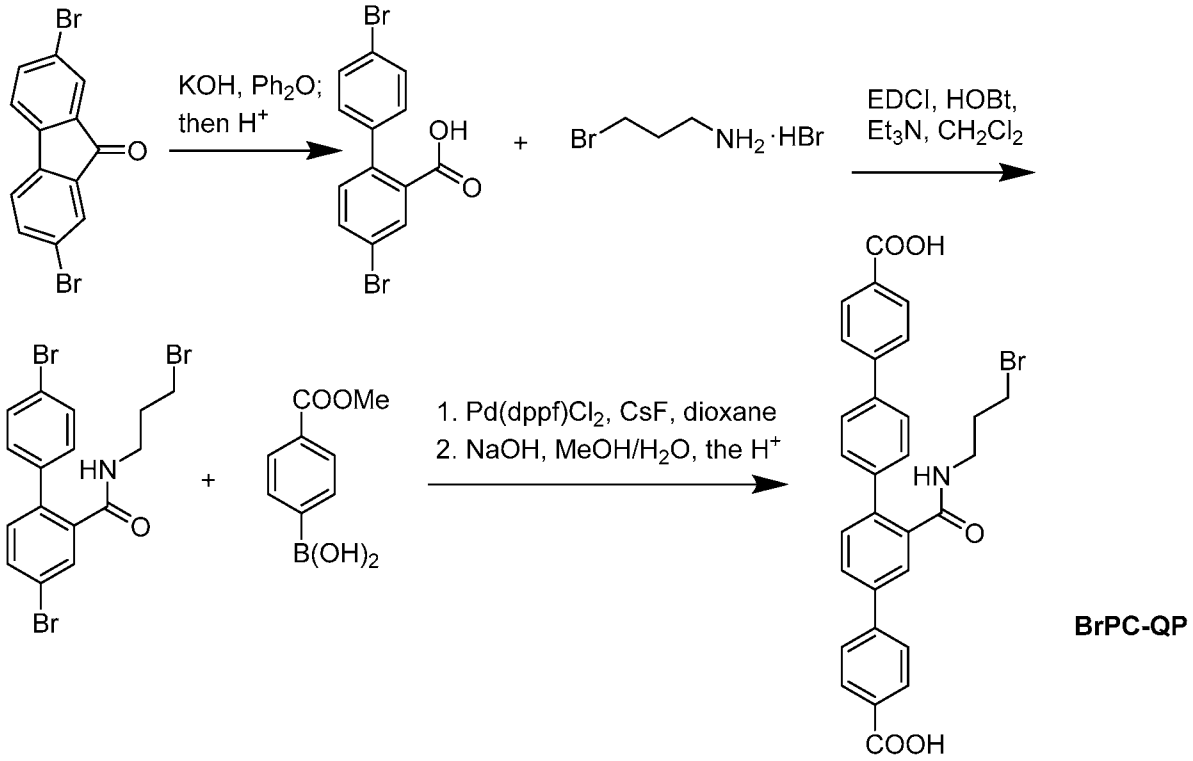

Scheme 8. Synthesis of BrPC-QP.

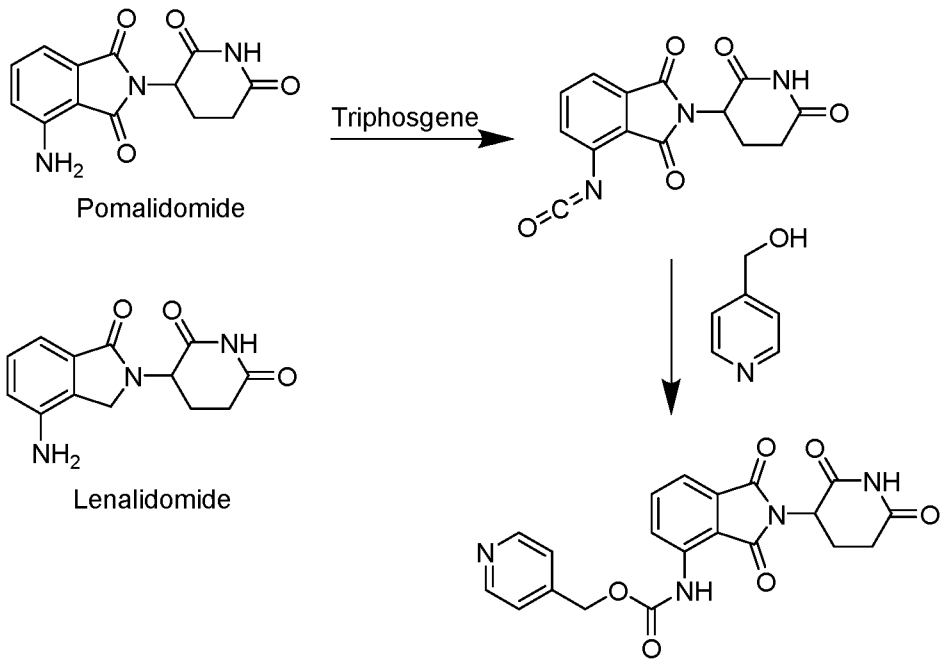

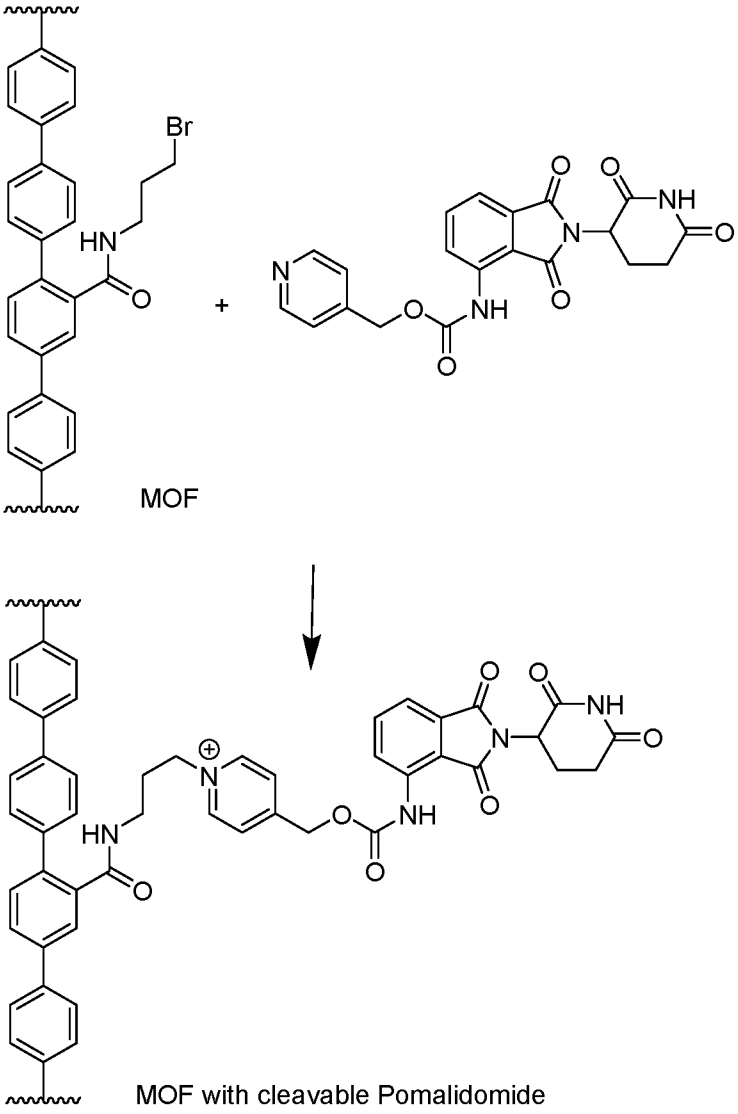

Scheme 9. Synthesis of MOF with QP-Pomalidomide

As shown in Scheme 8, above, the quaterphenyl dicarboxylic acid with a *N*-3-bromopropyl carbamate (**BrPC-QP**) was synthesized from 2,7-dibromo-9*H*-fluoren-9-one in 4 steps via intramolecular ring-opening, amide formation with 3-bromopropamine, Suzuki coupling with (4-(methoxycarbonyl)phenyl)boronic acid, and base-catalyzed hydrolysis. As shown in Scheme 9, above, a pyridine-substituted carbamate of small molecule chemotherapeutic pomalidomide was prepared by reacting pomalidomide with phosgene and then with 4-(hydroxymethylpyridine). Other chemotherapeutics, such as lenalidomide, can be used in place of pomalidomide. A mix-ligand nMOF, Hf-DBP-QP-BrPC, was synthesized solvothermally by heating a mixture of $HfCl_4$, H_2DBP, BrPC-QP, acetic acid, and water in *N, N*-dimethylformamide at 80 °C for 1 day. Finally, Hf-DBP-QP-PC was post-synthetically modified by treatment with the pyridine-substituted carbamate of pomalidomide afford Hf-

DBP-QP-pomalidamide, i.e., a nMOF with pomalidomide covalently linked to a QP ligand by a X-ray sensitive picolinium linkage.

REFERENCES

All references listed herein including but not limited to all patents, patent applications and publications thereof, scientific journal articles, and database entries are incorporated herein by reference in their entireties to the extent that they supplement, explain, provide a background for, or teach methodology, techniques, and/or compositions employed herein.

(1) Horcajada, P.; Gref, R.; Baati, T.; Allan, P. K.; Maurin, G.; Couvreur, P.; Férey, G.; Morris, R. E.; Serre, C., Metal–Organic Frameworks in Biomedicine. *Chem. Rev.* **2012,** *112* (2), 1232-1268.

(2) McKinlay, A. C.; Morris, R. E.; Horcajada, P.; Férey, G.; Gref, R.; Couvreur, P.; Serre, C., BioMOFs: Metal–Organic Frameworks for Biological and Medical Applications. *Angew. Chem. Int. Ed.* **2010,** *49* (36), 6260-6266.

(3) Yang, J.; Yang, Y.-W., Metal–Organic Frameworks for Biomedical Applications. *Small* **2020,** *16* (10), 1906846.

(4) Ge, X.; Wong, R.; Anisa, A.; Ma, S., Recent development of metal-organic framework nanocomposites for biomedical applications. *Biomaterials* **2022,** *281*, 121322.

(5) Sun, Y.; Zheng, L.; Yang, Y.; Qian, X.; Fu, T.; Li, X.; Yang, Z.; Yan, H.; Cui, C.; Tan, W., Metal–Organic Framework Nanocarriers for Drug Delivery in Biomedical Applications. *Nano-Micro Lett.* **2020,** *12* (1), 103.

(6) Horcajada, P.; Chalati, T.; Serre, C.; Gillet, B.; Sebrie, C.; Baati, T.; Eubank, J. F.; Heurtaux, D.; Clayette, P.; Kreuz, C.; Chang, J.-S.; Hwang, Y. K.; Marsaud, V.; Bories, P.-N.; Cynober, L.; Gil, S.; Férey, G.; Couvreur, P.; Gref, R., Porous metal–organic-framework nanoscale carriers as a potential platform for drug delivery and imaging. *Nat. Mater.* **2010,** *9* (2), 172-178.

(7) Horcajada, P.; Serre, C.; Maurin, G.; Ramsahye, N. A.; Balas, F.; Vallet-Regí, M.; Sebban, M.; Taulelle, F.; Férey, G., Flexible Porous Metal-Organic Frameworks for a Controlled Drug Delivery. *J. Am. Chem. Soc.* **2008,** *130* (21), 6774-6780.

(8) Orellana-Tavra, C.; Baxter, E. F.; Tian, T.; Bennett, T. D.; Slater, N. K. H.; Cheetham, A. K.; Fairen-Jimenez, D., Amorphous metal–organic frameworks for drug delivery. *Chem. Commun.* **2015,** *51* (73), 13878-13881.

(9) Teplensky, M. H.; Fantham, M.; Li, P.; Wang, T. C.; Mehta, J. P.; Young, L. J.; Moghadam, P. Z.; Hupp, J. T.; Farha, O. K.; Kaminski, C. F.; Fairen-Jimenez, D., Temperature Treatment of Highly Porous Zirconium-Containing Metal–Organic Frameworks Extends Drug Delivery Release. *J. Am. Chem. Soc.* **2017,** *139* (22), 7522-7532.

(10) Orellana-Tavra, C.; Marshall, R. J.; Baxter, E. F.; Lázaro, I. A.; Tao, A.; Cheetham, A. K.; Forgan, R. S.; Fairen-Jimenez, D., Drug delivery and controlled release from biocompatible metal–organic frameworks using mechanical amorphization. *J. Mater. Chem. B* **2016,** *4* (47), 7697-7707.

(11) He, C.; Lu, K.; Liu, D.; Lin, W., Nanoscale Metal–Organic Frameworks for the Co-Delivery of Cisplatin and Pooled siRNAs to Enhance Therapeutic Efficacy in Drug-Resistant Ovarian Cancer Cells. *J. Am. Chem. Soc.* **2014,** *136* (14), 5181-5184.

(12) Sun, C.-Y.; Qin, C.; Wang, C.-G.; Su, Z.-M.; Wang, S.; Wang, X.-L.; Yang, G.-S.; Shao, K.-Z.; Lan, Y.-Q.; Wang, E.-B., Chiral Nanoporous Metal-Organic Frameworks with High Porosity as Materials for Drug Delivery. *Adv. Mater.* **2011,** *23* (47), 5629-5632.

(13) Luo, T.; Nash, G. T.; Jiang, X.; Feng, X.; Mao, J.; Liu, J.; Juloori, A.; Pearson, A. T.; Lin, W., A 2D Nanoradiosensitizer Enhances Radiotherapy and Delivers STING Agonists to Potentiate Cancer Immunotherapy. *Adv. Mater.* **2022,** *34*, 2110588.

(14) Morris, W.; Briley, W. E.; Auyeung, E.; Cabezas, M. D.; Mirkin, C. A., Nucleic Acid–Metal Organic Framework (MOF) Nanoparticle Conjugates. *J. Am. Chem. Soc.* **2014,** *136* (20), 7261-7264.

(15) Zhao, N.; Yan, L.; Zhao, X.; Chen, X.; Li, A.; Zheng, D.; Zhou, X.; Dai, X.; Xu, F.-J., Versatile Types of Organic/Inorganic Nanohybrids: From Strategic Design to Biomedical Applications. *Chem. Rev.* **2019,** *119* (3), 1666-1762.

(16) Zhou, Z.; Vázquez-González, M.; Willner, I., Stimuli-responsive metal–organic framework nanoparticles for controlled drug delivery and medical applications. *Chem. Soc. Rev.* **2021,** *50* (7), 4541-4563.

(17) Wang, Y.; Yan, J.; Wen, N.; Xiong, H.; Cai, S.; He, Q.; Hu, Y.; Peng, D.; Liu, Z.; Liu, Y., Metal-organic frameworks for stimuli-responsive drug delivery. *Biomaterials* **2020,** *230*, 119619.

(18) Li, Y.; Teng, X.; Wang, Y.; Yang, C.; Yan, X.; Li, J., Neutrophil Delivered Hollow Titania Covered Persistent Luminescent Nanosensitizer for Ultrosound Augmented Chemo/Immuno Glioblastoma Therapy. *Adv. Sci.* **2021,** *8* (17), 2004381.

(19) Li, Y.; Teng, X.; Yang, C.; Wang, Y.; Wang, L.; Dai, Y.; Sun, H.; Li, J., Ultrasound Controlled Anti-Inflammatory Polarization of Platelet Decorated Microglia for Targeted Ischemic Stroke Therapy. *Angew. Chem. Int. Ed.* **2021,** *60* (10), 5083-5090.

(20) Zhang, C.; Wang, X.; Liu, G.; Ren, H.; Li, J.; Jiang, Z.; Liu, J.; Lovell, J. F.; Zhang, Y., Metal coordination micelles for anti-cancer treatment by gene-editing and phototherapy. *J. Controlled Release* **2023,** *357*, 210-221.

(21) Liu, G.; Jiang, Z.; Lovell, J. F.; Zhang, L.; Zhang, Y., Design of a Thiol-Responsive, Traceless Prodrug with Rapid Self-Immolation for Cancer Chemotherapy. *ACS Appl. Bio Mater.* **2021,** *4* (6), 4982-4989.

(22) Kilian, H. I.; Pradhan, A. J.; Jahagirdar, D.; Ortega, J.; Atilla-Gokcumen, G. E.; Lovell, J. F., Light-Triggered Release of Large Biomacromolecules from Porphyrin-Phospholipid Liposomes. *Langmuir* **2021,** *37* (36), 10859-10865.

(23) Lu, S.; Hao, D.; Xiang, X.; Pei, Q.; Xie, Z., Carboxylated paclitaxel prodrug nanofibers for enhanced chemotherapy. *J. Controlled Release* **2023,** *355*, 528-537.

(24) Hao, D.; Meng, Q.; Jiang, B.; Lu, S.; Xiang, X.; Pei, Q.; Yu, H.; Jing, X.; Xie, Z., Hypoxia-Activated PEGylated Paclitaxel Prodrug Nanoparticles for Potentiated Chemotherapy. *ACS Nano* **2022,** *16* (9), 14693-14702.

(25) Lu, S.; Xia, R.; Wang, J.; Pei, Q.; Xie, Z.; Jing, X., Engineering Paclitaxel Prodrug Nanoparticles via Redox-Activatable Linkage and Effective Carriers for Enhanced Chemotherapy. *ACS Appl. Mater. Interfaces* **2021,** *13* (39), 46291-46302.

(26) Spring, B. Q.; Bryan Sears, R.; Zheng, L. Z.; Mai, Z.; Watanabe, R.; Sherwood, M. E.; Schoenfeld, D. A.; Pogue, B. W.; Pereira, S. P.; Villa, E.; Hasan, T., A photoactivable multi-inhibitor nanoliposome for tumour control and simultaneous inhibition of treatment escape pathways. *Nat. Nanotechnol.* **2016,** *11* (4), 378-387.

(27) Xie, J.; Gonzalez-Carter, D.; Tockary, T. A.; Nakamura, N.; Xue, Y.; Nakakido, M.; Akiba, H.; Dirisala, A.; Liu, X.; Toh, K.; Yang, T.; Wang, Z.; Fukushima, S.; Li, J.; Quader, S.; Tsumoto, K.; Yokota, T.; Anraku, Y.; Kataoka, K., Dual-Sensitive Nanomicelles Enhancing Systemic Delivery of Therapeutically Active Antibodies Specifically into the Brain. *ACS Nano* **2020,** *14* (6), 6729-6742.

(28) Liu, J.; Saw, R. E.; Kiang, Y. H., Calculation of Effective Penetration Depth in X-Ray Diffraction for Pharmaceutical Solids. *J. Pharm. Sci.* **2010,** *99* (9), 3807-3814.

(29) Dawson, L. A.; Sharpe, M. B., Image-guided radiotherapy: rationale, benefits, and limitations. *Lancet Oncol.* **2006,** *7* (10), 848-858.

(30) Verellen, D.; Ridder, M. D.; Linthout, N.; Tournel, K.; Soete, G.; Storme, G., Innovations in image-guided radiotherapy. *Nat. Rev. Cancer* **2007,** *7* (12), 949-960.

(31) Barker, H. E.; Paget, J. T. E.; Khan, A. A.; Harrington, K. J., The tumour microenvironment after radiotherapy: mechanisms of resistance and recurrence. *Nat. Rev. Cancer* **2015,** *15* (7), 409-425.

(32) Yang, C.; Yang, Y.; Li, Y.; Ni, Q.; Li, J., Radiotherapy-Triggered Proteolysis Targeting Chimera Prodrug Activation in Tumors. *J. Am. Chem. Soc.* **2023,** *145* (1), 385-391.

(33) Ding, Z.; Guo, Z.; Zheng, Y.; Wang, Z.; Fu, Q.; Liu, Z., Radiotherapy Reduces N-Oxides for Prodrug Activation in Tumors. *J. Am. Chem. Soc.* **2022,** *144* (21), 9458-9464.

(34) Quintana, J. M.; Arboleda, D.; Hu, H.; Scott, E.; Luthria, G.; Pai, S.; Parangi, S.; Weissleder, R.; Miller, M. A., Radiation Cleaved Drug-Conjugate Linkers Enable Local Payload Release. *Bioconjugate Chem.* **2022,** *33* (8), 1474-1484.

(35) Tuo, W.; Renault, J.-P.; Rajpal, A.; Pin, S.; Le Gall, T.; Taran, F., Radiation-Responsive Benzothiazolines as Potential Cleavable Fluorogenic Linkers for Drug Delivery. *Chem. Eur. J.* **2023,** *n/a* (n/a), e202300358.

(36) Takakura, H.; Matsuhiro, S.; Inanami, O.; Kobayashi, M.; Saita, K.; Yamashita, M.; Nakajima, K.; Suzuki, M.; Miyamoto, N.; Taketsugu, T.; Ogawa, M., Ligand release from silicon phthalocyanine dyes triggered by X-ray irradiation. *Org. Biomol. Chem.* **2022,** *20* (36), 7270-7277.

(37) Guo, Z.; Hong, H.; Zheng, Y.; Wang, Z.; Ding, Z.; Fu, Q.; Liu, Z., Radiotherapy-Induced Cleavage of Quaternary Ammonium Groups Activates Prodrugs in Tumors. *Angew. Chem. Int. Ed.* **2022,** *61* (34), e202205014.

(38) Fu, Q.; Li, H.; Duan, D.; Wang, C.; Shen, S.; Ma, H.; Liu, Z., External-Radiation-Induced Local Hydroxylation Enables Remote Release of Functional Molecules in Tumors. *Angew. Chem. Int. Ed.* **2020,** *59* (48), 21546-21552.

(39) Lu, K.; He, C.; Guo, N.; Chan, C.; Ni, K.; Lan, G.; Tang, H.; Pelizzari, C.; Fu, Y.-X.; Spiotto, M. T.; Weichselbaum, R. R.; Lin, W., Low-dose X-ray radiotherapy–radiodynamic therapy via nanoscale metal–organic frameworks enhances checkpoint blockade immunotherapy. *Nat. Biomed. Eng.* **2018,** *2* (8), 600-610.

(40) Xu, Z.; Ni, K.; Mao, J.; Luo, T.; Lin, W., Monte Carlo Simulations Reveal New Design Principles for Efficient Nanoradiosensitizers Based on Nanoscale Metal–Organic Frameworks. *Adv. Mater.* **2021,** *33* (40), 2104249.

(41) Zhen, W.; Weichselbaum, R. R.; Lin, W., Nanoparticle-Mediated Radiotherapy Remodels the Tumor Microenvironment to Enhance Antitumor Efficacy. *Adv. Mater.* **2023,** *35* (21), 2206370.

(42) Li, Y.; Xie, M.; Jones, J. B.; Zhang, Z.; Wang, Z.; Dang, T.; Wang, X.; Lipowska, M.; Mao, H., Targeted Delivery of DNA Topoisomerase Inhibitor SN38 to Intracranial Tumors of Glioblastoma Using Sub-5 Ultrafine Iron Oxide Nanoparticles. *Adv. Healthc. Mater.* **2022,** *11* (14), 2102816.

(43) Bottero, V.; Busuttil, V. r.; Loubat, A. s.; Magné, N.; Fischel, J.-L.; Milano, G. r.; Peyron, J.-F. o., Activation of Nuclear Factor κB through the IKK Complex by the Topoisomerase Poisons SN38 and Doxorubicin: A Brake to Apoptosis in HeLa Human Carcinoma Cells1. *Cancer Res.* **2001,** *61* (21), 7785-7791.

(44) Ni, K.; Lan, G.; Chan, C.; Quigley, B.; Lu, K.; Aung, T.; Guo, N.; La Riviere, P.; Weichselbaum, R. R.; Lin, W., Nanoscale metal-organic frameworks enhance radiotherapy to potentiate checkpoint blockade immunotherapy. *Nat. Commun.* **2018,** *9* (1), 2351.

(45) Chu, J.; Ke, F.-S.; Wang, Y.; Feng, X.; Chen, W.; Ai, X.; Yang, H.; Cao, Y., Facile and reversible digestion and regeneration of zirconium-based metal-organic frameworks. *Commun. Chem* **2020,** *3* (1), 5.

(46) Ju, E.; Dong, K.; Chen, Z.; Liu, Z.; Liu, C.; Huang, Y.; Wang, Z.; Pu, F.; Ren, J.; Qu, X., Copper(II)–Graphitic Carbon Nitride Triggered Synergy: Improved ROS Generation and Reduced Glutathione Levels for Enhanced Photodynamic Therapy. *Angew. Chem. Int. Ed.* **2016,** *55* (38), 11467-11471.

(47) Halliwell, B.; Gutteridge, J. M. C.; Aruoma, O. I., The deoxyribose method: A simple "test-tube" assay for determination of rate constants for reactions of hydroxyl radicals. *Anal. Biochem.* **1987,** *165* (1), 215-219.

(48) Wang, L.; Xia, J.; Fan, H.; Hou, M.; Wang, H.; Wang, X.; Zhang, K.; Cao, L.; Liu, X.; Ling, J.; Yu, H.; Wu, X.; Sun, J., A tumor microenvironment responsive nanosystem for chemodynamic/chemical synergistic theranostics of colorectal cancer. *Theranostics* **2021,** *11* (18), 8909-8925.

(49) Fan, L.; Peng, G.; Sahgal, N.; Fazli, L.; Gleave, M.; Zhang, Y.; Hussain, A.; Rassool, F.; Qi, J., Abstract 1981: Histone demethyalase JMJD1A promotes the DNA damage response of prostate cancer cells. *Cancer Res.* **2016,** *76* (14_Supplement), 1981-1981.

(50) Xia, D.; Hang, D.; Li, Y.; Jiang, W.; Zhu, J.; Ding, Y.; Gu, H.; Hu, Y., Au–Hemoglobin Loaded Platelet Alleviating Tumor Hypoxia and Enhancing the Radiotherapy Effect with Low-Dose X-ray. *ACS Nano* **2020,** *14* (11), 15654-15668.

(51) Fracaroli, A. M.; Furukawa, H.; Suzuki, M.; Dodd, M.; Okajima, S.; Gándara, F.; Reimer, J. A.; Yaghi, O. M., Metal–Organic Frameworks with Precisely Designed Interior for Carbon Dioxide Capture in the Presence of Water. *J. Am. Chem. Soc.* **2014,** *136* (25), 8863-8866.

(52) Ni, K.; Lan, G.; Chan, C.; Duan, X.; Guo, N.; Veroneau, S. S.; Weichselbaum, R. R.; Lin, W., Ultrathin Metal-Organic-Layer Mediated Radiotherapy-Radiodynamic Therapy. *Matter* **2019,** *1* (5), 1331-1353.

(53) Johnstone, T. C.; Suntharalingam, K.; Lippard, S. J., The Next Generation of Platinum Drugs: Targeted Pt(II) Agents, Nanoparticle Delivery, and Pt(IV) Prodrugs. *Chem. Rev.* **2016,** *116* (5), 3436-3486.

(54) Chabner, B. A.; Roberts, T. G., Chemotherapy and the war on cancer. *Nat. Rev. Cancer* **2005,** *5* (1), 65-72.

(55) Xu, X.; Zeng, Z.; Ding, X.; Shan, T.; Liu, Q.; Chen, M.; Chen, J.; Xia, M.; He, Y.; Huang, Z.; Huang, Y.; Zhao, C., Reactive oxygen species-activatable self-amplifying Watson-Crick base pairing-inspired supramolecular nanoprodrug for tumor-specific therapy. *Biomaterials* **2021,** *277*, 121128.

(56) Zhang, Y.; Xu, C.; Yang, X.; Pu, K., Photoactivatable Protherapeutic Nanomedicine for Cancer. *Adv. Mater.* **2020,** *32* (34), 2002661.

(57) Abet, V.; Filace, F.; Recio, J.; Alvarez-Builla, J.; Burgos, C., Prodrug approach: An overview of recent cases. *Eur. J. Med. Chem.* **2017,** *127*, 810-827.

(58) Zubrod, C. G., Selective Toxicity of Anticancer Drugs: Presidential Address1. *Cancer Res.* **1978,** *38* (12), 4377-4384.

(59) Albert, A., Chemical aspects of selective toxicity. *Nature* **1958,** *182*, 421-423.

(60) Dong, X.; Brahma, R. K.; Fang, C.; Yao, S. Q., Stimulus-responsive self-assembled prodrugs in cancer therapy. *Chem. Sci.* **2022,** *13* (15), 4239-4269.

(61) Hao, Y.; Chen, Y.; He, X.; Yu, Y.; Han, R.; Li, Y.; Yang, C.; Hu, D.; Qian, Z., Polymeric Nanoparticles with ROS-Responsive Prodrug and Platinum Nanozyme for Enhanced Chemophotodynamic Therapy of Colon Cancer. *Adv. Sci.* **2020,** *7* (20), 2001853.

(62) Chu, B.; Qu, Y.; He, X.; Hao, Y.; Yang, C.; Yang, Y.; Hu, D.; Wang, F.; Qian, Z., ROS-Responsive Camptothecin Prodrug Nanoparticles for On-Demand Drug Release and

Combination of Chemotherapy and Photodynamic Therapy. *Adv. Funct. Mater.* **2020,** *30* (52), 2005918.

(63) Zhen, W.; An, S.; Wang, S.; Hu, W.; Li, Y.; Jiang, X.; Li, J., Precise Subcellular Organelle Targeting for Boosting Endogenous-Stimuli-Mediated Tumor Therapy. *Adv. Mater.* **2021,** *33* (51), 2101572.

(64) Luo, C.; Sun, J.; Liu, D.; Sun, B.; Miao, L.; Musetti, S.; Li, J.; Han, X.; Du, Y.; Li, L.; Huang, L.; He, Z., Self-Assembled Redox Dual-Responsive Prodrug-Nanosystem Formed by Single Thioether-Bridged Paclitaxel-Fatty Acid Conjugate for Cancer Chemotherapy. *Nano Lett.* **2016,** *16* (9), 5401-5408.

(65) Zhou, F.; Feng, B.; Wang, T.; Wang, D.; Cui, Z.; Wang, S.; Ding, C.; Zhang, Z.; Liu, J.; Yu, H.; Li, Y., Theranostic Prodrug Vesicles for Reactive Oxygen Species-Triggered Ultrafast Drug Release and Local-Regional Therapy of Metastatic Triple-Negative Breast Cancer. *Adv. Funct. Mater.* **2017,** *27* (46), 1703674.

(66) Zhang, W.; Hu, X.; Shen, Q.; Xing, D., Mitochondria-specific drug release and reactive oxygen species burst induced by polyprodrug nanoreactors can enhance chemotherapy. *Nat. Commun.* **2019,** *10* (1), 1704.

(67) Li, X.; Lovell, J. F.; Yoon, J.; Chen, X., Clinical development and potential of photothermal and photodynamic therapies for cancer. *Nat. Rev. Clin. Oncol.* **2020,** *17* (11), 657-674.

(68) Pham, T. C.; Nguyen, V.-N.; Choi, Y.; Lee, S.; Yoon, J., Recent Strategies to Develop Innovative Photosensitizers for Enhanced Photodynamic Therapy. *Chem. Rev.* **2021,** *121* (21), 13454-13619.

(69) Yang, B.; Chen, Y.; Shi, J., Reactive Oxygen Species (ROS)-Based Nanomedicine. *Chem. Rev.* **2019,** *119* (8), 4881-4985.

(70) Yang, K.; Yang, Z.; Yu, G.; Nie, Z.; Wang, R.; Chen, X., Polyprodrug Nanomedicines: An Emerging Paradigm for Cancer Therapy. *Adv. Mater.* **2022,** *34* (6), 2107434.

(71) Vaidya, S. P.; Patra, M., X-rays Actuate Anticancer Drugs: Opening New Vistas in Prodrug Therapy. *ChemBioChem* **2021,** *22* (21), 2998-3000.

(72) Pan, Y.; Tang, W.; Fan, W.; Zhang, J.; Chen, X., Development of nanotechnology-mediated precision radiotherapy for anti-metastasis and radioprotection. *Chem. Soc. Rev.* **2022,** *51* (23), 9759-9830.

(73) Wang, D.; He, I. W.; Liu, J.; Jana, D.; Wu, Y.; Zhang, X.; Qian, C.; Guo, Y.; Chen, X.; Bindra, A. K.; Zhao, Y., Missing-Linker-Assisted Artesunate Delivery by Metal–

Organic Frameworks for Synergistic Cancer Treatment. *Angew. Chem. Int. Ed.* **2021,** *60* (50), 26254-26259.

(74) Lismont, M.; Dreesen, L.; Wuttke, S., Metal-Organic Framework Nanoparticles in Photodynamic Therapy: Current Status and Perspectives. *Adv. Funct. Mater.* **2017,** *27* (14), 1606314.

(75) Simon-Yarza, T.; Giménez-Marqués, M.; Mrimi, R.; Mielcarek, A.; Gref, R.; Horcajada, P.; Serre, C.; Couvreur, P., A Smart Metal–Organic Framework Nanomaterial for Lung Targeting. *Angew. Chem. Int. Ed.* **2017,** *56* (49), 15565-15569.

(76) Alyami, M. Z.; Alsaiari, S. K.; Li, Y.; Qutub, S. S.; Aleisa, F. A.; Sougrat, R.; Merzaban, J. S.; Khashab, N. M., Cell-Type-Specific CRISPR/Cas9 Delivery by Biomimetic Metal Organic Frameworks. *J. Am. Chem. Soc.* **2020,** *142* (4), 1715-1720.

(77) Haddad, S.; Abánades Lázaro, I.; Fantham, M.; Mishra, A.; Silvestre-Albero, J.; Osterrieth, J. W. M.; Kaminski Schierle, G. S.; Kaminski, C. F.; Forgan, R. S.; Fairen-Jimenez, D., Design of a Functionalized Metal–Organic Framework System for Enhanced Targeted Delivery to Mitochondria. *J. Am. Chem. Soc.* **2020,** *142* (14), 6661-6674.

(78) Lu, K.; Aung, T.; Guo, N.; Weichselbaum, R.; Lin, W., Nanoscale Metal–Organic Frameworks for Therapeutic, Imaging, and Sensing Applications. *Adv. Mater.* **2018,** *30* (37), 1707634.

(79) Ramesh, M.; Ahlawat, P.; Srinivas, N. R., Irinotecan and its active metabolite, SN-38: review of bioanalytical methods and recent update from clinical pharmacology perspectives. *Biomed. Chromatogr.* **2010,** *24* (1), 104-123.

(80) Lan, G.; Ni, K.; Veroneau, S. S.; Song, Y.; Lin, W., Nanoscale Metal–Organic Layers for Radiotherapy–Radiodynamic Therapy. *J. Am. Chem. Soc.* **2018,** *140* (49), 16971-16975.

(81) Lu, K.; He, C.; Lin, W., Nanoscale Metal–Organic Framework for Highly Effective Photodynamic Therapy of Resistant Head and Neck Cancer. *J. Am. Chem. Soc.* **2014,** *136* (48), 16712-16715.

(82) Zhong, X.; Wang, X.; Zhan, G.; Tang, Y. a.; Yao, Y.; Dong, Z.; Hou, L.; Zhao, H.; Zeng, S.; Hu, J.; Cheng, L.; Yang, X., NaCeF4:Gd,Tb Scintillator as an X-ray Responsive Photosensitizer for Multimodal Imaging-Guided Synchronous Radio/Radiodynamic Therapy. *Nano Lett.* **2019,** *19* (11), 8234-8244.

(83) Liu, J.; Hu, F.; Wu, M.; Tian, L.; Gong, F.; Zhong, X.; Chen, M.; Liu, Z.; Liu, B., Bioorthogonal Coordination Polymer Nanoparticles with Aggregation-Induced Emission

for Deep Tumor-Penetrating Radio- and Radiodynamic Therapy. *Adv. Mater.* **2021,** *33* (9), 2007888.

(84) Franken, N. A. P.; Rodermond, H. M.; Stap, J.; Haveman, J.; van Bree, C., Clonogenic assay of cells in vitro. *Nat. Protoc.* **2006,** *1* (5), 2315-2319.

(85) Fu, Q.; Gu, Z.; Shen, S.; Bai, Y.; Wang, X.; Xu, M.; Sun, P.; Chen, J.; Li, D.; Liu, Z., Radiotherapy activates picolinium prodrugs in tumors. *Nature Chemistry* **2024**. doi.org/10/1038/s41557-024-01501-4.

It will be understood that various details of the presently disclosed subject matter may be changed without departing from the scope of the presently disclosed subject matter. Furthermore, the foregoing description is for the purpose of illustration only, and not for the purpose of limitation.

CLAIMS

What is claimed is:

1. A metal organic framework (MOF) comprising an X-ray sensitive prodrug, wherein the MOF comprises metal-containing secondary building units (SBUs) linked together via organic bridging ligands,

wherein at least one of the SBUs comprises a metal cation capable of absorbing X-rays, and

wherein at least one of the organic bridging ligands is substituted by a group having the formula: -L-D, wherein L is a bivalent linker group comprising one or more bonds capable of radical-promoted bond cleavage and wherein D is a monovalent moiety of a therapeutic agent.

2. The MOF of claim 1, wherein the metal cation capable of absorbing X-rays is selected from the group consisting of Hf, a lanthanide metal, Ta, W, Re, Os, Ir, Pt, Au, and Bi.

3. The MOF of claim 2, wherein the metal cation capable of absorbing X-rays is an Hf cation, optionally wherein one or more of the SBUs comprise a Hf oxo cluster, optionally a Hf_6 oxo cluster or a Hf_{12} oxo cluster.

4. The MOF of any one of claims 1-3, wherein L has the structure:

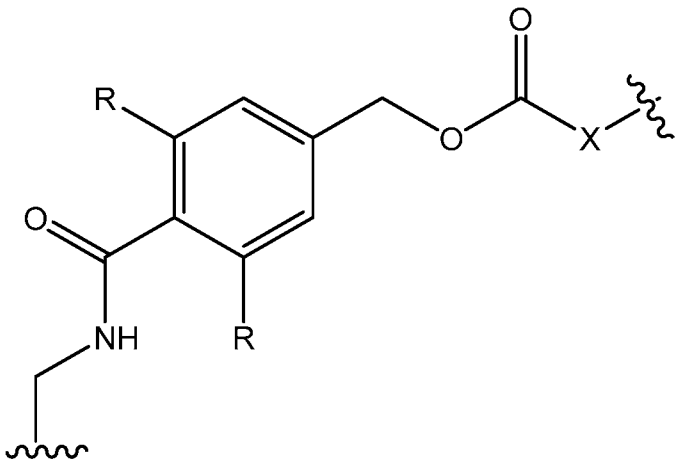

or

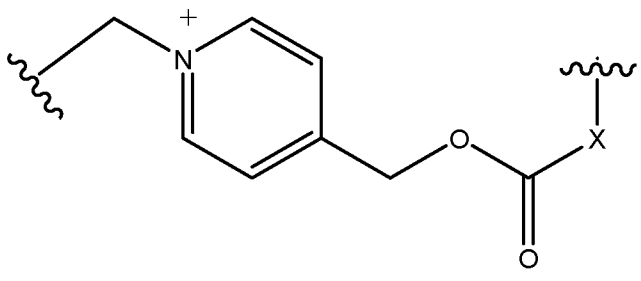

wherein:

X is -O-, -NR'-, -O-X_1-O-, or NH-X_1-NH-, wherein R' is selected from H and alkyl, and X_1 is alkylene, optionally wherein R' is H or methyl and/or X_1 is propylene or ethylene; and

each R is hydroxyl, oxyalkyl, optionally methoxy, or dialkylamino, optionally dimethylamino.

5. The MOF of any one of claims 1-4, wherein the therapeutic agent is a therapeutic agent that comprises at least one functional group selected from a primary amino group, a secondary amino group, -C(=O)-NH_2, -C(=O)OH, a hydroxyl group, and a phenol.

6. The MOF of any one of claims 1-5, wherein the therapeutic agent is a chemotherapeutic agent or an immune modulator, optionally a TLR agonist or a STING agonist.

7. The MOF of any one of claims 1-6, wherein the therapeutic agent is selected from the group consisting of SN38, R848, imiquimod, VTX-378, DSR-6434, ioxoribine, TLR7/8 agonist 1, Cu-712-9, neoseptin-3, and diABZI.

8. The MOF of any one of claims 1-7, wherein the at least one organic bridging ligand substituted by a group having the formula -L-D is an organic bridging ligand comprising a terphenyl (TP) moiety or a quaterphenyl (QP) moiety and at least two groups, which can be the same or different, selected from the group consisting of a carboxylate group, an aromatic or non-aromatic nitrogen-containing group, a phenol, an acetylacetonate, a phosphonate, and a phosphate; optionally wherein the at least one organic bridging ligand has a structure selected from:

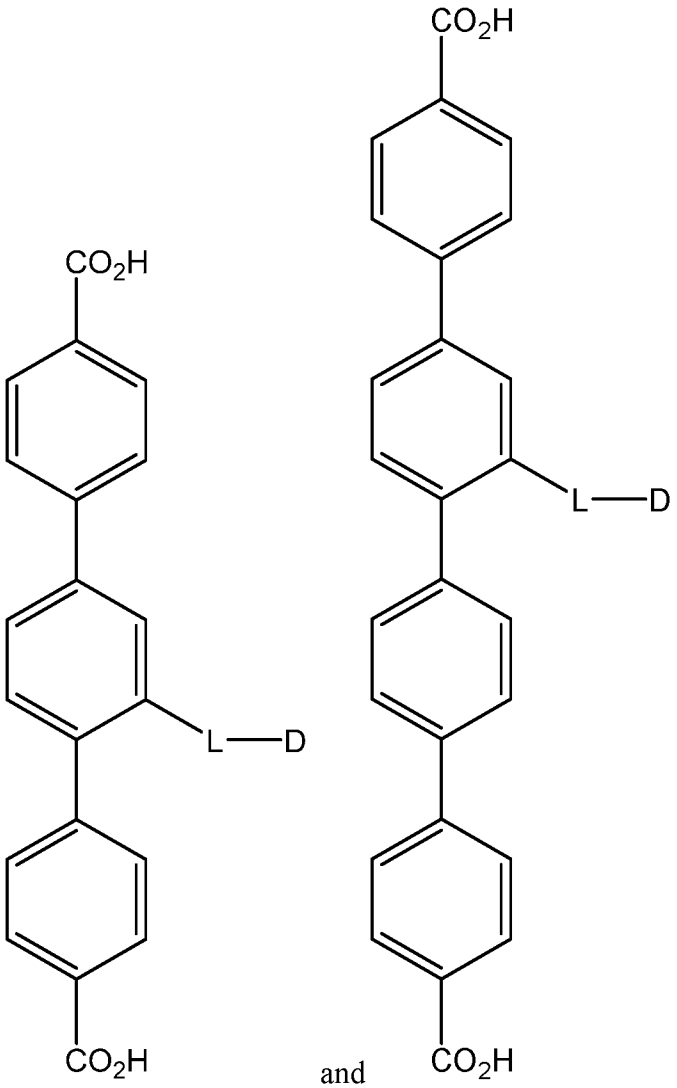

9. The MOF of any one of claims 1-8, further comprising at least one photosensitizer, optionally wherein the MOF comprises at least one organic bridging ligand selected from the group consisting of a porphyrin, a chlorin, a chlorophyll, a phthalocyanine, a ruthenium-bipyridine complex, an iridium-phenylpyridine complex, or an iridium-bipyridine complex.

10. The MOF of claim 9, wherein the MOF comprises at least one organic bridging ligand comprising a porphyrin, optionally bis(p-benzoato)porphyrin (DBP).

11. A pharmaceutical composition comprising an MOF of any one of claims 1-10.

12. A method of treating a disease in a subject in need thereof, the method comprising:

(a) administering to the subject a MOF of any one of claims 1-10, or a pharmaceutical composition of claim 11, and

(b) irradiating at least a portion of the subject with X-rays.

13. The method of claim 12, wherein the disease is cancer, optionally selected from the group consisting of a head tumor, a neck tumor, a head and neck tumor, a breast tumor, a gynecological tumor, a brain tumor, a colorectal cancer, a lung cancer, mesothelioma, a soft tissue sarcoma, and a pancreatic cancer.

14. The method of claim 12 or claim 13, wherein D is a monovalent moiety of a chemotherapeutic agent, thereby providing to the subject, upon performing (b), a combination of (i) chemotherapy and (ii) radiotherapy (RT) or radiotherapy-radiodynamic therapy (RT-RDT).

15. The method of claim 14, wherein the MOF comprises a photosensitizer, optionally DBP, thereby providing to the subject, upon performing (b), a combination of (i) chemotherapy and (ii) RT-RDT.

16. The method of any one of claims 12-15, wherein D is monovalent moiety of SN38 and wherein a higher percentage of SN38 is released from the MOF upon performing (b) compared to release from a comparable amount of a homogenous SN38 prodrug, optionally wherein the homogenous SN38 prodrug is MeO-SN.

17. The method of claim 12 or claim 13, wherein D is a monovalent moiety of an immune modulator, thereby providing to the subject, upon performing (b), a combination of (i) immunotherapy and (ii) RT or RT-RDT.

18. The method of claim 17, wherein the MOF comprises a photosensitizer, optionally DBP, thereby providing to the subject, upon performing (b) a combination of immunotherapy and RT-RDT.

19. The method of any one of claims 12-18, wherein the method provides selective cytotoxicity and/or immune activation in a tumor.

20. Use of an MOF of any one of claims 1-10, or a pharmaceutical composition of claim 11, in treating a disease, optionally cancer, in a subject in need thereof.

21. The use of claim 20, wherein the use provides selective cytotoxicity and/or immune activation in a tumor.

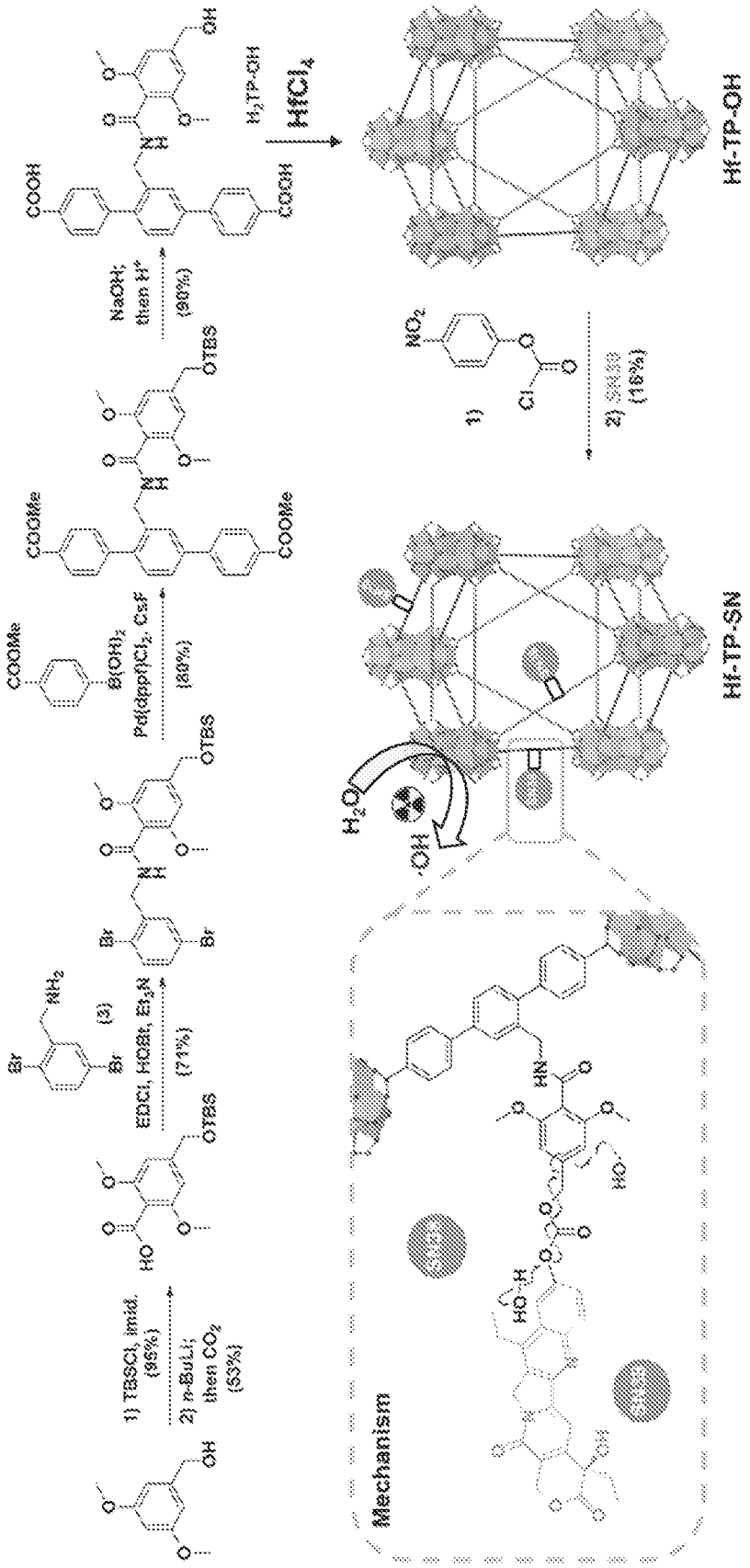

FIG. 1

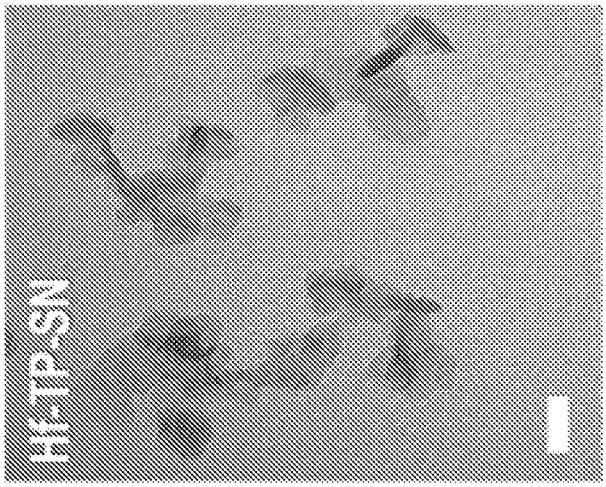

FIG. 2C

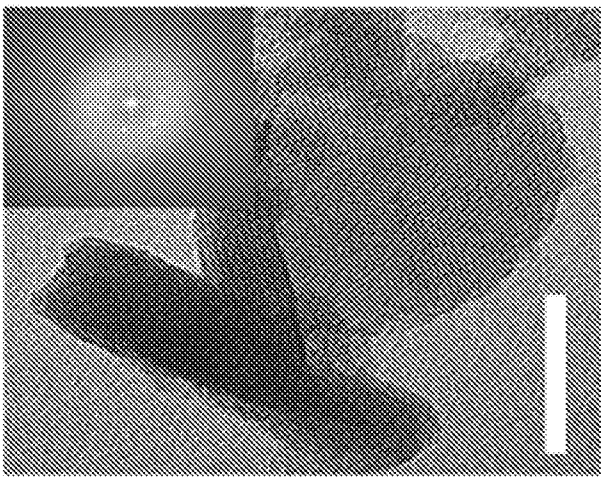

FIG. 2B

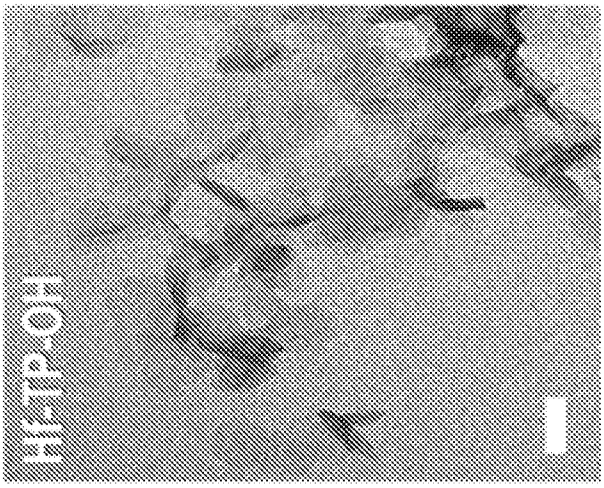

FIG. 2A

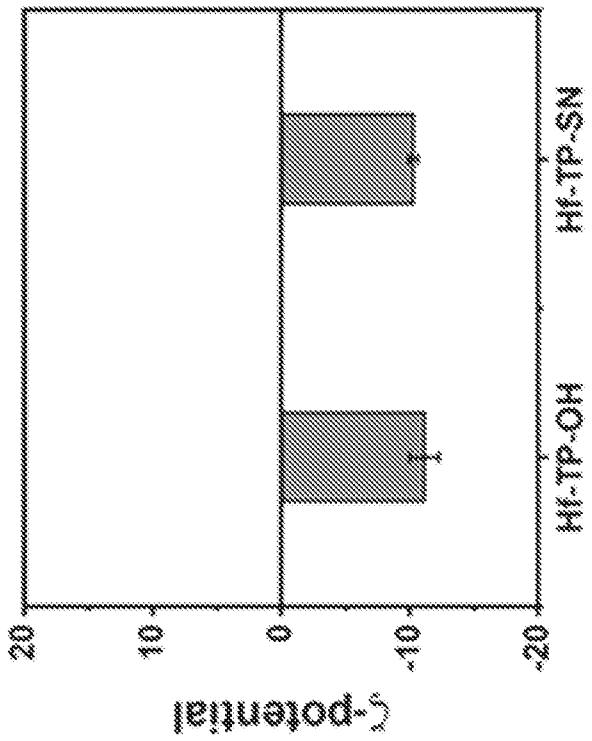
ζ-potential
20
10
0
-10
-20
Hf-TP-OH
Hf-TP-SN

FIG. 3B

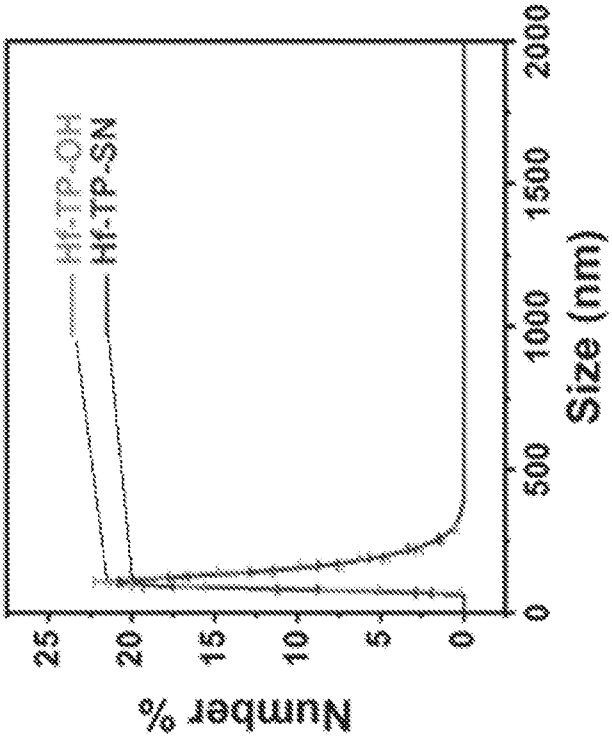
Number %
25
20
15
10
5
0
Size (nm)
0
500
1000
1500
2000
Hf-TP-OH
Hf-TP-SN

FIG. 3A

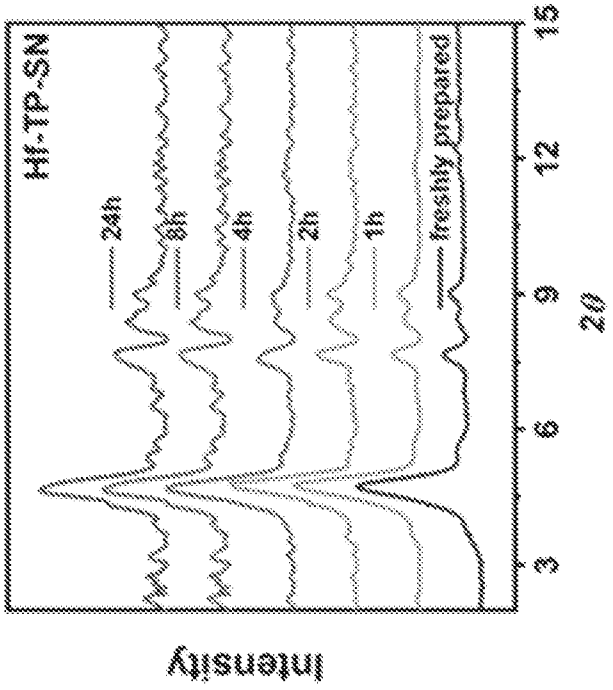
Hf-TP-SN
24h
8h
4h
2h
1h
freshly prepared
3
6
9
12
15
2θ
Intensity

FIG. 3D

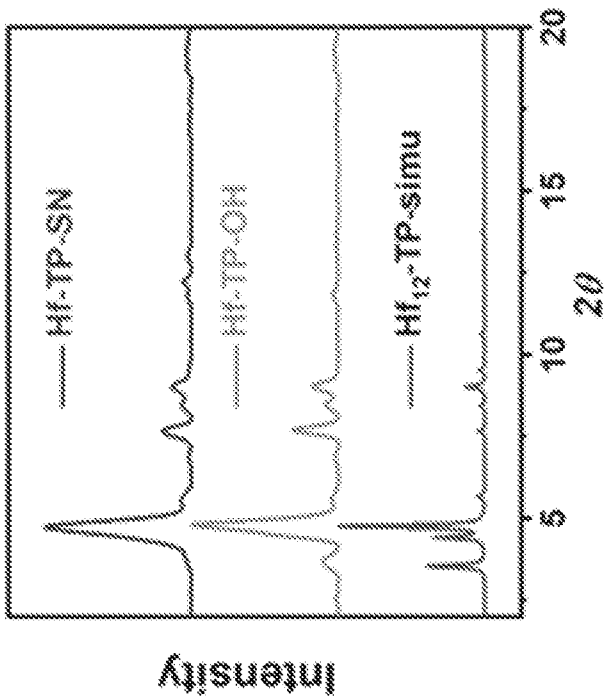
Hf-TP-SN
Hf-TP-OH
Hf12-TP-simu
5
10
15
20
2θ
Intensity

FIG. 3C

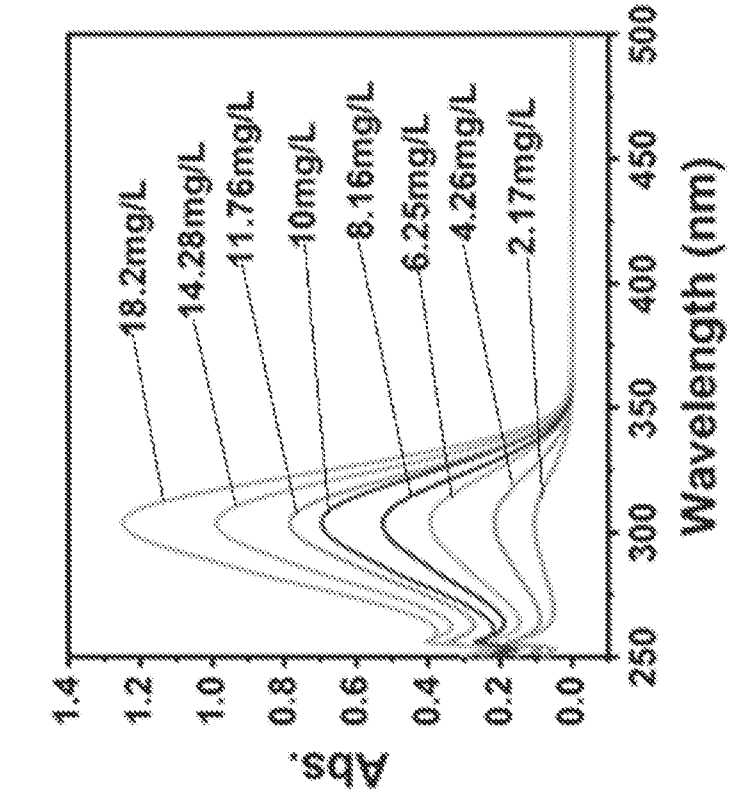
18.2mg/L
14.28mg/L
11.76mg/L
10mg/L
8.16mg/L
6.25mg/L
4.26mg/L
2.17mg/L
Abs.
Wavelength (nm)
1.4
1.2
1.0
0.8
0.6
0.4
0.2
0.0
250
300
350
400
450
500

FIG. 4B

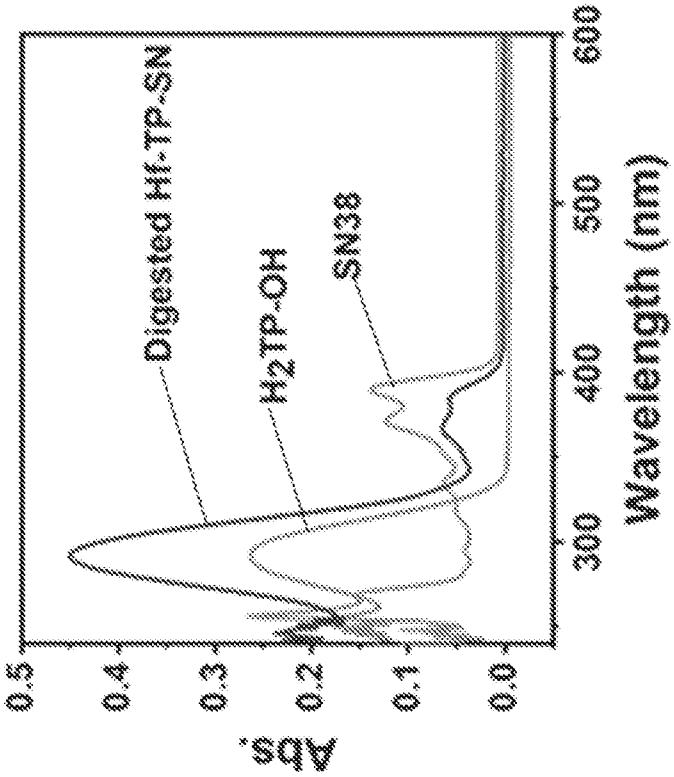
Digested Hf-TP-SN
H2TP-OH
SN38
Abs.
Wavelength (nm)
0.5
0.4
0.3
0.2
0.1
0.0
300
400
500
600

FIG. 4A

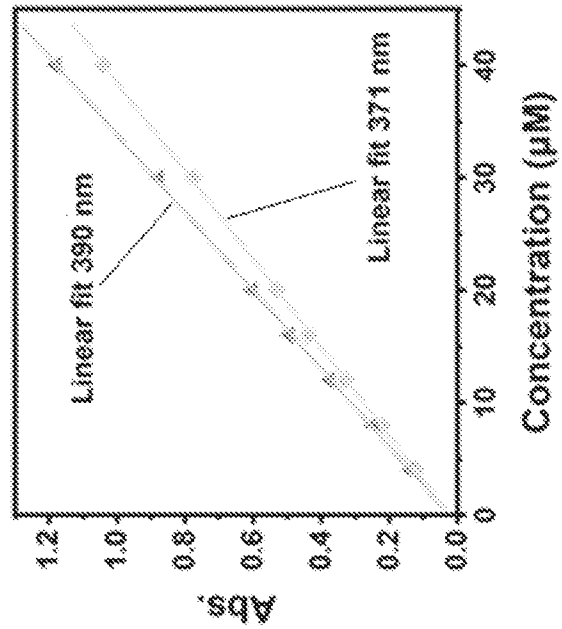

FIG. 4E

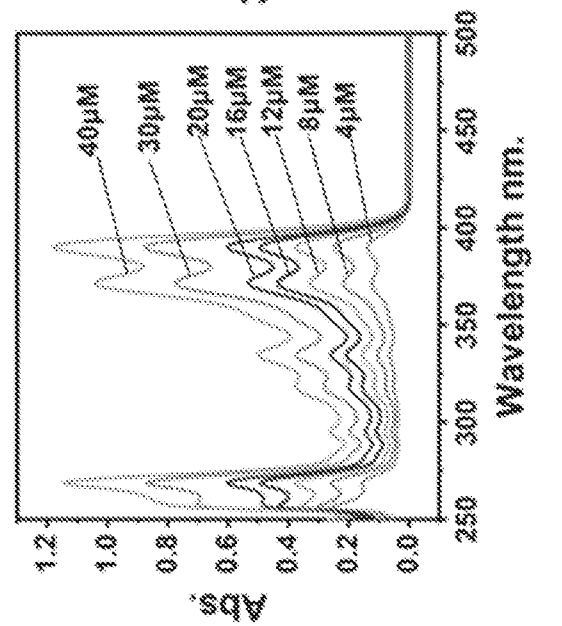

FIG. 4D

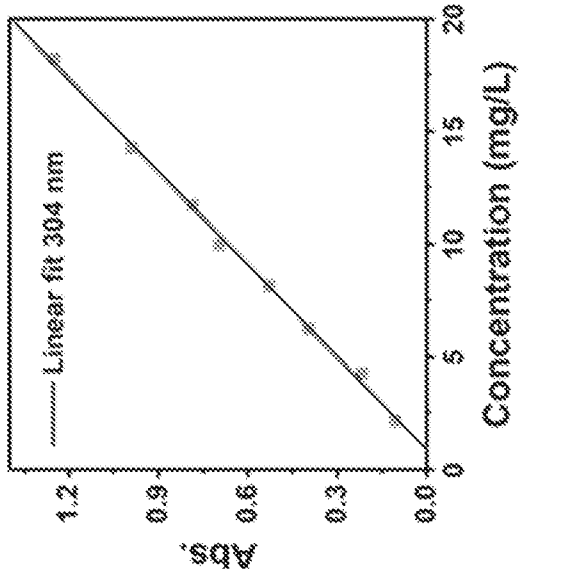

FIG. 4C

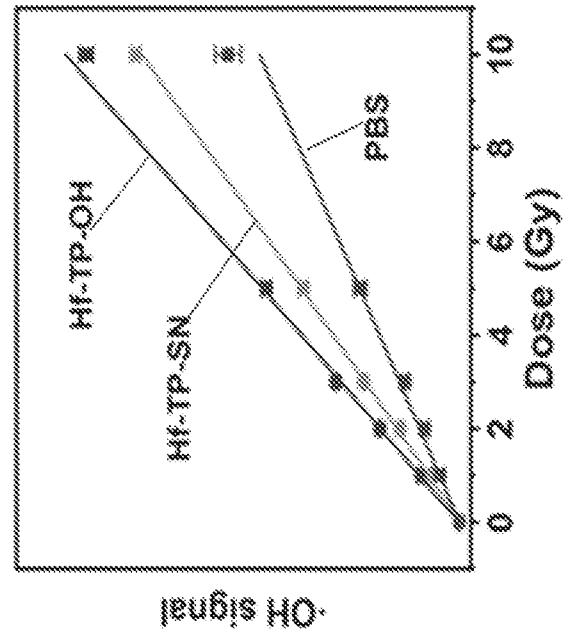

FIG. 5B

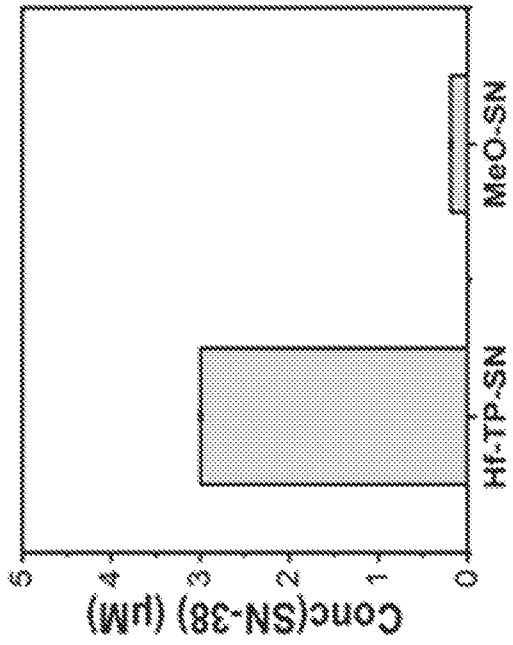

FIG. 5D

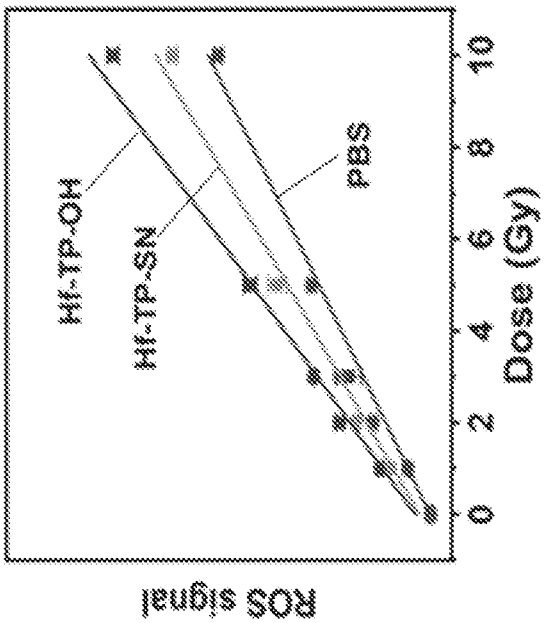

FIG. 5A

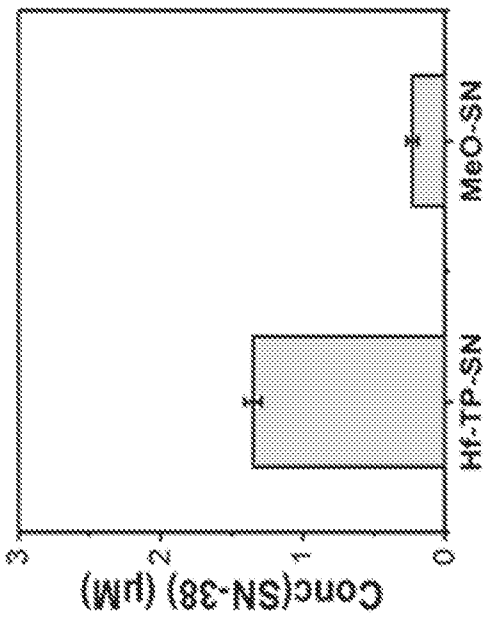

FIG. 5C

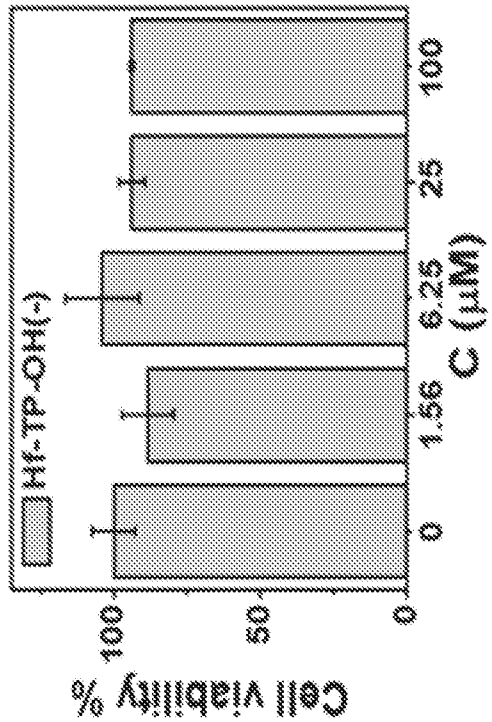

FIG. 6B

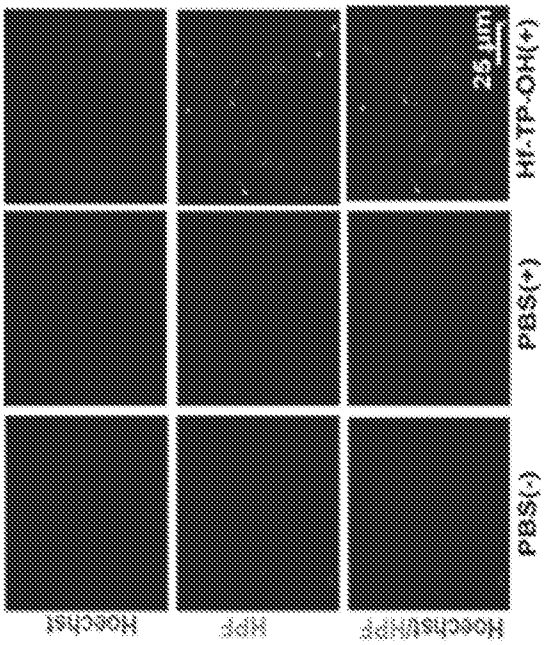

FIG. 6D

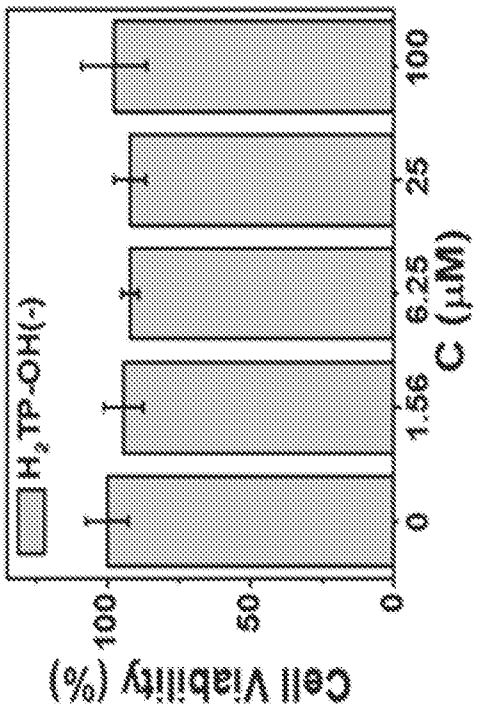

FIG. 6A

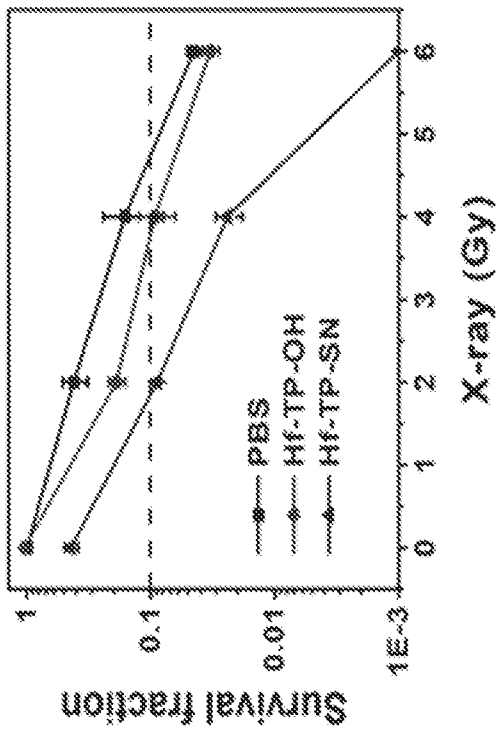

FIG. 6C

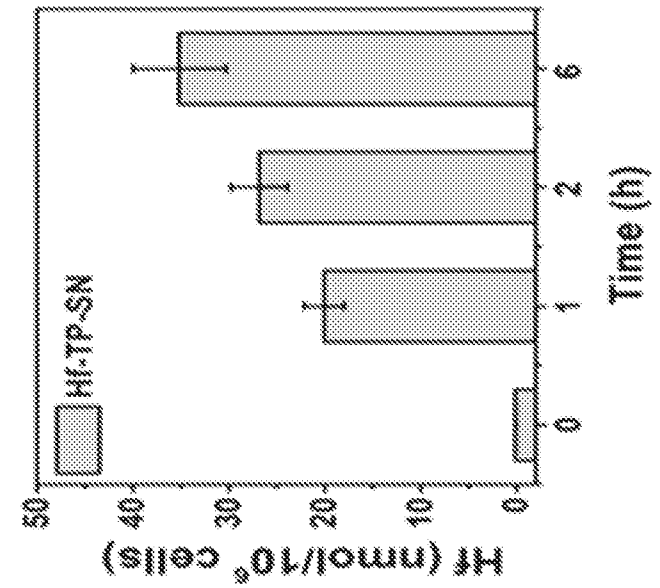

FIG. 7C

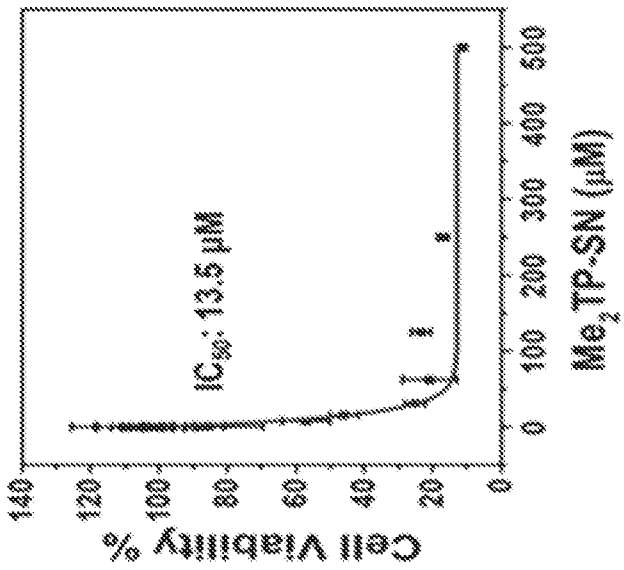

FIG. 7B

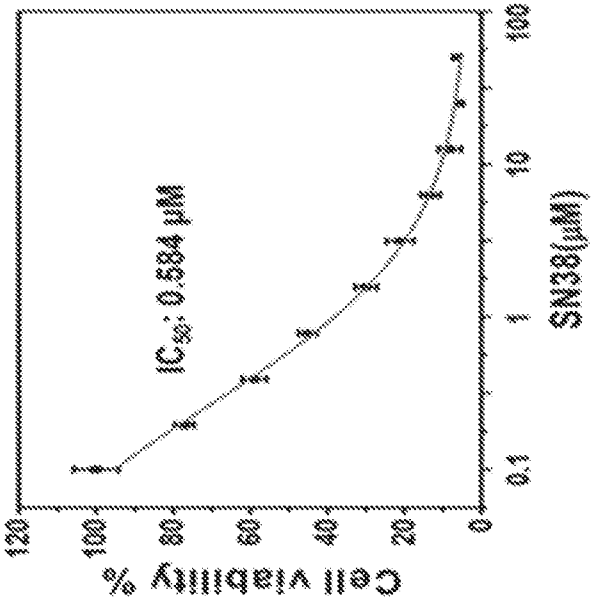

FIG. 7A

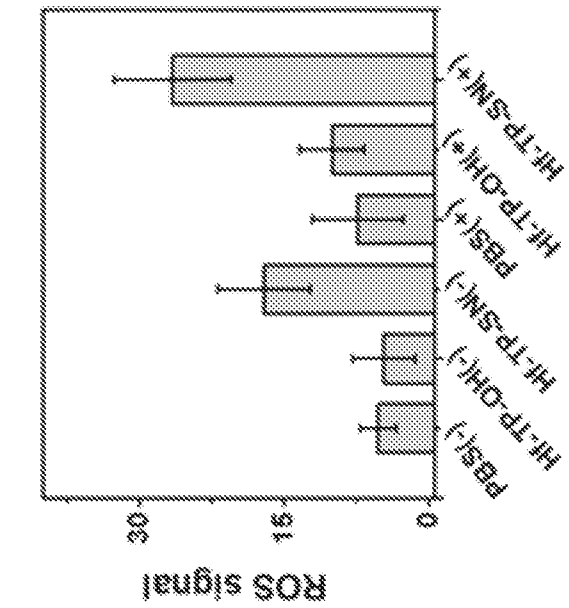
ROS signal
0
15
30
PBS(-)
HL-TP-OH(-)
HL-TP-SW(-)
PBS(+)
HL-TP-OH(+)
HL-TP-SW(+)

FIG. 8B

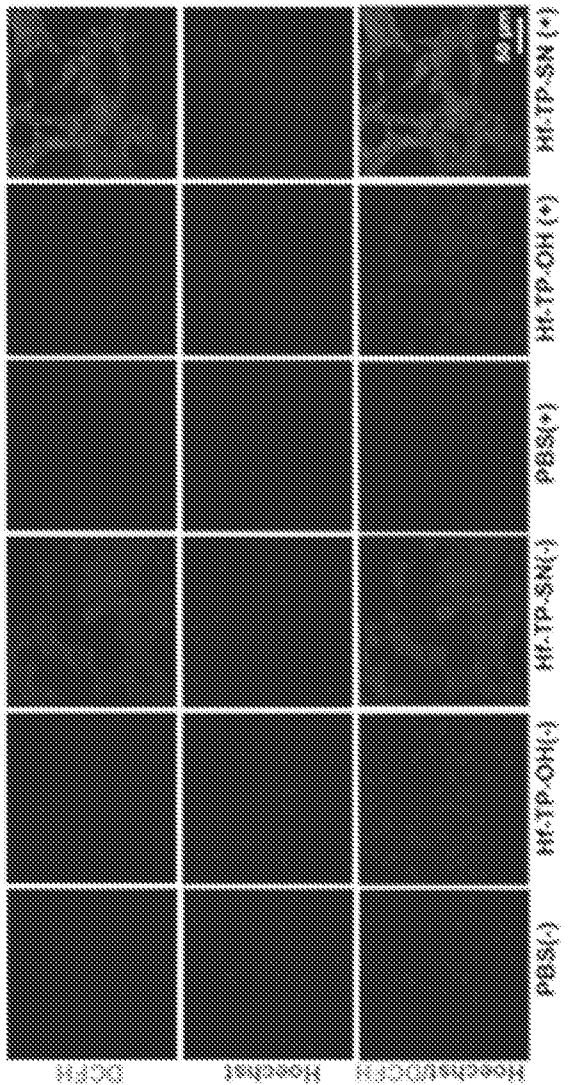
Hoechst/DCFH
Hoechst
DCFH
PBS(-)
HL-TP-OH(-)
HL-TP-SW(-)
PBS(+)
HL-TP-OH(+)
HL-TP-SW(+)

FIG. 8A

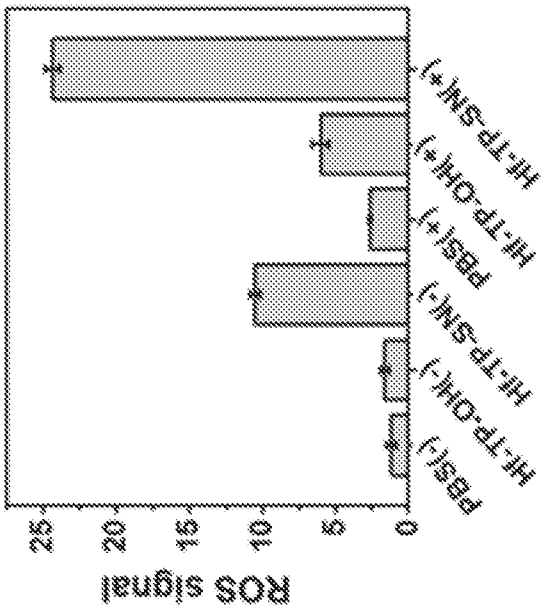
ROS signal
0
5
10
15
20
25
PBS(-)
HL-TP-OH(-)
HL-TP-SNH(-)
PBS(+)
HL-TP-OH(+)
HL-TP-SNH(+)

FIG. 8D

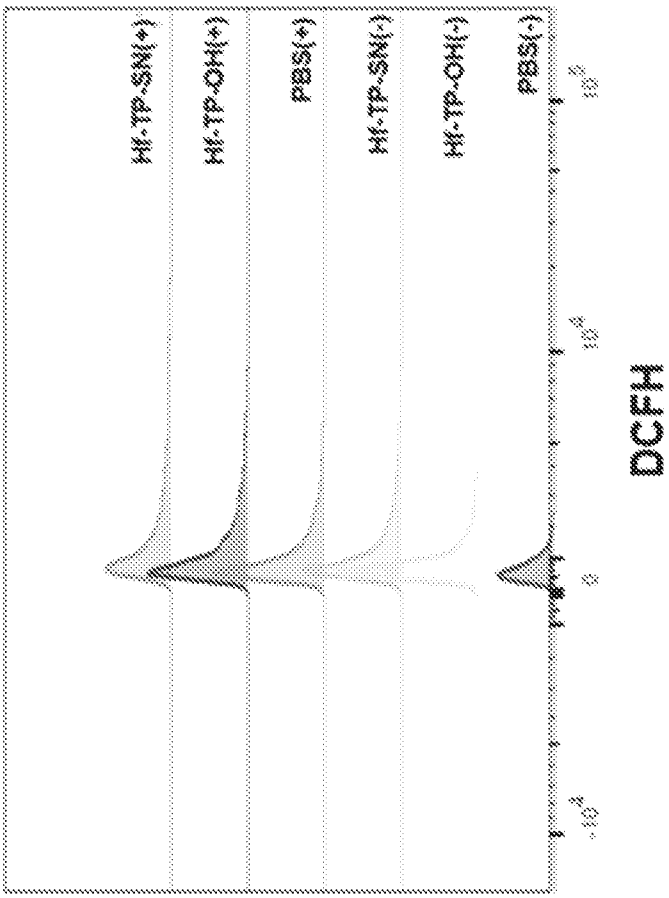
DCFH
PBS(-)
HL-TP-OH(-)
HL-TP-SNH(-)
PBS(+)
HL-TP-OH(+)
HL-TP-SNH(+)

FIG. 8C

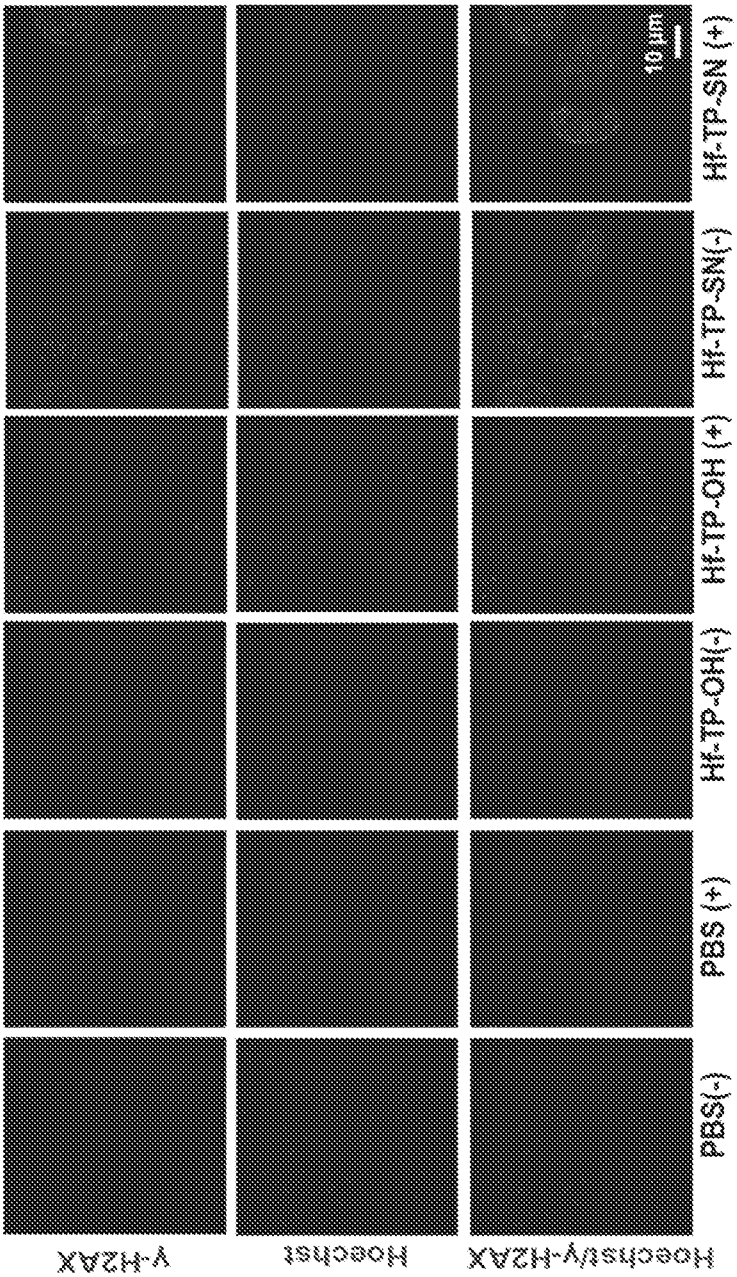
Hoechst/γ-H2AX
Hoechst
γ-H2AX
PBS(-)
PBS (+)
Hf-TP-OH(-)
Hf-TP-OH (+)
Hf-TP-SN(-)
Hf-TP-SN (+)
10 μm

FIG. 9

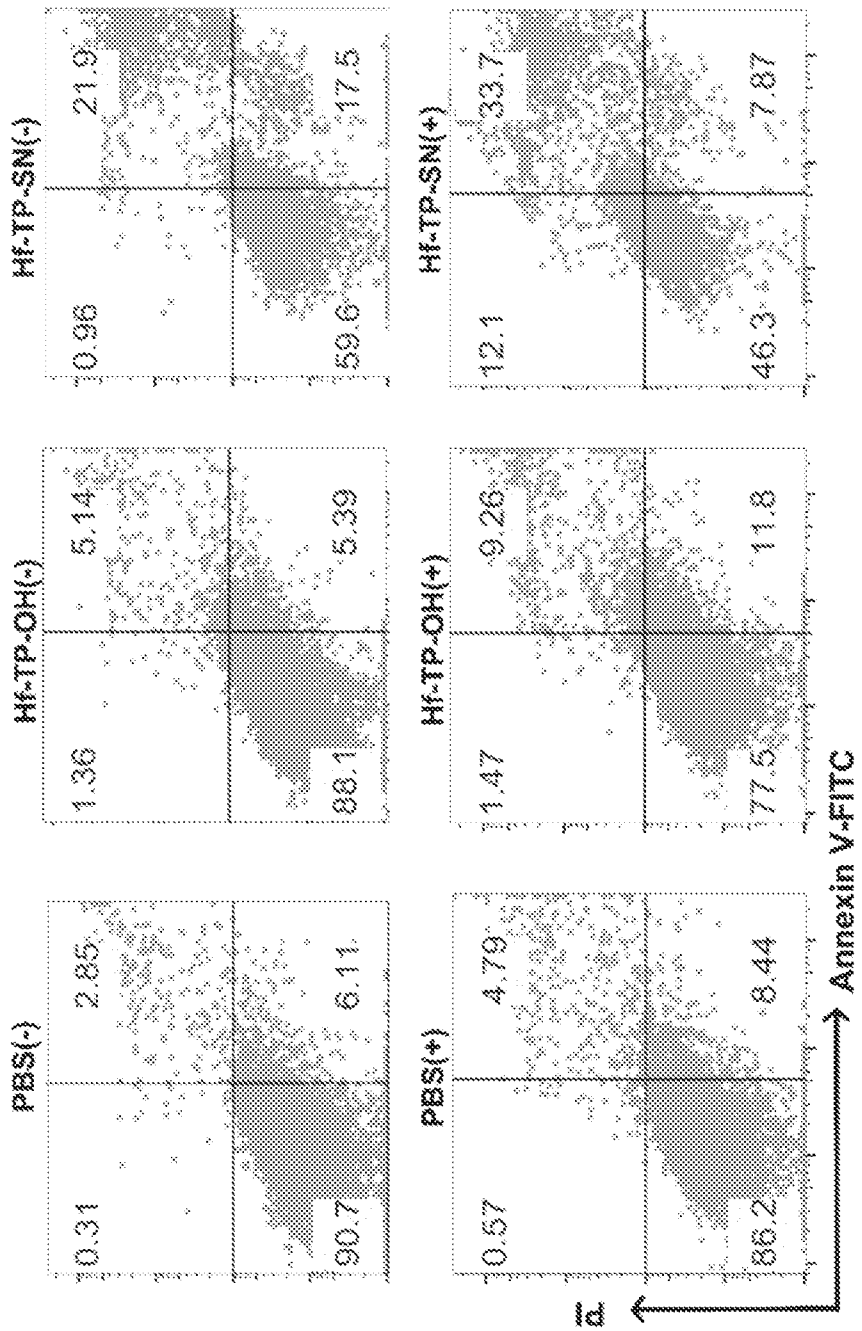
PBS(-)
Hf-TP-OH(-)
Hf-TP-SN(-)
PBS(+)
Hf-TP-OH(+)
Hf-TP-SN(+)
0.31
2.85
90.7
6.11
1.36
5.14
88.1
5.39
0.96
21.9
59.6
17.5
0.57
4.79
86.2
8.44
1.47
9.26
77.5
11.8
12.1
33.7
46.3
7.87
PI
Annexin V-FITC

FIG. 10

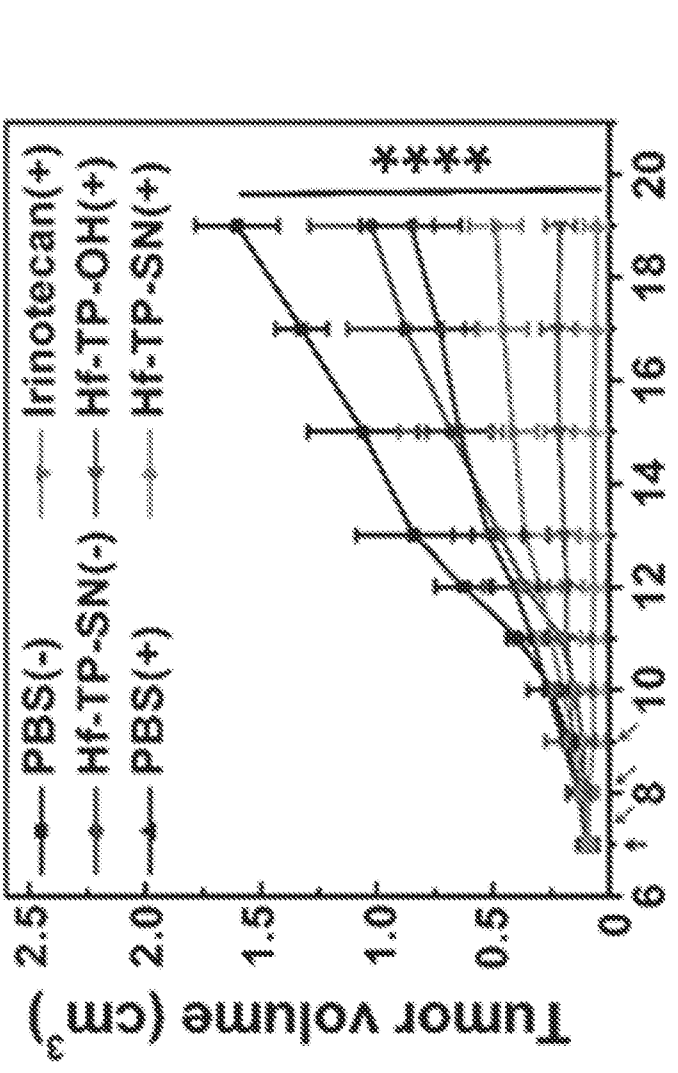

FIG. 11A

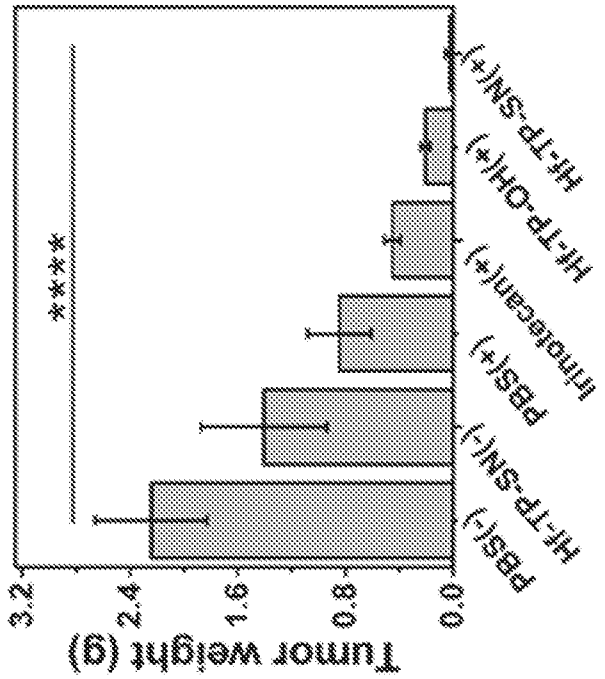

FIG. 11B

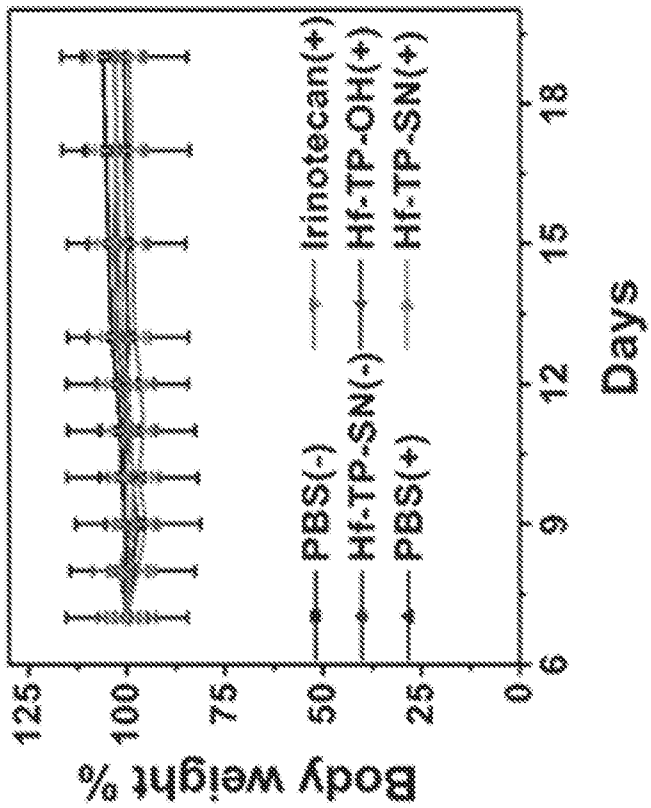

FIG. 11D

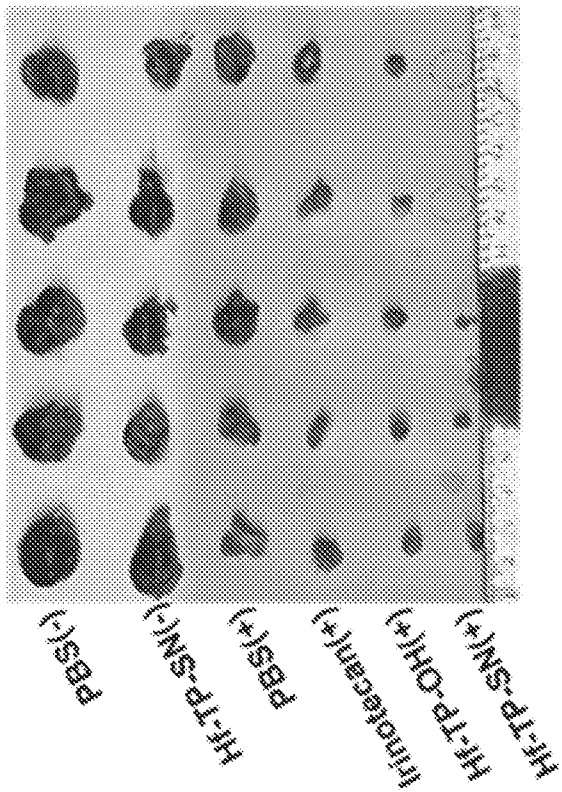

FIG. 11C

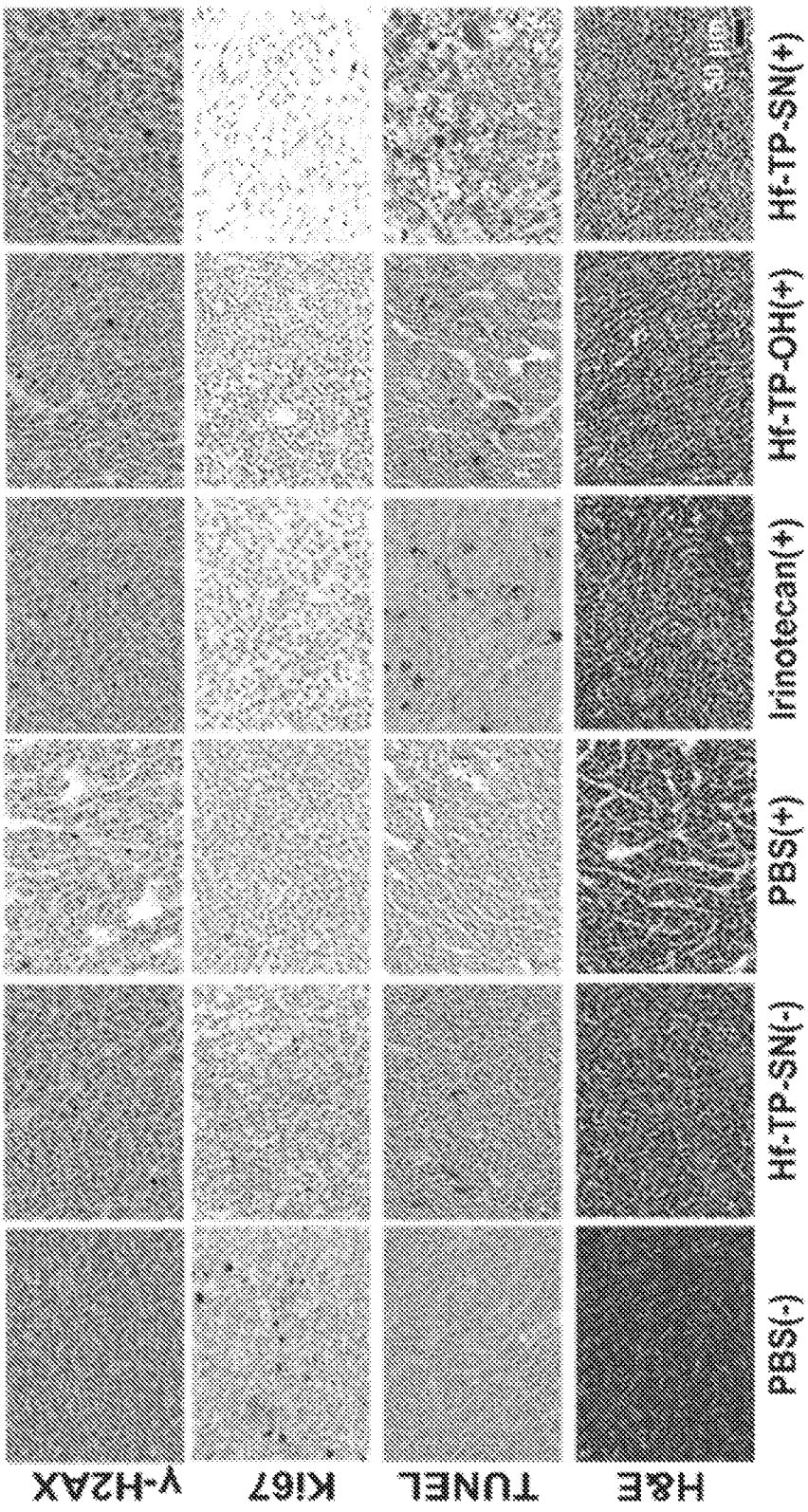
H&E
TUNEL
Ki67
γ-H2AX
PBS(-)
Hf-TP-SN(-)
PBS(+)
Irinotecan(+)
Hf-TP-OH(+)
Hf-TP-SN(+)
50 μm

FIG. 12

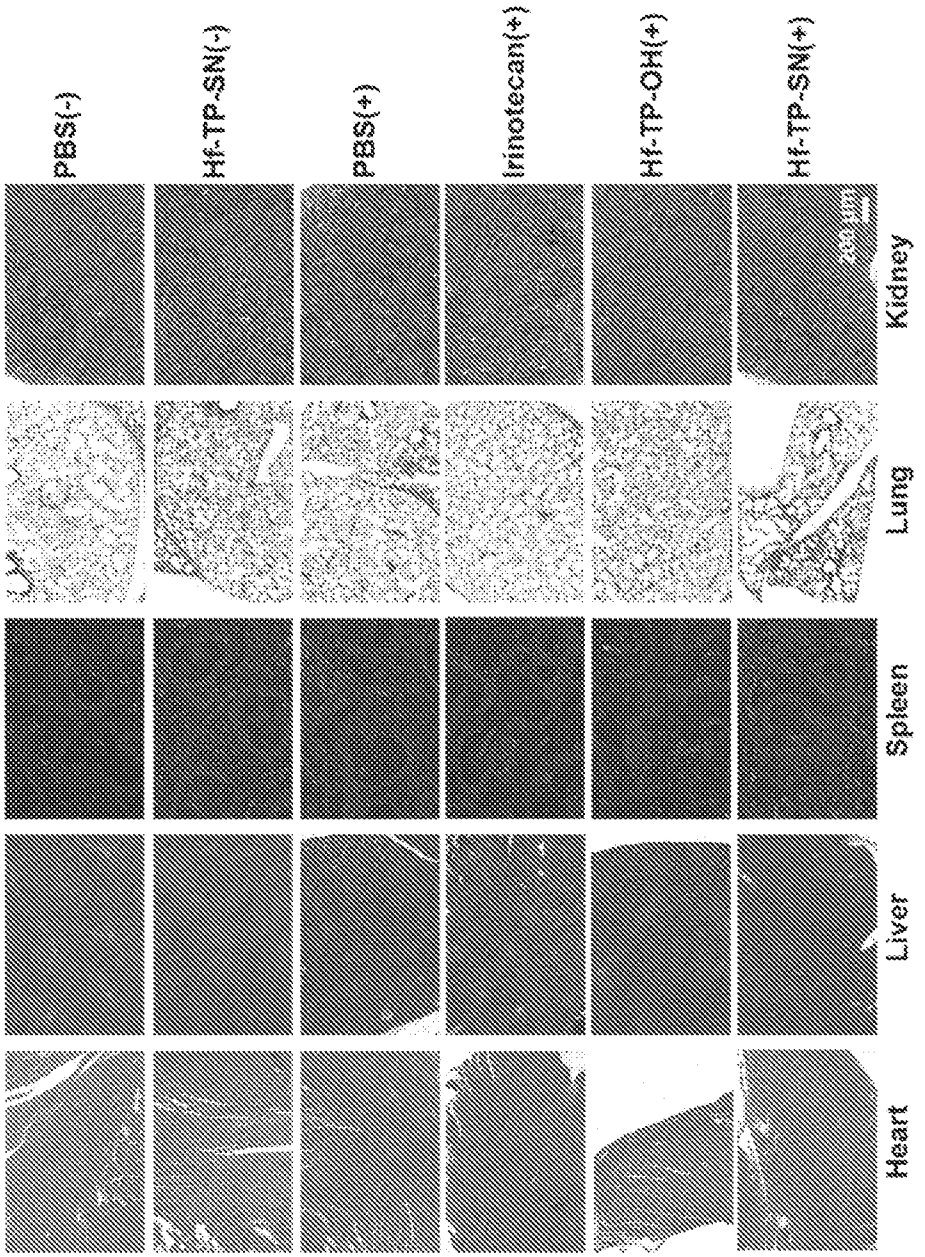
PBS(-)
Hf-TP-SN(-)
PBS(+)
Irinotecan(+)
Hf-TP-OH(+)
Hf-TP-SN(+)
Kidney
Lung
Spleen
Liver
Heart

FIG. 13

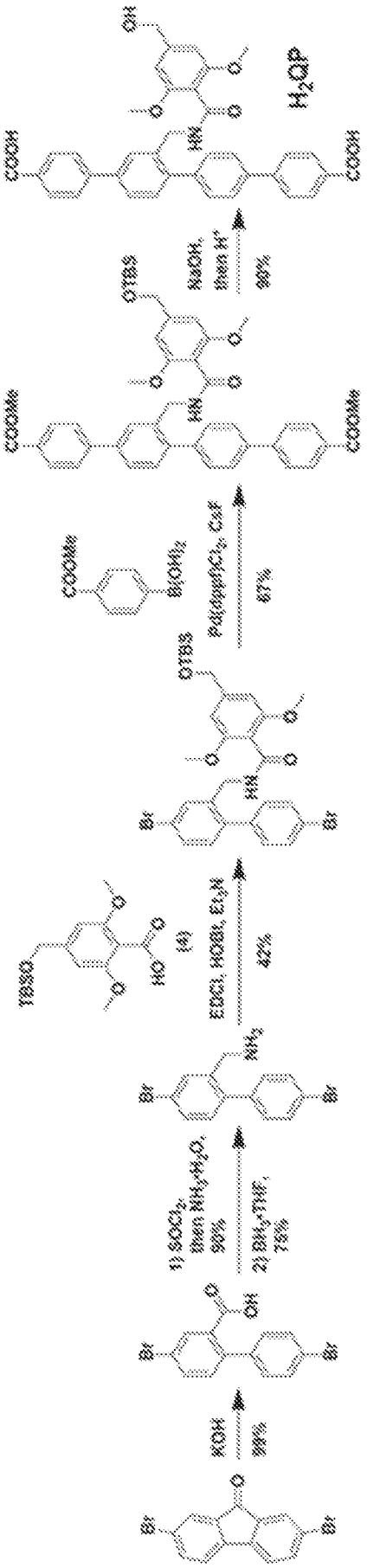
KOH
99%
1) SOCl2, then NH4+H2O, 90%
2) BH3-THF, 75%
EDCI, HOBt, Et3N
42%
Pd(dppf)Cl2, CsF
67%
NaOH, then H+
86%
H2QP

FIG. 14A

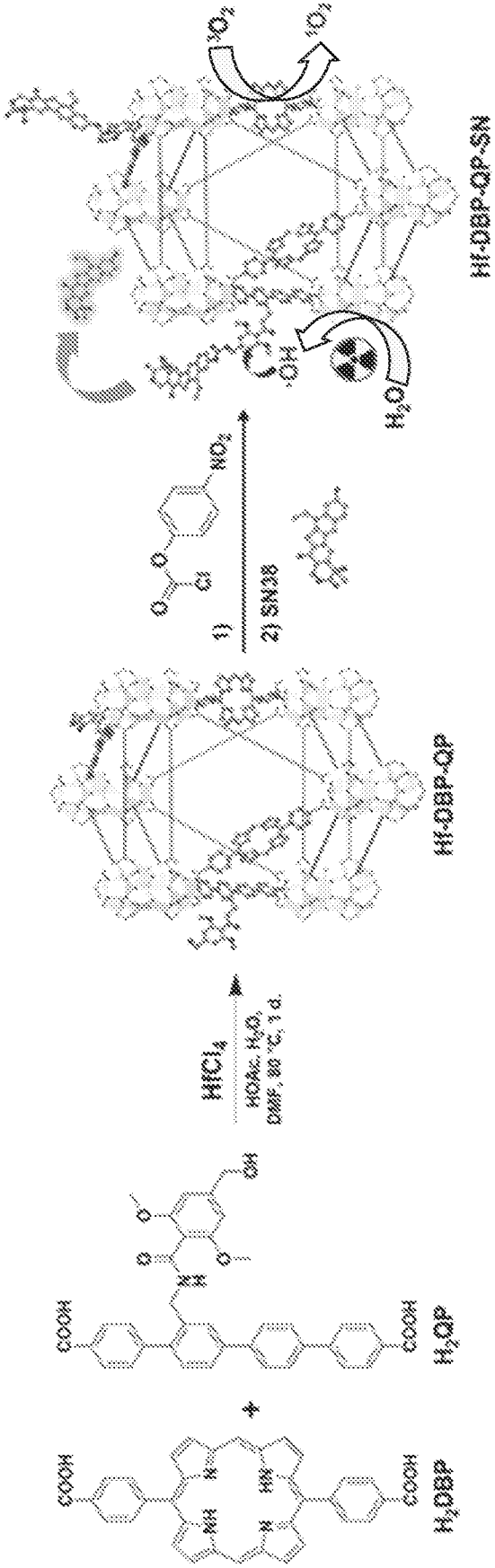
H4DBP
H4QP
HfCl4
HOAc, H2O,
DMF, 80 °C, 1 d.
Hf-DBP-QP
1)
2) SN38
Hf-DBP-QP-SN
1O2
1O2
H2O

FIG. 14B

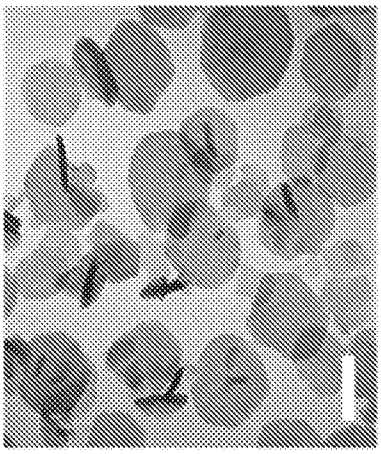

FIG. 15A

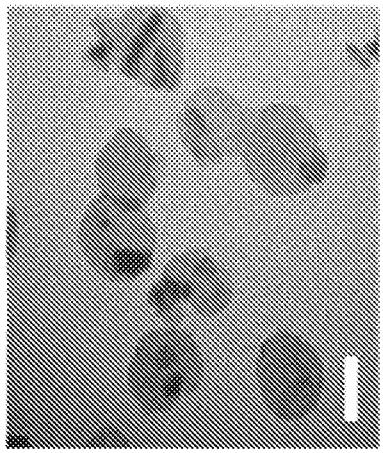

FIG. 15B

FIG. 15C

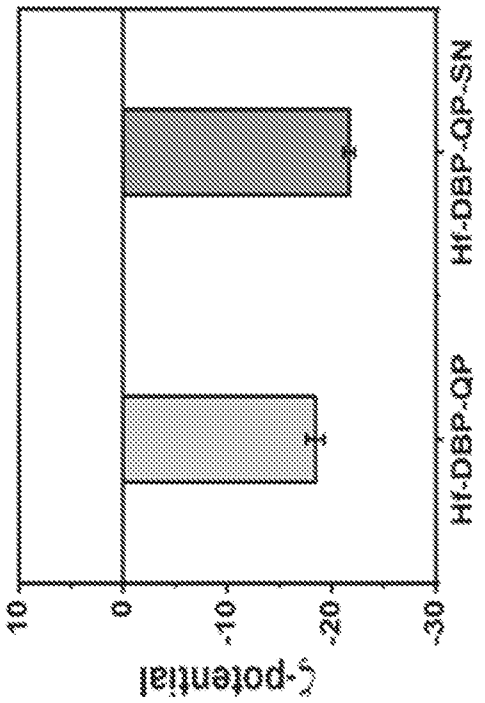

FIG. 15D

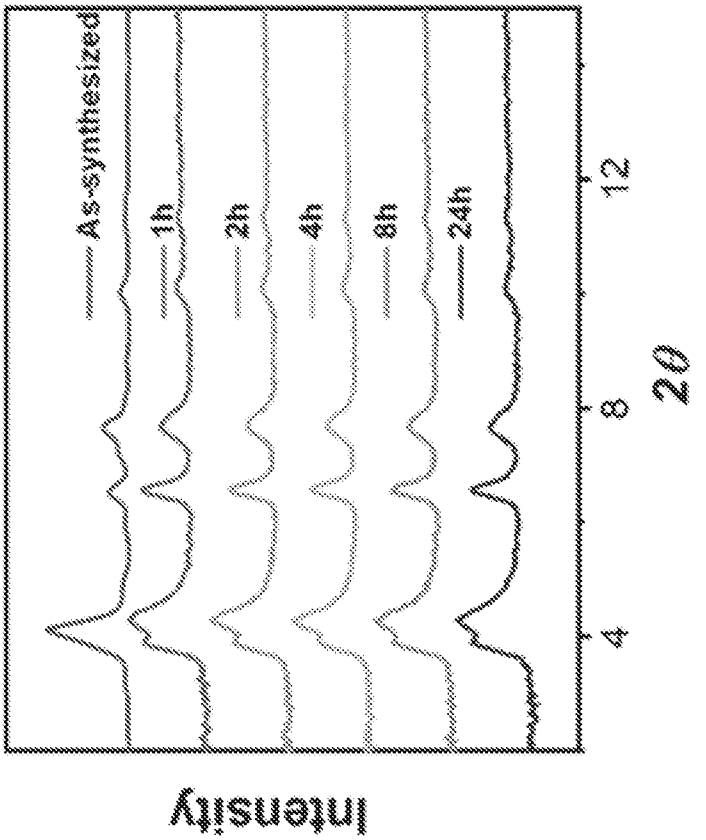

FIG. 16B

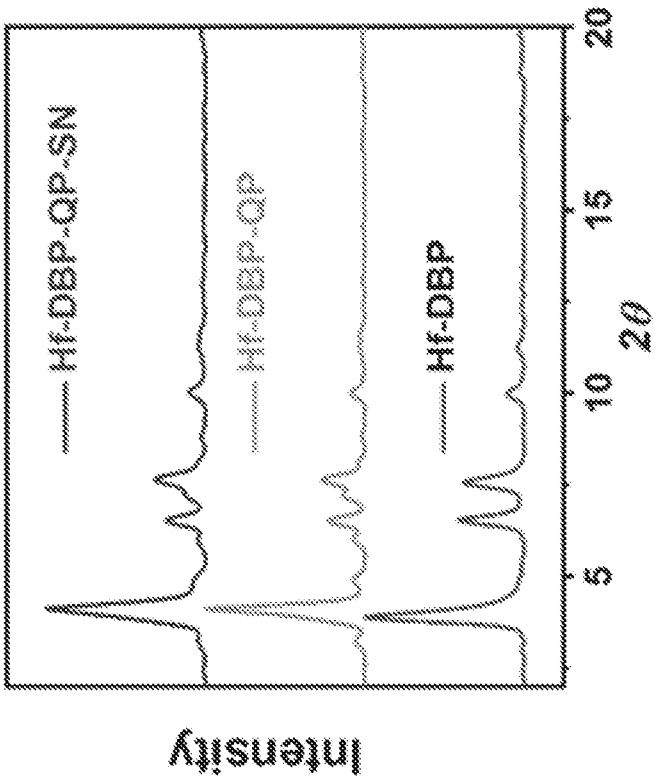

FIG. 16A

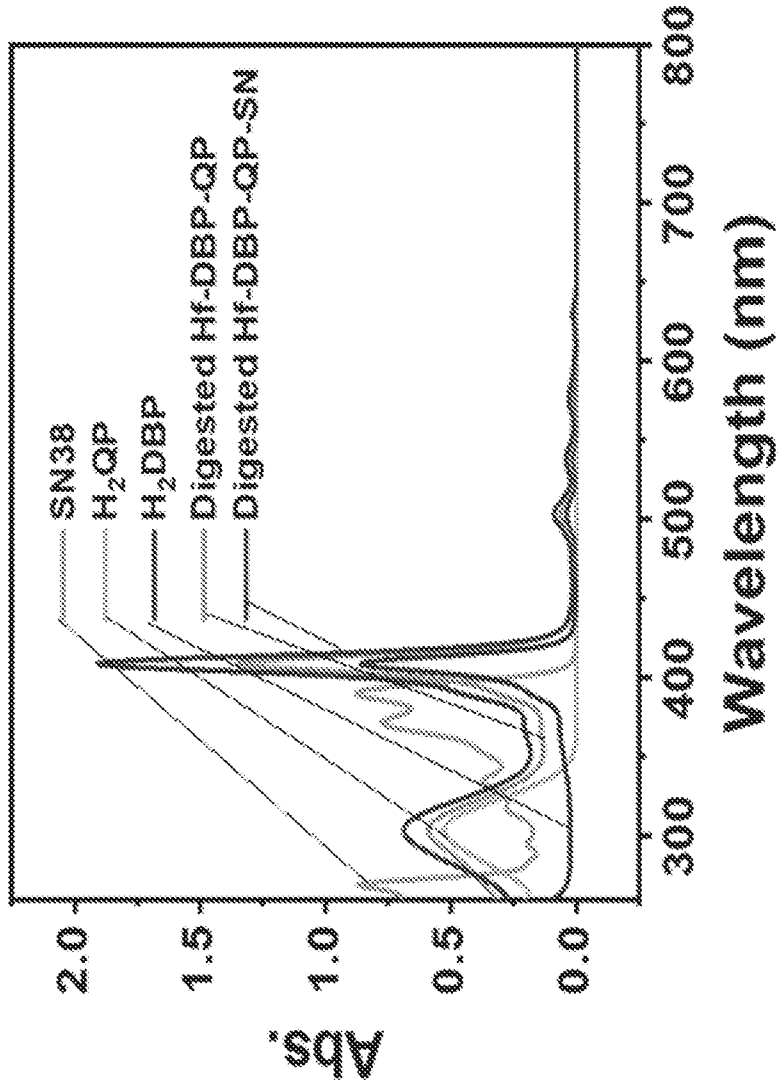
SN38
H_2QP
H_2DBP
Digested Hf-DBP-QP
Digested Hf-DBP-QP-SN
Abs.
2.0
1.5
1.0
0.5
0.0
300
400
500
600
700
800
Wavelength (nm)

FIG. 17

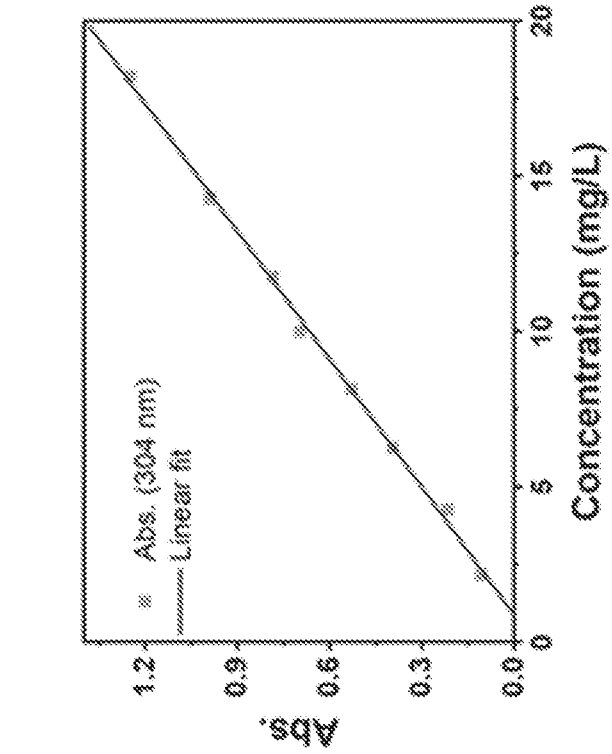

FIG. 18B

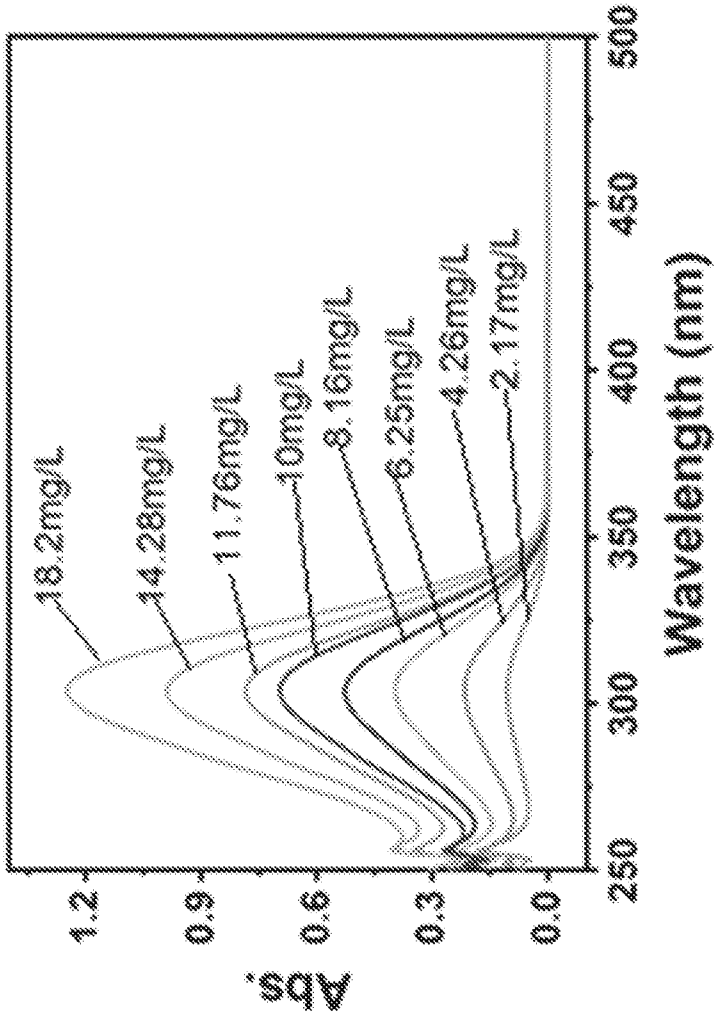

FIG. 18A

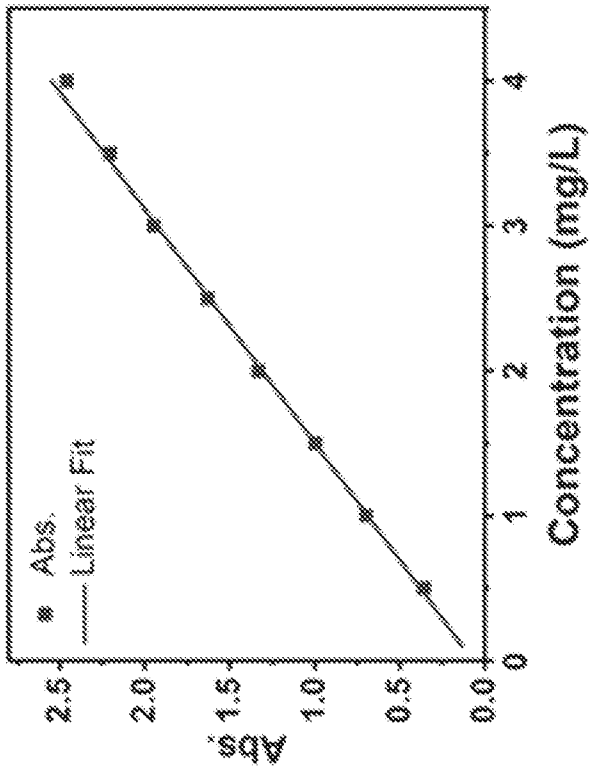

FIG. 18D

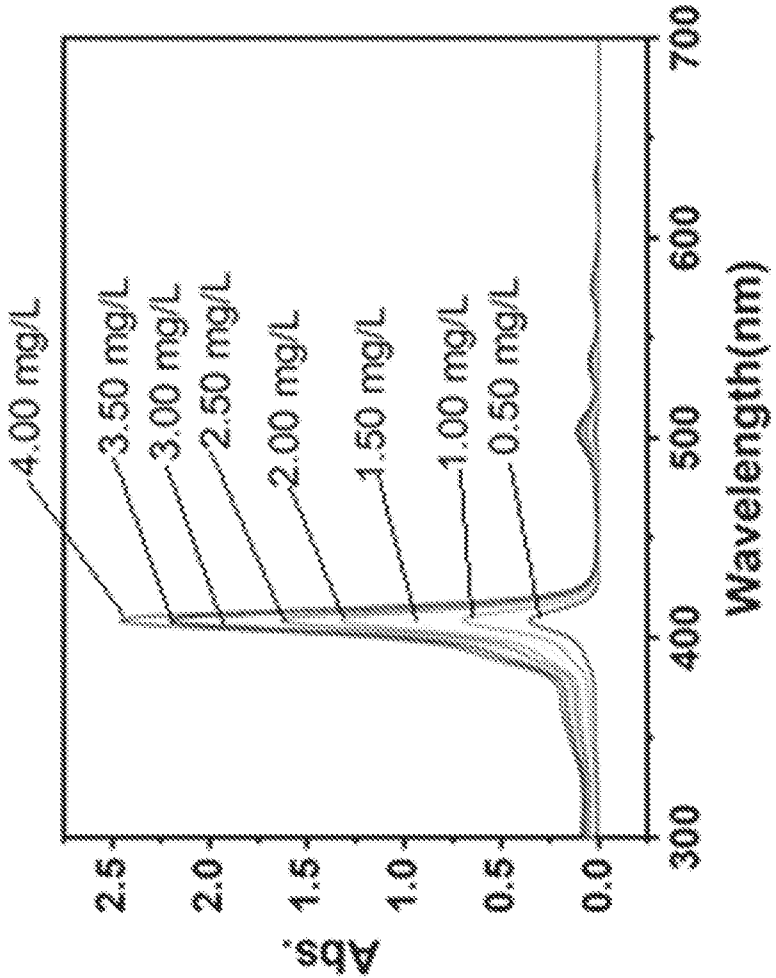

FIG. 18C

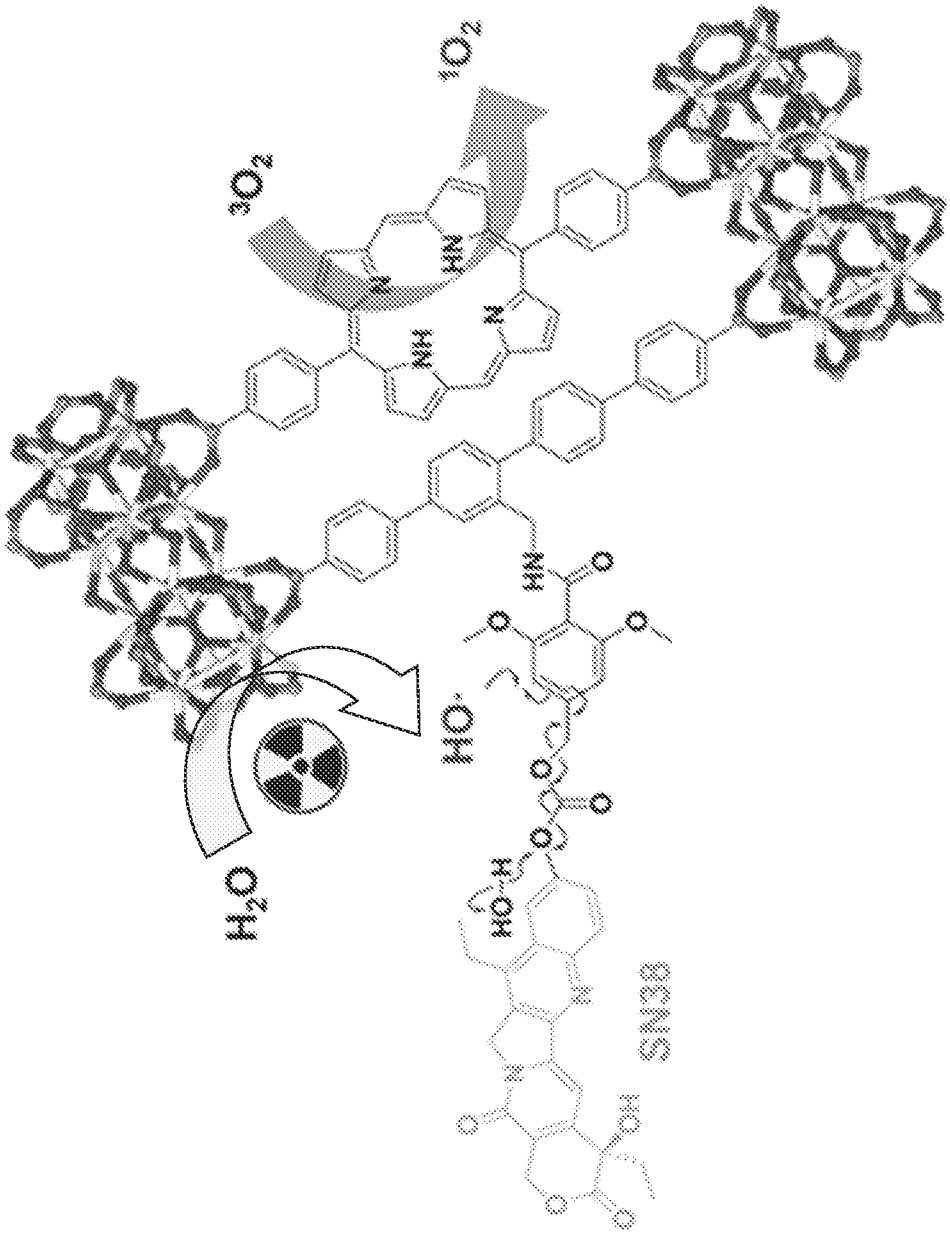

FIG. 19A

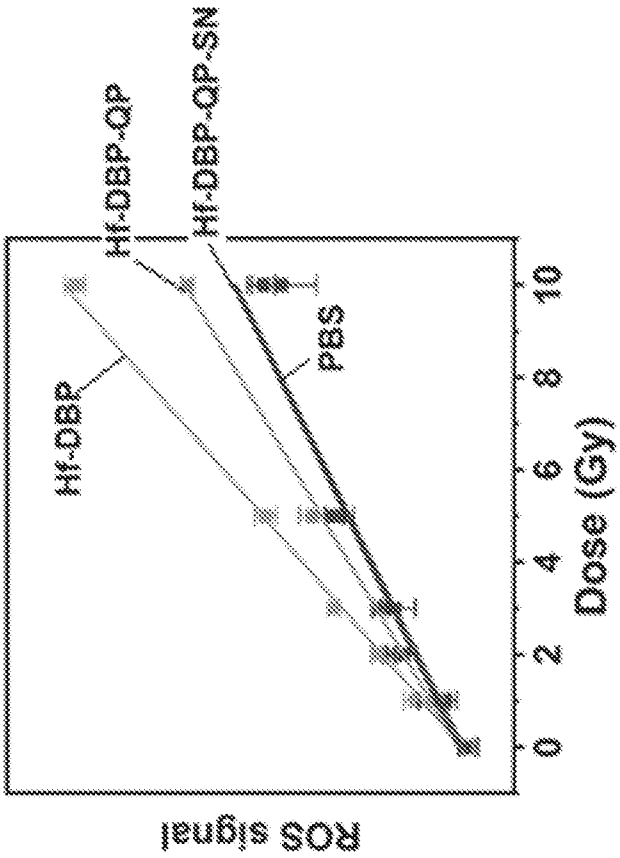

FIG. 19C

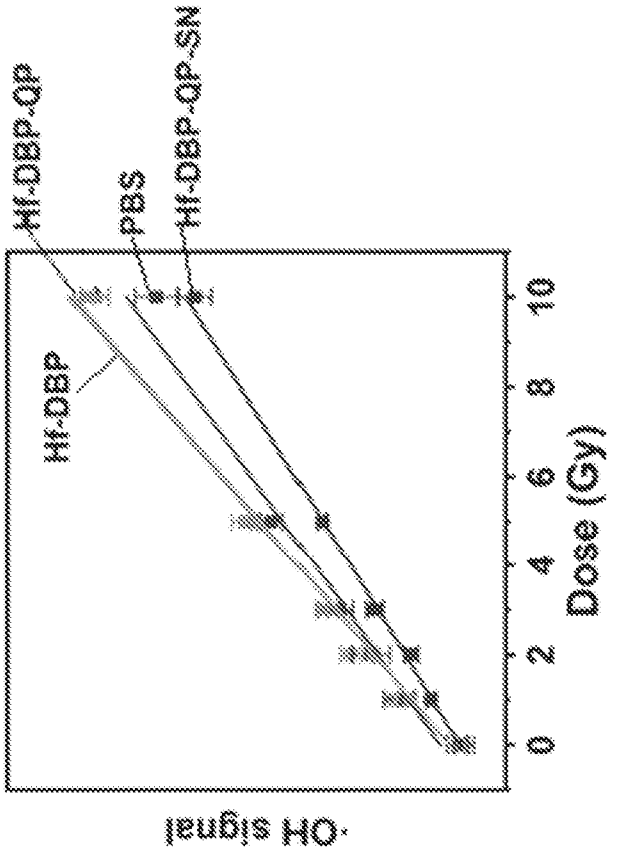

FIG. 19B

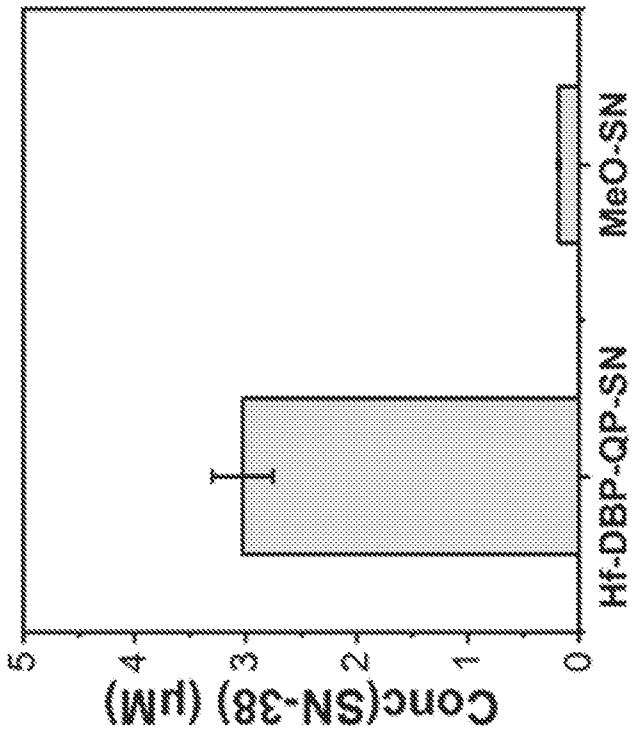

FIG. 20B

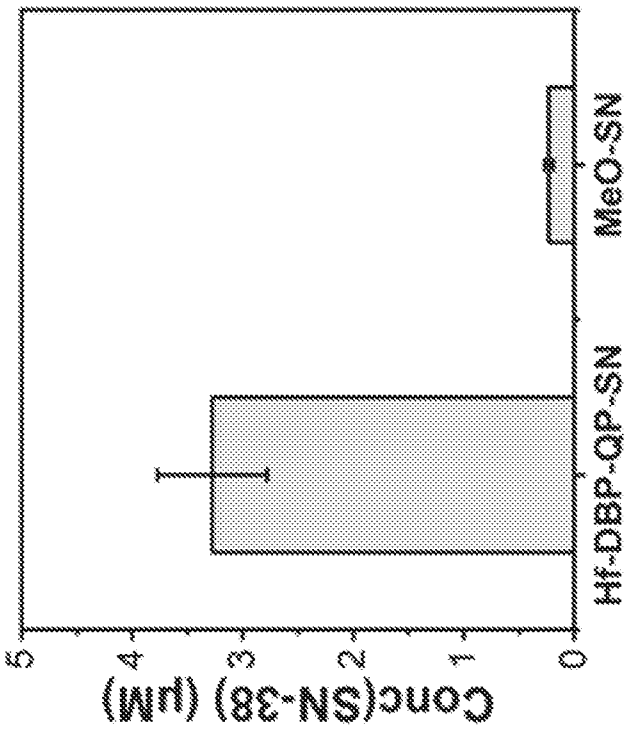

FIG. 20A

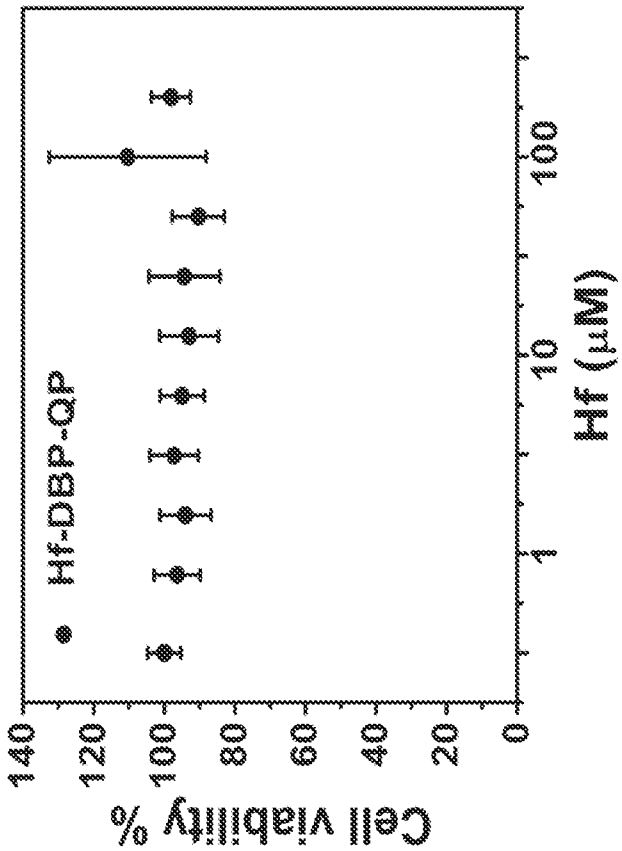

FIG. 21

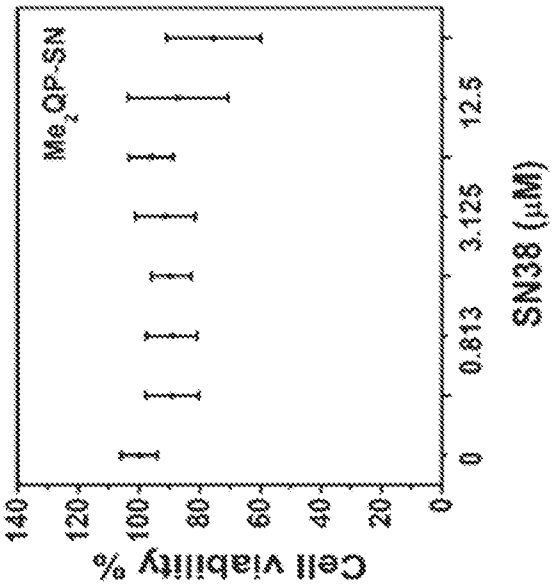

FIG. 22B

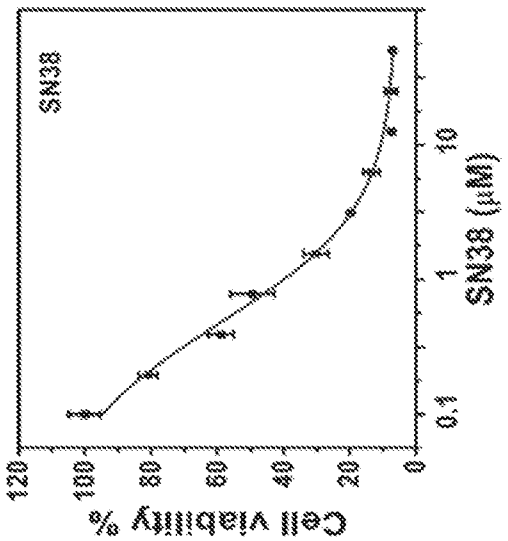

FIG. 22A

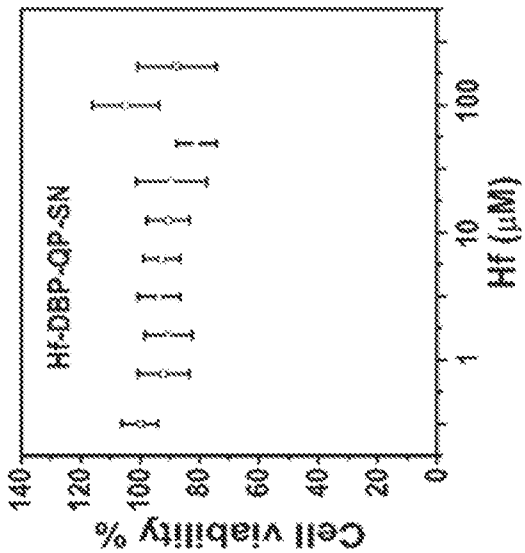

FIG. 22C

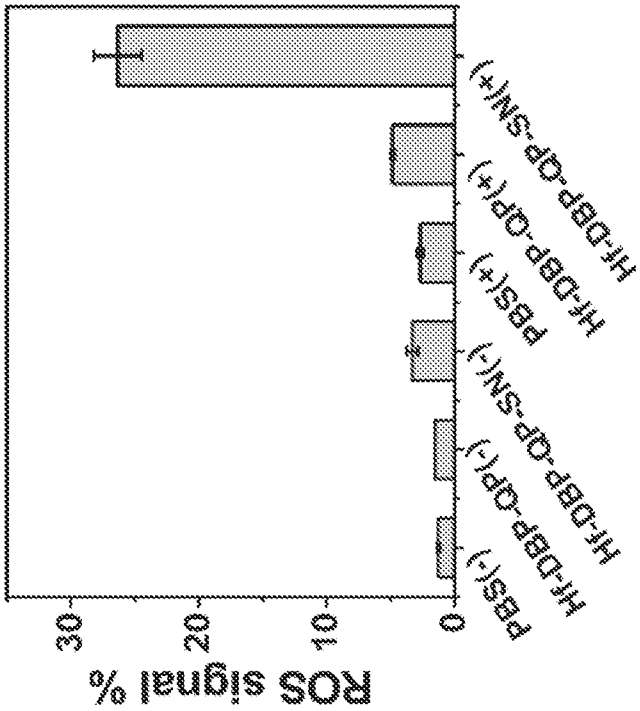
ROS signal %
0
10
20
30
PBS(-)
Hf-DBP-QP(-)
Hf-DBP-QP-SN(-)
PBS(+)
Hf-DBP-QP(+)
Hf-DBP-QP-SN(+)

FIG. 24

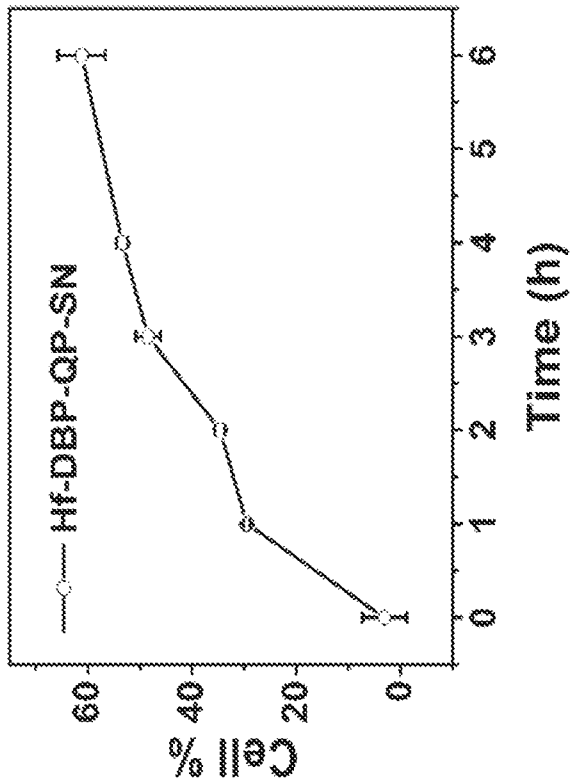
Cell %
0
20
40
60
Time (h)
0
1
2
3
4
5
6
Hf-DBP-QP-SN

FIG. 23

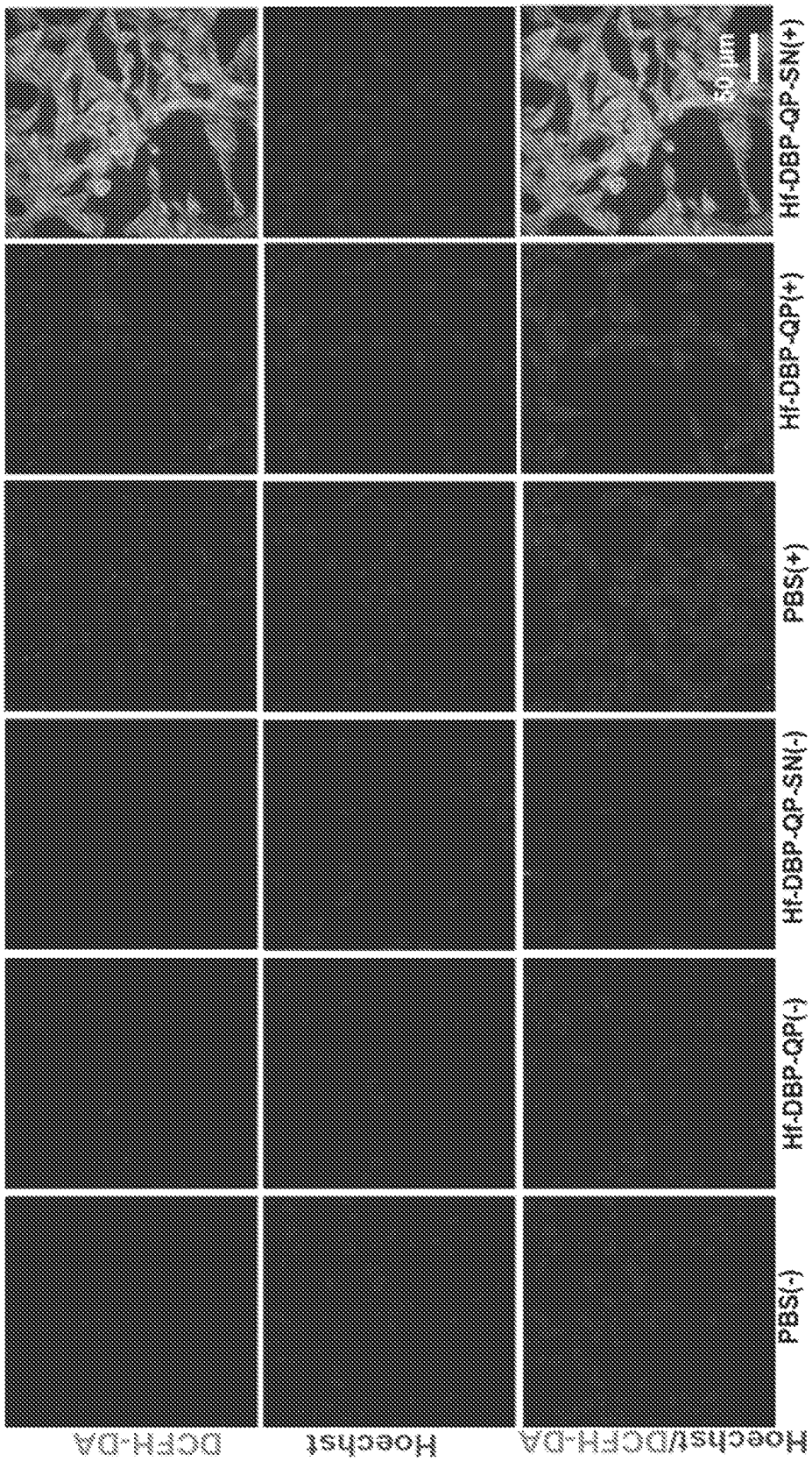
Hoechst/DCFH-DA
Hoechst
DCFH-DA
PBS(-)
Hf-DBP-QP(-)
Hf-DBP-QP-SN(-)
PBS(+)
Hf-DBP-QP(+)
Hf-DBP-QP-SN(+)
50 μm

FIG. 25

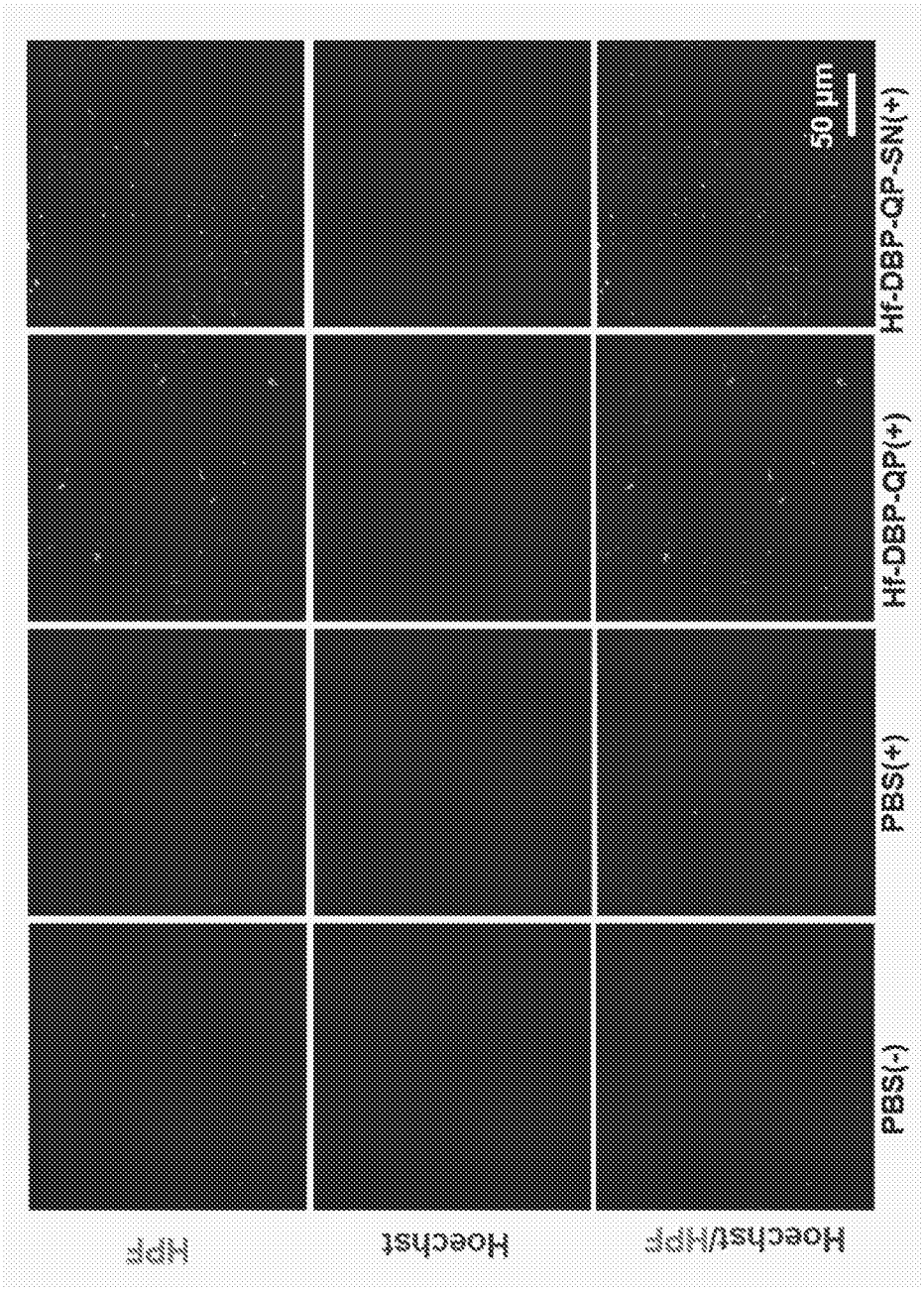

FIG. 26

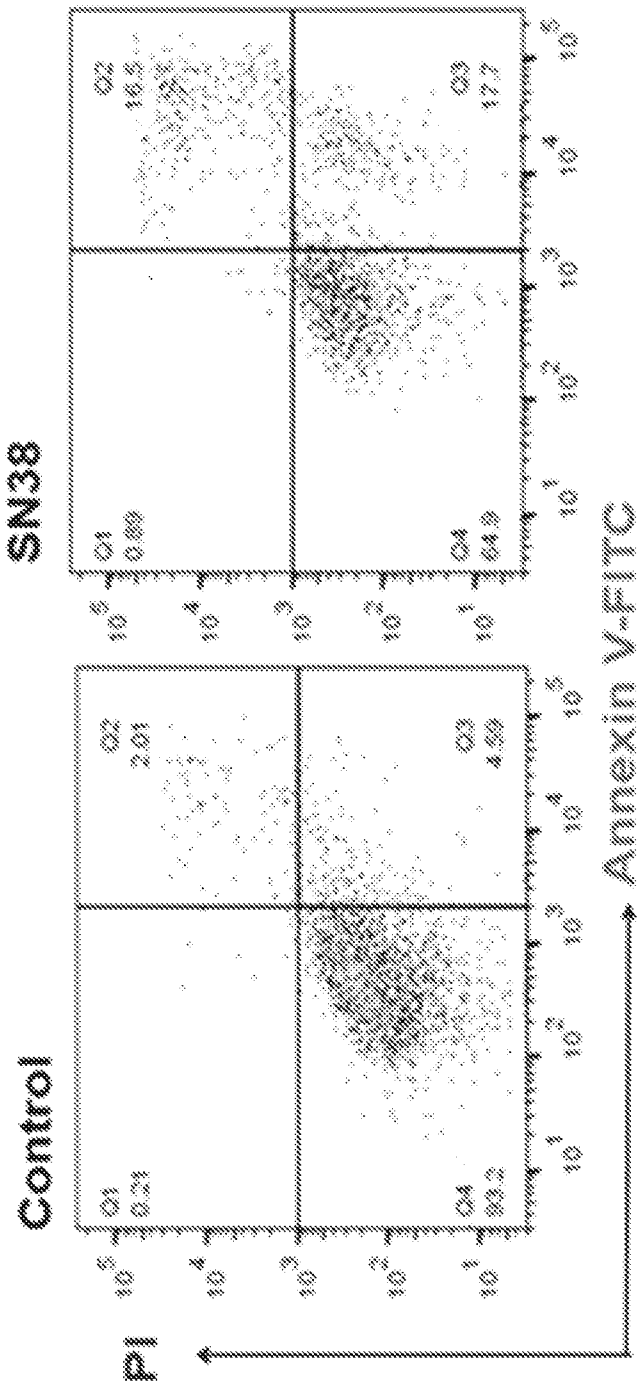
SN38
Control
PI
Annexin V-FITC
Q2
16.3
Q3
17.7
Q1
0.80
Q4
64.9
Q2
2.61
Q3
4.99
Q1
0.21
Q4
18.3

FIG. 27A

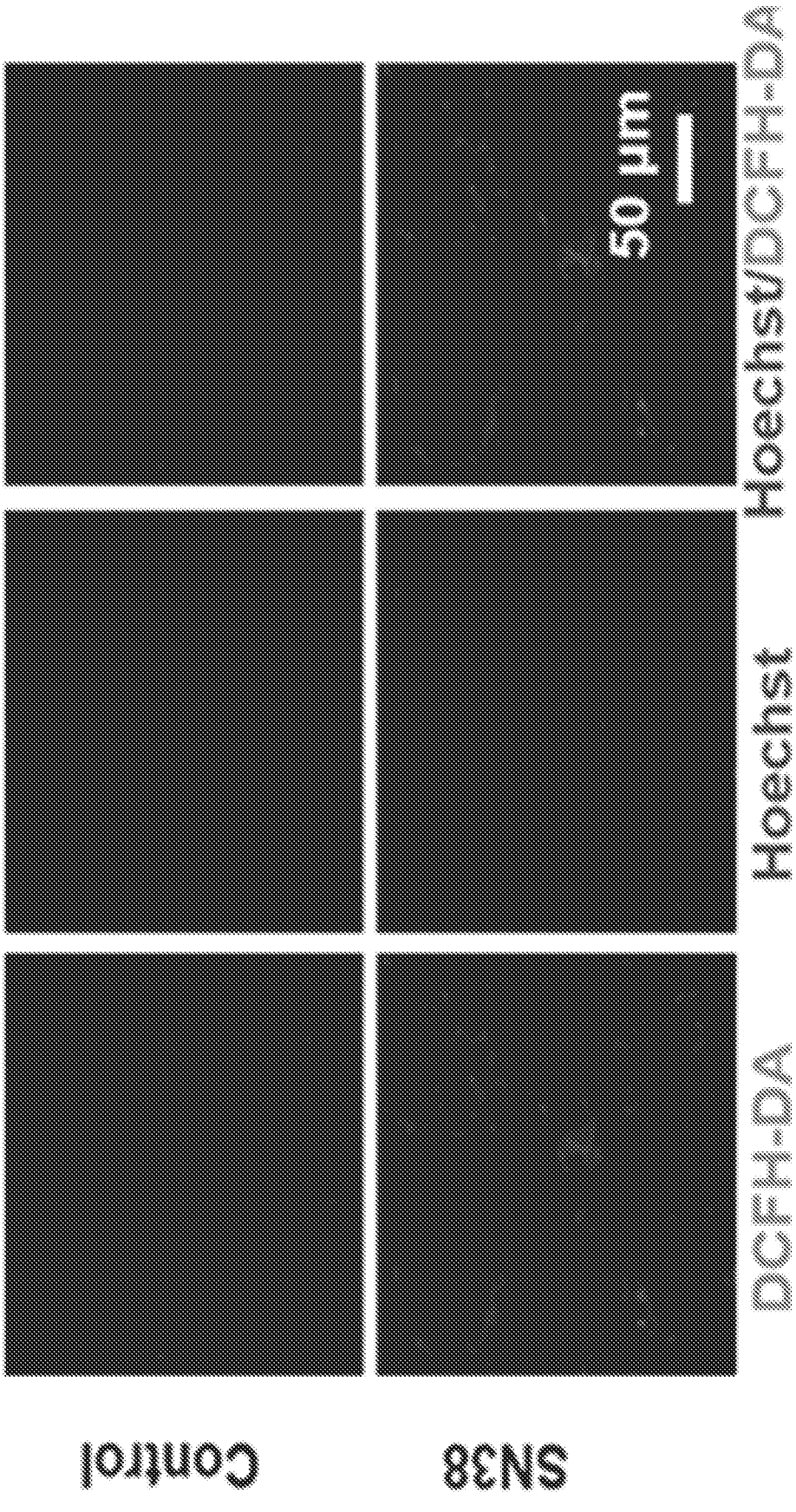

FIG. 27B

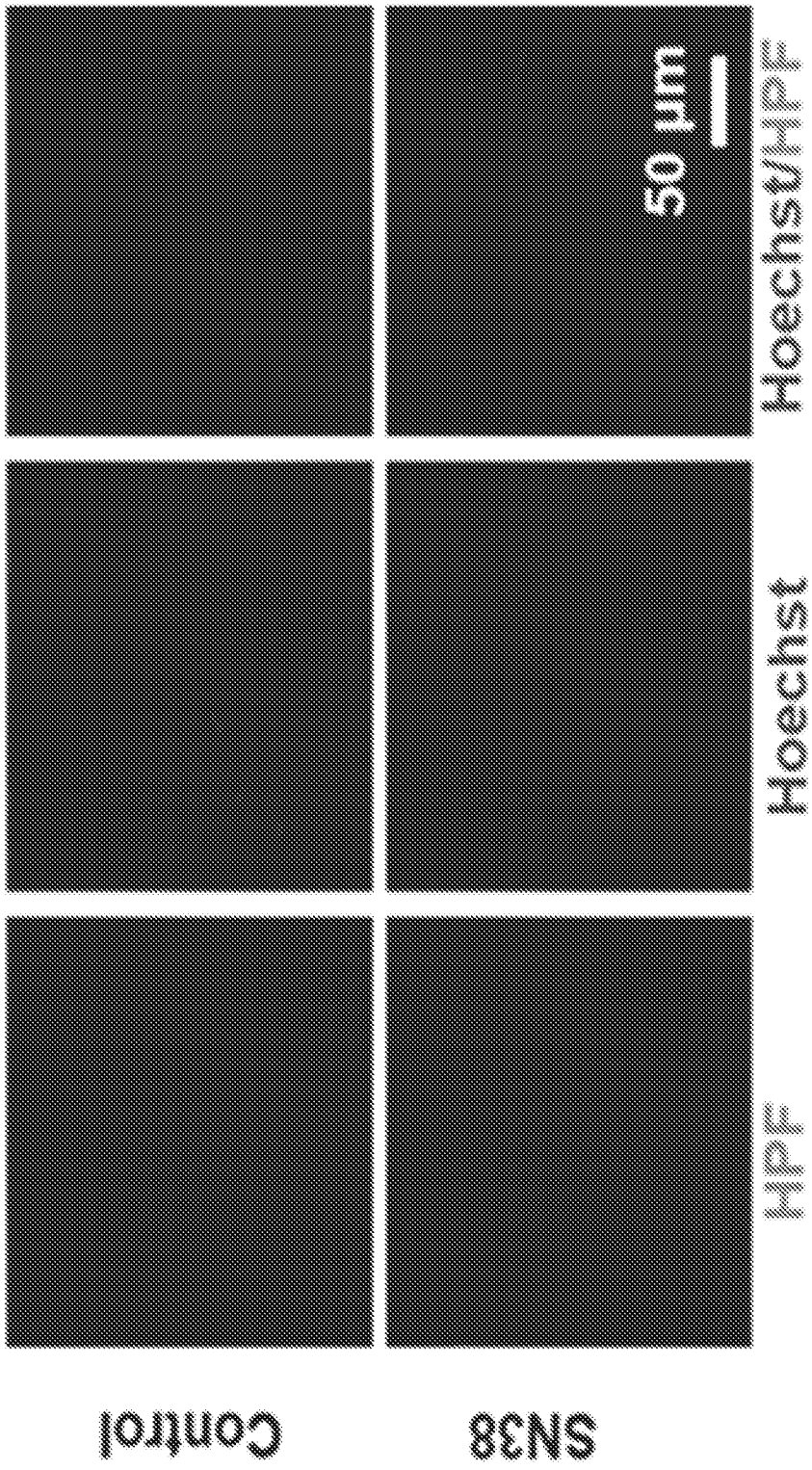

FIG. 27C

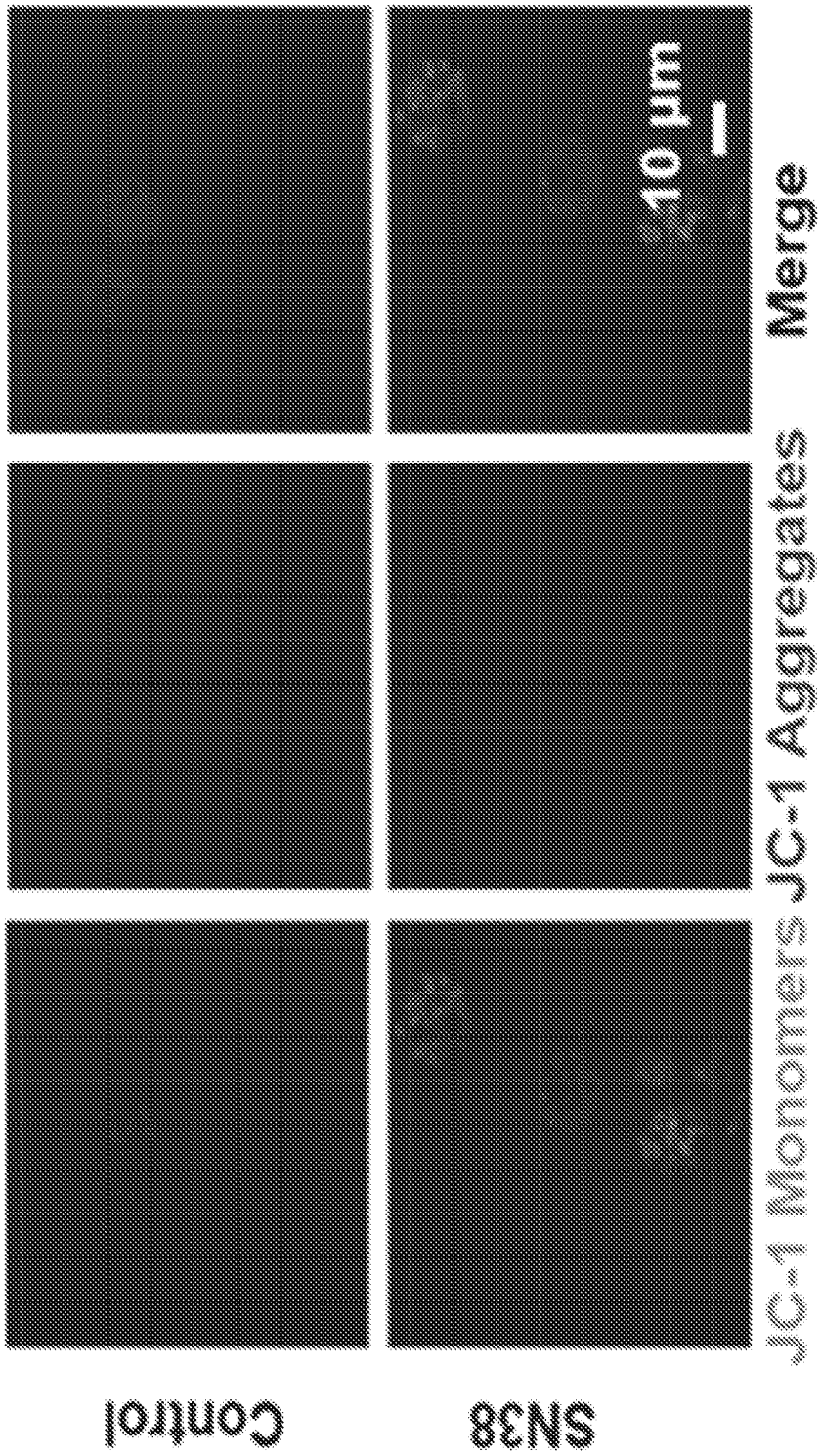

FIG. 27D

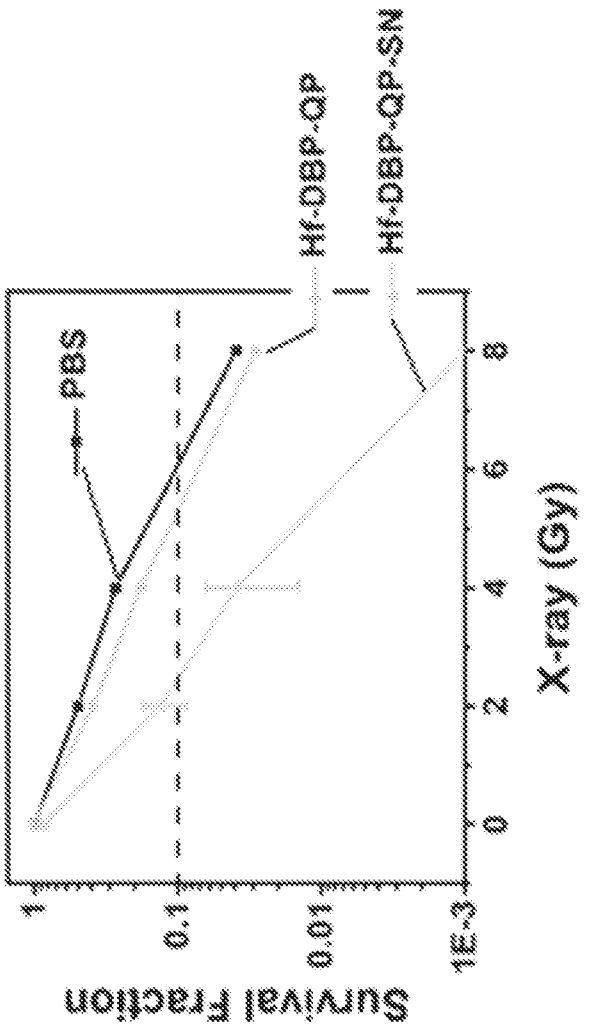
Survival Fraction
1
0.1
0.01
1E-3
0
2
4
6
8
X-ray (Gy)
PBS
Hf-DBP-QP
Hf-DBP-QP-SN

FIG. 28A

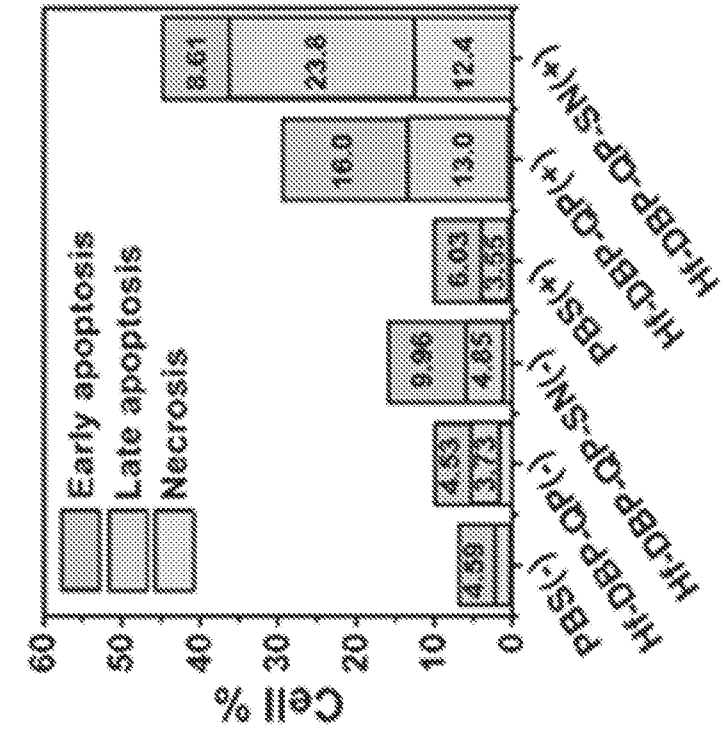

FIG. 28C

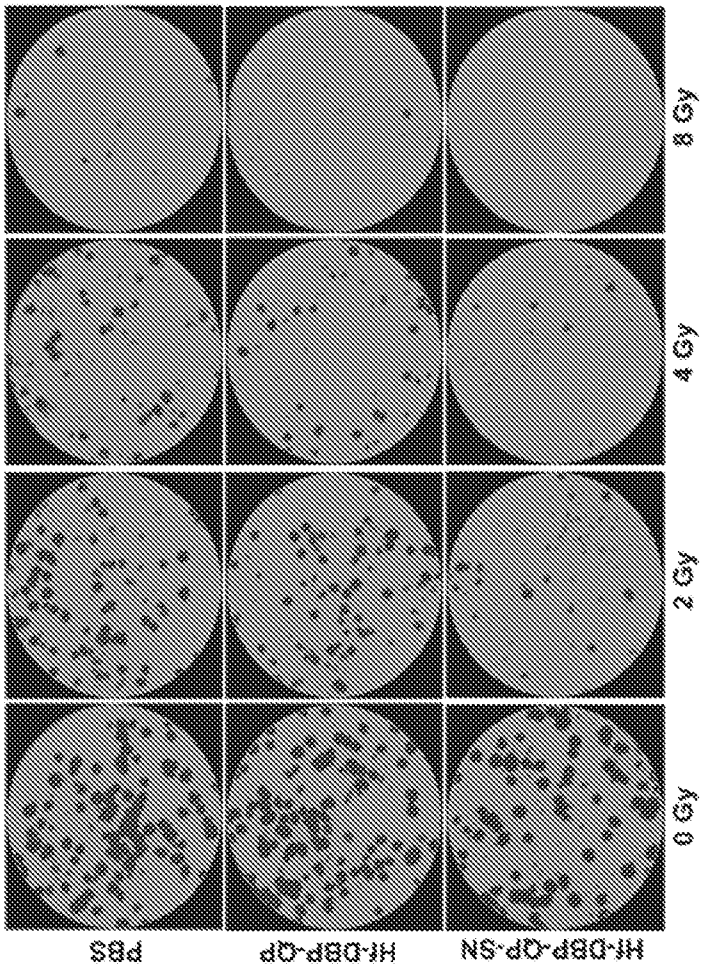

FIG. 28B

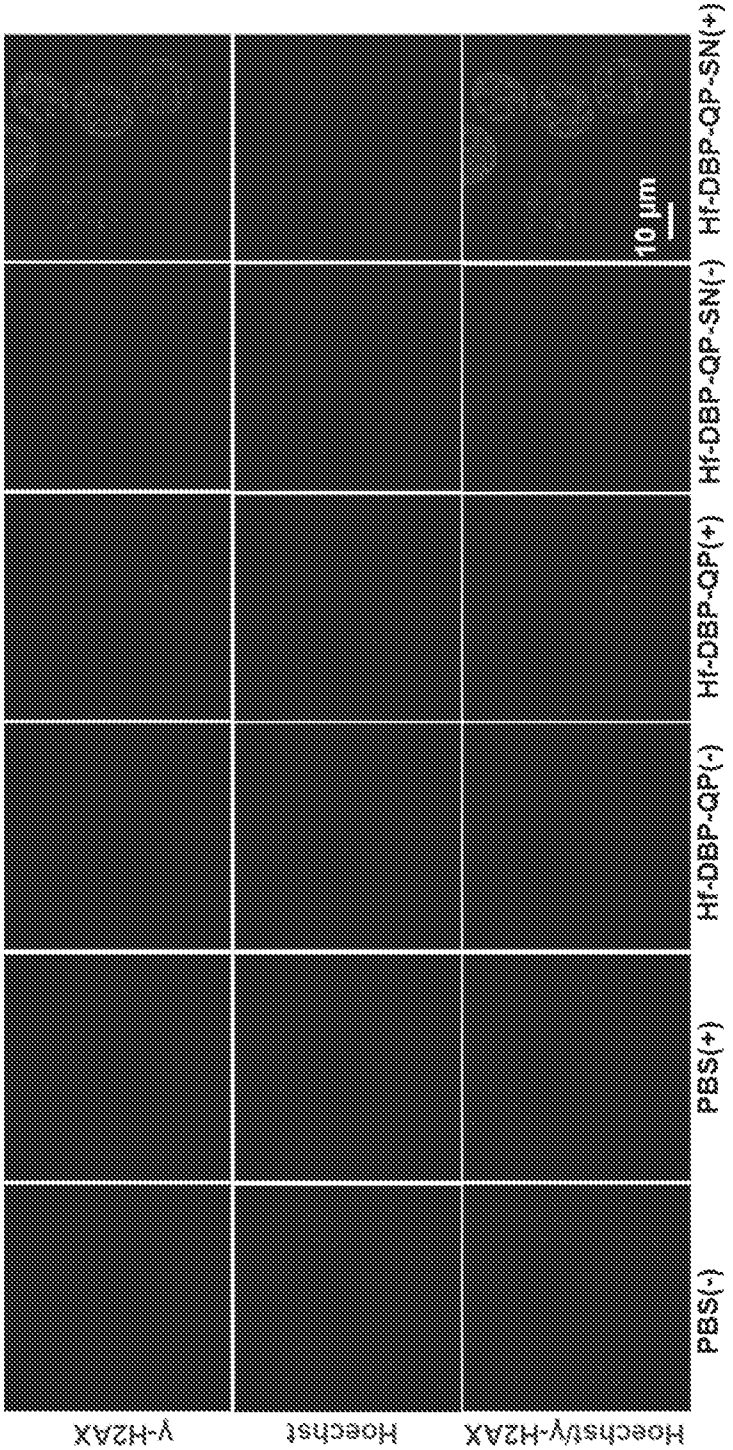
Hoechst/γ-H2AX
Hoechst
γ-H2AX
PBS(-)
PBS(+)
Hf-DBP-QP(-)
Hf-DBP-QP(+)
Hf-DBP-QP-SN(-)
Hf-DBP-QP-SN(+)
10 μm

FIG. 29

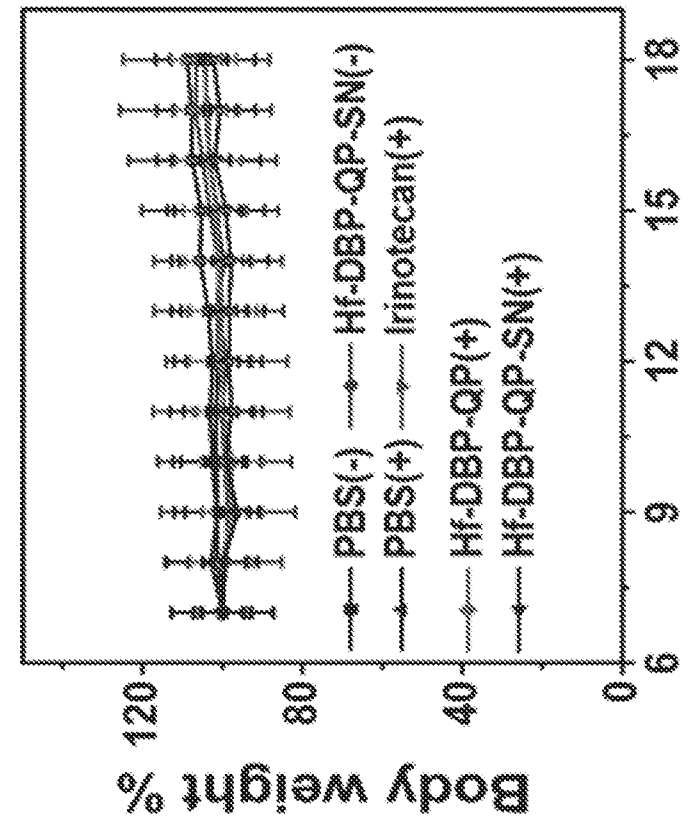

FIG. 30B

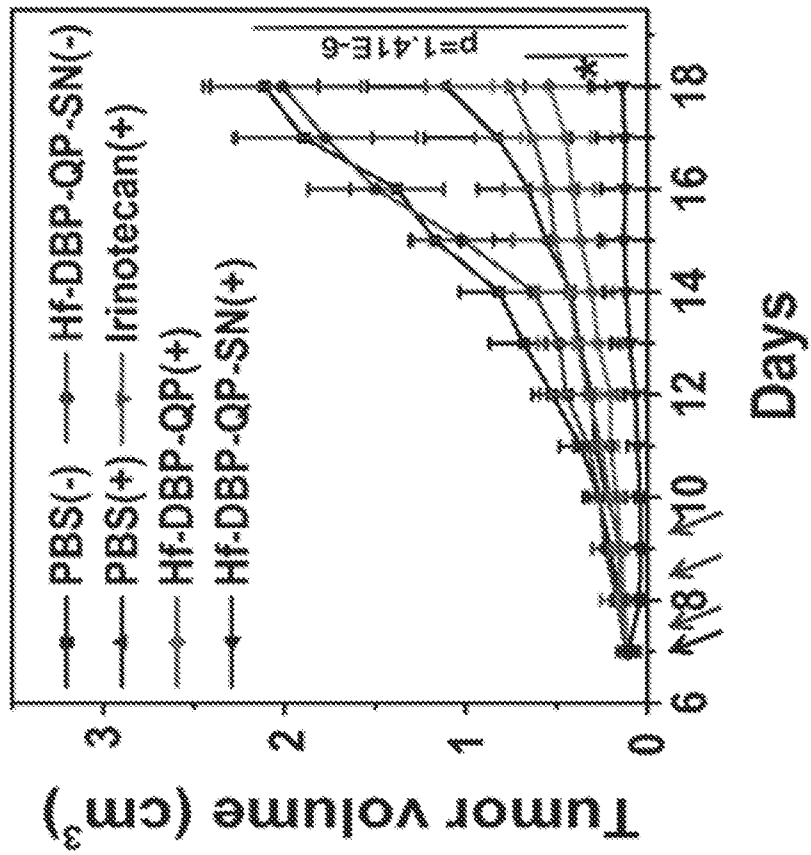

FIG. 30A

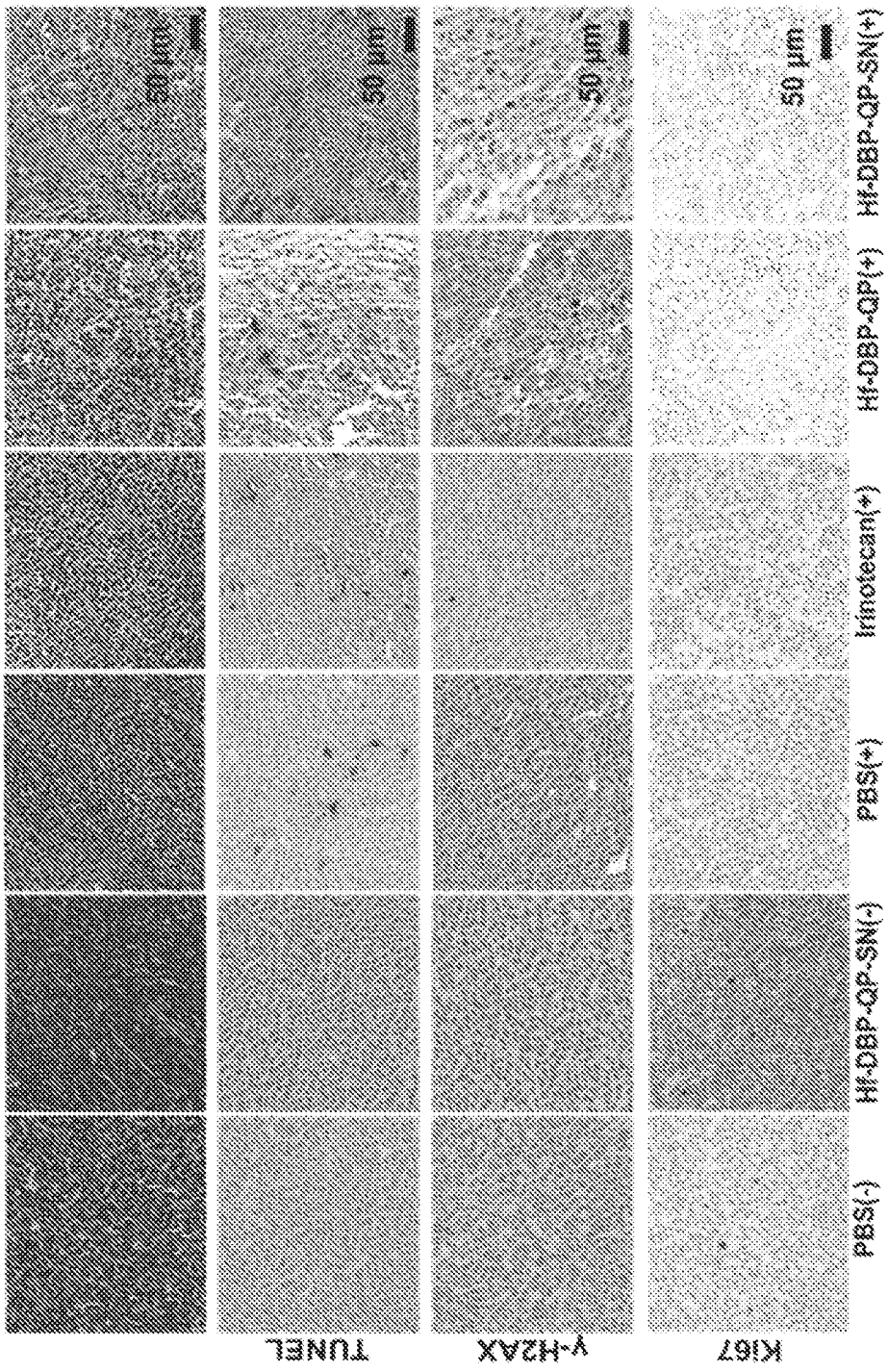
50 μm
50 μm
50 μm
50 μm
PBS(-)
Hf-DBP-QP-SN(-)
PBS(+)
Irinotecan(+)
Hf-DBP-QP(+)
Hf-DBP-QP-SN(+)
TUNEL
γ-H2AX
Ki67

FIG. 31

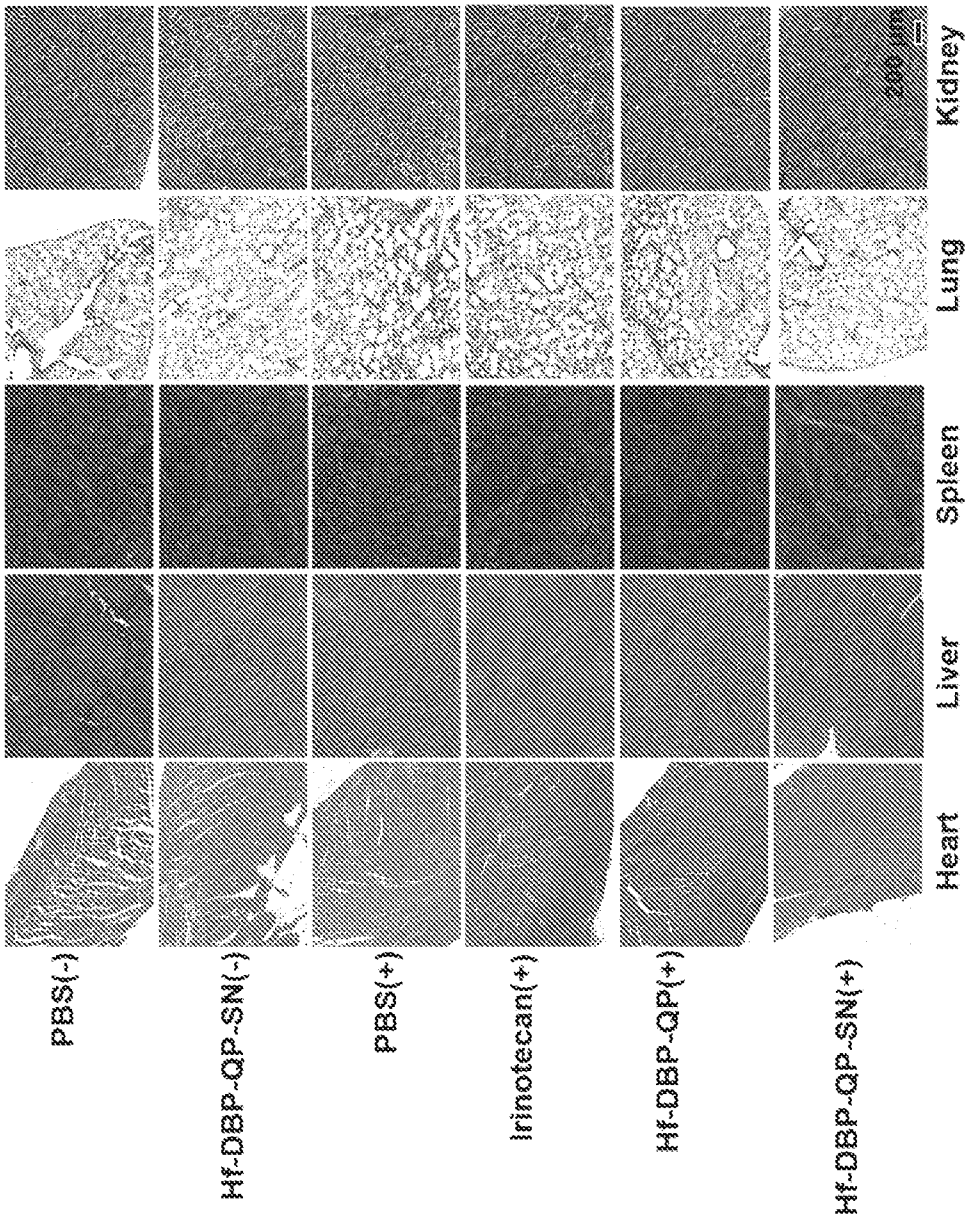
PBS(-)
Hf-DBP-QP-SN(-)
PBS(+)
Irinotecan(+)
Hf-DBP-QP(+)
Hf-DBP-QP-SN(+)
Heart
Liver
Spleen
Lung
Kidney
200 μm

FIG. 32

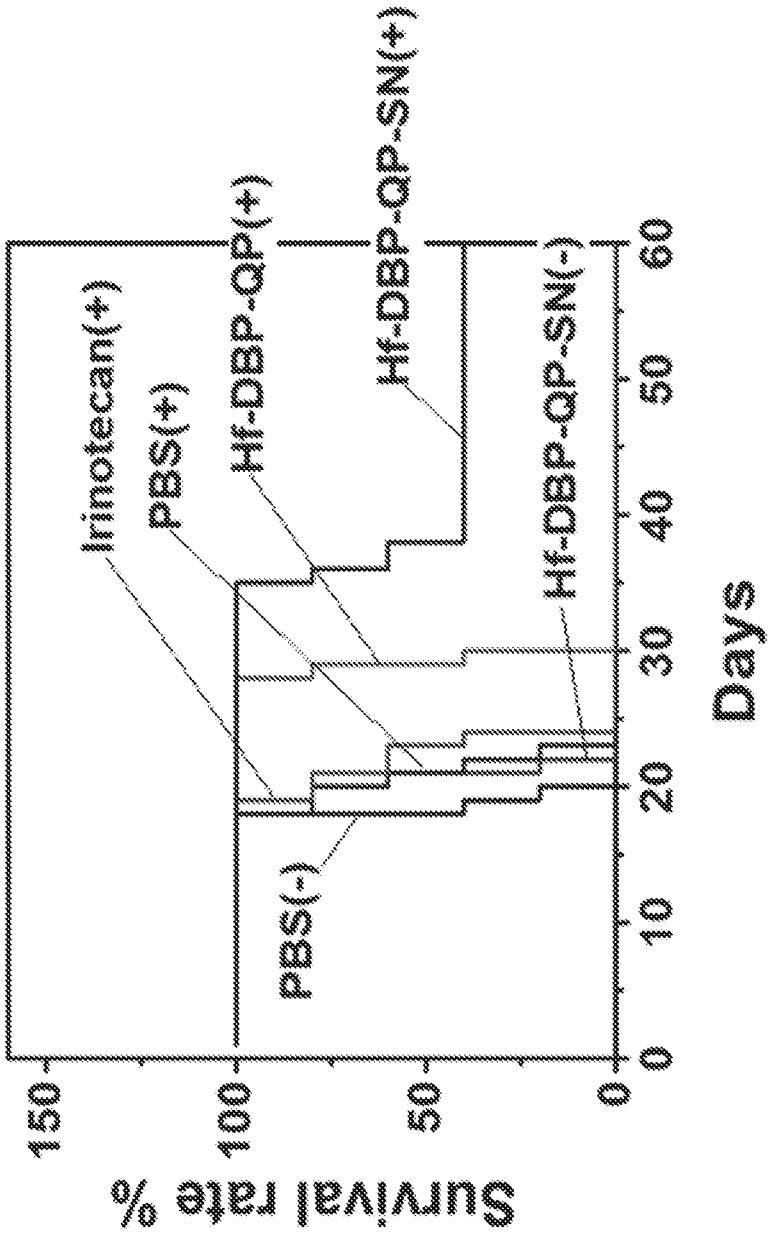
Survival rate %
150
100
50
0
0
10
20
30
40
50
60
Days
Irinotecan(+)
PBS(+)
Hf-DBP-QP(+)
Hf-DBP-QP-SN(+)
Hf-DBP-QP-SN(-)
PBS(-)

FIG. 33

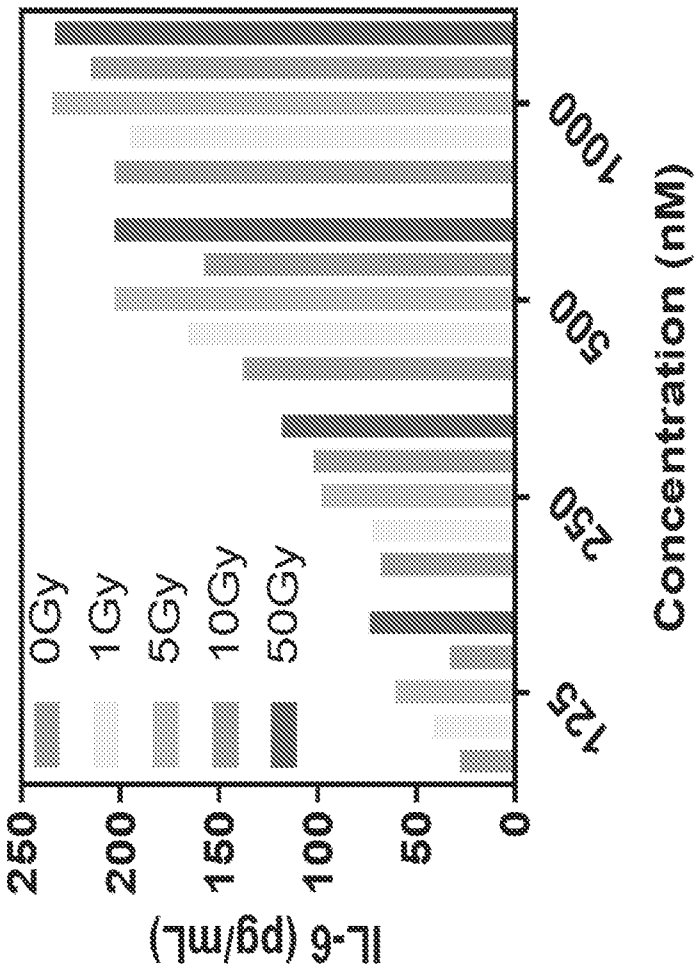
IL-6 (pg/mL)
250
200
150
100
50
0
0Gy
1Gy
5Gy
10Gy
50Gy
125
250
500
1000
Concentration (nM)

FIG. 34

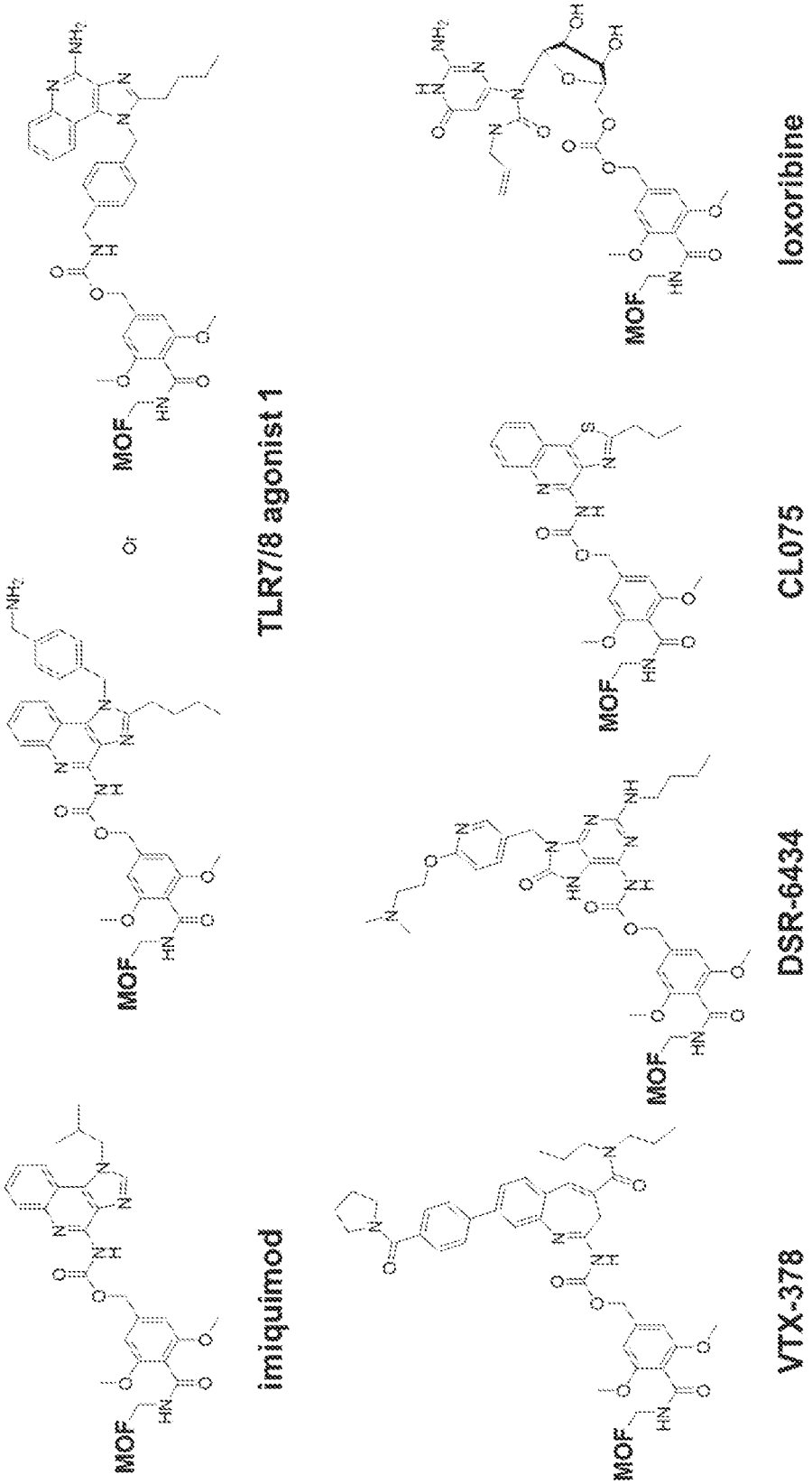
MOF
TLR7/8 agonist 1
or
MOF
imiquimod
MOF
loxoribine
MOF
CL075
MOF
DSR-6434
MOF
VTX-378

FIG. 35A

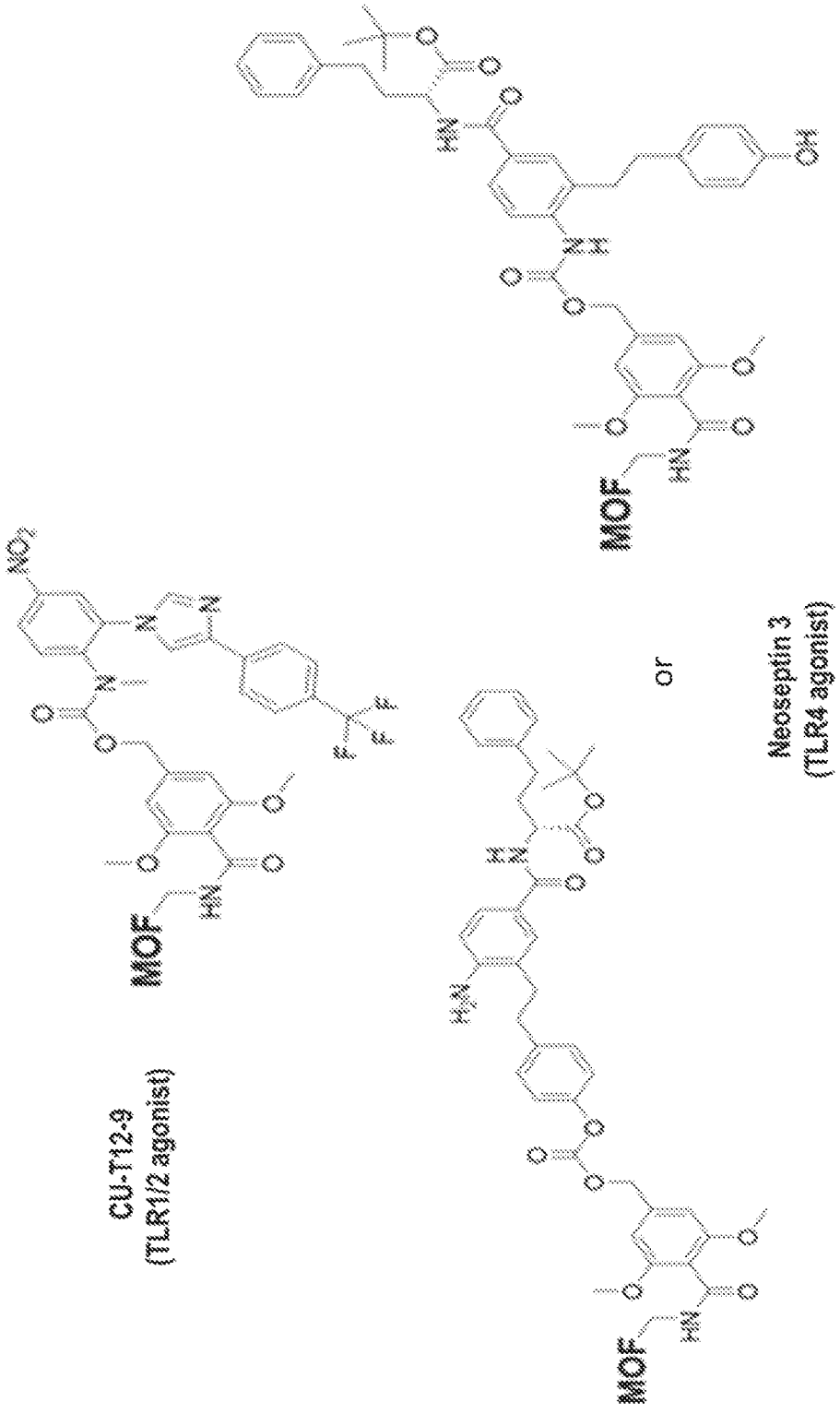

FIG. 35B

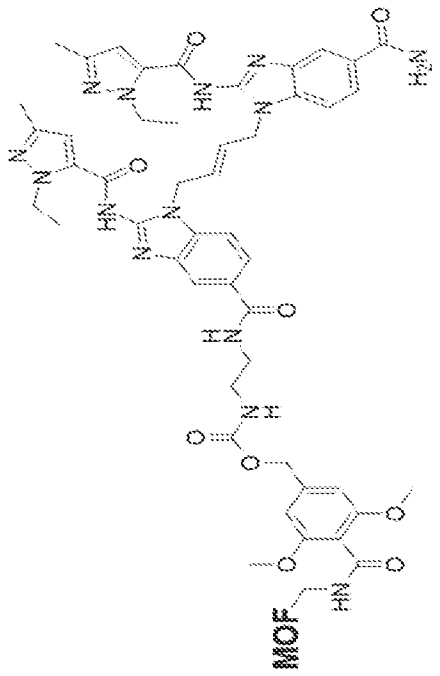

diABZI-C2-NH2 (diABZI derivative)

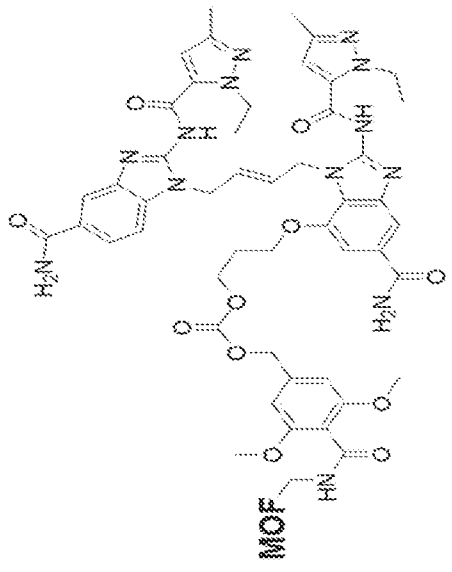

STING agonist-3 (diABZI derivative)

FIG. 35C